# CONVERSION OF CARBOHYDRATE BIOMASS TO VALUE ADDED CHEMICALS

**THESIS**

**SUBMITTED TO THE**

**SAVITRIBAI PHULE PUNE UNIVERSITY**

**FOR THE DEGREE OF**

**DOCTOR OF PHILOSOPHY**

IN

**CHEMISTRY**

BY

**NISHITA LUCAS**

**RESEARCH SUPERVISIOR**

**Dr. C.V.V. SATYANARAYANA**

**CATALYSIS DIVISION**

**CSIR - NATIONAL CHEMICAL LABORATORY**

**PUNE-411008, INDIA**

**MARCH 2015**

# CERTIFICATE

This is to certify that the work incorporated in the thesis entitled "**Conversion of carbohydrate biomass to value added chemicals**" submitted by **Ms. Nishita Lucas**, to the Savitribai Phule Pune University, for the degree of **Doctor of Philosophy** in Chemistry, was carried out by the candidate under my supervision at the Catalysis Division, CSIR-National Chemical Laboratory, Pune–411008, India. The material obtained from other sources has been duly acknowledged in the thesis. To the best of my knowledge, the present work or any part thereof has not been submitted to any other university for the award of any other degree or diploma.

Date:
Place: Pune

**Dr. C.V.V. SATYANARAYANA**
(Research Supervisor)
CSIR- National Chemical Laboratory,
Pune-411008, India

# DECLARATION BY RESEARCH SCHOLAR

I hereby declare that the thesis entitled **"Conversion of carbohydrate biomass to value added chemicals"** submitted for the Degree of **Doctor of Philosophy** in chemistry to the Savitribai Phule Pune University, has been carried out by me at the Catalysis and Inorganic Chemistry Division, National Chemical Laboratory, Pune – 411008, India, under the supervision of **Dr. C.V.V. Satyanarayana**. The material obtained from other sources has been duly acknowledged in this thesis. The work is original and has not been submitted in part or full by me for any other degree or diploma to this or any other University.

Date:
Place: Pune

**NISHITA LUCAS**
(Research Scholar)
CSIR- National Chemical Laboratory,
Pune-411008, India

*.....dedicated to my beloved parents and family*

***No problem can withstand the assault of sustained thinking.....***

***Voltaire***

## ***ACKNOWLEDGEMENTS…***

The completion of this thesis is credited to the support and encouragement of numerous people encompassing my family members, friends, colleagues and well wishers. At this point of accomplishment I am privileged to acknowledge all those people who made this thesis possible and an unforgettable experience for me. It is a pleasant task to reciprocate to the ones who contributed in many ways to the success of this study.

First and foremost, I would like to express my heartfelt and sincere gratitude to my research supervisor Dr. Satyanarayana Chilukuri who introduced me to a fascinating realm of chemistry. I am deeply indebted to him for his invaluable guidance and unconditional support. His constant inspiration and constructive criticism helped me immensely to focus my views in proper perspective. His tireless attitude has been an impetus for me throughout the course of study. He gave me the freedom to think and work; and I shall cherish my learning experience under his guidance. I also owe him towards his moral support which helped me immensely on my personal front. I take this opportunity to express my deepest sense of gratitude and reverence towards him for guiding me in the right direction throughout the research tenure.

Words fail me when I intend to express profound gratitude and indebtness to Dr. S.B. Halligudi for his professional and personal support. I believe the better way of thanking him would be through my future contribution to scientific community.

I extend my sincere thanks to the Director of CSIR-NCL Dr. Sourav Pal, Dr. Sivaram (former director) and Dr. D. Srinivas (Head, Catalysis division) for providing me the opportunity to accomplish my research work in this prestigious and well-equipped laboratory. My heartful thanks are due to Dr. P.N. Joshi, Dr. T. Raja, Dr. Nandini Devi, Dr. S. Sengupta, Dr. P. Dhepe, Dr. Vinod, Dr. Umbarkar, Ms. Violet Samuel, Mr.Madhu, Mr. Jha, Mr. Purushothaman and all other scientific and non-scientific staff for their help and support in scientific and technical matters during my tenure as a research student. I take this occasion to thank all my teachers, well-wishers classmates & friends in various stages for their teachings, love, encouragement, kind cooperation and good wishes that I received from them.

I extend my sincere thanks to Student Academic Office and University of Pune for the smooth documentation process during my doctoral studies. I am grateful to CSIR for awarding the research fellowship and Director, CSIR-National Chemical Laboratory for extending all infrastructural facilities.

I have high regards for all my lab seniors for their support and help during my Ph D. course. I am indebted to my labmates Dr. Narasimha, Hanmant, Richa, Lakshmi, Atul, Srikanth, Pranjal, and earlier labmates Kalpana, Lakshman, Aditya, Jay, Mangesh, Srinivasrao, Lalit, Gajanan, Swanand, Santosh, Amlan, Chandan for their love and encouragement.

I sincerely thank all my divisional friends for their timely help. A very special and warm thanks to my senior colleagues and friends Dr. Ankur, Dr. Shanbhag, Dr. Suman, Dr. Amol, Dr. Palraj, Dr. Neelesh and Sheetal for being the best supporters and awesome pals and teaching me the true value of friendship and becoming an inevitable part of my life.

Coming to the important people without whom the study would not have been conceptualized and accomplished. I am immensely pleased to thank my late grandparents especially and my parents, Shri Joel Praveen and Smt. Lipika for their nurturing, care, encouragement, blessings and essential parenting. I owe them for all the sacrifices and hardships endured for bringing me to this platform. I don't have words to express my gratitude to my husband Shri Satyendra for his undying love, support and positivity, for being the pillar and backbone of my courage and strength. Lastly, I would thank my daughter Mischelle for being a supportive & a mature child.

I would like to pay high regards to my in laws Shri Ajit and Smt. Dorothy, my brother Ashish, my sister Rebekah, my sister in law Ayojita, my brother in law Shri Saurabh and his wife Smt. Priyanka, all my cousins and kids (Ayush, Arush and Mayesha) for bestowing their affection, moral support, blessings, concern and constant encouragement on me.

Above all, I owe it all to Almighty God for granting the wisdom, health and belief to undertake research work for my thesis and enabling me to its completion.

***Nishita Lucas***

# Table of Contents

## Chapter 2 : Catalyst synthesis and characterization

# List of Figures

# List of Schemes



# List of Tables

## LIST OF ABBREVATIONS

| | |
|---|---|
| SBA | Santa Barbara Amorphous |
| BET | Brunauer-Emmett-Teller |
| GC | Gas chromatography |
| HPLC | High-Performance liquid chromatography |
| FID | Flame Ionization detector |
| FTIR | Fourier Transform Infra-red |
| ICP-OES | Inductively coupled plasma optical emission spectrometry |
| PXRD | Powder X-ray diffraction |
| SEM | Scanning electron microscopy |
| TEM | Transmission electron microscopy |
| TGA | Thermogravimetric analysis |
| TPD | Temperature programmed desorption |
| MS | Mass spectrometery |
| HMF | 5-Hydroxymethyl furfural |
| LA | Levulinic acid |
| IPA | Isopropyl amine |
| LCA | Lactic acid |
| Vs. | Versus |

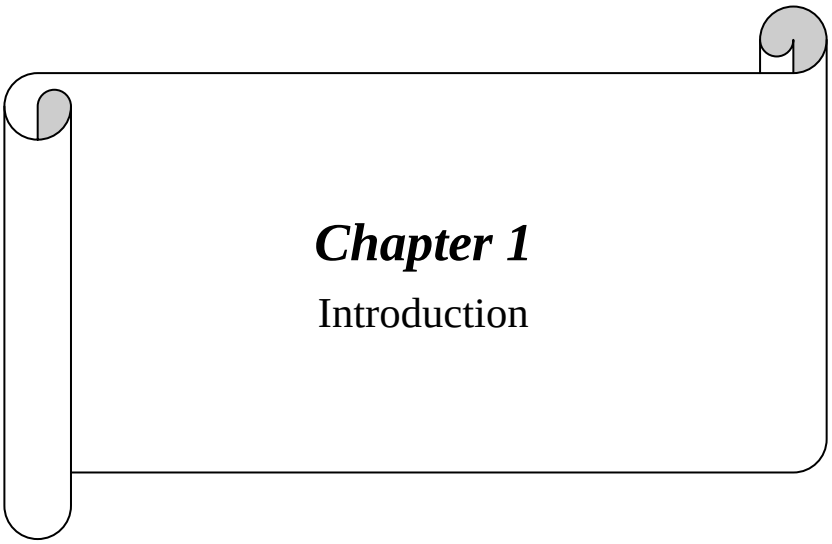

# *Chapter 1*

Introduction

## 1.1. Introduction

Catalysis plays an important role in the development of green, efficient and economical industrial processes for the production of chemicals, drug intermediates and fuels. The accomplishments of any chemical plant would depend on the catalyst technology it uses. Heterogeneous catalysis is the pillar of modern chemical technology. The continuous discovery of novel catalytic processes is leading to major innovations in chemical processing.

The word 'Catalysis', a Greek word implying 'loosen' and 'down', was coined by Berzelius in 1836 when he observed that chemical reactions occurred by catalytic contact [1-3]. Later in 1895, Ostwald proposed a definition which stated that "a catalyst accelerates a chemical reaction without affecting the position of the equilibrium" [4]. By the end of the $19^{th}$ century many catalytic processes were developed for selective oxidation, hydrogenation, dehydrogenation, isomerization, polymerization etc. All these catalytic processes triggered the industrial revolution [5]. Sulfuric acid synthesis (Contact Process), nitric acid synthesis (Ostwald Process), ammonia synthesis (Haber-Bosch Process), Fischer Tropsch synthesis, HCN synthesis (Andrussov Oxidation), Olefin polymerization (Ziegler Natta polymerization), desulfurization of petroleum (hydrodesulfurization), olefin metathesis, methanol conversion to hydrocarbons, sharpless epoxidation etc. are some of the important industrial processes [4,6]. Thus, the catalysis became backbone to the chemical industry contributing substantially to our societal needs and wealth.

During the industrial revolution, prime focus was on the discovery of new processes, but not on sustainability and waste minimization. As a result, lot of waste was generated from various chemical and pharmaceutical processes. This alarming environmental devastation was indicative of imperative transition from traditional methodology of reactivity and yields towards greener processes which focused on eliminating the use of toxic materials, waste elimination and 100% utilization of raw materials.

## 1.2. Sustainability and green chemistry

The need for transforming the orthodox reaction concepts to the environmental benign industrial process paved the way for sustainable chemistry. The *Brundtland Report* [7] came with the ideology of sustainable development which was defined as:

*Meeting the needs of the present generation without compromising the ability of future generations to meet their own needs.*

Subsequently, the concept of sustainability has seen greater attention, in which 'Green chemistry' has become an integral part. If sustainability is the ultimate objective, then the vital tool to accomplish it is Green chemistry. The term 'Green Chemistry' was coined in the early 1990's by Anastas *et al* [8] of the US Environmental Protection Agency (EPA) as:

*Green chemistry efficiently utilizes (preferably renewable) raw materials, eliminates waste and avoids the use of toxic and/or hazardous reagents and solvents in the manufacture and application of chemical products.*

This concept is embodied in the 12 Principles of Green Chemistry [9] which can be paraphrased as

1. Waste prevention instead of remediation
2. Atom efficiency
3. Less hazardous/toxic chemicals
4. Safer products by design
5. Innocuous solvents and auxiliaries
6. Energy efficient by design
7. Preferably renewable raw materials
8. Shorter syntheses route (avoid derivatization)
9. Catalytic rather than stoichiometric reagents
10. Design products for degradation
11. Analytical methodologies for pollution prevention
12. Inherently safer processes

The doctrine of green chemistry calls for the development of new reaction conditions and chemical reactivity that would benefit the chemical synthesis in context of enhanced environmental safety, better health, improvised resources and energy efficiency, increased product selectivity and simplicity in operation.

The industry and academia have widely accepted the principles of green chemistry, atom efficiency, effective concepts pertaining to waste reduction and E factors. Replacements of outdated processes using stoichiometric reagents with greener catalytic alternatives have led to significant minimization in waste generation. The next step towards achieving sustainable chemical industry will be the one in

which the renewable resources would be deployed for synthesis of chemicals, in accordance to the seventh principle of Green chemistry.

### 1.3. Renewable raw materials: the ultimate efficiency

Plant biomass was an excellent source for meeting the energy needs of the society before the discovery of fossil fuels. The discovery of crude oil in 19$^{th}$ century led to rapid industrialization and improved standard of living. Thus, fossil fuels became the major source of chemicals, energy and materials of the modern society.

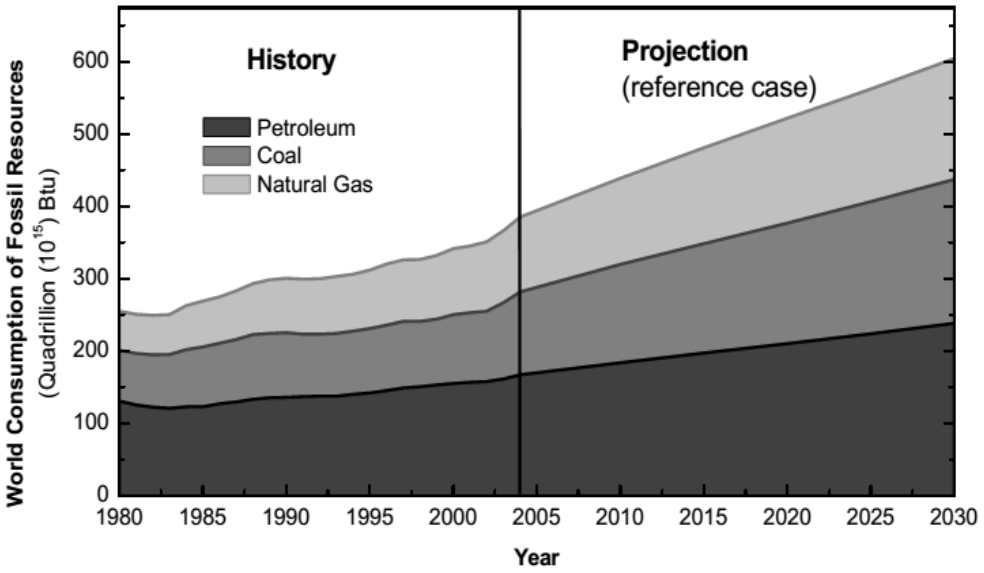


**Fig. 1.1.** World consumption of fossil fuels from 1980-2030.

Currently, fossil fuels such as petroleum, coal and natural gas meets 90% of the energy demand [10]. During 1980-2004, rate of consumption of fossil resources has increased to 50%, as shown in Fig. 1.1. It is projected that by 2030, $600\times10^{15}$ Btu of fossil resources would be needed to meet the energy demand of the world [11]. But, the fossil fuel reserves are limited and continuous increase in their demand particularly from developing countries will cause their rapid depletion in near future [12]. Moreover, the consumption of fossil fuels leads to net $CO_2$ emissions to the atmosphere, which has a detrimental effect on environment as it contributes to global warming and climatic change [13]. These issues have compelled the society to look for alternative sources of chemicals and energy. In this context, the ambitious objective of producing 25 % of chemicals and 20% of fuels from renewable sources (by 2030) are the apt approaches for a gradual transformation of fossil based economy into a renewable one.

## 1.4. Biomass valorization

### 1.4.1. Superiority, incentives and scope

A modern economy calls for efficacious use of renewables using new technologies. Various renewable resources include wind, water, solar and biomass. The potential energy of wind and kinetic energy of water is used for the generation of electricity, solar flux provides heat and thermal energy and biomass provides chemical energy stored as chemical bonds. Biomass stands unrivalled among the other renewable resources because it is only source that possess the energy in the form of chemical bonds. This striking feature of biomass allows it to be utilized for manufacturing numerous chemicals and fuels in addition to electricity and heat generation.

The term 'biomass' refers to any plant derived organic matter available on a renewable basis, that includes waste and residues of agricultural crop, wood, aquatic animal and plants, municipal and other waste materials [15]. Hence, availability of biomass is widespread, abundant and inexpensive [16-18]. Biggest advantage of biomass is that it is distributed across all regions of the world. These characteristics make biomass a superior and sustainable source for future demands of energy and chemicals.

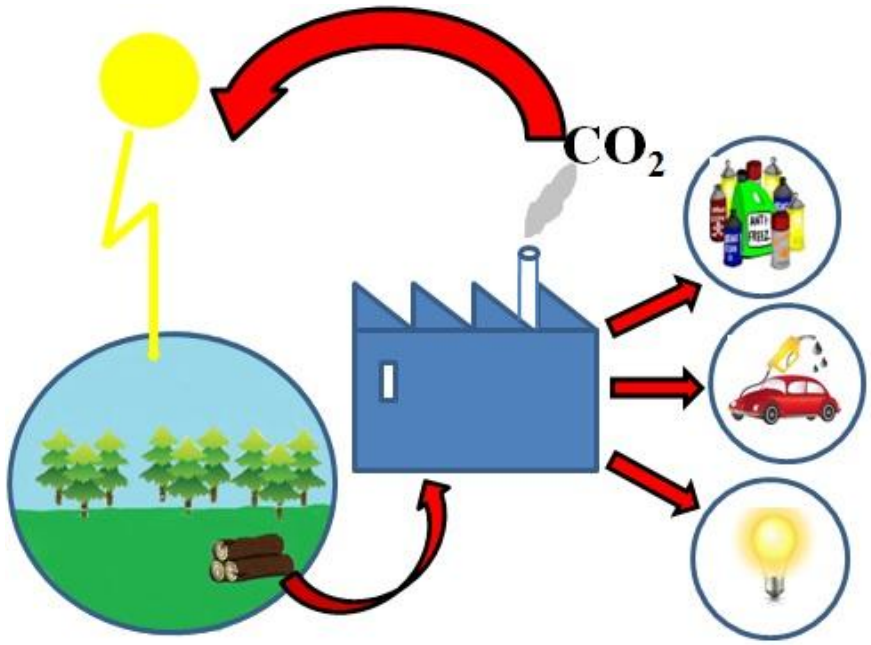


**Fig. 1.2.** Sustainable production of chemicals and fuels from biomass.

Biomass can be processed, either chemically or biologically in a biorefinery. According to the American National Renewable Energy Laboratory (NREL), '*biorefinery is a facility that integrates biomass conversion processes and equipment to produce fuels, power and chemicals from biomass'* [19]. The $CO_2$ released from the use of renewable product is used for photosynthesis for the production of biomass (Fig. 1.2.). The process is cyclical which makes biomass a renewable feedstock with useful carbon atoms [20]. However, to attain the objectives of sustainable development, biorefineries should play a significant role in the near future.

### 1.4.2. Composition of biomass

The most prolific class of biomass is the lignocellulosic biomass since it contributes to structural integrity of the plants and is always present in them. It has received tremendous attention over the past decade due to its abundance and ease of availability [21-24]. In general, the feedstocks used for energy/chemical production are lignocellulosic (crops and waste biomass) e.g. agricultural residues, switch grass, miscanthus, wastes from wood processing and municipality. Thus, this plant biomass is the most viable resource for production of chemicals and fuels [25-28] in a sustainable manner. Lignocellulose is comprised of three different fractions: cellulose, hemicellulose and lignin.

#### 1.4.2.1. Cellulose

Cellulose is a linear polysaccharide which consists of 1,4 linkages of D-glucopyranose monomers (Fig. 1.3). It is a crystalline material with an extended, flat, 2-fold helical conformation [29]. The hydrogen bonds present in the cellulose help to maintain and reinforce the linear, flat conformation of the chain. The top and bottom of these chains are entirely hydrophobic but the sides are hydrophilic and capable of hydrogen bonding. The presence of aliphatic hydrogen atoms in the axial positions and the polar hydroxyl groups in the equatorial positions are responsible for hydrogen bonding. Cellulose is entrapped within the complex lignin/hemicellulose matrix and it is largely inaccessible to hydrolysis in untreated biomass. This imparts the structure with rigid crystallinity. The degree of polymerization of cellulose varies from source to source; it is approximately 10,000 to 15,000 glucopyranose monomer units for wood and cotton respectively [30]. Biomass pre-treatment processes like milling and physical/chemical treatments serves to pervade lignin and extract hemicelluloses, so

that subsequent hydrolysis steps are more effective. Partial acid hydrolysis of cellulose gives cellobiose (glucose dimer), cellotriose (glucose trimer) and cello-tetrose (glucose tetramer), while complete acid hydrolysis breaks it into glucose [31]. It constitutes 40-50% of the total lignocellulosic biomass.

#### 1.4.2.2. Hemicellulose

Hemicellulose is a polymeric material which constitutes 20-40 wt % of the plant biomass [32]. In contrast to cellulose, the hemicellulose component is a branched polymer of five different sugars (pentoses and hexoses). The main sugars are xylose and arabinose (pentoses) and galactose, glucose and mannose (hexoses), all of which are highly substituted with acetic acid. Hemicellulose is bound to lignin and cellulose strands are interwoven with it (Fig 1.3.). Its extraction can be achieved through various physical and chemical methods. The most copious building block of hemicellulose is xylan (a polymer of xylose linked at the 1 and 4 positions). The branched nature of hemicellulose imparts it amorphous nature and it is relatively easy to carry out acid hydrolysis, compared to cellulose, yielding its monomer sugars.

#### 1.4.2.3. Lignin

The lignin fraction of biomass is a highly cross linked, amorphous polymer comprised of methoxylated phenylpropane structures, like coumaryl alcohol, sinapyl alcohol and coniferyl alcohol. High degree of cross linking makes the plant structurally stringent and provides a hydrophobic vascular system for the movement of solutes and water [33]. Lignin encompasses the cellulose, hemicellulose fractions and it acts like an adhesive holding these fibers together (Fig. 1.3.). Effective biomass pretreatment processes are required to split the lignin seal making the carbohydrate portions easily accessible. This irregular polymer is formed by an enzyme-initiated free-radical polymerization of the alcohol precursors [34]. Its extractives are defined as those compounds that are not an integral part of the biomass structure. Extractives are soluble in solvents like ethers, methanol, hot and cold waters. Different types of carbohydrates such as amylase from corn grains and sucrose from sugarcane are a part of these extractives. Being rich in oxygenated aromatic species, lignin is an ideal feedstock for the production of phenolic resins and researchers have demonstrated strategies for the production of aromatics and bio-oils from lignin [35]. It constitutes 15-30% of the total lignocellulosic biomass.

Being the most renewable feedstock, the conversion technologies of lignocellulosic biomass to generate fuels and chemicals are not effective and still remain a major challenge worldwide. The cause is the structural and chemical complexity of biomass which hinders its conversion towards targeted products with high yield and selectivity. There are numerous methods for transforming lignocellulose to fuels and chemicals but the prominent ones are pyrolysis, gasification and hydrolysis. The first two approaches convert the biomass to fuels while the last one converts it to chemicals. Through hydrolysis the chemicals which are obtained can be further upgraded by adopting interesting transformations revealing the potential of this technology in obtaining wider array of products. All these technologies are discussed in detailed in upcoming sections.

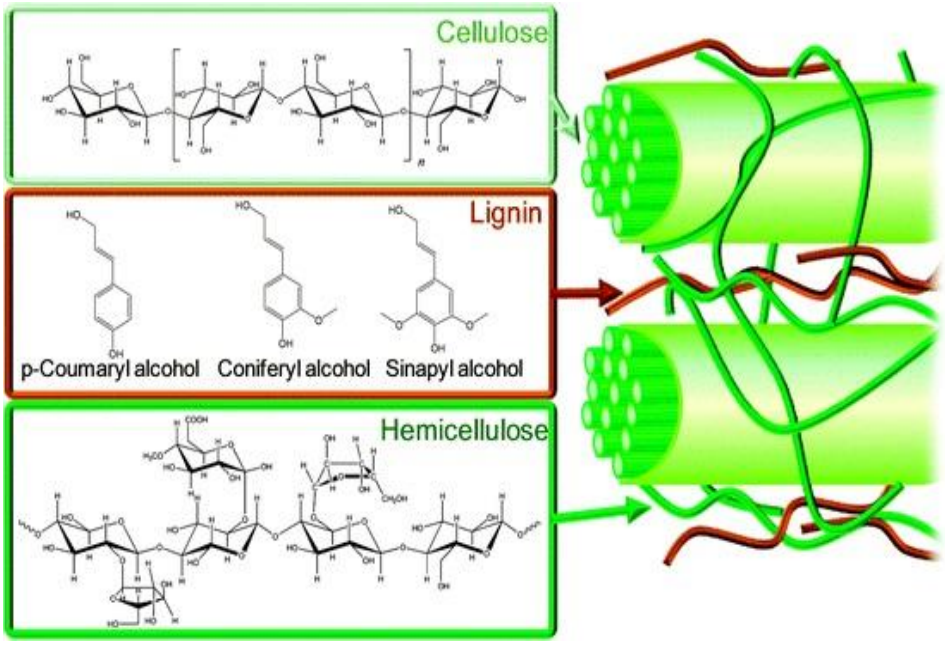


**Fig. 1.3.** Composition of lignocellulosic biomass.

### 1.4.3. Processes for conversion of biomass to fuels and chemicals

#### 1.4.3.1. Gasification

Biomass gasification is a thermal method of transforming biomass to a mixture of CO and $H_2$ (i.e. syn gas). This is carried at very high temperatures as the reaction process is highly endothermic (800°C) [36].Partial combustion of biomass happens during gasification with steam and air. Syn gas obtained as a result of this can be transformed into liquid hydrocarbons through Fischer-Tropsch approach [37-39] or methanol synthesis [40,41]. Streams rich in $H_2$ can be produced by tuning the

ratio of reactants in the syn gas, by carrying out water gas shift (WGS) reaction [42] or by insitu $CO_2$ absorption pathways [43]. Despite the fact that all three components of lignocellulosic biomass can be employed for gasification there are associated drawbacks with it. There are some challenges that are to be resolved in this route like highly dilute or poor quality syn gas stream [44], consumption of huge amount of biomass, also the moisture content of biomass which in turn affects the thermal efficiency of the process. These shortcomings increase the overall economy of the process [45-47].

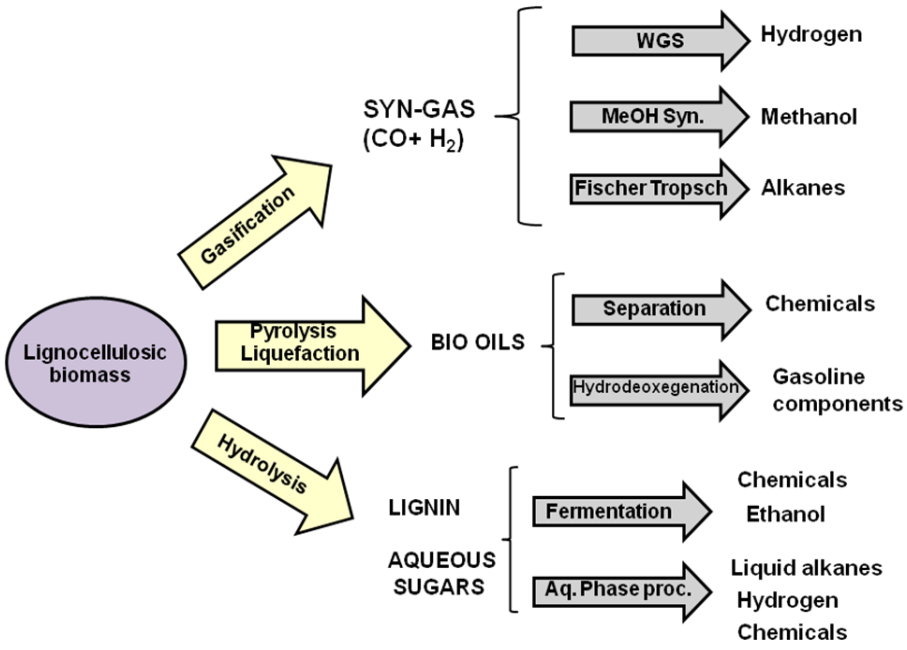


**Fig. 1.4.** Conversion routes of lignocellulosic biomass to fuels and chemicals [13].

### 1.4.3.2. Pyrolysis/Liquefaction

Another method for valorization of biomass is pyrolysis or liquefaction. In this method, biomass is heated in an inert atmosphere at lower temperatures (300 – 700 °C) to give bio-oil, a dark organic liquid [36,48]. Various polymeric carbohydrates, oxygenated compounds, lignin fragments and water (~25wt%) constitute this oil [48]. Due to diverse constituents of bio-oil it is an excellent source of chemicals. However, the energy efficiency is low which can be ascribed to higher oxygen content in it demanding further processing to enhance its fuel properties. This can be achieved by deoxygenation in presence of external $H_2$ [49,50] or its conversion to aromatics using zeolites [51]. The operational simplicity of the process is

neutralized by costly isolation and up gradation methods and lack of product selectivity.

#### 1.4.3.3. Hydrolysis

Enzymatic and acid hydrolysis is a process in which the individual components of lignocellulosic biomass (polymeric sugars and lignin) could be obtained with ease. This methodology is superior to pyrolysis and gasification since the operational temperatures are low. Lignocellulose possess a highly complex and rigid structure resulting in low surface area and high crystallinity. This makes its depolymerization to sugars a strenuous task [52,53]. Breaking such complex feedstocks into monomers calls for very efficacious pretreatment methods. During the pretreatment process the outermost and rigid lignin seal is ruptured exposing the cellulosic and hemicellulosic fraction. These fractions then become more accessible for the enzymes or acids for hydrolysis and could be converted to sugars (hexose or pentose). Visualizing the importance of such pretreatment methods they are of diverse origins ranging from physical, chemical or biological [54,55]. On hydrolysis, the morphology and network of lignin gets altered under the mild reaction conditions with simultaneous hydrolysis of hemicellulose fraction with acids. Since cellulose is linear and crystalline more austere conditions are required for its depolymerization. Conclusively, through hydrolysis the sugars could be derived from complex biomass feedstocks at a low cost. This biomass derived carbohydrates possess great potential to be transformed into value added chemicals. The present thesis embarks the utilization of these carbohydrates into highly important chemicals.

## 1.5. Value added chemicals from carbohydrate biomass

Every year, 170 billion metric tons of biomass is produced through photosynthesis, 75% of which can be allocated to carbohydrates, 20% lignin and 5% other natural products like oils, nucleic acid, fats, alkaloids, proteins and terpenes [56-59]. Hence, it is important to look for effective approaches to exploit them. These carbohydrates not only contribute to a major fraction of plant biomass but also have several applications in various sectors like food, paper, fermentation, petroleum production and pharmaceutical industries [60]. So it can be concluded that carbohydrates are plentiful, varied and reusable source of carbon.

Carbohydrates are macromolecules of oxygen, carbon and hydrogen with the empirical formula $C_m(H_2O)_n$ (m is not equal to n). They are classified as mono, di, oligo and polysaccharide where the mono and dimers are called sugars. The monosaccharide is the simplest carbohydrate (monomer) and other macromolecules/ polymers are composed of this monomer with the empirical formula $(CH_2O)_n$, where n is three or more. Hexoses and pentoses i.e. C-6 and C-5 sugars respectively, are the most common and abundant biomass primary compounds.

**Table 1.1.** List of biomass derived platform chemicals.

| Carbon species | Important platform chemicals |
|---|---|
| C2 | Acids (acetic, glycolic, oxalic), ethanol, ethylene. |
| C3 | Acids (3-hydroxypropionic, lactic, propionic, acrylic), acetone glycerol and propane diols. |
| C4 | Acids (fumaric, succinic, asperic, malic, asperic, butyric), 1,2,4-butane triol, 1-butanol, acetoin and 2,3-butane diol. |
| C5 | Acids (levulinic, itaconic, glutamic), furfural and sugars ( Xylose and arabinose) |
| C6 | Acids (adipic, citric, gluconic), sucrose, sorbitol, 5-hydroxymethyl furfural and lysine |

The chemicals obtained from petrochemical feedstocks which can serve as platform chemicals consist of alkanes (ethane and butane), aromatics (benzene, xylene, toluene), propylene, 1,3,-butadiene [61]. Currently, a similar approach is adopted in deriving chemicals from carbohydrates and lignin which can be identified as platform molecules. Researchers have recognized some compounds which have the potential to act as building blocks, which are listed in Table 1.1. The biomass primary products (cellulose, starch, hemicellulose, lignin, proteins and oils) are the reactants from which these chemicals can be attained [62]. Amongst those listed, many can be produced from carbohydrate as reactant. Because of high functionality and reactivity, low volatility, processing of biomass is preferably pursued by liquid-phase technologies [63]. In general, numerous important fuels and chemical intermediates (Fig. 1.5.) can be produced from carbohydrates by biotechnical/chemical pathway [64,65]. They can be transformed into alcohols [66, 67], furanics [68,69] and acids [70,71] which have been identified as the top 12 value added chemicals by US DOE

[72]. Effective conversion of these compounds into chemicals and energy is the measure of successful biomass utilization strategy.

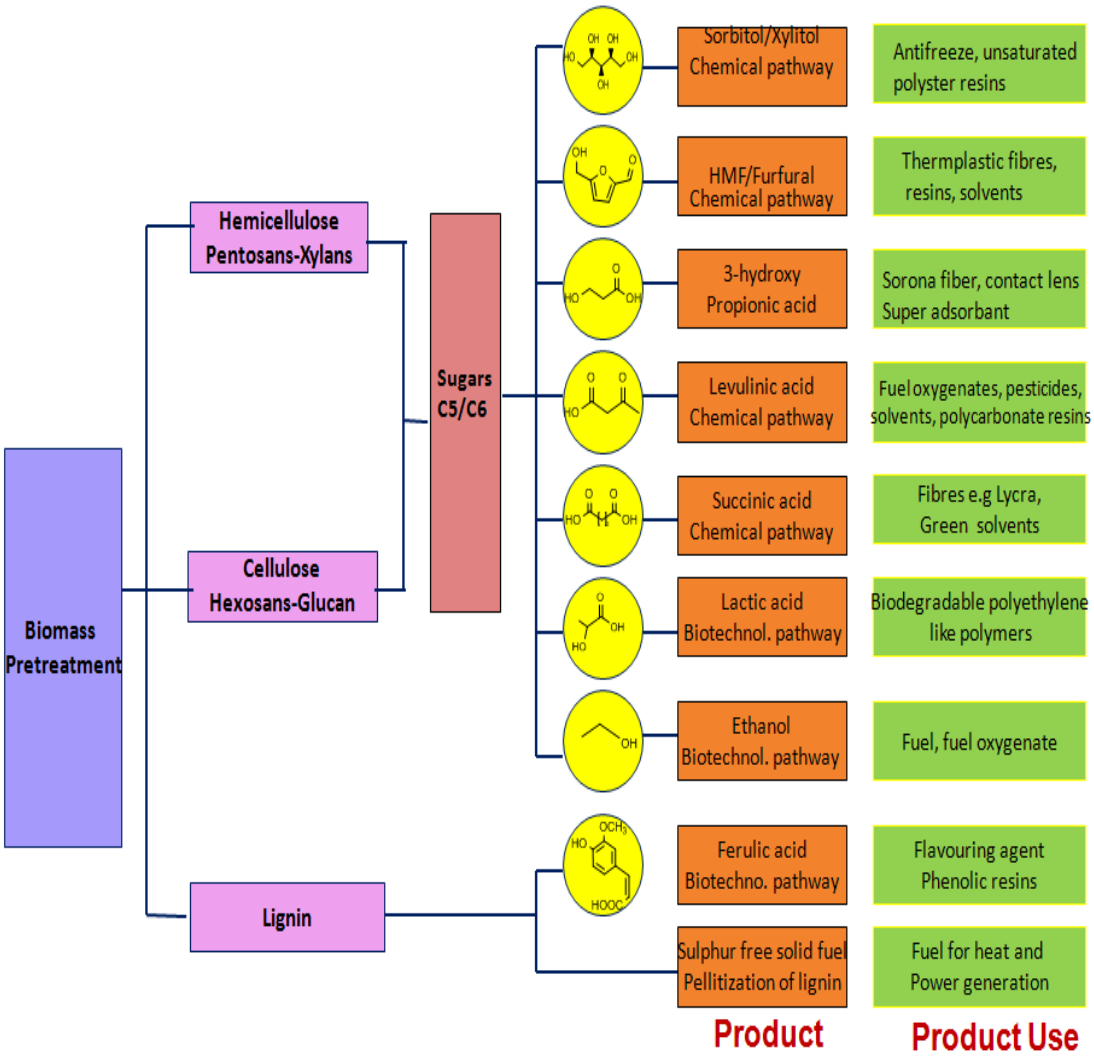


**Fig. 1.5.** Value added chemicals from carbohydrate biomass [72]**.**

The chemical transformation of sugars employs various types of reactions including hydrolysis, dehydration, isomerization, aldol condensation, hydrogenation, reforming and oxidation of sugars to give important chemicals with significant applications [73]. Figure1.6. depicts the organic transformation of sugars to render an array of useful chemicals.

Among the various transformations, dehydration of sugars appears to be the most attractive and promising approach. Through this, three important chemicals, viz., 5-hydroxymethyl furfural (HMF) through dehydration of hexoses, levulinic acid on rehydration of HMF and furfural by dehydration of pentoses are obtained. The present thesis focuses on the dehydration of sugars to HMF and levulinic acid by dehydration-

rehydration processes. Hence, various aspects of these important chemical feedstocks are discussed below in more detail.

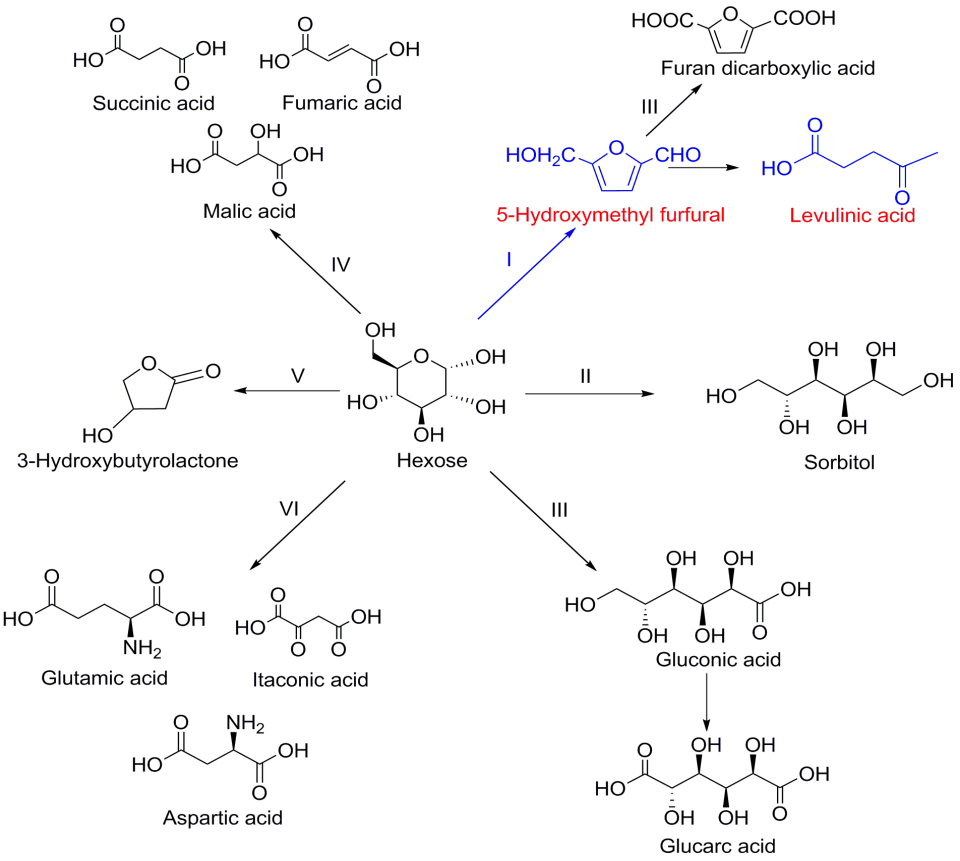


**Fig. 1.6.** Transformation of hexoses (I) dehydration (II) hydrogenation (III) oxidation (IV) fermentation Kerb's pathway (V) fermentation and oxidation (VI) fermentation.

### 1.5.1. 5-Hydroxymethyl furfural as "platform chemical"

The term "platform chemical" is used to describe a compound that can undergo multiple transformations to give numerous useful products. Furanics are heterocyclic compounds with an aromatic ring comprised of four carbon atoms and an oxygen atom that can be obtained from hexose sugars. One such furanic that is increasingly becoming important is HMF. It is comprised of a furan ring system with an aldehyde and a hydroxymethyl group at the 2 and 5 positions respectively. It was reported in 19$^{th}$ century by Dull *et al* [74] for the first time. He has synthesized it by heating inulin and oxalic acid under pressure. Later, Kiermayer [75] synthesized HMF from sugarcane juice using a similar procedure. Later, after intensive research, it was generalized that HMF can be obtained from sugars on heating under acidic conditions [76]. Additionally, HMF has been detected in foods such as cereals, dried fruits, coffee and baking products [77-80]. The daily intake of HMF is estimated to be 30–

150 mg per person [81]. HMF can be toxic to humans when ingested at concentrations of 75 mg per kg of body weight or greater. An excellent review by Rosatalle *et al* summarizes the biological properties and synthetic applications of HMF [82].

The actual value of HMF is in the truth that it can be changed into various useful compounds via. simple chemical transformations (Fig. 1.7.). The potential applications of HMF includes its selective oxidation to furan-2,5-dicarboxylic acid (FDCA) and 2,5-diformylfuran (DFF). The former is of vital interest because it can be used as a replacement for isophthalic and terephthalic acids which are used for synthesizing polyurethanes, polyesters, and polyamides [83,84]. Hydrogenation of HMF transforms it to 2,5-diformyl-tetrahydrofuran (DF-THF) and 2,5-bis(hydroxymethyl) tetrahydrofuran (DHM-THF). These products on condensation generate polymers which have the potential to become liquid alkanes [85]. HMF on hydrogenolysis renders 2,5-dimethylfuran (DMF), 2-methyltetrahydrofuran (MTHF) and 2,5-dimethyltetrahydrofuran (DMTHF). Amongst them, DMF has great significance as a biofuel as it is immicible with water, have high energy density and low volatility [86]. HMF rehydration decomposes it into formic and levulinic acid [87], both being important commodity chemicals. Additionally, levulinic acid serves as a precursor for γ-valerolactone; a liquid fuel [88]. Moreover, numerous phenolic resins and polymerizable furanic compounds with promising properties have been prepared from HMF [89,90].

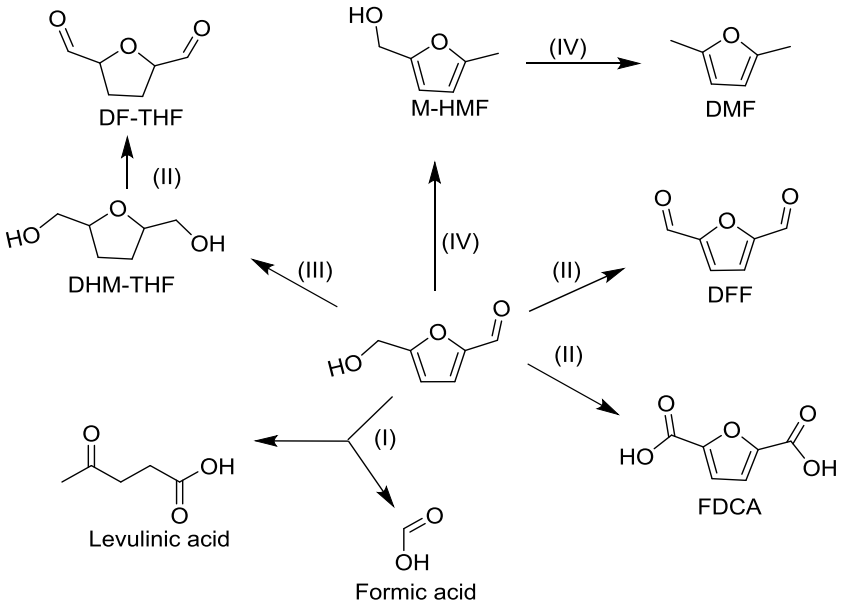


**Fig. 1.7.** Synthetic routes from HMF by (I) rehydration (II) oxidation (III) reduction (IV) hydrogenolysis.

The mechanism of HMF formation from fructose was first studied by Haworth and Jones [91]. After them many researchers [92-94] attempted similar mechanistic studies and exhibited two plausible pathways for HMF formation from aldoses and ketose (Scheme 1.1). The first pathway depicted the formation of HMF based on transformation of ring systems and second pathway shows that HMF is formed through a series of acyclic intermediates. Moreover, they demonstrated that the chemistry of the formation of HMF is very complex. Apart from dehydration, other competitive and inevitable side reactions such as isomerization, fragmentation and condensation occurred, which strongly influenced the yield of the process [93]. Van Dam [92] and Cottier [95] showed that aqueous and non-aqueous dehydration processes led to about 37 products. Therefore getting HMF in good yields is a challenging task.

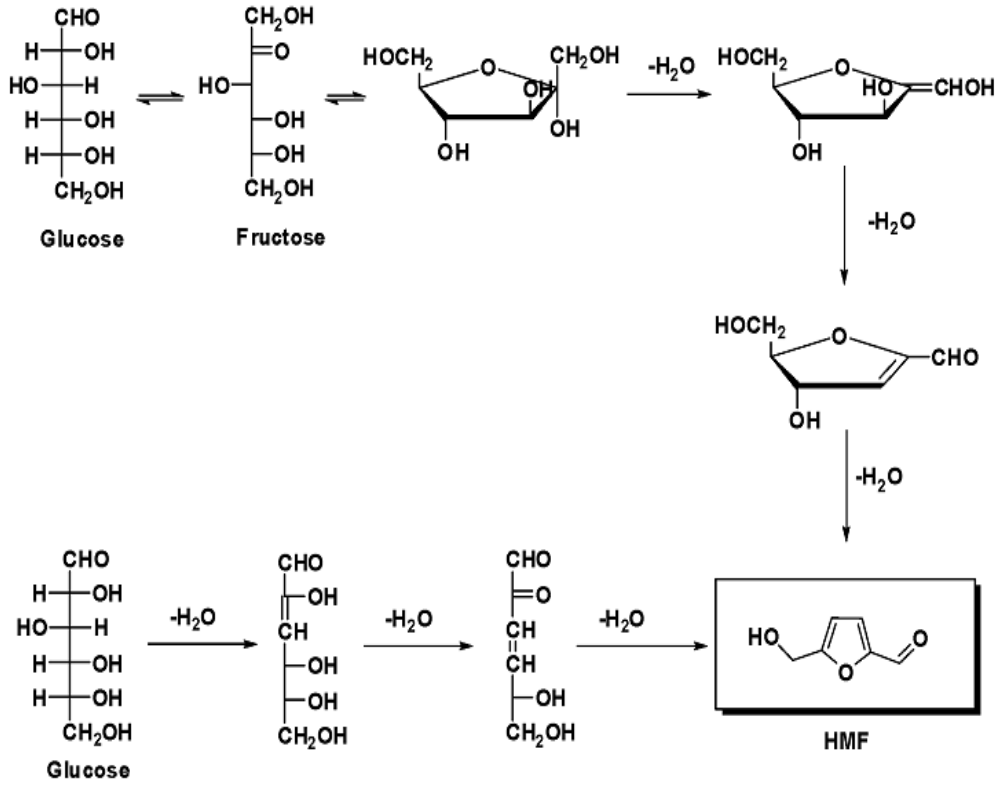


**Scheme 1.1.** Pathways for dehydration of hexose.

Researchers have synthesized HMF in various reaction medium ranging from organic solvents (DMSO), water, biphasic medium, ionic liquids and in supercritical solvent conditions. However poor yields and economic feasibility of the processes hinders its industrial scale up. Because of the highly reactive nature of the reaction, the role of acidity must be envisaged as it can change the reaction pathway leading to

unwanted side reactions. Therefore in the present investigations, HMF synthesis was attempted in various mediums along with the fine tuning of the acidity to study its effect and furnish insights into the desired acidity for such complex reactions.

### 1.5.2. Levulinic acid

Levulinic acid (LA), or 4-oxopentanoic acid or γ-ketovaleric acid or, is categorized under a $C_5$-chemical with a pair of multifunctional group, consisting of mono ketonic and mono carboxylic group. The presence of bifunctional groups makes LA a highly reactive molecule from which a wide array of chemicals can be obtained. Other striking features are its chemical properties like solubility and acidity. LA is readily soluble in aqueous, polar and non-polar, protic and aprotic organic solvents like ethanol, diethyl ether, acetone, and many others. The dissociation constant (pKa = 4.59) of LA was comparable with aliphatic carboxylic acids having low molecular weight ($C_3$-$C_5$) [96].

Levulinic acid is recognised as a platform chemical for rendering various interesting derivatives [97], as depicted in Fig. 1.8. LA derivates are a result of organic transformation of the functional groups (keto, carboxylic and methyl) and reduction and oxidation. Each derivative is of utmost industrial importance. One of the important approaches of transforming the carboxylic group is the production of various esters through esterification of LA.

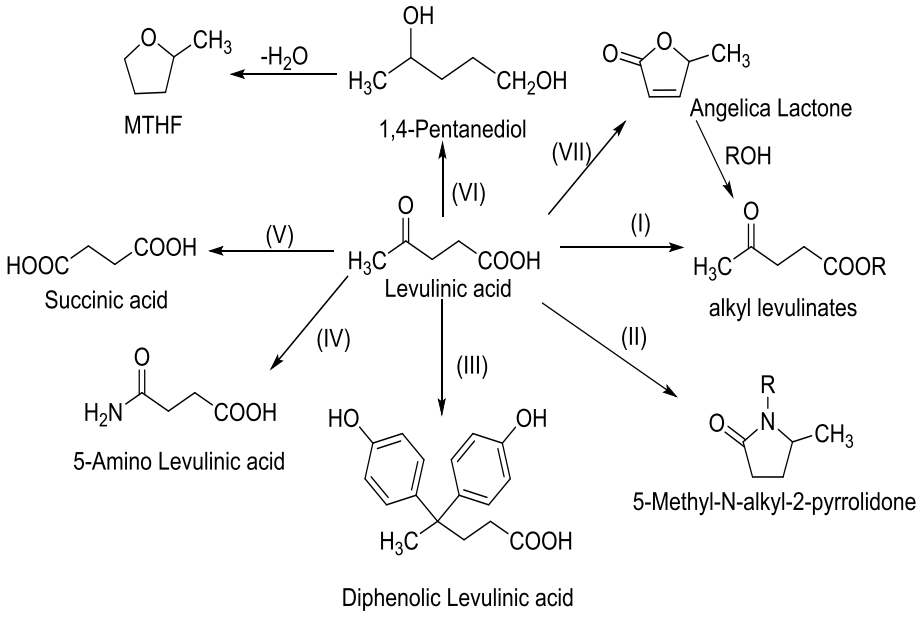


**Fig. 1.8.** Organic transformation of LA (I) esterification (II) reductive amination (III) condensation (IV) enzymatic (V) oxidation (VI) hydrogenation (VII) dehydration

Levulinic esters can be used as fuel additives, solvents and plasticizers [98]. Additionally, they have potential to serve as kerosene replacement in firing of gas turbines [99]. Reductive amination of the carbonyl group gives amides which are attractive because of their biological activity. δ-Aminolevulinate has an established market ($9.1–13.6\times10^4$ tons $year^{-1}$) since it is used as an ingredient of renowned biodegradable herbicide [72]. Among other reactions of carbonyl group, the important one is the condensation reaction with cyclic or aromatic alcohols to give diphenolic acids which can be used in producing paints, lubricants, polymers and fire-retardant materials [100]. Halogenation of methyl group by chloride or bromide is an effective way of transforming them to organic halides. 5-Bromolevulinic acid is a precursor for δ-aminolevulinic acid. Levulinic acid can be oxidized to numerous interesting compounds. Succinic acid is an important chemical resulting from LA oxidation, its uses and reactions are very well documented in literature [101]. Catalytic hydrogenation of LA gives γ-valerolactone (GVL) which is deployed as adhesives, insecticides and solvent for lacquers [102]. Methyl tetra hydro furan (MTHF); an important derivative of GVL, is used as gasoline oxygenate and possesses remarkable market potential ($2.6\times10$ $5m^3year^{-1}$) [103]. Apart from these, LA itself finds numerous applications. It is used as solvent, food flavouring agent and as an inhibitor for synthesis of chlorophyll. It is used in the preparation of rubber, nylon and synthetic resins and as a constituent of hydraulic brake fluids. Researchers have demonstrated that its sodium salt can be used as an antifreeze compound instead of ethylene glycols [104].

The mechanism of LA formation was studied by Horvat *et al* [105] which show that its formation proceeds through the formation of HMF as intermediate. Fructose is dehydrated to HMF which again rehydrates to give LA (Scheme 1.2.) On rehydration, water molecule adds to the C2-C3 double bond of the furan which leads to ring opening and the formation of unstable intermediate. This intermediate then decomposes to give the final products, LA and formic acid (FA). LA was first prepared in the 1840's by the Dutch professor G.J. Mulder when sucrose was heated at high temperature with mineral acids [106]. Still this approach is the most common and attractive for preparing LA from biomass. Starting from C6 sugars the theoretical yield of LA is estimated to be 64.5 wt % (or 100 mol %) because of the simultaneous production of formic acid [107]. Generally, low LA yields are obtained (less than or equal to two thirds of theoretical value) due to the formation of humins (solid black

residue) which are condensation products and the by-product furfural produced from the decomposition of C5-sugars.

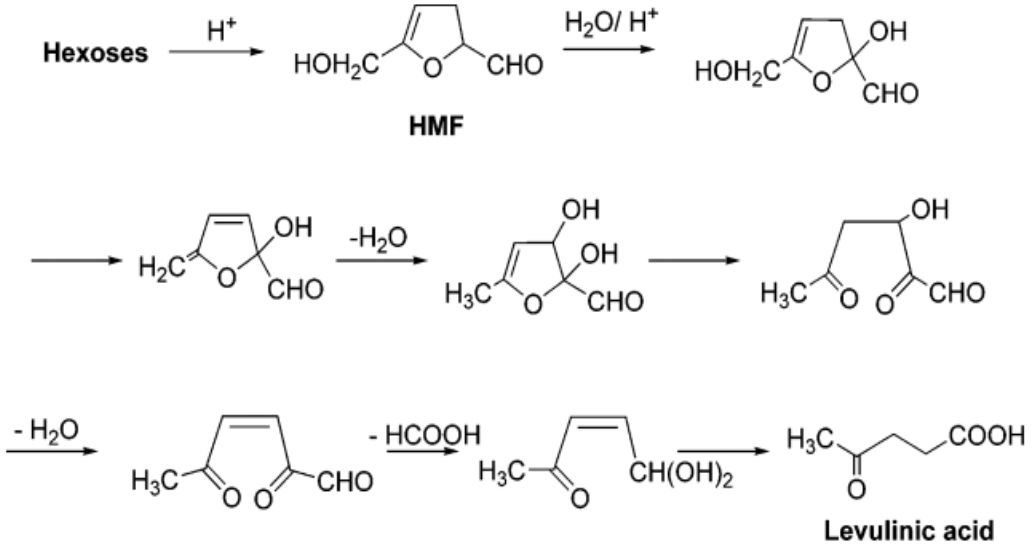


**Scheme 1.2.** Pathway for conversion of hexose to LA.

Levulinic acid is produced industrially from agricultural wastes and wood processing containing cellulose or hemicellulose (up to 75%) by their acid treatment [108]. Initially these feedstocks are treated with strong acids (HCl and $H_2SO_4$) at atmospheric pressures around 100 °C. This hydrolyses the polymeric sugars to monomers. The resulting hydrolysate is boiled in dilute HCl solution for 20-48 h. After reaction, the solid (humic acids) are separated by filtration and the liquid concentrate is used for LA extraction. It is extracted with organic solvents like ethyl acetate, ethers or is separated through distillation [108]. 40% LA yield with respect to hexose content is obtained. Performing reactions at higher temperatures and under pressures leads to a considerable gain of time [109]. BioMetics Inc. has developed a continuous process (Biorefine process) for the production of LA from cellulosic feedstocks like agricultural residues and wood wastes [110]. In this process carbohydrate containing material is continuously supplied to the first reactor where it is hydrolyzed at 215°C and 31 bar in the presence of 2-5 wt% of $H_2SO_4$ for 15 s. The HMF produced from the first reactor is continuously removed and fed into a second reactor operating at a temperature of 193 °C, 14.6 bar pressure for 12 min, finally yielding 60-70 % (of theoretical yields) of LA. The process has progressed through a pilot plant and is close to becoming a commercial reality.

Further sections give the general introduction of the heterogeneous catalysts viz. mesoporous materials, clays, zeolites and rare earth phosphates (lanthanide phosphates) which are used for dehydration reactions.

## 1.6. Mesoporous materials

Porous solids find applications in adsorption (for separation), ion exchange and catalysis. Zeolites which are microporous (pore diameter < 20 Å) crystalline aluminosilicates, are the most widely used catalysts in industry. However their use in different applications is limited to a maximum pore size of 13 Å [111]. Important industrial applications like treating heavy feeds, separation and selective synthesis of large molecules demanded expansion of the pore sizes of zeolites from micropore to mesopore region. Mesoporous materials (pore diameters between 20 and 500 Å) were therefore a welcome addition to classical zeolites. In 1990, Kuroda *et al* first reported the synthesis of mesoporous silica (FSM-16, Folded sheet materials) having uniform pore size using layered polysilicate kanemite as a template [112]. A significant breakthrough in the research of mesoporous materials was witnessed when Mobil scientists discovered the M41S family of silicate/aluminosilicate mesoporous molecular sieves with exceptionally large uniform pore structures which has resulted in a worldwide renaissance in this area [113].

### 1.6.1. M41S and SBA-15

M41S family of mesoporous materials are characterized by a regular array of pores, in the 20–100 Å range, with uniform diameter, high specific surface area and pore volume, which are advantageous for the adsorption and catalytic conversion of bulky molecules. Three different mesophases in this family have been identified, i.e. lamellar (MCM-50) [114] hexagonal (MCM-41) [115] and cubic phases (MCM-48) [116]. Amongst them, MCM-41 has been investigated extensively owing to simple synthesis protocols and because the other members in this family are either thermally unstable or difficult to obtain. MCM-41 possess honeycomb arrays of nonintersecting uniformly sized channels with diameters ranging from 15 to 100 Å depending on the template used, the addition of auxiliary organics and the synthesis parameters. Later in addition to cationic amphiphiles, neutral block copolymers were employed as templating agents to produce well-ordered hexagonal array of mesopores. Using this approach Stucky and coworkers synthesized SBA-15 from poly(ethylene oxide)–

poly(propylene oxide)–poly(ethylene oxide) (PEO–PPO–PEO) triblock copolymer (called as P123) in acidic media [117]. This synthesis strategy gave mesoporous materials with higher pore diameters (30-300Å for SBA-15 compared to 20-100 Å for MCM-41) and enhanced wall thickness leading to improved hydrothermal stability [118]. Thus, SBA-15 has emerged as a better candidate than MCM-41 offering new opportunities for applications in catalysis and advanced composite materials.

### 1.6.2. Mechanism of the formation of mesoporous materials

Two synthesis mechanisms were proposed by Mobil researchers [119]. In the first route, the cationic surfactant species organize into lyotropic liquid crystal phase, which can serve as template for the formation of hexagonal structure. Surfactant micelles aggregate into hexagonal array of rods, followed by the interaction of silicate anions present in the reaction mixture with the cationic head groups of the surfactant species. The condensation of the silicate species further leads to the formation of an inorganic polymeric species. The template is removed by calcination to get hexagonally arranged inorganic hollow cylinders (Scheme 1.3).

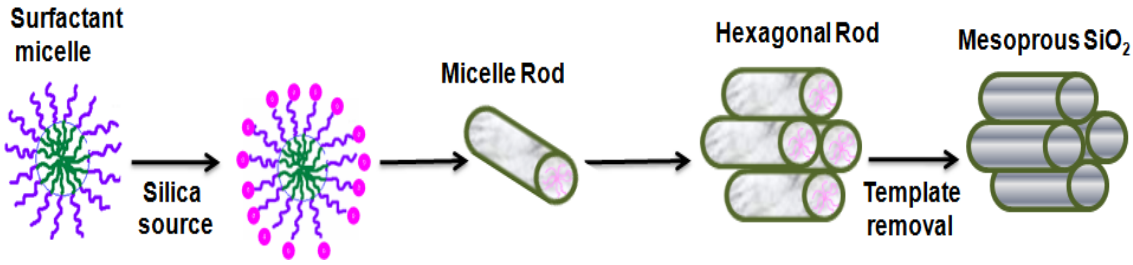


**Scheme 1.3.** Mechanism of formation of mesoporous materials.

In the second route, the hexagonal ordering is assumed to be initiated by the presence of silicate species in the reaction mixture. Chen *et al* [120] proposed that randomly distributed surfactant micelles interact with silicate oligomers by columbic interactions which results in randomly oriented surfactant micelles surrounded by two or three silica monolayers. These species spontaneously pack into a highly ordered mesoporous phase with an energetically favorable hexagonal arrangement, accompanied by silicate condensation. Further condensation between silicate species on adjacent rods occurs on heating and the inorganic wall continues to condense to form the stable hexagonal network. Some other mechanisms for the formation of

mesoporous silica like charge density matching, folded sheet mechanism and silicatropic liquid crystal models have also been proposed.

### 1.6.3. Mechanism of the formation of SBA-15

Monnier *et al* [121] and Tanev [122] showed that the assembly of mesoporous materials can also be driven by hydrogen bonds in the case of neutral templates such as nonionic poly (ethylene oxide) (PEO) surfactants and inorganic precursors. The assembly of the mesoporous silica organized by non-ionic alkyl-ethylene oxide (alkene oxide) triblock copolymer species in acid media occurs through an $(S^0H^+)$ $(X^-I^+)$ path way. First, alkoxysilane species are hydrolysed at a pH less than 2.

$$Si(OEt)_4 + nH_3O^+ \xrightarrow[pH<2]{Hydrolysis} Si(OEt)_{4-n}(OH_2^+)_n$$

This is followed by partial oligomerization of the silica. The EO moieties of the surfactant in strong acid media associating with hydronium ions

$$REO_m + yHX \xrightarrow{H_2O} REO_{m-y}[(EO)H_3O^+]_y + yX^-$$

Where, R = alkyl, poly (propylene oxide) and $X^- = Cl^-, I^-, Br^-, NO_3^-, H_ySO_4^{-2+y}$, $H_yPO_4^{-3+y}$

According to the mechanism proposed by Zhao *et al* [118], formation of SBA-15 proceeds through a scheme where the silica source is first hydrolyzed at low pH to form $Si(OMe)_{4-n}(OH_2^+)_n$ species. The PEO moieties of the block copolymer combine with hydronium ions. Then, the charged cationic silica species and PEO units congregate through $Cl^-$, by a combination of hydrogen bonding, Vander Waals and electrostatic interactions to form $REO^{m-y}[(EOH_3O^+]y\ldots yX^-\ldots I^+$, which can be designated as $(S^0H^+)(X^-I^+)$. Coordination sphere expansion around Si by anion coordination of the form $X^-Si^-OH_2^+$ may play a vital role. Further condensation of the silica species and the organization of the surfactant and inorganic species leads to the formation of silica-surfactant mesophase structure with the lowest energy, allowed by the solidifying inorganic network. Furthermore, the time required for silica mesopore precipitation depends on the acid anion and is found to be the least in the presence of $Cl^-$ when used in the form of HCl. It was exhibited that the EO-length determines the

silica mesostructure and wall thickness of the material. The hydrophobic PO unit affects the pore diameter and its length influences the templating ability as a longer PO-block results in more highly ordered domains and better defined particles.

### 1.6.4. Aluminium substituted mesoporous molecular sieves

Ion-exchange, catalytic and adsorptive properties of molecular sieve materials originate from acid sites which arise from the presence of accessible hydroxyl groups associated with tetrahedral framework aluminium in a silica matrix [123]. Purely siliceous molecular sieve materials have an electrically neutral framework and consequently no acid sites. Hence, substantial efforts were made for the introduction of Al into silica frameworks. For Al incorporation in siliceous framework, 'direct synthesis' methods are employed in which an aluminium precursor is taken into the synthesis gel prior to hydrothermal synthesis. This method often demands specific synthesis conditions depending on the required structures of the materials and Al insertion in the silica matrix produces inferior ordered materials.

SBA-15 is a purely siliceous phase synthesized in strong acidic media (2 M HCl solution). Since most of the aluminium sources dissolve in strong acids, precipitation to incorporate framework aluminium into silica matrix by direct synthesis seems improbable. Researchers have demonstrated incorporation of Al into siliceous materials using post-synthesis modifications by grafting Al onto SBA-15 wall surfaces with anhydrous aluminium isopropoxide, anhydrous $AlCl_3$ or with sodium aluminate in aqueous solution followed by calcination [124]. The materials produced via these post-synthesis procedures have superior structural integrity, acidity and catalytic activity compared to the ones prepared by direct synthesis.

Aluminium incorporated molecular sieves, AlSBA-15 in particular, have been shown to catalyze numerous organic transformations such as acylation, alkylation, oxidative ring opening and cracking, hydrodesulfurization, with high activity and selectivity [125, 126]. They are also used as supports for metal oxides and complexes and used in many organic transformations [127]. Fine tuning of the acidity makes them more versatile in catalytic applications.

## 1.7. Clays

Clay has always played a dominant role in human life. Interesting and wide-ranging properties like geochemical purity, easy access, high resistance to

atmospheric conditions and low price make them attractive materials. Clay minerals are the basic constituents of clay raw materials which consists of sheets (hence the terms phyllosilicates or sheet silicates) firmly arranged in structural layers. Each layer is made of two, three or four sheets. The sheets are composed of $SiO_4^-$ tetrahedrons (abbreviated as T) or $[XO_3(OH)_3]^{6-}$ octahedron (abbreviated as O) where X = Al, Mg or Fe. The interior of octahedra and terahedra contains smaller metal cations. The apex of these cations is occupied by oxygens which are further connected with protons (as OH). All these fundamental structural elements assemble to form a hexagonal network in each sheet [128].

Many properties of clays such as sorption, ion exchange and medicinal properties have been exploited from its genesis, but its utility for catalytic applications was explored only in the $20^{th}$ century. Presently clay is an essential material with varied applications in oil drilling, ceramics, metal and paper industry and liners for waste disposal [129]. It is additionally used as decoloration agent, for ion exchange, as adsorbent and as catalyst [130].

### 1.7.1. Origin of clays

Clays are formed by three principle processes which are the outcome of alterations that occur during geochemical cycle including soil formation or weathering. These processes are: (a) detrital inheritance (specifically for soil), where clay minerals are inherited from pre-existing parent or weathered rock. Such clays are extremely complex and diverse in nature. They possess the characteristic feature of parent material along with properties induced during the weathering; (b) trans-formation, where the original silicate structure of the clay mineral is restored but there are significant changes in the interlayer region e.g. illite-vermiculite-smectite and (c) neoformation, where the clays are formed through crystallization of solutions or gels. The formation of clay minerals through this process is dependent on physicochemical conditions during weathering, such as concentration/composition of the soil solutions, nature of the starting material, pH, temperature, rainfall and percolation rate. Montmorillonite and kaoline are classical products of such clays [131].

### 1.7.2. Montmorillonite clay

Montmorillonite is the most widely used smectite clay which belongs to TOT type (dioctahedral) clays. The structure of montmorillonite K-10 is shown in Fig. 1.9,

which represents schematic representation of crystal lattice of montmorillonite. They have an octahedral aluminate layer sandwiched between two tetrahedral silicate layers (TOT or 2:1 layer) [132]. The layers contain $Fe^{3+}$ and $Mg^{2+}$, which are present in small amounts as impurities. The interstitial cations such as $Na^{+}$, $K^{+}$ and $Ca^{2+}$ are too large to be accommodated in the interior of the crystal and are trapped as freely moving ions between negatively charged planes. These charge compensating cations on the layer surfaces can be easily replaced by other cations when available in solution and hence they are called exchangeable cations and the process is referred to as ion exchange. The concentration of these cations expressed in milli equivalents per 100 gram of dry clay, is called CEC (cation exchange capacity). Natural montmorillonite has limited acid catalytic activity. Acid treatment can increase this activity many folds [133]. The labile proton is a great source of Brönsted acidity and the presence of $Al^{3+}$ and $Fe^{3+}$ act as Lewis centers. A wide variety of acid treated montmorillonite clays are manufactured by Sud Chemie AG such as montmorillonite K5, K10, K20, K30, KSF, KSFO etc. which are prepared from naturally occurring clay. Researchers have tremendously exploited them as solid acid catalysts for numerous reactions. An excellent review by Adams summarises the interesting properties and potential applications of acid treated clays [134].

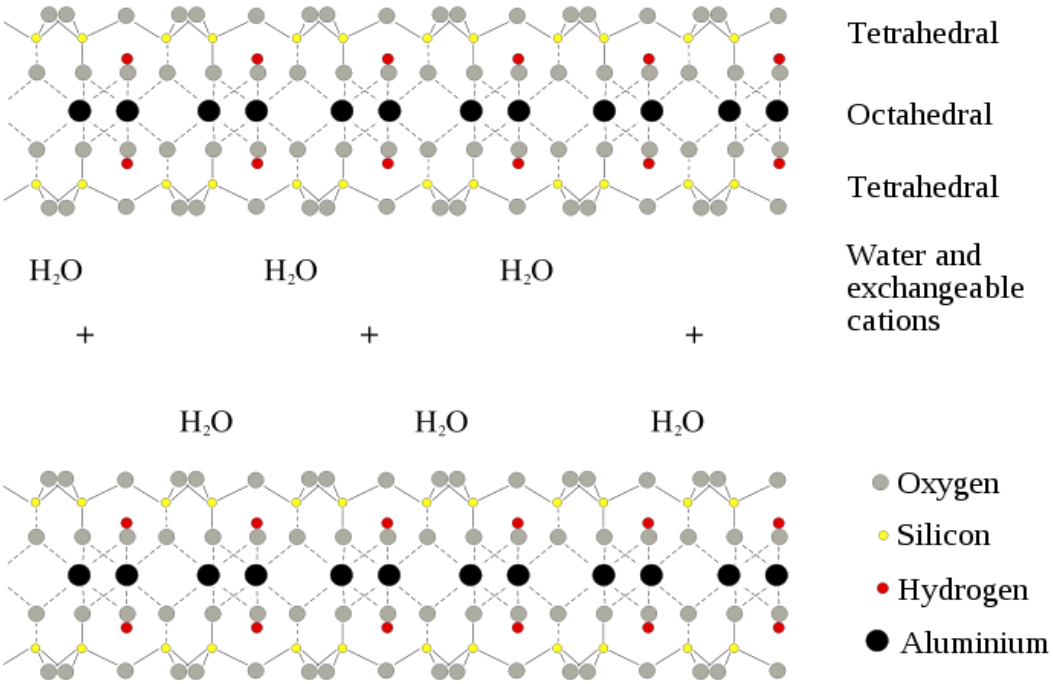


**Fig. 1.9.** Structure of montmorillonite clay.

### 1.7.3. Aluminium pillared clay

When the oil industry faced problems concerning processing of heavy fractions of crude oil components, research was initiated towards development of catalysts with relatively large pore sizes, and with good thermal/hydrothermal stability. This spurred interest in the concept of pillared clays. The concept of intercalation in clays was demonstrated by McLeod and Barrer in 1955 [135]. Inorganic hydrated polyoxocations are used as pillaring agents which leads to basal expansion (upto 20 Å), improved thermal stability (upto 500 °C) and enhanced specific surface area (upto 500 $m^2/g$). Until now most of the research on pillared clays has been focused mostly on the $Al_{13}$ polyoxocation $[AlO_4Al_{12}(OH)_{24}(H_2O)_{12}]^{7+}$ as a pillaring agent. This polyoxocation is prepared by a reported method [136], which is mixed with dilute clay suspension followed by careful washing. It was found that these $Al_{13}$ cations exchange with the interlayer cation, as shown by Sterte and Otterstedt [137]. Apart from the above mentioned properties of the pillared clays, the presence of surface acidity in them makes them an efficient candidate for various catalytic applications. Pillared clays possess both Brönsted and Lewis acidity arising from surface hydroxyl groups and metal oxide pillars respectively. The amount and strength of the acidity can be fine tuned by changing the parent clay material and the metal oxide pillars. This property widens the scope of the pillared clays for variety of acid catalyzed organic transformation. Different types of reactions have been studied using pillared clays like dehydration, esterification, alkylation, disproportionation hydroisomerisation, dehydrogenation, hydrogenation and aromatization [138-140]. The contribution of pillared clays towards the synthesis of chemicals and fine chemicals remains outstanding.

## 1.8. Zeolites

Zeolites are crystalline microporous aluminosilicates possessing highly ordered structures either of natural or synthetic origin [141]. They contain tetrahedral of $SiO_4$ and $AlO_4^-$ that are connected through shared oxygen atoms resulting into a three dimensional network of channels and in few cases cavities. The presence of trivalent Al atoms in the framework renders it excess negative charge which is compensated by the cations which are mostly exchanged alkali metal ions present in the intrazeolitic channels along with adsorbed water molecules. These alkali metal cations can in turn be exchanged for protons. Thus, the Si/Al molar ratio corroborate

to the acid sites in the zeolites. Thus the interior of the pores turns to active surface of zeolites. This inner pore structure is dependent on the type of zeolite/cations and its composition. The crystallographic unit cell of the zeolites may be represented as:

$$\mathbf{M_{y/n}\,[(SiO_2)_x(AlO_2)_y].zH_2O}$$

where, M is a charge compensating cation with valency 'n'. The ratio x/y can have the value 1 to ∞. The 'z' denotes the number of water molecules, which can be reversibly adsorbed/desorbed in the zeolite pores. The structure of zeolites render them with excellent properties like high surface area and adsorption properties, active acid sites, shape selectivity due to uniform pores and channels, good hydrothermal/thermal stability and ease of regeneration. These properties make them potential candidates for gas separation, ion exchange, as adsorbents, detergent builders and catalysis especially in oil refining, petrochemical sector and production of fine and specialty chemicals [142].

### 1.8.1. Nomenclature

Although, there is no systematic nomenclature for molecular sieve materials, the structure commission of International zeolite association (IZA) and IUPAC have assigned a three capital alphabets as structural codes to synthetic and natural zeolites [143,144]. These three capital letters have been used to identify structure types (Table 1.2). The codes for zeolite identification have generally been derived from the names of the type of species, and do not include numbers and characters other than roman letters. Structure type codes are independent of chemical composition, distribution of various possible T atoms, (e.g. $Si^{4+}$, $Ti^{4+}$, $Al^{3+}$ etc.), cell dimensions or crystal symmetry.

**Table 1.2.** Some common structural codes of zeolites.

| Structure Code | Zeolite |
|---|---|
| FAU | Faujasite: X and Y |
| MFI | Mobil Five: ZSM-5 |
| MEL | Mobil Eleven: ZSM-11 |
| MOR | Mordenite |
| FER | Ferrierite |
| BEA | Beta |

### 1.8.2. Classification

Various attempts have been made to classify the families of zeolites on the basis of their crystal structure, chemical composition, effective pore diameter and natural occurrence which are discussed in the further sections.

#### 1.8.2.1. Nature of secondary building units

Fischer, Breck and Smith [145-147] categorized zeolites on the basis of differences in the secondary building units (SBU). The SBU's are the aluminosilicate oligomers having ring, chain and cage like structures, which are basic building units of zeolite framework structure. The different SBU's are pictorially presented in Fig.1.10. These SBU's unite in different combination to form zeolite structures. All known zeolitic structures can be synthesized using the SBU's mentioned here.

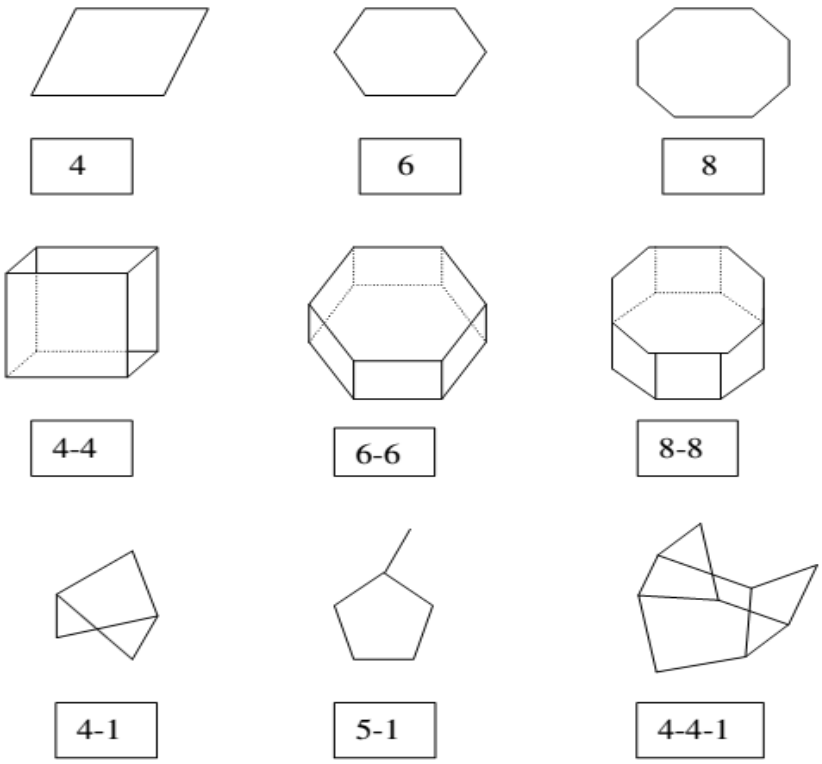


**Fig. 1.10.** Secondary building units (SBU) in zeolite synthesis.

#### 1.8.2.2. Chemical composition

Flanigen categorized zeolites using their chemical composition [148]. Depending on Si/Al ratio, zeolites are classified as low silica, intermediate silica, high silica and pure silica zeolites (silicalites) (Table 1.3).

**Table 1.3:** Classification of zeolites on the basis of chemical composition.

| Type | Si/Al ratios | Examples |
|---|---|---|
| Low silica | 1.0 to 1.5 | Sodalite, A, X |
| Intermediate silica | 2 to 5 | L, Mordenite, Omega, FAU |
| High silica | 5 to thousands | ZSM-5, EU-1 |
| Silicate (all silica) | ∞ | Silicate-1, Silicate-2 |

#### 1.8.2.3. Pore size

Zeolites have also been classified according to their pore diameter. The pore diameter of the zeolite depends upon the number of tetrahedra present in the ring aperture. On the basis of pore openings, zeolites are commonly classified into small pore (6 or 8-member ring), medium pore (10-member ring), large pore (12-member ring) [149]. Table 1.4 illustrates the examples on the basis of pore size classification.

**Table 1.4:** Classification of zeolites on the basis of pore size.

| **Small Pore (8 MR)** | **Medium Pore (10 MR)** | **Large pore (12 MR)** |
|---|---|---|
| MTN | Ferrierite (FER) | Cancrinite |
| NU-1 | ZSM-5 (MFI) | Linde X,Y, L. |
| Chabazite | ZSM-11(MEL) | Mazzite |
| Erionite | EU-1 (ZSM-50) | Mordenite |
| Clinoptillolite | Stilbite | Offretite |
| ZK-5 | ZSM-23 | ZSM-12 (MTW) |
| Linde A | Theta-1 (ZSM-22) | Omega |
| Rho | ZSM-48 (EU-2) | Beta (BEA) |

MR-Membered ring

### 1.8.3. Beta zeolite

The beta (BEA-type) zeolite possesses a three dimensional network of 12-membered rings. It has two comparable straight channels in a and b directions (0.76 X 0.64 nm) and one sinusoidal channel in the c direction (0.55 X 0.55 nm) [144]. The interconnection of these channels forms the three-dimensional pore structure with high accessibility, as also suggested by the fully exchangeable charge compensating cations. Zeolite beta is devoid of supercages, but at the intersections of the channels the large empty spaces have a diameter of ca. 1.2 nm which can accommodate large

molecules that would not necessarily diffuse through the micropores. The intriguing structural and chemical properties of zeolite beta make it an important material in diverse acid-catalyzed reactions. This zeolite was first prepared by Wadlinger *et al* in 1967 [150]. Zeolite beta is obtained as a high-silica material with crystallite sizes in the nanometer range. The typical Si/Al ratio of synthetic zeolite beta is in the range of 12 to 30 [151]. Zeolite beta is built from an intergrown structure of two or three types of polymorphs: polymorph A (***BEA**, $P4_122$, a = 12.632 Å and c = 26.186 Å), polymorph B (C2/c, a = 17.896 Å, b = 17.920 Å, c = 14.328 Å, and β = 114.8°) and polymorph C (BEC, $P4_2/mmc$, a = 12.769 Å and c = 12.977 Å) [152]. The different polymorphs are built from different stacking of the same building layer (Fig.1.11). The stacking results into highly faulty materials.

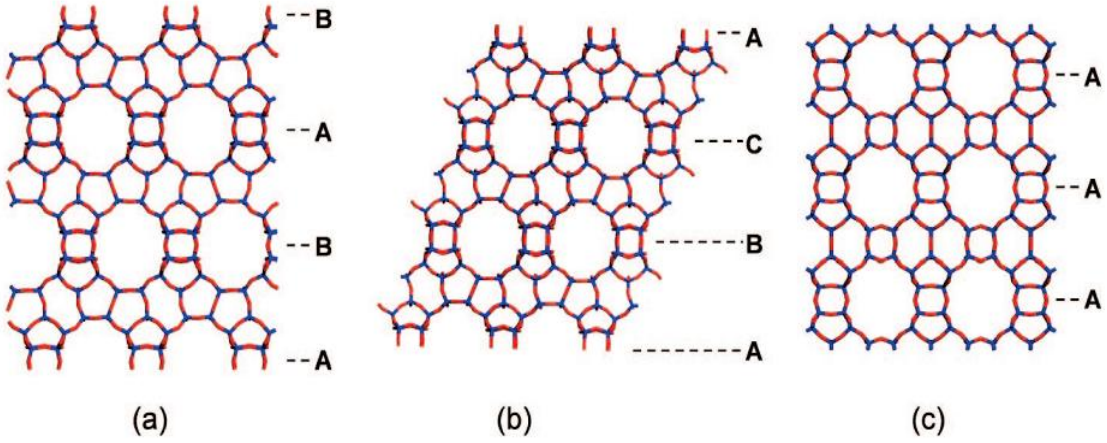


**Fig 1.11.** Framework structures of (a) Polymorph A , (b) Polymorph B and (c) Polymorph C of zeolite beta, showing the different stackings of the 12-ring pores as (a) ABAB. ., (b) ABCABC. . ., and (c) AA. . ..

### 1.8.4. Dealumination of beta zeolite

Beta zeolite is an interesting material owing to its high acidity and peculiar pore system. The acidity in zeolites is associated with the coordination of Al atoms. The aluminium coordination in zeolites is tetrahedral which are the source of Brönsted acidity and the presence of $Al^{3+}$ serves as Lewis acid centers [153]. Researchers have demonstrated the presence of octahedrally coordinated aluminium partly attached to beta framework. The flexibility of Al coordination in zeolites can be used for the fine tuning of the acidity which widens its scope as acid catalyst. This aroused interest in structural modification of the zeolite by the post synthesis modifications like dealumination which gave high silica zeolites with enhanced thermal/hydrothermal stability.

Dealumination is a process of removal of framework aluminium without destroying the micropore structure. The framework aluminium can be removed by hydrolysis of Al-O-Si bonds. Several methods like acid leaching combined with steaming, complexation of aluminium by oxalic acid, replacing aluminium by silicon by treating it with gaseous silicon tetrachloride are employed for removal of framework aluminium [154]. As a result of modification a secondary pore system is generated that comprises of mesopores which aids diffusion in the zeolite micropores by reducing diffusion paths. Dealumination causes an uncontrolled loss of framework Al cations leading to a decrease in the number of active acid sites. By varying the extent of dealumination the acidity in the materials can be controlled. The resulting high silica materials have increased hydrophobicity and finds important industrial applications.

## 1.9. Nanomaterials

Being dominated by interfaces and surfaces the nanomaterials often exhibit astonishing electronic, physical, mechanical and catalytic properties. Nanomaterials are materials with structured components having at least one dimension < 100 nm. They can be categorized as two dimensional nanoscale materials like nanorods, nanowires and nanotubes and three dimensional nanoscale materials like colloids, quantum dots and precipitates. Nanocrystalline materials composing of nanometer-sized grains are inculcated in this category [155]. In catalysis, the adsorption-desorption is surface oriented; there is a need to increase the numbers of sites by enhancing the surface area which is attained by reducing the particle size. This decrease in particle size results into higher surface area-to volume ratios and alters the intrinsic catalytic performance. This has important implications for chemical reactions. Hence, the goal is to learn the preparation and designing of catalysts with the most effective size and structure.

### 1.9.1. Rare earth phosphate as nanocrystalline materials

The lanthanide phosphate ($LnPO_4$) nanomaterials are most important from academic and industrial point of view due to their unique properties. Rare earth orthophosphates possess a variety of potentially beneficial properties such as high thermal stability (~ 2300 °C) [156], low solubility in water ($K_{sp} = 10^{-25}$ to $10^{-27}$) [157], a high refractive index (n=1.5), a high concentration of lasing ions (~$1.8X10^{21}$ ions

$cm^{-3}$) [158] and acidity [159]. Rare earth compounds have been extensively used in high performance luminescent devices, magnets, lasing materials, ceramics, proton conductors, moisture sensors, heat resistant materials, host for radioactive wastes, green phosphor in fluorescent lamps, scintillators for X-ray and γ-ray detection in medical science, biochemical probes and medical diagnostics [160]. Besides this, rare earth phosphates showed catalytic activity in various reactions; some are decomposition of $CF_4$, NO decomposition, highly enantioselective Diels-Alder reaction and oxidative dehydrogenation of isobutane to isobutene [161-164].

### 1.9.2. Crystal structure and the possible growth mechanism of $LnPO_4$

The properties of lanthanide compounds depend strongly on their composition and structure, which are sensitive to the bonding states of Ln ions. If lanthanide compounds are fabricated in the form of 1D nanostructure (e.g. nanorods/nanowires) with a different crystal structure, they would have new functionalities as a result of their marked specific shape. This embarked the synthesis of $LnPO_4$ (Ln = La to Dy) nanorods/nanowires (exhibiting anisotropic growth) having a hexagonal crystal structure. These $LnPO_4$ materials were synthesized using different materials such as wet chemical precipitation, sol-gel, hydrothermal or high temperature solid state reactions [165]. The final physico-chemical properties arise from the synthesis route adopted. By far the wet chemical precipitation (solution precipitation) method is the most widely used and economical method for the synthesis of these nanomaterials.

To date, the shape of metal nanoparticles or semiconductor nanocrystals has mainly been controlled by the presence of polymers, surfactants or strong chelating ligands. Peng *et al* presented a three-stage shape evolution mechanism based on the spherical diffusion controlled crystal growth theory for elucidation of the shape evolution of CdSe nanocrystals [166,167]. The theory explains the mechanism of the formation of nanorods/nanowires. The aspect ratios and length of nanorods or nanowires is strongly dependent on the pH. The pH influences the concentration of $[PO_4^{3-}]$ and $[Ln^{3+}]$ in the solution. It was inferred that by controlling the pH the apt concentration of solute ions can be maintained at the required stage which drives the one dimensional growth of lanthanide phosphates. Apart from the role of pH another important finding was deduced by Fang *et al* [168] in which they demonstrated the crucial role of anisotropy. Since, these phosphate materials are synthesized by solution phase process, the anisotropic nature of reactant ions (building blocks) affects

the morphology of the final product. This leads to the characteristic one dimensional formation of linear infinite chains of hexagonal structured rare earth or lanthanide phosphates $LnPO_4$ (Ln = La to Dy). They studied the growth mechanism in $CePO_4$ (Fig. 1.11.). In $CePO_4$, each cerous ion is coordinated to eight oxygen atoms, four at distances of 2.34 Å and four at 2.66 Å. The shorter distances are to the corners of four different tetrahedra, linking atoms which are practically coplanar. The longer distances extend to pairs of oxygens forming the edges of two tetrahedral each above and below the plane of the four shorter distances. A given phosphate group is coordinated to six cerous ions, each corner by one short bonding distance and opposite edges by longer bonding distances. The Ce-Ce separation is 4.13 Å. The $PO_4^{3-}$ ion has been taken to be a tetrahedral grouping of oxygens about phosphorus, with the P-O distance fixed at 1.56 Å (Fig. 1.12a). The overall structure of $CePO_4$ may be exhibited as columns built up of alternate $Ce^{3+}$ and $PO_4^{3-}$, extending along the c axis. Each column is linked to four neighboring columns in such a manner that open channels run through the structure along the hexagonal axis (Fig. 1.12b).

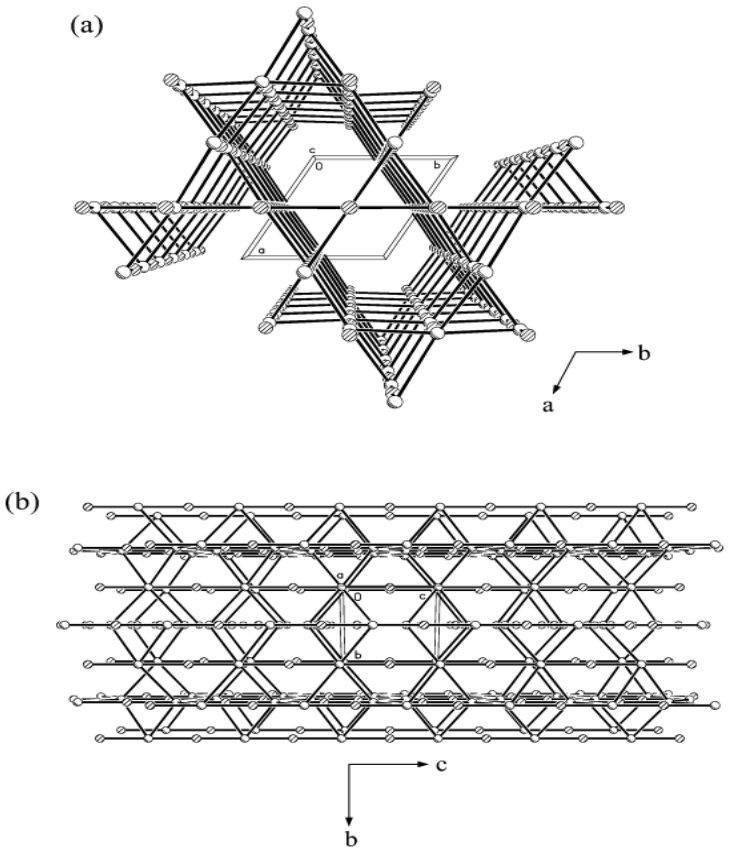


**Fig. 1.12.** (a) Packing view of $CePO_4$ along the 'c' axis. (b) Packing view of $CePO_4$ along the 'a' axis. [Source: Ref. 173].

extending along the ‘c’ axis. Visualized from thermodynamic perspective, the activation energy for the growth of hexagonal $LnPO_4$ along the ‘c’ axis is lower than that of growth perpendicular to the ‘c’ axis [169]. This means higher growth rate along the ‘c’ axis and a lower one perpendicular to the ‘c’ axis to form $LnPO_4$ nanowires/nanorods that grow preferentially along the [001]. Hexagonal $LnPO_4$ (Ln = La, Pr, Nd, Sm, Eu, Gd, Tb and Dy) are isostructural with hexagonal $CePO_4$; therefore, the formation of other $LnPO_4$ nanowires/nanorods can also be explained based on its highly anisotropic character along the ‘c’ axis. It is this structural feature that plays a key role in the highly intrinsic preferential growth along the ‘’c axis of $LnPO_4$ (Ln = La to Dy) nanorods/nanowires.

### 1.10. Scope and objectives of thesis

Conversion of renewable biomass to value added chemicals is an area of current interest. 5-Hydroxymethyl furfural (5-HMF) and levulinic acid (LA) are two important chemicals with great potential which can be obtained from dehydration of carbohydrate biomass. In pursuit of this, the scope and objectives of this thesis are to derive these chemicals from carbohydrates using solid acid catalysts. 5-HMF is synthesized in biphasic medium using Al incorporated SBA-15 (varying Si/Al ratio) and chemically treated clays (K10, K20, K30 and Al pillared clay). Levulinic acid was synthesized using beta zeolite (varying $SiO_2/Al_2O_3$ ratio). In quest of stable catalysts, it was also synthesized in aqueous medium using nanocrystalline rare earth phosphates ($LnPO_4$ where Ln = La-Dy). All the catalyst systems were characterized by various physiochemical techniques and their catalytic properties were investigated. The acidity of each catalyst system was fine tuned and its effect on yield of targeted products was studied. Since this reaction involves reactive reactants/products, it is of utmost importance to envisage the role of acidity. The thesis attempts to furnish insights into the types of acidity required for 5-HMF and LA formation. Factors influencing the activity of these catalysts are investigated.

## 1.11. Organization of the Thesis

The thesis is divided into six chapters. A brief description of the contents of each chapter is given below.

**Chapter 1: Introduction**

Chapter 1 gives a general introduction to heterogeneous catalysis, which includes a brief description of various methods used for the preparation of catalysts reported in the thesis. This chapter presents an introduction to the potential of biomass derived carbohydrates for the production of chemicals. Prime importance is given to dehydration of sugars to 5-HMF; an important platform chemical and LA an important bulk chemical. Their properties and industrial significance are discussed. It also describes the various catalysts used like Al incorporated SBA-15, rare earth phosphates, zeolites and chemically treated clays. A review of the literature to date in these areas is included. Finally, the aim of the thesis is outlined briefly.

**Chapter 2: Catalyst synthesis and experimental techniques for characterization**

Chapter 2 describes the methods of catalyst synthesis and experimental techniques employed for their characterization. The catalysts synthesized were Al incorporated SBA-15, rare earth phosphates ($LaPO_4$-$DyPO_4$), whereas zeolite beta (with different $SiO_2/Al_2O_3$ ratios) and acid treated/pillared clays were commercially procured. They were characterized by various physico-chemical techniques including X-ray diffraction (XRD), $N_2$ sorption, scanning and transmission electron microscopy (SEM & TEM), $^{27}Al/^{29}Si$ nuclear magnetic resonance (NMR), infrared spectroscopy (FTIR), Raman spectroscopy, temperature programmed desorption of ammonia (TPD-$NH_3$), temperature programmed desorption coupled with mass spectrometry (TPD-MS) and IR of pyridine desorbed. Theory and experimental procedures of each of these techniques have been described in this chapter.

**Chapter 3: Synthesis of 5-hydroxymethyl furfural (HMF) in biphasic medium over solid acid catalysts.**

Chapter 3 provides detailed introduction to dehydration of hexose to HMF. This transformation is catalyzed with two types of solid acid catalysts. Therefore, the chapter is divided into two parts: 3A and 3B. Part 3A deals with investigations pertaining to Al incorporated SBA-15 as catalysts for dehydration of fructose to HMF in biphasic medium. It presents the characterization results of AlSBA-15 catalysts

using XRD, SEM and TEM to study their structure and morphology before and after Al incorporation. The results from $^{27}$Al MAS NMR, $NH_3$-TPD, TPD-MS, $N_2$ sorption, etc. are also discussed in detail. The activity of catalysts in dehydration of fructose to HMF and optimization of reaction conditions are also depicted in this part. Part 3B deals with the synthesis of HMF from fructose in biphasic medium using acid treated/pillared clays. It exhibits the characterization results of clay catalyst using XRD, $^{27}$Al MAS NMR, $^{29}$Si NMR, $N_2$ sorption, Pyridine IR etc. and the catalytic activity of the clay for the synthesis of an important platform chemical HMF.

Our investigations show that AlSBA-15 effectively catalyzes the dehydration of fructose to furans due to its mesoporosity and fine tuning of the acidity. The acidity was correlated with HMF yields. The presence of moderately strong acidity is crucial for higher yield/selectivity of HMF. The yield of HMF decreased at higher reaction temperatures, high contact time and with high acidity. The condensation of reactant/product to give soluble oligomers and humins (insoluble organic compounds) is dominant side reaction which leads to decrease in the yields. Leaching of aluminium occurs under hydrothermal conditions, if solvent mixtures containing water are used, while activity can be substantially retained if DMSO is used as solvent.

Among various clay catalysts, the acid treated clays exhibited superior catalytic activity as compared to pillared clays. The HMF yields were correlated with type of acidity. The presence of Brönsted acid sites was found to be crucial for higher yields of HMF. Conclusions were drawn based on the catalytic studies and their correlation with the characterization results, which are given at the end of each section.

**Chapter 4: Synthesis of biomass derived levulinic acid using beta zeolite catalysts**

Chapter 4 provides detailed introduction to LA synthesis from biomass, its rationale and significance. The need of zeolites as catalyst and fine tuning of their acidity is addressed. This chapter is divided into two parts. Part-A describes the characterization of catalysts (with various $SiO_2/Al_2O_3$ ratio) with XRD, SEM, $^{27}$Al MAS NMR, $N_2$ sorption, $NH_3$-TPD, TPD-MS using isopropyl amine etc. Part-B describes catalytic activity of these catalysts for dehydration of sucrose/glucose to LA, a highly important bulk chemical.

Beta zeolite catalysts show superior activity for the dehydration of sugars to LA owing to their appropriate acidity, three dimensional pore structure and smaller crystallite size. Levulinic acid yield increased with the presence of moderately strong acidity. Additionally, a good linear correlation with Brönsted acidity (from TPD-MS) was obtained. This clearly demonstrates that moderately strong to medium Brönsted acid sites are required for LA formation. For the dehydration of carbohydrate to LA, reaction temperature, time, substrate concentration, catalyst weight plays vital role in obtaining higher yield of the acid. Importantly, various mono/di/polysaccharides could be converted to LA. By conducting the reaction in ethanol; ethyl levulinate which is a renewable fuel additive was obtained in good yield and the catalyst could be effectively recycled. Kinetic studies were conducted and activation energy of the reaction was calculated. The characterization results were corroborated with the catalytic performance at the end of chapter.

**Chapter 5: Synthesis of 5-hydroxymethyl furfural and levulinic acid using nanocrystalline rare earth phosphates**

Chapter 5 deals with the synthesis of HMF from fructose in aqueous medium followed by dehydration of various polysaccharides to LA using rare earth phosphates as catalysts. This chapter is also divided into two parts. Part-A describes the synthesis and characterization of $LnPO_4$ catalysts (Ln=La to Dy). Characterization of these materials was carried out using XRD, SEM, TEM, ICP-OES, TEM, $NH_3$-TPD, TPD-MS, $N_2$ sorption, Raman and FTIR. Part-B describes the catalytic activity of these catalysts for dehydration of renewable feed stocks to value added chemicals.

Nanocrystalline $LnPO_4$ (Ln=La-Dy) materials were explored as catalysts for the dehydration reaction. The effect of lanthanide contraction on crystallinity, morphology, acidity and catalytic activity was investigated. Effect of acidity on HMF/LA yield was studied. A linear correlation was obtained for HMF/LA yield with moderate Brönsted acidity. The role of reaction conditions on dehydration/rehydration was also investigated. Catalyst recyclability in drastic hydrothermal reaction conditions was also witnessed. The conclusions drawn from the above studies are included at the end of the chapter.

**Chapter 6: Summary and Conclusions**

This chapter describes the inferences and conclusions drawn upon the investigations conducted with regard to various catalysts in the dehydration of carbohydrate biomass to value added chemicals. Since, it is also mandatory to summarize the work for the benefit of the reader; this chapter summarizes the results of this work while comparing it with reported results. Further, at the end of this chapter, it offers suggestions for further research in these areas.

## 1.12. References


1. S. Green, Industrial Catalysis, Macmillan Company, New York, 1928.
2. J.J Berzelius, Årsberättelsen om framstegi fysik och kemi, Royal Swedish Academy of Sciences, 1835.
3. J.J. Berzelius, Reseanteckningar, P.A. Norstedt & Söner, Stockholm, 1903.
4. B.H. Davis, G. Ertl, H. Knözinger, J. Weitkamp (Eds.), Handbook of Heterogeneous Catalysis, Vol. 1, VCH, Weinheim, 1997.
5. B. Lindstroma, L.J. Petterson, Cat. Tech. 7 (2003) 130.
6. J. Hagen, Industrial Catalysis: A Practical Approach, 2nd ed. VCH, Weinheim, 2006.
7. C.G. Brundtland, Our Common Future, The World Commission on Environmental Development, Oxford University Press, Oxford, 1987.
8. P. Anastas, J.C. Warner, Green Chemistry: Theory and Practice, Oxford University Press, Oxford, 1998.
9. S.L.Y. Tang, R.L. Smith, M. Poliakoff, Green Chem. 7 (2005) 761.
10. D.A. Simonetti, J.A. Dumesic, ChemSusChem 1 (2008) 725.
11. Energy Information Administration (EIA) International Energy Outlook 2007. http://www.eia.doe.gov/oiaf/ieo/index.html
12. D.Y. Goswami, F. Kreith, Handbook of Energy Efficiency and Renewable Energy, CRC Press/Taylor & Francis, Boca Raton, 2007.
13. Intergov. Panel Climate Change (IPCC) 007. http://www.aaas.org/news/press_room/climate_change/media/fourth_spm2feb07.pdf
14. J.C. Ruiz, R.M. West, J.A. Dumesic, Annu. Rev. Chem. Biomol. Eng. 1 (2010) 79.
15. A. Pandey, Hanbook of plant based biofuels, CRC Press/Taylor & Francis, Boca Raton, 2008.
16. R.H. He, P. Ye, B.C. English, J.A. Satrio, Bioresour. Technol. 100 (2009) 5305.
17. Y.Y. Wu, Z.H. Fu, D.L. Yin, Q. Xu, F.L. Liu, C.L. Lu, L.Q. Mao, Green Chem. 12 (2010) 696.

18. H. Roper, C. Vilvoorde, Starke 54 (2002) 89.
19. National Renewable Energy Laboratory, Conceptual biorefinery, 2005 http://www.nrel.gov/biomass/biorefinery.html
20. D.L. Klass, Biomass for Renewable Energy, Fuels and Chemicals, Academic Press, San Diego, 1998.
21. C. Somerville, H. Youngs, C. Taylor, S.C. Davis and S.P. Long, Science 329 (2010) 790.
22. E. Taarning, C.M. Osmundsen, X.B. Yang, B. Voss, S.I. Andersen and C.H. Christensen, Energy Environ. Sci. 4 (2011) 793.
23. W. Boerjan, J. Ralph , M. Baucher, Annu. Rev. Plant Biol. 54 (2003) 519.
24. L. Shuai and X.J. Pan, Research Progress In Paper Industry And Biorefinery ($4^{th}$ Isetpp) 1-3 (2010) 1293.
25. D.M. Alonso, J.Q. Bond, J.A. Dumesic, Green Chem. 12 (2010) 1493.
26. S.S. Chundawat, G.T. Beckham, M.E. Himmel, B.E. Dale, Annu. Rev. Chem. Biomol. Eng. 2 (2011) 121.
27. J.B. Binder, R.T. Raines, J. Am. Chem. Soc. 131 (2009) 1979.
28. C.H. Zhou, X. Xia, C.X. Lin, D.S. Tong, J. Beltramini, Chem. Soc. Rev. 40 (2011) 5588.
29. C.E. Wyman, S.R. Decker, M.E. Himmel, J.W. Brady, C.E. Skopec, L. Viikari, In Polysaccharides, $2^{nd}$ ed., S. Dumitriu, Marcel Dekker (Eds.) New York, 2005.
30. A.C. O'Sullivan, Cellulose 4 (1997) 173.
31. T.A. Hsu, M.R. Ladisch, G.T. Tsao, Chem. Technol. 10 (1980) 315.
32. U.S. Department of Energy, Feedstock Composition Gallery, U.S. Department of Energy, Washington DC, 2005. http://www.eere.energy.gov/biomass/feedstock_glossary.html
33. R.J. Evans, T.A. Milne, M.N. Soltys, J. Anal. Appl. Pyrolysis 9 (1986) 207.
34. E. Adler, Wood Sci. Technol. 11 (1977) 169.
35. Y. Zhao, L. Deng, B. Liao, Y. Fu, Q.X. Guo, Energ. Fuels 24 (2010) 5735.
36. J.P. Lange, Biofuels Bioprod. Bioref. 1 (2007) 39.

37. E. Iglesia, S.C. Reyes, R.J. Madon, S.L. Soled, Adv. Catal. 39 (1993) 221.
38. L. Caldwell, Selectivity in Fischer-Tropsch synthesis: review and recommendations for further work 1980. http://www.fischer-tropsch.org/DOE/DOE_reports/81223596/pb81223596.pdf
39. M.E. Dry, Catal. Today 71 (2002) 227.
40. K. Klier, Adv. Catal. 31 (1982) 243.
41. J.P. Lange, Catal. Today 64 (2001) 3.
42. E.L. Kunke, R.R. Soares, D.A. Simonetti, J.A. Dumesic, Appl. Catal. B 90 (2009) 693.
43. S. Koppatz, C. Pfeifer, R. Rauch, H. Hofbauer, T. Marquard-Moellensted, M. Specht, Fuel Process. Technol. 90 (2009) 914.
44. R.R. Soares, D.A. Simonetti, J.A. Dumesic, Angew. Chem. Int. Ed. 45 (2006) 3982.
45. G.W. Huber, S. Iborra, A. Corma, Chem. Rev. 106 (2006) 4044.
46. C.N. Hamelinck, R.A. Surs, A.P.C. Faaij, Biomass Bioenergy 29 (2005) 114.
47. P.L. Spath, D.C. Dayton, Preliminary screening—technical and economic assessment of synthesis gas to fuels and chemicals with emphasis on the potential for biomass-derived syngas. Rep. NREL/TP-510-34929. U.S. Dep. Energy, Natl. Renew. Energy Lab., 2003. http://www.nrel.gov/docs/fy04osti/34929.pdf
48. D. Mohan, C.U. Pittman, P.H. Steele, Energy Fuels 20 (2006) 848.
49. S.R.A. Kersten, W.P.M. van Swaai, L. Lefferts, K. Seshan, Options for catalysis in the thermochemical conversion of biomass into fuels. In Catalysis for Renewables: From Feedstock to Energy Production, G. Centi, R.A. van Santen (Eds.), Weinheim: Wiley-VCH, 2007.
50. D.C. Elliott, Energy Fuels 21 (2007) 1792.
51. T.R. Carlson, T.P. Vispute, G.W. Huber, ChemSusChem 1(2008) 397.
52. Y. Shun, J. Cheng, Bioresour. Technol. 83 (2002) 1.

53. N. Mosiera, C. Wyman, B. Dale, R. Elander, Y.Y. Lee, Bioresour. Technol. 96 (2005) 673.
54. P. Kumar, D.M. Barrett, M.J. Delwiche, P. Stroeve, Ind. Eng. Chem. Res. 48 (2009) 3713.
55. A. Carroll, C. Somerville, Annu. Rev. Plant Biol. 60 (2009) 165
56. S. Lima, M.M. Antunes, M. Pillinger, A.A. Valente, ChemCatChem. 3 (2011) 1686.
57. T. Stahlberg, W.J. Fu, J.M. Woodley, ChemSusChem. 4 (2011) 451.
58. M.E. Zakrzewska, E. Bogel-Lukasik, R. Bogel-Lukasik, Chem.Rev. 111(2) (2011) 397.
59. X.H. Qi, M. Watanabe, T.M. Aida, R.L. Smith, Bioresour.Technol. 109 (2012) 224.
60. F.W. Lichtenthaler, InMethods and Reagents for Green Chemistry: An Introduction, P. Tundo, A. Perosa, F. Zecchini (Eds.), John Wiley & Sons, Inc., New York, 2007.
61. A. Boisen, T.B. Christensen, W. Fu, Y.Y. Gorbanev, T.S. Hansen, J.S. Jensen, S.K. Klitgaard, S. Pedersen, A. Riisager, T. Ståhlberg, J.M. Woodley, Chem. Eng. Res. Des. (2009) 1318.
62. M.E. Zakrzewska, E.B. Lukasik, R.B. Lukasik, Chem. Rev. 111 (2011) 397-417.
63. J.N. Cheda, G.W. Huber, J.A. Dumesic. Angew. Chem. Int. Ed. 46 (2007) 7164.
64. M.J. Climent, A. Corma, S. Iborra, Green Chem. 13 (2011) 520.
65. R.M. West, E.L. Kunkes, D.A. Simonetti, J.A. Dumesic, Catal. Today 147 (2009) 115.
66. N. Yan, C. Zhao, C. Luo, P.J. Dyson, H.C. Liu, Y. Kou, J. Am. Chem. Soc. 128 (2006) 8714.
67. C. Luo, S.A. Wang, H.C. Liu, Angew. Chem. 119 (2007) 7780.
68. L. Hu, G. Zhao, W. Hao, X. Tang, Y. Sun, L. Lin, S. Liu, RSC Adv. 2 (2012) 11184.
69. X. Tong, Y. Ma, Y. Li, Appl. Catal. A. 385 (2010) 1.
70. S. Okino, R. Noburyu, M. Suda, T. Jojima, M. Inui, H. Yukawa, Appl. Microbiol. Biotechnol. 81 (2008) 459.

71. M.S. Holm, S. Saravanamurugan, E. Taarning, Science 328 (2010) 602.
72. T. Werpy, G. Petersen, "Top Value Added Chemicals from Biomass: Vol. 1-Results of Screening for Potential Candidates from Sugars and Synthesis Gas", Report No. NREL/TP-510-35523; National Renewable Energy Laboratory, Golden, CO, 2004. http://www.osti.gov/bridge.
73. A. Corma, S. Iborra, A. Velty, Chem. Rev. 107 (2007) 2411.
74. G. Dull, Chem. Ztg. 19 (1895) 216.
75. J. Kiermayer, Chem. Ztg. 19 (1895) 1003.
76. R.J. Ulbricht, S.J. Northup, J.A. Thomas, Fund. Appl. Toxicol. 4 (1984) 843.
77. M. Murkovic, N. Pichler, Mol. Nutr. Food Res. 50 (2006) 842.
78. J.A. Rufi´ an-Henares, C. Delgado-Andrade, F.J. Morales, J. Cereal Sci. 43 (2006) 63.
79. R.L. Prior, X. Wu, L. Gu, J. Agric. Food Chem. 54 (2006) 3744.
80. T. Husoy, M. Haugen, M. Murkovic, D. Jobstl, L.H. Stolen, T. Bjellaas, C. Ronningborg, H. Glatt and J. Alexander, Food Chem. Toxicol. 46 (2008) 3697.
81. C. Janzowski, V. Glaab, E. Samimi, J. Schlatter, G. Eisenbrand, Food Chem. Toxicol. 38 (2000) 801.
82. A.A. Rosatella, S.P. Simeonov, R.F. Frade, C.A. Afonso, Green Chem. 13 (2011) 754.
83. S.E. Davis, L. Houk, E.C. Tamargo, A.K. Datye, R.J. Davis, Catal. Today 160 (2011) 55.
84. N.K. Gupta, S. Nishimura, A. Takagaki, K. Ebitani, Green Chem. 13 (2011) 824.
85. R. Alamillo, M. Tucker, M. Chia, Y.P. Torres, J.A. Dumesic, Green Chem. 14 (2014) 1413.
86. Y. Leshkov, C.J. Barett, Z.Y. Liu, J.A. Dumesic, Nature 447 (2007) 982.
87. B. Girisuta, L.P. Janssen, H.J. Heeres, Green Chem. 8 (2006) 701.
88. M. Chia, J.A. Dumesic, Chem. Commun. 47 (2011) 12233.

89. A. Gandini, M.N. Belcacem, Prog. Polym. Sci. 22 (1997) 1203.
90. H. Koch, F. Krause, R. Steffan, H.U. Woelk, Starke 35 (1983) 304.
91. W.N. Haworth, W.G.M. Jones, J. Chem. Soc. (1944) 667.
92. H.E. Van Dam, A.P.G. Kieboom, H. Van Bekkum, Starch-Starke 38 (1986) 95.
93. M.J. Antal, W.S.L. Mok, G.N. Richards, Carbohydr. Res. 199 (1990) 91.
94. B.F.M. Kuster, Starch-Starke 42 (1990) 314.
95. L. Cottier, G. Descotes, Trends Heterocycl. Chem. 2 (1991) 233.
96. B. V. Timokhin, V. A. Baransky, G.D. Eliseeva, Russ. Chem. Rev. 68 (1) (1999) 73.
97. R. H. Leonard, Ind. Eng. Chem. 48 (8) (1956) 1330.
98. P.D. Bloom, US Patent 20100216915 (2010).
99. W. E. Erner, US patent 4364743 (1982).
100. R.E. Holmen, US patent 3471554 (1969).
101. C. Fumagalli, Succinic acid and succinic anhydride. In Kirk-Othmer Encyclopedia of Chemical Technology, 4th ed., J. Kroschwitz, M. Home-Grant (Eds.), John Wiley and Sons, New York, 22 (1997) 1074.
102. A.P. Dunlop, J.W. Madden, US patent 2786852 (1957).
103. J.J. Bozell, L. Moens, D.C. Elliott, Y. Wang, G.G. Neuenscwander, S.W. Fitzpatrick, R.J. Bilski, J.L. Jarnefeld, Resour. Conserv. Recycl. 28 (2000) 227.
104. V. Ghorpade, M. Hanna, US Patent 5859263 (1996).
105. J. Horvat, B. Klaic, B. Metelko, V. Sunjic,Tetrahedron Lett. 26 (1985) 2111.
106. G.J. Mulder, J. Prakt. Chem. 21 (1840) 219.
107. R.H. Leonard, Ind. Eng. Chem. 48(8) (1956) 1330.
108. V. Sunjik, J. Horvat, B. Klaic, Kem. Ind. 33 (1984) 599.
109. C.P. Sassenrath, W.L. Shilling, US Patent 3258481 (1962).
110. S.W. Fitzpatrick, WO Patent 9640609 (1996).
111. L.B. McCusker, C. Baerlocher, M. Biilow, Zeolites 11 (1991) 308.
112. T. Yanagisawa, T. Shimizu, K. Kuroda, C. Kato, Bull. Chem. Soc. Jpn. 63 (1990) 988.

113. C.T. Kresge, M.E. Leonowicz, W.J. Roth, J.C. Vartulli, J.S. Beck, Nature 359 (1992) 710.

114. M. Dubois, Th. Gulik-krzywicki, B. Cabane, Langmuir 9 (1993) 673.

115. J.S. Beck, J.C. Vartulli, W.J. Roth, M.E. Leonowicz, C.T. Kresge, K.D. Schmitt, C.T.W. Chu, D.H. Olson, E.W. Sheppard, S.B. McCullen, J.B. Higgins, J.L. Schlenker, J. Am. Chem. Soc. 114 (1992) 10834.

116. J.C. Vartulli, K.D. Schmitt, C.T. Kresge, W.J. Roth, M.E. Leonowicz, S.B. McCullen, S.D. Hellring, J.S. Beck, J.L. Schlenker, D.H. Olson, E.W. Sheppard, Chem. Mater. 6 (1994) 2317.

117. D. Zhao, J. Feng, Q. Huo, N. Melosh, G.H. Fredrickson, B.F. Chmelka, G.D. Stucky, Science 279 (1998) 548.

118. D. Zhao, Q. Huo, J. Feng, B.F. Chmelka, G.D. Stucky, J. Am. Chem. Soc. 120 (1998) 6024.

119. C.T. Kresge, M.E. Leonowicz, W.J. Roth, J.C. Vartulli, J.S. Beck, Nature 359 (1992) 710.

120. C.Y. Chen, S.L. Burkett, H. Li, M. Davis, Microporous Mater. 2 (1993) 27.

121. A. Monnier, F. Schuth, Q. Huo, D. Kumar, D. Margolese, R.S. Maxwell, G. Stucky, M. Krishnamurty, P. Petroff, A. Firouzi, M. Janicke, B. Chmelka, Science 261 (1993) 1299.

122. P.T. Tanev , T.J. Pinnavaia, Science 267 (1995) 865

123. A. Corma, V. Forne, M.T. Navarro, J.P. Pariente, J. Catal. 148 (1994) 148.

124. Z. Luan, M. Hartman, D. Zhao, W. Zhou, L. Kevan, Chem. Mater. 11 (1999) 1621.

125. N. Lucas, A.P. Amrute, K. Palraj, G.V. Shanbhag, A. Vinu, S.B. Halligudi, J. Mol. Catal. A: Chem. 295 (2008) 29.

126. Y. Zheng, J. Li, N. Zhao, W. Wei, Y. Sun, Micropor. Mesopor.Mater. 92 (2006) 195.

127. S. Sahoo, P. Kumar, F. Lefebvre, S.B. Halligudi, J. Mol. Catal. A: Chem. 273 (2007) 102.

128. J. Konta, Appl. Clay Sci. 10 (1995) 275.

129. A. Corma, Chem. Rev. 97 (1997) 2373.
130. L. Fowden, R.M. Barrer, R.B. Tinker, eds. Philosophical Transactions of the Royal Society of London, Series A, Mathematical and Physical Sciences, 1984.
131. M.J. Wilson, Clay Miner. 34 (1999) 7.
132. L.M. Barclay, D.W. Thompson, Nature 222 (1969) 263.
133. G.A. Mills, J. Holmes, E.B. Cornelius, J. Phy. Coll. Chem. 54 (1950) 1170.
134. J.M. Adams, Appl. Clay Sci. 2 (1987) 309.
135. R.M. Barrer, D.M. McLeod, Trans Faraday Soc. 51 (1955) 1290.
136. J.T. Kloprogge, D. Seykens, J.H. Jansen, J.W. Geus, J. Non-Cryst. Solids 142 (1992) 94.
137. J.P. Sterte , J.E. Otterstedt, Preparation of Catalysts IV, B. Delmon, P. Grange, P.A. Jacobs, G. Poncelet (Eds.) Elsevier, Amsterdam (1987).
138. Z. Ding, J.T. Kloprogge, R.L. Frost, J. Porous Mater. 8 (2001) 273.
139. I. Benito, A. del Riego, M. MartõÂnez, C. Blanco, C. Pesquera, F. GonzaÂlez, Appl. Catal. A. 180 (1999) 175.
140. F. Figueras, Catal. Rev. Sci. Eng. 30 (3) (1988) 457.
141. R.M. Barrer, Hydrothermal Chemistry of Zeolites academic press, New York 1982.
142. L.V.C. Rees, Nature 296 (1992) 492.
143. R. M. Barrer, Pure and Appl. Chem. 51 (1979) 1091.
144. W.M. Meier, D.H. Olson, Atlas of Zeolite Structure Types, Butterworths (1987).
145. J.V. Smith, Mineral Soc. Amer. Spec. paper 1 (1963).
146. K.F. Fischer, W.M. Meier, Fortschi Mineral 42 (1965) 50.
147. D.W. Breck, Molecular Sieves Zeolites, Adv. Chem. Ser., Amer. Chem. Soc., Washington DC, 101 (1971) 1.
148. E.M. Flanigen, In Proceedings of the fifth Interanational Conference of Zeolites, (L.V.C Rees Eds.) Naples, Italy, June 2-6, (1980) 760.
149. L.B. Sand, Econ. Geol. (1967) 161.
150. R.L. Wadlinger, G.T. Kerr, E.J. Rosinski, US patent 33080691 (1967).

151. S. Mintova, V. Valtchev, T. Onfroy, C. Marichal, H. Knozinger, T. Bein, Micropor. Mesopor. Mater. 90 (2006) 237.

152. A. Corma, M. Moliner, A. Cantin, M.J. Cabanas, J.L. Jorda, X. Zou, Chem. Mater. 20 (2008) 3218.

153. D. Barthomeuf, Cat. Rev.–Sci. Eng. 38:4 (1996) 521.

154. M. Muller, G. Harvey, R. Prins, Micropor. Mesopor. Mater. 34 (2000) 135.

155. S. Chaturvedi, P.N. Dave, J. Saudi Chem. Soc. 16 (2012) 307.

156. Y. Hikichi, T. Nomura, J. Am. Ceram. Soc. 70 (1987) C 252.

157. F.H. Firsching, S.N. Brune, J. Chem. Eng. Data 36 (1991) 93.

158. Y. Guo, P. Woznicki, A. Barkatt, E.E. Saad, I.G. Talmy, J. Mater. Res. 11 (1996) 639.

159. L.N. Ho, H. Nishiguchi, K. Nagaoka, Y. Takiya, J. Porous Mater. 13 (2006) 237.

160. R. Patra, G. Alexandra, S. Patra, D.S. Jacob, A. Gedanken, A. Landau, Y. Gofer, New J. Chem. 29 (2005) 733.

161. Y. Takita, M. Ninomiya, H. Miyake, H. Wakamatsu, Y. Yoshinaga, T. Ishihara, Phys. Chem. Chem. Phys. 1 (1999) 4501.

162. H. Tamai, T. Ikeya, F. Nishiyama, H. Yasuda, K. Ilida, S. Nojima, J. Mater. Science 35 (2000) 4945.

163. H. Furuno, T. Kambara, Y. Tanaka, T. Hanamoto, T. Kagawa, J. Inanaga, Terahed. Lett. 44 (2003) 6129.

164. Y. Takita, K. Sano, T. Muraya, H. Nishiguchi, N. Kawata, M. Ito, T. Akbay, T. Ishihara, Appl. Catal. A. 170 (1998) 23.

165. S. Lucas, E. Champion, D. Bregiroux, D. B. Assollant, F. Audubert, J. Solid State Chem. 177 (2004) 1302.

166. Z.A. Peng, X.G. Peng, J. Am. Chem. Soc. 123 (2001) 1389.

167. Z.A. Peng, X.G. Peng, J. Am. Chem. Soc. 124 (2002) 3343.

168. Y.P. Fang, A.W. Xu, R.Q. Song, H.X. Zhang, L.P. You, J.C. You, H.Q. Lui, J. Am. Chem. Soc. 125 (2003) 16025.

169. K.E. Murphy, M.B. Altman, B.J. Wunderlich, Appl. Phys.48 (1977) 4122.

# *Chapter 2*

Catalyst synthesis and characterization

## 2.1. Introduction

It is desired that a good heterogeneous catalyst should demonstrate excellent catalytic activity, 100% selectivity to the desired product and should have acceptable on-stream stability. In the context of catalyst development, characterization of catalytic materials is highly essential as it provides insights into the relation between activity of the catalyst and its physico-chemical properties. If the structure and composition of a catalyst can be correlated with its activity and selectivity, the performance of the catalyst can be understood, thus helping in its reproducibility.

This chapter describes the synthesis of various catalyst materials used in this thesis and experimental methods deployed for their characterization. Aluminium incorporated SBA-15 and lanthanide phosphate catalysts were prepared for execution of this work, while beta zeolite with various compositions ($SiO_2/Al_2O_3$ = 28, 38, 75, 150) and chemically treated clays (K-10, K-20, K-30, Al pillared clay) were commercially procured for the present study. For detailed physico-chemical characterization of these catalyst materials; X-ray diffraction, scanning and transmission electron microscopy, Infrared, Raman spectroscopy and methods based on adsorption and desorption of probe molecules are quite useful. These investigations are expected to provide information about phase structure, crystallinity, crystallite size, surface structure, textural properties, nature of active sites, morphology, particle size, nature of acidity and other characteristic features. The structure-activity relationship is better understood by these techniques, which helps to improve the activity of the catalyst for various applications.

The above listed catalysts were subjected to different characterization techniques. The formation of the desired phase, structural integrity and various physicochemical properties of the catalysts were investigated by X-ray diffraction (XRD), Fourier transform infrared spectroscopy (FTIR), Raman spectroscopy (RS), $N_2$-sorption, thermo gravimetric analysis (TGA), scanning electron microscopy (SEM), transmission electron microscopy (TEM), inductively coupled plasma-optical emission spectrometry (ICP-OES) and $^{27}Al/^{29}Si$ magic angle spinning nuclear magnetic resonance (MASNMR). The total acidity was measured using temperature programmed desorption of ammonia (TPD-$NH_3$), while the Brönsted acidity was measured using isopropyl amine as a probe molecule. Also, the nature of acidi sites (Brönsted and Lewis) was investigated by FTIR using pyridine as probe molecule.

## 2.2. Catalyst preparation

### 2.2.1. Preparation of SBA-15 and Al incorporated SBA-15

Mesoporous siliceous SBA-15 was synthesized according to the procedure reported by Stucky and co-workers [1]. About 4 g of amphiphilic triblock copolymer, poly(ethylene glycol)-block-poly(propylene glycol)-block-poly(ethylene glycol) (average molecular weight, 5800) was dispersed in 30 mL of water, to which 120 g of 2 M HCl solution was added to get a homogeneous solution. To this solution, 8 g of tetra ethyl orthosilicate (TEOS) was added slowly under stirring. This mixture was continuously stirred at 40 °C for 24 h and transferred to a teflon-lined autoclave for crystallization at 100 °C for 2 days. The solid obtained after crystallization was filtered, washed with distilled water and dried at 100 °C for 12 h. The crystalline material was then calcined in flowing air at 550 °C for 6 h in order to decompose and remove the tri-block copolymer to yield mesoporous SBA-15.

A post-synthesis route similar to the procedure reported by Luan *et al* [2] was employed for the preparation of AlSBA-15. In a typical synthesis, anhydrous $AlCl_3$ was dissolved in dry ethanol (25 mL). To this solution, SBA-15 (1 g) was added and refluxed for 10 h under stirring. The material was then filtered, washed repeatedly with ethanol and dried at room temperature followed by calcination at 550 °C for 5 h to give AlSBA-15 catalysts. By varying the $AlCl_3$ content, a series of AlSBA-15 catalysts (with Si/Al ratio ranging 10–40) were prepared.

### 2.2.2. Preparation of $ZrO_2$ supported tungstophosphoric acid (TPA)

This catalyst was prepared by wet impregnation method following the procedure described elsewhere [3]. The support zirconium oxyhydroxide was prepared by adding 5 wt% $NH_3$ solution to 0.5M solution of $ZrOCl_2.8H_2O$, drop wise under continuous stirring till a final pH of 9.5 was reached. The precipitate was filtered, washed repeatedly (till free of chloride ions), dried at 110 °C for 14 h and crushed to get white zirconium oxyhydroxide powder. To the methanolic solution of TPA (0.15 g in 20 mL), zirconium oxyhydroxide (1g) was added and stirred for 12 h at room temperature. The solvent was slowly evaporated to dryness and material was dried at 80 °C overnight, crushed and calcined at 750 °C for 5 h to get 15 wt% TPA/$ZrO_2$-750 (15TZ750). Catalyst with 15 wt% $WO_3$ on $ZrO_2$ (15WZ750) was also prepared in a similar manner for which aqueous solution of ammonium metatungstate

(0.16 g in 20 mL) was taken as the $WO_3$ precursor. After evaporation of the solvent, the material was dried at 100 °C overnight followed by calcination.

### 2.2.3. Preparation of lanthanide phosphates

These catalysts were prepared by aqueous precipitation method following the procedure described by Lucas *et al* [4]. In a typical synthesis, 40 mL of ammonium dihydrogenphosphate ($NH_4H_2PO_4$) solution (0.42 M) was added dropwise to 150 mL of lanthanide salt solution (0.11 M) at a flow rate of 0.3 $mL.min^{-1}$. Upon addition, colloidal white precipitate was obtained; the slurry was then digested at 50 °C for 18 h. The precipitate was washed with distilled water and separated by centrifugation (1000 RPM, 0.5h) and dried at 100 °C overnight. The other lanthanide (Ce, Nd, Sm, Tb and Dy) phosphates were prepared in a similar manner, using corresponding nitrate salts for La, Ce, Nd, Sm and chloride salts for Tb and Dy. The dried materials were crushed and calcined at 500 °C for 4 h in air. The catalysts were designated as $LaPO_4$, $CePO_4$, $PrPO_4$, $NdPO_4$, $SmPO_4$, $TbPO_4$ and $DyPO_4$. However, for the synthesis of $GdPO_4$, 3.92 g of gadolinium oxide was added to 5.8398 g of 70% $HNO_3$ and heated slightly for complete dissolution of the oxide, the solution was then diluted to 150 mL. To this, 40 mL of $NH_4H_2PO_4$ solution (0.42 M) was added dropwise to give $GdPO_4$ precipitate which was digested, washed, centrifuged and calcined following similar procedure used for the other phosphates.

## 2.3. Characterization of catalysts

Characterization of the above materials helps to understand the properties of the catalysts in a better way, so that materials can be improved or designed to meet the requirements. The following write-up provides a brief account of the theory and principle of various characterization techniques used for the current study. The procedure used for each experimental technique is also described in this part.

### 2.3.1. X-ray Diffraction (XRD)

X-Ray diffraction is one of the fundamental techniques employed for catalyst characterization. It has been an important technique for determining the structure of materials characterized by long-range order. It is used to identify crystalline phase(s) of the catalyst by means of lattice structural parameters and crystallinity [5]. X-rays are highly intrusive electromagnetic radiations which are electrically neutral. Their frequency lies between the ultra-violet (UV) and gamma radiations and their

wavelength (λ) range from approximately 0.04 Å to 1000 Å. For diffraction applications, X-rays with only shorter wavelengths ranging from few Å to 0.1 Å (1-12keV) are used because these are comparable to the size of the atoms. Therefore the X-rays are ideally suited for deducing the structural arrangement of atoms and molecules for various materials.

The diffraction method involves the interaction of the incident monochromatized X-rays (like Cu Kα) with the atoms of a periodic lattice. X-rays scattered by atoms in an ordered lattice interfere constructively in directions given by Bragg's law [6]:

$$\mathbf{n\lambda = 2\ d\ \sin\theta};\ n = 1, 2, 3,\ldots \qquad (2.1)$$

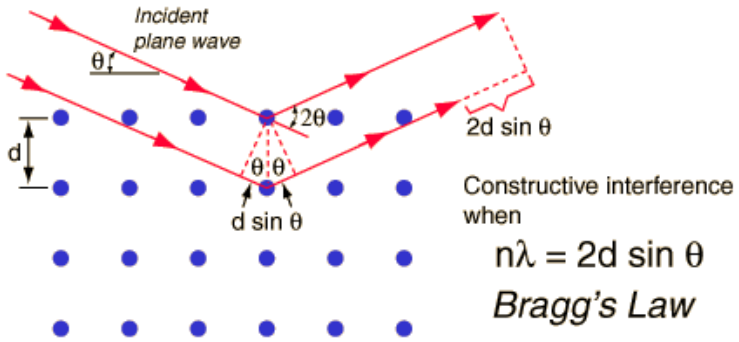


**Fig. 2.1.** Principle of Bragg's law.

where, λ is the wavelength of the X-rays, d is the distance between two lattice planes, θ is the angle between the incoming X-rays and the normal to the reflecting lattice plane and n is the integer called order of the reflection.

By measuring the angle 2θ, under which constructively interfering X-rays leave the crystal, the Bragg's equation gives the corresponding lattice spacing, which is characteristic for a particular compound. Width of the diffraction peaks signifies the dimension of the reflecting planes. It is known that the width of a diffraction peak increases when the crystallite size is reduced below a certain limit (<100 nm). Therefore, XRD patterns can be used to estimate the average crystallite size of very small crystallites using XRD line broadening by applying the Scherrer formula [7];

$$\mathbf{t = 0.9\lambda / \beta Cos\ \theta} \qquad (2.2)$$

where, t is the thickness of the crystallites (in Å), λ is the wavelength of X-rays, θ is the diffraction angle and β is the full width at half maxima of the diffraction peak.

X-ray diffraction pattern of all the catalysts reported in this thesis were collected using PANalytical X'pert Pro dual goniometer. The data were collected with a step size of 0.02 ° at a scan rate of 0.5 °$min^{-1}$. The sample was rotated throughout the scan for better counting statistics. The incident radiation used was Ni filtered Cu$K_\alpha$ ($\lambda$= 1.5406 Å, 40 kV, 30 mA) and the data collection was carried out using a flat holder in Bragg–Brentano geometry (0.2 °).

Low-angle X-ray diffraction patterns were collected in the 2θ range 0.5–5°, with an X'celerator detector, using the real time multiple strip (RTMS) detection technique, at a scan rate of 0.5$^o$ $min^{-1}$.

### 2.3.2. $N_2$ Physisorption

The most accepted method of measuring surface area of catalytic materials is the one that is based on the theory developed by Brunauer, Emmett and Teller in 1938 considering the multilayer adsorption. Its assumptions are (i) adsorption energy remains constant from zero to full coverage for the primary layer of the adsorbate and each successive layers above (ii) enthalpy of adsorption is the same for any other layer except the first one (iii) there is no inter molecular interaction, however they attract and retain molecules striking them from the gas phase (iv) a new layer can be initiated before the completion of the one under formation. The Brunauer-Emmett-Teller (BET) equation 2.3 is [8];

$$\mathbf{P/V(P_0-P) = 1/CV_m + [(C-1)/CV_m] (P/P_0)} \qquad (2.3)$$

where, $P_0$ is saturation vapor pressure of the adsorbate at the experimental temperature, P is adsorption equilibrium pressure, $V_m$ is the volume of adsorbate required for monolayer coverage, V is volume of gas adsorbed at pressure P and C is a constant related to the heat of adsorption and liquefaction. In order to quantify the amount of nitrogen adsorbed, a linear relationship between $P/P_0$ and $P/V(P_0/P)$ is required. This linear portion is only restricted to a limited portion of the entire isotherm, generally for $P/P_0$ of 0.05 to 0.30. The slope of the straight line S is equal to $(C-1)/CV_m$ and the intercept I is equal to $1/CV_m$. Both the parameters are used to calculate the monolayer volume, $V_m$ given by 1/(S+I). The surface area of the catalyst ($S_{BET}$) is related to $V_m$, by the equation,

$$\mathbf{S_{BET} = (V_m/22414) N_a \sigma} \qquad (2.4)$$

where $N_a$ is Avogadro number and σ is mean cross sectional area covered by one adsorbate molecule. Nitrogen gas is most widely used for surface area determinations as it exhibits intermediate C values (50-250) on most solid surfaces, impeding localized adsorption or behavior as two dimensional gas. It has been demonstrated that the C influences the value of the cross-sectional area of an adsorbate. Therefore, the acceptable range of C for nitrogen makes it possible to calculate its cross-sectional area from its bulk liquid properties [9]. For the hexagonal close-packed nitrogen monolayer at -196 °C, the cross-sectional area σ for nitrogen is 16.2 Å.

The $N_2$ adsorption experiments were conducted using Quantachrome autosorb IQ analyser. Nitrogen physisorption was carried out at -196 °C after degassing the samples at 300 °C (except for clay samples which were degassed at 175 °C) for 3 h in vacuum. The isotherms were analyzed in a conventional manner in the region of the relative pressure, $P/P_0$ = 0.005 to 1.0. Pore volumes were calculated using the t-plot method of De Boer. The BJH method and the corrected Kelvin equation was used to determine the pore size distributions from the adsorption/desorption branches of the isotherms [10].

### 2.3.3. Electron microscopy

The electron microscopy has many variants. In this section, we deal only with scanning electron microscopy and transmission electron microscopy. The former is useful for the examination of physical features of the sample, like size and shape of crystals in the material. On the other hand TEM is much more useful to study the nano structure of the material along with the metal dispersion.

#### 2.3.3.1. Scanning electron microscopy (SEM)

SEM is a type of electron microscopy that images the sample surface by scanning it with a high-energy beam of electrons in a raster scan pattern. It is a straightforward technique to probe the morphological features of the materials. SEM scans over a sample surface with a probe of electrons (5-50 eV) and detects the yield of either secondary or back-scattered electrons as a function of the position of the primary beam. Contrast is generally caused by the orientation that parts of the surface facing the detector appear brighter than parts of the surface with their surface normal pointing away from the detector. The interaction between the electron beam and the sample produces different types of signals providing detailed information about the

surface structure and morphology of the sample [11, 12]. A major advantage of SEM is that bulk samples can also be directly studied by this technique.

The SEM micrographs of the samples were obtained on a Leo Leica Cambridge UK Model Stereoscan 440 scanning electron microscope. The samples were loaded on stubs and sputtered with thin gold film to prevent surface charging and also to protect from thermal damage due to electron beam [13].

#### 2.3.3.2. Transmission electron microscopy (TEM)

TEM is basically used for high resolution imaging of thin films of a solid sample for compositional and micro structural analysis. In this technique a very thin sample is irradiated with high energy electron beam emitted by a cathode and formed by magnetic lenses. This beam which is partially transmitted through the specimens is diffracted by the lattices of a semi crystalline or crystalline material and propagates along different directions. Thus, the beam carries information about the structure of the specimen. This is followed by imaging and angular distribution analysis of the forward scattered electrons (unlike SEM where backscattered electrons are detected) and energy analysis of the emitted X-rays [14]. The image is then magnified by a series of magnetic lenses until it is recorded by hitting a fluorescent screen, photographic plate, or light sensitive sensor such as a CCD (charge-coupled device) camera. The image detected by the CCD may be displayed in real time on a monitor or computer.

The ability to determine the positions of atoms within materials has made the TEM an interesting and indispensable tool for research and development in the fields of nano-technologies, development of semiconductor devices for electronics and photonics and heterogeneous catalysis.

Transmission electron microscopy of the samples was carried out using FEI Technai TF-30 instrument operating at 300 kV. The samples for TEM measurements were prepared by placing a droplet of the sample suspension, prepared in isopropyl alcohol using ultrasonification on a carbon coated copper grid (mesh 200) by leaving them for drying at room temperature. The difference in the alignment of the two microscopy's is depicted in Fig. 2.2.

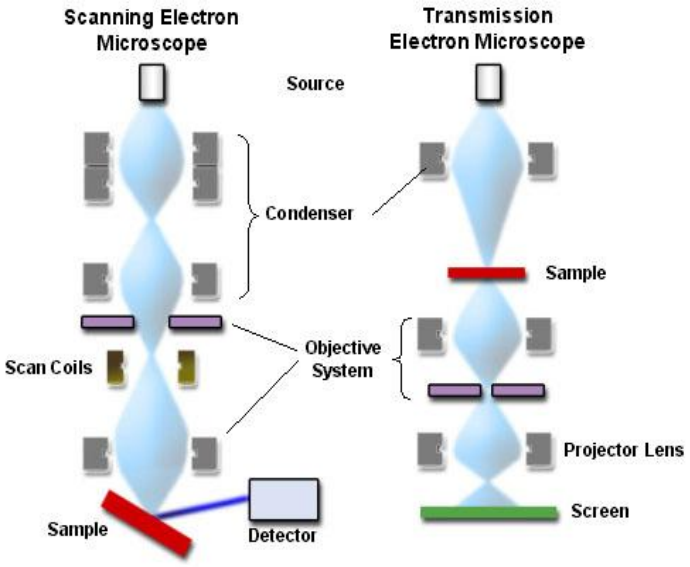


**Fig. 2.2.** Alignment of SEM and TEM.

### 2.3.4. Solid state magic angle spinning nuclear magnetic resonance spectroscopy

In liquid state, all the anisotropic (directionally dependent) interactions are averaged resulting narrow NMR peaks. However, in solid state such averaging is not feasible. In solid-state NMR, the line shape is determined by dipolar and quadrupolar interactions. The lines are usually broader as the rigid structure of the solid prevents the averaging of the dipolar interaction (HD) by motions. Since, the first order quadrupolar and dipolar interactions are proportional to $(3\cos^2\theta - 1)$, where $\theta$ is the angle between an inter nuclear vector and the magnetic field, these interactions can be removed, to a first order approximation, by spinning the sample around the so-called magic angle $\beta$ with respect to the external magnetic field, for which $3\cos^2\beta - 1 = 0$, i.e. $\beta = 54.74°$. Hence this technique is known as magic angle spinning (MAS) [15].

$^{27}$Al Magic-angle spinning (MAS) NMR spectra were recorded on a Bruker DSX300 spectrometer at 7.05 T magnetic field. The sample was rotated at 6000 Hz at the magic angle, while collecting the data. A delay of 2 s was maintained between two 45° pulses. External $Al(H_2O)_6^{3+}$ was used as a reference. For $^{29}$Si NMR spectra, the sample was rotated at 4000 Hz and $Si(CH_3)_4$ was used as external reference.

### 2.3.5. Inductively coupled plasma-optical emission spectrometry (ICP-OES)

ICP-OES is one of the most powerful and popular analytical tools for the determination of trace elements in a myriad of sample types. It was developed by

Fassal at Iowa state university in US and by Greenfield at Albright & Wilson, in the UK Ltd. in the mid 1960s [16]. The technique is based on the spontaneous emission of photons from atoms and ions that have been excited in a RF discharge. Liquid and gas samples may be injected directly into the instrument, while solid samples require extraction or acid digestion so that the analytes are present in a solution.

The sample solution is converted in to an aerosol and directed into the central channel of the plasma. At its core, the inductively coupled plasma (ICP) sustains a temperature of approximately 9727 °C, so the aerosol is quickly vaporized. Analyte elements are liberated as free atoms in the gaseous state. Further collisional excitation within the plasma imparts additional energy to the atoms, promoting them to the excited states. Sufficient energy is often available to convert the atoms to ions and subsequently promote the ions to excited states. Both the atomic and ionic excited state species may then relax to the ground state via the emission of a photon. These photons have characteristic energies that are determined by the quantized energy level structure for the atoms or ions. Thus the wavelength of the photons can be used to identify the elements from which they originated. The total number of photons is directly proportional to the concentration of the originating element in the sample. Sample introduction is depicted in Fig. 2.3.

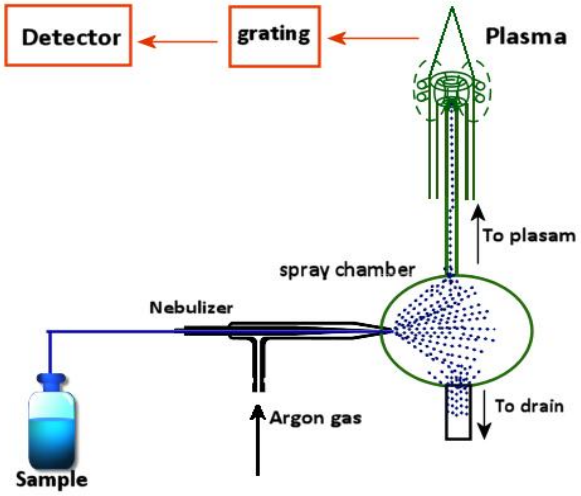


**Fig. 2.3.** Depiction of sample introduction to ICP-OES.

ICP-OES analysis was carried out on a Spectro Arcos instrument equipped with the Winlab software (FHS-12). Metals can be analyzed by either a radial or an axial plasma configuration. Standard solutions containing different elements were used for the calibration purpose. The rare earth phosphate catalysts were dissolved in

conc. HCl and were made up to 100 mL of aqueous solution, and analyzed using an ICP-OES instrument. For AlSBA-15 and clay catalysts, about 0.5 g of the sample was weighed into a platinum crucible and 2 mL concentrated $H_2SO_4$ followed by 5mL of HF (40% solution) was added to it, which was evaporated to dryness on a sand bath. The treatment was repeated thrice. The residue was then heated to red-hot intensity using a Bunsen burner for 0.75 h. The sample was then cooled and weighed. The residue was then dissolved in a 1:1 mixture of conc. HCl and diluted with water to 250 mL. The solution was analyzed using an ICP-OES instrument.

### 2.3.6. Infrared Spectroscopy (IR)

Infrared spectroscopy is the first and the most important of the modern spectroscopic techniques that has found profound applications in the field of catalysis. This is primarily due to the fact that IR provides actual information on the structure, geometry and orientation of practically all molecules that are present in the sample, irrespective of the physical state, temperature or pressure. It is therefore a useful tool to identify phases that are present in the catalyst or its precursor stages, the adsorbed species, adsorption sites and the way in which the adsorbed species are chemisorbed on the surface of the catalyst [17,18].

Infrared spectroscopy is the most common form of vibrational spectroscopy and it depends on the excitation of vibrations in molecules or in solid lattices by the absorption of photons, which occurs if a dipole moment changes during the vibration. The intensity of the infrared band is proportional to the change in dipole moment. A variety of IR techniques have been used to get information on the surface chemistry of different solids. With respect to the characterization of solid catalysts, two techniques largely predominate, namely, the transmission/absorption and the diffuse reflection techniques. In the first case, the sample consists typically of 10-100 mg of catalyst, pressed into a self-supporting disc of approximately 1 $cm^2$ and a few tenths of a millimeter thickness. In diffuse reflectance mode (DRIFT), samples can be measured by simply depositing on a sample holder, avoiding the tedious preparation of wafers. This technique is especially useful for strongly scattering or absorbing samples. The infrared absorption spectrum is described by Kubelka Munk function [19]

$$\mathbf{F(R_\infty) = (1-R_\infty)^2/2R_\infty = K/S} \qquad (2.5)$$

where, K is the absorption coefficient, which is a function of the frequency ν, S is the scattering coefficient and $R_\infty$ is the reflectivity of a sample of infinite thickness, measured as a function of ν.

The Fourier transform-infrared spectra of the catalysts reported here were recorded on Bruker Tensor 27 FT-IR spectrometer at ambient conditions. The spectra were recorded using thin self-supporting discs made by pressing the mixture of catalyst sample and KBr.

### 2.3.7. Infrared adsorption studies - Pyridine adsorption

The most common application of IR in catalysis is to identify adsorbed species and to study the way in which these species are chemisorbed on the surface of the catalyst [20-22]. More specifically, IR spectroscopy has been used to study the adsorption of typical probe molecules like ammonia, pyridine and other bases, hydrocarbons and carbon dioxide, which can monitor the basic sites on oxide catalysts [23]. Investigation of adsorbed species in relation to their behavior in catalytic reactions is the main field of application of IR spectroscopy.

The nature of acid sites (Brönsted and Lewis) of various catalyst samples was studied by in-situ FTIR with chemisorbed pyridine in drift mode on Bruker Tensor 27 instrument with 4 $cm^{-1}$ resolution. These studies were performed after heating the pre-calcined powder samples in-situ from room temperature to 400 °C (the temperature was 175 °C for clay samples) at a heating rate of 5 °C $min^{-1}$ in $N_2$ flow (40 mL.$min^{-1}$). The samples were kept at the activation temperature for 3 h and then cooled to 100 °C; prior to introduction of pyridine vapors (30 µL) in $N_2$ flow. The IR spectra were recorded at a resolution 4 $cm^{-1}$, after degassing the sample at 200 °C by averaging the spectra after about 400 scans.

### 2.3.8. Thermal analysis

Thermo analytical techniques involve the measurements of the response of a solid under study (energy or mass released or consumed) as a function of temperature (or time), when it is heated in programmed way. Thermogravimetry (TG) is a technique which measures the change in mass of a material as a function of temperature and time, in a controlled manner. This variation in mass can be either a loss of mass (vapor emission) or a gain of mass (gas fixation). It is ideally used to assess volatile content, thermal stability, degradation characteristics, aging/lifetime

breakdown, sintering behavior and reaction kinetics. Differential thermal analysis (DTA) is a technique which measures the temperature difference of the sample versus a reference, caused by thermal events in a material. It is ideally used to determine melting point, glass transition temperature, crystallinity, degree of curing, heat capacity, impurities present etc [24].

In the present work, thermogravimetry measurements of the samples were performed with a Mettler Toledo TGA/SDTA 851 apparatus. The analyses were carried out in air (40 $mL.min^{-1}$) at a heating rate of 10 °C $min^{-1}$ from 30 °C to 800 °C using about 10 mg of sample in a platinum pan. Calcium oxalate was used to calibrate the instrument. TGA curves are depicted as the first derivative (DTG) of the direct weight change with heating.

### 2.3.9. Temperature programmed desorption

Temperature programmed desorption (TPD), temperature programmed reduction (TPR), temperature programmed oxidation (TPO) and reaction spectroscopy (TPRS) typically involve monitoring surface or bulk processes between the solid catalyst and its gaseous environment via continuous analysis of the gas phase composition as the temperature is raised linearly with time. Instrumentation for temperature-programmed investigations consists of a reactor charged with the catalyst in a furnace that can be temperature programmed and a thermal conductivity detector (TCD) to measure the conductivity of gas stream passing through the sample before and after interaction, to find out its change in concentration. Mass Spectrometer can be coupled with the detector for identification of various species formed or evolved during the desorption process.

Temperature programmed desorption of ammonia ($NH_3$-TPD) is one of the most widely used and flexible techniques for characterizing the acid sites on surfaces. Determining the quantity and strength of the acid sites is crucial to understand and predict the performance of a catalyst. Upon contacting with a surface, probe molecule (ammonia) is sorbed onto the surface either by physisorption, chemisorption, or by the formation of chemical bonds, minimizing the energy of the species. On increasing the sample temperature, the species is desorbed from the surface. The amount of ammonia desorbed is proportional to the acid concentration.

However using ammonia as a probe does not differentiate the site specific adsorption as the adsorption may occur at Brönsted sites, Lewis sites, or as a result of

any combination of surface/vapor attractive forces. This problem can be circumvented by using other amines like alkyl amines. The chief advantage of the use of alkyl amines as a probe for acid-site densities is that the temperature-programmed decomposition reaction occurs only at Brönsted sites (eq. 2.9), providing an efficient method for direct quantification of Brönsted acidity [25].

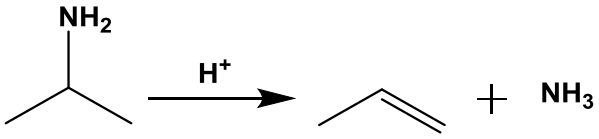


(2.6)

The acidity of the catalysts was investigated by $NH_3$-TPD using Micromeritics Autochem-2920 instrument. Prior to TPD run, the sample was activated at 450 ºC in He flow (40 mL.min$^{-1}$) for 1 h to remove all physisorbed impurities. Subsequently, the temperature was brought down to 80 ºC and the sample was exposed to a stream of 10% $NH_3$ in He (30 mL.min$^{-1}$) for 0.5 h. The temperature was then raised to 100 ºC and flushed with He for 1 h at 100 ºC to remove the physisorbed $NH_3$. The $NH_3$ desorption was carried out in He flow (40 mL.min$^{-1}$) by increasing the temperature to desired level (550 ºC or 800 ºC at 10 ºCmin$^{-1}$), while monitoring the concentration of $NH_3$ desorbed using thermal conductivity detector of the instrument.

The presence of Brönsted acid sites was determined by temperature programmed desorption of isopropyl amine as probe molecule (TPD-IPA) using Micromeritics Autochem-2920 equipped with a Thermostar TM mass spectrometer. Initially, the sample was activated at 400 ºC in He flow (40 mL.min$^{-1}$) for 1 h. Subsequently, the temperature was brought down to 80 ºC and IPA was sorbed by exposing the samples to vapors of IPA (flask temperature = 50 ºC) in He (25 mL.min$^{-1}$). The dosing was repeated 20 times for complete sorption. The temperature was then raised to 100 ºC and flushed with He for 1 h at 100 ºC to remove the physisorbed IPA. The desorption of IPA was carried out in He flow (40 mL.min$^{-1}$) by increasing the temperature to 800 ºC at 10 ºC min$^{-1}$, while monitoring the concentration of desorbed species using a mass spectrometer.

### 2.3.10. Raman Spectroscopy

Raman spectroscopy is based on the inelastic scattering of photons, which loose energy by exciting vibrations in the sample. Photons of the laser are absorbed by the sample and then re-emitted. Frequency of the re-emitted photons is shifted up

or down in comparison with original monochromatic frequency, which is called the Raman effect. This shift provides information about vibrational, rotational and other low frequency transitions in molecules. A vibration is Raman active if it changes the polarizability of the molecule. Raman and infrared spectroscopy complement each other, in particular for highly symmetrical molecules e.g. $CO_2$. Raman spectroscopy is commonly used in chemistry, since vibrational information is specific to the chemical bonds and symmetry of molecules. Therefore, it provides a fingerprint by which the molecule can be identified. From Raman spectral data, we can determine the composition of material, crystal symmetry and orientation, quality of crystal, amount of material, stress or strain etc.

Raman spectra were recorded using Horiba JY Lab RAM HR 800 with a Czerny-Turner type spectrograph with 800 mm focal length and achromatic flat field monochromator along with mirror-based reflective optics and charge-couple device (CCD) detector. The scanned wavelength region was 200-1200 $cm^{-1}$, using Ar (632.8 nm, 20 mW) laser.

## 2.4. References


1. D. Zhao, J. Feng, Q. Huo, N. Melosh, G.H. Fedrickson, B.F. Chemlka, G.D. Stucky, Science 279 (1998) 548.
2. Z. Luan, M. Hartmann, D. Zhao, W. Zhou, L. Kevan, Chem. Mater. 11 (1999) 1621.
3. B.M. Devassy, S.B. Halligudi, S.G. Hegde, A.B. Halgeri, F. Lefebvre, Chem. Commun. 10 (2002) 1074.
4. S. Lucas, E. Champion, D. Bregiroux, D.B. Assollant, F. Audubert, J. Solid State Chem. 177 (2004) 1302.
5. J.W. Niemantsverdriet, Spectroscopic methods in Heterogeneous catalysis, VCH, Weinheim, 1993.
6. B.D. Cullity , S.R. Stock, Elements of X-ray Diffraction, Prentice Hall, 3rd ed. (2001).
7. N.F.M. Henry, J. Lipson , W.A. Wooster, The interpretation of X-ray diffraction photographs, Macmillan and Co Ltd., London, (1951).
8. S. Brunauer, P.H. Emmett, E. Teller, J. Am. Chem. Soc. 60 (1938) 309.
9. (a) A.V. Kiselev , Y.A. Eltekov , World Congress on Surface Activity, Vol. II, p. 228, Butterworths, London, 1957. (b) S. Lowell, J. Shields, G. Charalambous and J. Manzione, J. Colloid Interface Sci. 86 (1982) 191.
10. E.P. Barrett, L.G. Joyner, P.P. Halenda, J. Am. Chem. Soc. 73 (1951) 373.
11. J.I. Goldstein, H. Yakowitz (Eds.), Practical Scanning Electron Microscopy, Plenum Press, New York, 1975.
12. G. Lawes, Scanning Electron Microscopy and X-Ray Microanalysis, John Wiley and Sons Ltd., Chichester, 1987.
13. P.J. Goodhew, J. Humphreys, R. Beanland, Electron Microscopy and Analysis, 3rd edition, 2001.
14. J.R. Fryer, Chemical Applications of Transmission Electron Microscopy, Academic Press, San Diego, 1979.
15. R.A. Wind, A.I. Popov, K. Hallenga (Eds.), Modern NMR Techniques and Their Application in Chemistry, p. 156, Marcel Dekker, Inc., New York, 1991.
16. C.B. Boss, K.J. Fredeen, Concept, Instrumentation and Techniques in Inductively Coupled Plasma Optical Emission Spectrometry, 2nd edition, Perkin-Elmer, Norwalk, CT, 1997.

17. J.M. Thomas, O. Terasaki, P.L. Gai, W. Zhou, J. Gonzalez-Calbet, Acc. Chem. Res. 34 (2001) 583.
18. R.P. Eischens, W.A. Pliskin, Adv. Catal. 10 (1958) 1.
19. (a) P. Kubelka, F. Munk, Z. Tech. Phys. 12 (1931) 593. (b) P. Kortum, W. Braun, C. Harzog, Angew. Chem. Int. Ed. 2 (1963) 333.
20. M.D. Baker, Catal. Rev. Sci. & Eng., 29 (1987) 269.
21. J.A. Lercher, C. Grundling, G. Eder-Mirth, Catal. Today, 27 (1996) 353.
22. J.C. Lavalley, Catal. Today, 27 (1996) 377.
23. M.C. Kung, H.H. Kung, Catal. Rev. Sci. & Eng., 27 (1985) 425.
24. M.B. Kluwer Introduction to Thermal Analysis Techniques and applications 2nd edition, Academic pubishiers, (2001).
25. W.E. Farneth, R.J. Gorte, Chem. Rev. 95 (1995) 615.

# *Chapter 3*

Synthesis of 5-HMF in biphasic medium over solid acid catalyst

## 3.1. Introduction

It is an accepted proposition that present petroleum based chemicals need to be replaced with renewables as a result of the dwindling fossil fuel reserves. Moreover, rapid ecological changes taking place as a result of fossil fuel use makes it imperative to replace them with renewable fuels to attain a sustainable and renewable society. In this context, effective utilization of biomass for the production of fuels and chemicals has emerged as an important area of research. Saccharides have attracted greater attention as a promising carbon based alternative source as they are renewable chemical feedstocks [1,2]. Hence, their conversion to useful chemicals has been intensely explored [3]. However, problems of low volatility, poor solubility in desired medium and polyfunctionality of carbohydrates is hindering their effective conversion to value added chemicals. This necessitates development of innovative processes and catalyst systems to facilitate and accelerate their utilization. Since, 5-hydroxymethylfurfural (HMF) is an important platform chemical, it's synthesis through dehydration of hexoses is extensively studied [4]. The potential applications of HMF includes its selective oxidation to 2,5-furandicarboxylic acid which can be used as a replacement for terephthalic acid in the production of polyesters [5-8], its reduction to 2,5-dihydroxymethylfuran and 2,5-bis(hydroxymethyl)tetrahydrofuran [9,10], which can serve as alcohol components in the production of polyesters, its hydrogenolysis to 2,5 dimethyl furan (DMF), with excellent fuel properties to replace gasoline [11], its rehydration to levulinic acid (LA) an important chemical building block with versatile applications [12,13]. Moreover, numerous phenolic resins and polymerizable furanic compounds with promising properties have been prepared from HMF [14, 15]. As a result of above described versatile applications, successful efforts were made to produce HMF using both homogeneous and heterogeneous catalysts. The following sections give a detailed literature background of HMF synthesis from carbohydrates.

## 3.2. Literature background on the synthesis of HMF from carbohydrates

It is generally accepted that the synthesis of HMF results from triple dehydration of hexose [16] in the presence of an acid catalyst in various reaction medium. Apart from hexoses, other substrates that can be used are oligo- and polysaccharides. The HMF processes can be categorized as

1. Processes in non-aqueous media

2. Processes in aqueous media
3. Processes in mixed solvent systems
4. Processes in other systems

These processes described below in detail.

### 3.2.1. Dehydration in non-aqueous media

The dehydration of hexoses to HMF in non-aqueous media was found to be more effective in terms of reaction temperature and HMF yield as compared to those in aqueous media. The excellent HMF yields obtained in non-aqueous solvents can be attributed to the inhibition of the degradation of HMF to acids (levulinic and formic acid). Various organic solvents including dimethylsulfoxide (DMSO), alcohols, acetone, 1,4-dioxane, polyglycol ether, dimethylformamide (DMFa), dimethyl acetamide (DMAc), γ-valerlactone (GVL), N-methyl pyrrolidone (NMP), tetrahydrofuran (THF) etc. have been used as the reaction medium in the dehydration of carbohydrates. For a better understanding, these are further categorized as polar aprotic solvent systems and green solvents.

#### 3.2.1.1. Polar aprotic organic solvent systems

Among the numerous organic solvents used for dehydration of sugars, DMSO is the most common because it offers higher reactant solubility and enhanced product stability. The product HMF is stable in DMSO because it inhibits the formation of humins and acids; the most inevitable byproducts. Fructose dehydration in DMSO could proceed even without catalysts [17,18]. The mechanism for the same was explained by Amarasekara *et al* using NMR spectroscopy [19]. However the need to obtain nearly quantitative yields compelled the researchers to employ acid catalysts for the dehydration reaction.

For carbohydrate dehydration various catalysts (heterogeneous and homogeneous) were screened in DMSO. Excellent HMF yields were achieved from fructose in case of varied catalyst systems. Ishida *et al* used 2.5 mol% of $LaCl_3$ as catalyst in DMSO and achieved 95 % of HMF yield in 4 h at 100 °C [20]. Replacing DMSO by DMAc and DMFa did not alter the yields much. But the use of dioxane or 1-butanol as solvents resulted in lower yields (~ 25%). Fang *et al* used lanthanide triflates as catalysts and obtained 83 % HMF yield in 2 h at 120 °C with 10 wt% of $Sc(OTf)_3$ [21]. Saha *et al* used $AlCl_3$ catalyst for HMF from fructose and attained

71% HMF yield with 50 wt% catalyst at 120 ºC within 5 min [22]. The first HMF synthesis in DMSO using solid acid catalyst was reported in 1980 with Diaion PK-216 resin which gave 90% of HMF yield [23]. This was followed by Halliday and co-workers who used Dowex-type ion exchange resin for fructose dehydration and achieved 85 % HMF yield at 110 °C in 5 h [24]. Later several solid acid catalysts were screened for the reaction. Sulphated oxides/mixed oxides could effectively catalyze the reaction. Tong *et al* used $SO_4^{2-}/GeO_2$ and got 68% yield at 150 °C in 1.66 h [25]. Wang *et al* used $SO_4^{2-}/SnO_2$-$ZrO_2$ and attained 75% yield at 120 ºC in 2.5 h [26]. Other sulphated oxides like zirconia and niobia were tested and gave good yields of HMF (~ 75% yield) [27,28]. Several functionalized materials were also found to be catalytically active. Wu *et al* [29] studied bifunctionalized silica nano particle (MSN) solid catalyst having $HSO_3$ acid and [EMIM] $Cl/CrCl_2$ ionic liquid moieties. This resulted in enhanced production of HMF under milder conditions. The authors credited the effectiveness of the bi-functionalized MSN to the acidic moieties present on silica.

Wang *et al* used acid functionalized carbon as a recyclable catalyst and attained 91% HMF yield in 1 h at 130 ºC [30]. Recently $SO_3H$ functionalized metal organic framework was used as catalyst by Chen *et al* to get HMF yields of 90% at 120 ºC in 1 h. The catalyst was recycled several times without any loss of catalytic activity [31]. Many more interesting approaches were developed in the hunt for good catalyst systems. Ionic liquids were immobilized by Sidhpuria *et al* onto silica nano particles called as supported ionic liquid particles (SIPLs) which worked as good heterogeneous catalyst for HMF synthesis from fructose giving 63% yield [32]. Lan *et al* developed a magnetic catalyst comprising of Cr exchanged hydroxyapatite encapsulated $\gamma$-$Fe_2O_3$ in order to accomplish easy catalyst separation and recyclability. They got 89% HMF yield at 120 ºC in 4 h [33].

Apart from using different catalysts, modification of process conditions has also led to better results. Satsuma *et al* [34] explored the dehydration in organic solvent DMSO with several heterogeneous catalysts (zeolite, hetropoly acid and acidic resin). For water removal, the reactions were performed in vacuum ($0.97X10^5$ Pa) which improved the HMF yield to 97% with $FePW_{12}O_{40}$ in 2 h at 120 °C. Even without the removal of water nearly quantitative yields were attained when Amberlyst-15 was powdered (0.15–0.053 mm) and the catalyst exhibited excellent recyclability without any deactivation.

Research was also focused on employing other aprotic solvents like DMAc [20,21], DMFa [35], NMP [36,37] and mixtures of DMSO with other solvents [27,38]. A mixed system comprising of acetone and DMSO was used by Smith *et al* for dehydrating fructose using acidic resin (DOWEX 50WX8) as catalyst. They obtained very good yield of HMF (88%) in 0.33 h at 140 °C. The catalyst was recyclable and stable with minor deactivation. When sulfated zirconia was used as catalyst in the same system moderate yields were achieved (60-66%) [27,38]. Another important accomplishment was achieved by Binder and Raines in the synthesis of HMF from cellulose, glucose and fructose in DMAc with metal bromides and iodides. Among all reactants, fructose gave a maximum yield of 90% (100 °C, 2 h). This was an impressive study since very high yields were obtained in DMAc (alternative to DMSO) and polysaccharides like cellulose could also be efficiently transformed [39].

Since glucose is an abundant and cheapest monosaccharide, its conversion to HMF is economically favorable. However, the mechanism of dehydrating glucose involves two steps. First is its isomerization to fructose which is feasible over Lewis acidic or basic sites and second is fructose dehydration to HMF. Therefore the catalyst system should possess required sites for carrying out both the transformation. Glucose isomerisation to fructose proceeds in the presence of Lewis base or Lewis acid while fructose to HMF is a typical acid catalyzed reaction. Hence the obvious way is to incorporate sites for isomerization in the existing acid catalyst. For the isomerization reaction, tin [40] and chromium [39] were found to be highly effective. Rare earth metal salts ($ScCl_3$, $YCl_3$, $LaCl_3$) could give 30% HMF yield in DMAc at 200 °C in < 0.16 h [41]. Apart from these, chloride salt of Ge and Al were also catalytically active for isomerization [42,43]. Instead of the chloride the iodide salt of aluminium showed better catalytic activity as demonstrated by Ren *et al* [44]. With $AlCl_3$ as catalyst and DMAc as solvent 52% HMF yield was attained in 15 min at 120 °C using glucose as substrate. Solid acid catalyst like $ZrO_2$ [45], $SO_4^{2-}/ZrO_2$ [46], dealuminated zeolites [47], Sn exchanged phyllosilicates [48] where the metal centers acted as Lewis acid sites could effectively catalyze glucose dehydration giving HMF in moderate yields. Simultaneous use of acid and base in one pot was also found to be efficient for aldose transformation. Ohara *et al* used hydrotalcite with Amberlyst-15 in DMF solvent and achieved 42% yield of HMF from glucose at 100 °C in 3 h [49]. Raines *et al* also converted glucose to HMF in good yields of 50 % over phenyl boronic-acid catalyst using excessive of $MgCl_2$ [50]. Based on these results, it can be inferred that using

glucose or cellulose as reactant moderate to high yields of HMF can be obtained when isomerization catalyst are deployed in aprotic solvents as reaction medium, while much lower yield of the furan (< 20%) was achieved when no isomerization component is present in the catalyst.

Dehydration of carbohydrates in aprotic solvents with high boiling point is a good process for attaining high yields of HMF. However, the problem is of product isolation. For such systems, usually extraction or distillation has to be employed for product recovery, which makes the overall process energy intensive. Thus the quest for economic and green solvents to get high yields of HMF continues.

### 3.2.1.2. Green and economic solvent systems

Due to the reasons discussed above, there is renewed interest in the use of low boiling, cost effective and greener solvent for dehydration reaction. Alcohols are the most attractive as they have better dissolution of sugars and some of them are renewable since they can be derived from biomass. Additionally they are cost effective and environmental friendly. All these potential benefits qualify them to be used as a solvent for sugar dehydration. Bicker *et al* [51] carried out fructose dehydration in supercritical methanol at 180-240 °C, 15-35 MPa using 10 mmol $H_2SO_4$ as catalyst and obtained 78% yield of 5-methyoxymethyl 2-furfural (MMF) in 2-30 s. Lai *et al* tested the dehydration reaction in alcohol medium by using variety of alcohols like methanol, ethanol, 1-propanol, 2-propanol, 1-butanol; catalyzed by HCl (5 mol%). With 2-propanol, they attained 87 % yield of HMF at 120 °C in 3 h. Other alcohols gave a mixture of HMF-ether & HMF. Use of solid acid catalyst (Amberlyst-15) in 2-propanol resulted in lower yields, though catalyst and solvent were recyclable, while HMF could be recovered by simple distillation of solvent [52]. Similar observations were made by Chernyak *et al* [53] who employed lower temperatures for fructose dehydration in alcohols. Instead of HMF, its ethers were the dominant product (60-66% yield) when the reactions were conducted at 80–90 °C in 1-butanol using $H_2SO_4$ as catalyst (1.8 M). Interestingly, Liu *et al* were able to achieve good yields in ethanol with several ammonium salts and metal halides. With $NH_4Cl$ as the catalyst, HMF yield was 71% with the reaction being conducted at 100 °C [54]. Currently, carbohydrate dehydration in alcohols as reaction medium have gained immense attention [55, 56].

Apart from alcohols various other low boiling solvents were used as reaction medium. Jeong *et al* developed a process in which high fructose corn syrup could be dehydrated to HMF in very good yields (80%) over Amberlyst-15 in 1,4 dioxane as solvent working at 100 °C in 2 h. Interesting feature of the study was solvent and catalyst recyclability [57]. Biobased solvents were explored by Dumesic's group in which a combination of Sn-beta and Amberlyst-15 were used as solid acid catalyst in solvents like GVL, THF and γ-hexalactone and got 59%, 63% and 55% of HMF yields, respectively [58]. These findings have paved the way for an efficient, cost effective and green synthesis of HMF.

### 3.2.2. Dehydration in aqueous media

Water is an environmentally benign and ideal solvent for carrying out chemical transformations. In the beginning, research was focused on the development of efficient methods for HMF production from carbohydrates in aqueous mineral acid catalyzed systems. HMF was produced from glucose [59], fructose [60] and other polysaccharides like wood chips [61] and corn starch [59] using mineral acids, organic acids and in non-catalytic systems in the temperature range of 100-300 °C while reaction time was altered from hours to seconds. But, the yields of HMF were very low (<50% even from fructose). Though the water was most economic, green and best polar solvent, it was ineffective as the product HMF was unstable in aqueous acidic conditions. Rehydration of HMF to acids and its condensation to polymeric compounds (humins) are also dominant reactions in this system. This makes HMF synthesis in aqueous medium a challenging task. Though accompanied with certain drawbacks, water always had the attention of the researchers.

Several catalyst systems including metal halides [17], organic acids [62], metal oxides [63, 64] and metal phosphates [65] were employed for the reaction. Catalyst Fe exchanged vanadyl phosphate gave the best yields of HMF (60%) at 80 °C for 1 h. However, there was no catalyst recyclability study, which is an important aspect especially in the harsh acidic reaction conditions. Yanqin *et al* reported that mesoporous niobium phosphate excelled as an acid catalyst for the synthesis of HMF from fructose in water and they got good yield of HMF (45%) owing to mesoporosity of the catalyst [66]. Yoshida *et al* executed the reaction in sub-critical water (sub-CW) with zirconium phosphate catalyst and at 240 °C in 0.033 h attained 48% yield of

HMF [67]. Recently other solid acid catalysts like silicotungstic acid, niobic acid were used as catalyst and could render ~ 50% HMF yield from fructose [68].

For dehydrating glucose mostly oxides [64] and metal salts [69] were used. But they could deliver very low yields. The best result was reported by Saha *et al* [17] in which $AlCl_3$ (50 mol%) was used as catalyst to get 40% yield under microwave irradiation (120 °C, 20 min). Similarly various polysaccharides were used as feedstocks but the yields were less (< 50% for inulin and < 20% for cellulose) [65, 70]. Excellent results were obtained by Zhao *et al* when they used Brönsted Lewis surfactant combined heteropoly acid $Cr[(DS)H_2PW_{12}O_{40}]_3$ catalyst for cellulose dehydration in water systems and achieved 53% yield at 150 °C in 2 h [71].

Though the water is an ideal solvent, even after extensive screening of many catalysts, low yield of HMF is an issue to be addressed. Low selectivity arising from decomposition to acids, difficult isolation due to high solubility in water, limits its realistic application.

### 3.2.3. Dehydration in mixed solvent systems

As discussed in previous sections, the decomposition of HMF in aqueous systems is the major problem. To overcome it, a biphasic system consisting of an immiscible organic solvent along with water was popularly employed. The HMF is dissolved in organic solvent, which prevents it from degradation leading to its enhanced yield. Dumesic's research group pioneered the synthesis of HMF in biphasic systems [72-74] by extensively studying it under various conditions. Methyl isobutyl ketone (MIBK) was used as an extracting solvent in combination with water and attained HMF yield of about 55% from fructose using HCl as catalyst. In order to increase the yields, the aqueous phase was modified by addition of salt (chloride salts were beneficial), to achieve yields up to 87%. They also used solid acid catalysts such as polymer modified silica and ion exchange resin and got good yields of HMF. Further work was carried on the modification of the organic phase by addition of co-solvents like DMSO, 2-butanol, NMP etc. Water-alcohol and water (DMSO)-$CH_2Cl_2$ were also tested and alcohol modification gave the best HMF yields (84%). Even glucose dehydration was targeted to achieve 62% HMF yield with homogeneous $AlCl_3$ catalyst [74]. Apart from all these investigations, the biggest accomplishment of Dumesic's work was further organic transformation of HMF without separating it from solvent. The HMF produced was further converted to DMF, a biofuel using

Ru/C catalyst [75]. So this approach could directly give the biofuels from fructose through the formation of HMF as intermediate and avoiding its isolation. This study was a vital one in the scenario of overcoming challenges associated with HMF isolation. Visualizing this, several other studies were undertaken in which sugars were directly converted to wider array of products using HMF as an intermediate and following its downstream conversions [76].

Biphasic systems have been extensively studied by many other research groups, while a variety of acid catalysts were tried for the conversion of glucose and fructose. Moreau *et al* [77] used H-mordenites for fructose dehydration and achieved 74% yield at 165 °C in 1.5 h in water/MIBK biphasic systems. This was followed by Nijuis *et al* who performed a comparative study of different zeolites and other solid acids to investigate the effect of acidity and pore dimensionality [78]. Zhao *et al* used Cs exchanged heteropoly acid as catalyst and obtained 74 % yield at 110 °C in 1 h under biphasic system [79]. Tantalum compounds were also investigated, Lopez *et al* used [80] acidic mesoporous tantalum phosphate catalyst and achieved 32% HMF yield from glucose at 170 °C in 1 h whereas Yang *et al* [81] used tantalum hydroxide as catalyst in water/2-butanol biphasic systems and could efficiently convert various polysaccharides in HMF (inulin gave 79% yield, artichoke juice gave 50% yield) at 160 °C in 2.5 h. Glucose dehydration was studied by Davis *et al* using Sn-beta and HCl as catalyst in NaCl modified water/2-butanol system giving 57% yield of HMF at 160 °C in 1.5 h [82]. Other solid acid catalysts used were $SO_3H$ functionalized periodic mesoporous organosilicas [83], acidic resins [74], modified mesoporous silica [84], $TiO_2$ and Taa-A380 [85], SPC-108 [81], $Ag_3PW_{12}O_{40}$ [86] etc. that gave good yields from fructose while moderate yields were obtained from glucose.

Various homogeneous catalysts were screened for the dehydration of aldose and ketoses. Omar *et al* used $AlCl_3.6H_2O$ in NaCl modified water/THF system and achieved 61% yield from glucose at 160 °C in 10 min. Other polysaccharides like maltose, cellobiose gave 20-35% yields [87]. Slightly modified system was employed by Torres *et al* where the biphasic phase consisted of water/2-sec-butyl phenol, the catalyst was $AlCl_3$, $SnCl_4$ and lanthanide chlorides. This system gave 62% yield of HMF from glucose with $AlCl_3$ at 170 °C in 40 min, while other chloride salts gave moderate yields (30-35%) [88]. Shi *et al* carried cellulose dehydration in water/THF using metal sulphate catalyst and attained 53% HMF yield at 160 °C in 1 h [89]. Recently boric and formic acid were used to catalyze this transformation. Riisager *et*

*al* used boric acid with salts in water/MIBK biphasic system and achieved 60% HMF yield from fructose at 150 °C in 0.75 h, while glucose gave low yield (14%) even after prolonged time (5 h) [90]. Jiang *et al* used formic acid in water/2-butanol system and got 69% yield at 170 °C in ~ 1 h, whereas the same catalyst was used by Hassen and Yousuf for getting high HMF yields from bio-oil [91].

Aqueous/solvent biphasic systems can potentially be deployed on a large scale, especially when they are coupled with downstream HMF conversions.

### 3.2.4. Dehydration in other systems

Various other systems like supercritical solvents; microwave heating, ionic liquids *etc* have been explored for carbohydrate dehydration. Important accomplishments using supercritical solvents and microwave heating were described earlier, hence this section mainly focuses on dehydration using ionic liquids.

#### 3.2.4.1 Dehydration in ionic liquids

There has been tremendous interest in ionic liquids (IL) for effective biomass transformations to chemicals and fuels. Ionic liquids can be defined as salts that are liquid below 100 °C and exhibit unique characteristics like non flammability, high thermal stability, negligible vapor pressure and numerous structural variations. Geyas and Fayet were the first to use pyridinium chloride based ionic liquid for dehydration of fructose [92]. However, the work of Moreau *et al* ignited the renaissance in carbohydrate dehydration with IL's. They used 1-butyl-3-methylimidazolium tetrafluoroborate ([BMIM]$BF_4$) as reaction medium and Amberlyst-15 as catalyst for fructose dehydration achieving 52% yield at 80 °C in 3 h. When DMSO was used as a co-solvent, the yield improved to 87% [93]. This was followed by using a Brönsted IL methylimidazolium chloride [HMIM]Cl as reaction medium and catalyst which gave > 90% of HMF [94]. These findings paved the way for employing only acidic ILs as reaction medium as well as catalyst. In this context choline chloride, ammonium and immadazolium salts were used that gave very high HMF yield (> 90%) [95-97]. Another important approach was inculcated by Lima *et al* where the addition of MIBK or toluene in the IL [EMIM]/(HSO4) resulted in a biphasic system rendering 89% yield of HMF from fructose [98].

However, targeting HMF from glucose and other polysaccharides require the addition of active sites with the ILs. Therefore various Cr salts were used in different

IL's which was found to catalyze the glucose dehydration efficaciously. Zhao *et al* used $CrCl_2$ as catalyst in [EMIM]Cl attaining 65% HMF yield at 100 °C in 3 h [99]. For the same system, addition of N-heterocyclic carbene as ligands raised the yields to 81% [100]. Cellulose dehydration was also performed in ILs with Cr salts with altered conditions and impressive yield (50%) was obtained [101]. Other polysaccharides like starch, cellobiose, sucrose and pine wood also gave good yields in similar systems [102]. Since then various chromium nanoparticles, other salts and solid chromium catalyst have been extensively used for saccharide dehydration [103].

Other catalyst systems have been used with various ILs encompassing homogeneous salts and acids, heterogeneous oxides, resins, functionalized materials, zeolites, heteropoly acids etc. Informative reviews by Riisager [104] and Teong [105] gives a detailed account of results in carbohydrate dehydration using ILs, reflecting their scope and potential. However higher cost, mass transfer limitations, high HMF solubility in IL's poses major obstacles for their wide spread utilization.

Thus, it may be visualized that HMF synthesis has been explored in various media using variety of catalysts. However, to use heterogeneous catalysts, it is of prime importance to envisage the type and nature of acidic sites responsible for selective formation of HMF. Moreover, insights into the role of various acid sites are not furnished much in the literature. Hence, aim of the present thesis is to explore various aspects of acidity in the dehydration of fructose to HMF in biphasic solvent medium. The results of this chapter are divided into two parts. Part-3A deals with the dehydration of fructose to HMF using AlSBA-15 catalysts, while part-3B deals with the dehydration of fructose over clay catalysts.

## 3.3. Part 3A: Dehydration of fructose to HMF over ordered AlSBA-15 catalysts

During the last two decades, mesoporous materials have been investigated as catalysts or catalyst supports for many reactions, as the mesoporosity is found to be beneficial, especially when reactant or product molecules are bulky [106]. In addition to the mesoporosity, moderate acidity with their good thermal stability, offers further possibilities for designing more efficient and environmental friendly catalysts for the production of HMF. Visualizing this potential, we have explored Al incorporated SBA-15 for the dehydration of fructose to HMF. Aluminium was incorporated into SBA-15 by post synthesis methods. The acidity was tuned by varying the Al content in the sample to study its influence on the reaction. The synthesized materials were

subjected to detailed characterization to help in understanding the reactivity and selectivity/yield during dehydration of fructose. Various process parameters were also optimized for the dehydration reaction with an aim to improve the HMF selectivity and yield. Attempt was made to correlate the acidity with HMF yield.

### 3.3.1. Experimental procedures

#### 3.3.1.1. Materials

Fructose, glucose, sucrose, maltose, MIBK, 25% $NH_3$ solution, $ZrOCl_2.8H_2O$, dodecatungstophosphoric acid (hereafter TPA) and toluene were purchased from Loba Chemie Pvt. Ltd., $AlCl_3$, tetraethyl orthosilicate (TEOS) and poly(ethylene glycol)-block-poly(propylene glycol)-block-poly(ethylene glycol) (average molecular weight, 5800), were procured from Sigma-Aldrich, USA. Zeolites $NH_4^+$-mordenite (Si/Al=10) and $NH_4^+$-beta were (Si/Al=19) obtained from Zeolyst International, USA. These were calcined at 450 °C for 4 h in air flow before used for the reaction. The synthesis of AlSBA-15 with varying Si/Al ratio is described in Section.2.2.1.

#### 3.3.1.2. Catalytic activity

The dehydration reaction was carried out using 300 mL Parr (SS 316) autoclave that has a teflon liner. In a typical reaction, 1g of fructose was dissolved in 10 mL of Millipore water, to which 50 mL of MIBK and required amount of freshly activated catalyst were added. The closed vessel was purged with nitrogen and the reaction was conducted at the desired temperature. At the end of the reaction, the aqueous phase was filtered using nylon 0.22 μm filter and the filtrate was analyzed using HPLC, equipped with RI detector and $H^+$ Aminex column (305 mm × 7.8 mm) with 0.1% $H_3PO_4$ as the mobile phase at a flow rate of 0.6 $mL.min^{-1}$. The organic phase was analyzed by Varian 3800 GC, equipped with flame ionization detector (FID) and HP-5 capillary column (50 m × 0.32 mm × 1.05 μm film thickness). The products were identified by GC-MS and compared with authentic standards.

### 3.3.2. Result and discussion

#### 3.3.2.1. Catalyst characterization

##### 3.3.2.1.1. X-ray diffraction (XRD)

The XRD powder pattern of the AlSBA-15 (Si/Al = 10, 20, 30 and 40) samples are shown in Fig. 3.1. These consist of three well resolved peaks in the 2θ

range of 0.8-1.8°, which are similar to those recorded for SBA-15 in literature [107]. The presence of one strong reflection of (100) plane at 2θ = 0.8 and two weaker reflections of (110), (200) at higher 2θ are associated with the p6mm hexagonal symmetry in the materials. The similarity in XRD pattern of AlSBA-15 and SBA-15 clearly shows that with the post modification (alumination), no perturbation of the hexagonal mesoporous structure occurred. In addition, the XRD profiles do not show any other phase or amorphous material.

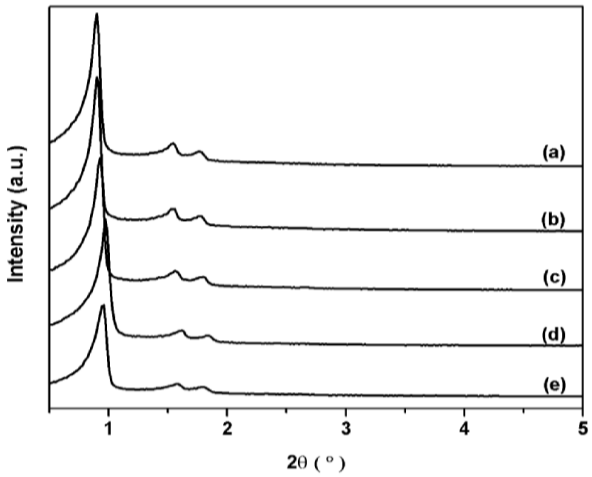


**Fig. 3.1.** XRD of (a) AlSBA-15 (Si/Al=10), (b) AlSBA-15 (Si/Al=20), (c) AlSBA-15 (Si/Al=30), (d) AlSBA-15 (Si/Al=40) and (e) SBA-15.

### 3.3.2.1.2. Surface area

Textural characteristics of the catalyst materials such as surface area, pore volume and pore size distribution were obtained from $N_2$ adsorption, these results are given in Table 3.1. The adsorption–desorption isotherms are given in Fig. 3.2.

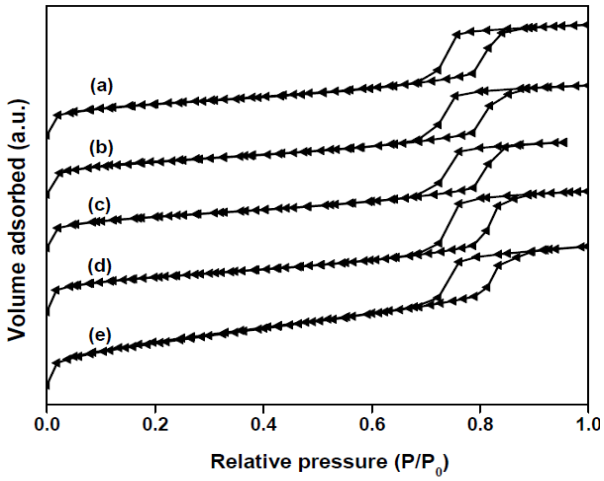


**Fig. 3.2.** $N_2$ adsorption and desorption isotherm of (a) AlSBA-15 (Si/Al=10), (b) AlSBA-15 (Si/Al=20), (c) AlSBA-15 (Si/Al=30), (d) AlSBA-15 (Si/Al=40) and (e) SBA-15.

All isotherms are of type IV and exhibit a H1-type broad hysteresis loop. The presence of large mesopores is confirmed from the sharp steep rise at a relative pressure ($P/P_0$) of 0.63–0.9, for all isotherms due to the capillary condensation of $N_2$ within mesopores where the $P/P_0$ position of the inflection point is correlated to the diameter of the mesopore. The SBA-15 has high surface area (808 $m^2g^{-1}$), with an average mesopore size of 60.5 Å (calculated using Kelvin equation). The surface areas and the pore volumes of aluminium containing samples were lower than the parent SBA-15. The pore volume also decreased with increasing Al content, probably due to presence of non-framework Al species as evidenced by $^{27}$Al NMR results.

**Table 3.1:** Textural-physiochemical properties of catalysts in fructose dehydration.

| Catalyst | Si/Al[@] | S.A. ($m^2$/g) | P.D. (Å) | P.V. (cc/g) | Acidity (mmol/g) | Fruct. conv. (mol %) | HMF Yield (mol%) | HMF Sel. (%) |
|---|---|---|---|---|---|---|---|---|
| SBA-15 | - | 808 | 60.5 | 0.870 | 0.002 | - | - | - |
| Al-SBA15 (Si/Al=10) | 19 | 549 | 53.7 | 0.727 | 0.267 | 68 | 40 | 59 |
| Al-SBA15 (Si/Al=20) | 42 | 560 | 54.1 | 0.703 | 0.243 | 65 | 42 | 65 |
| Al-SBA15 (Si/Al=30) | 58 | 541 | 53.9 | 0.685 | 0.188 | 63 | 49 | 78 |
| Al-SBA15 (Si/Al=40) | 65 | 611 | 60.1 | 0.784 | 0.147 | 59 | 52 | 88 |
| H-Beta | 19 | 632 | 5.7x7.5 6.5x 5.6 | - | 0.796 | 94 | 45 | 48 |
| | | | | | | 62[*] | 31 | 50 |
| H-Mord. | 10 | 490 | 6.5x7.0, 2.6x5.7 | - | 1.380 | 79 | 39 | 49 |
| | | | | | | 61[+] | 32 | 52 |
| H- ZSM5 | 23 | 350 | 5.4x5.6 5.5x5.1 | | 0.570 | 70 | 28 | 40 |
| | | | | | | 58[#] | 24 | 41 |
| 15TZ750 | - | 53 | - | - | 0.290 | 84 | 24 | 28 |
| | | | | | | 63[+] | 19 | 30 |

[@]determined by ICP-OES.

Reaction conditions: Fructose = 1 g (in 10mL water), temperature = 165 °C, catalyst = 0.15 g, water : MIBK= 1: 5 (v/v), reaction time = 1 h, RPM = 500.
[*] time = 35 min, [+] time = 45 min, [#] time = 50 min.

Legend: S. A. = surface area, P. D. = pore diameter, P. V. = pore volume, Fruct. conv. = fructose conversion, Sel. = selectivity, H-Mord. = H-Mordenite.

The presence of these extra framework species also leads to the reduction in surface area. However, no particular trend was observed in the variation of surface area values, which are in accordance with earlier findings [108].

### 3.3.2.1.3. Electron microscopy

The morphology of samples obtained using SEM is shown in Fig. 3.3. The rope like morphology of the parent SBA-15 is retained even after alumination. All the AlSBA-15 samples with varying Si/Al ratio retain the morphology indicating that morphology remains unchanged with variation in the Al content.

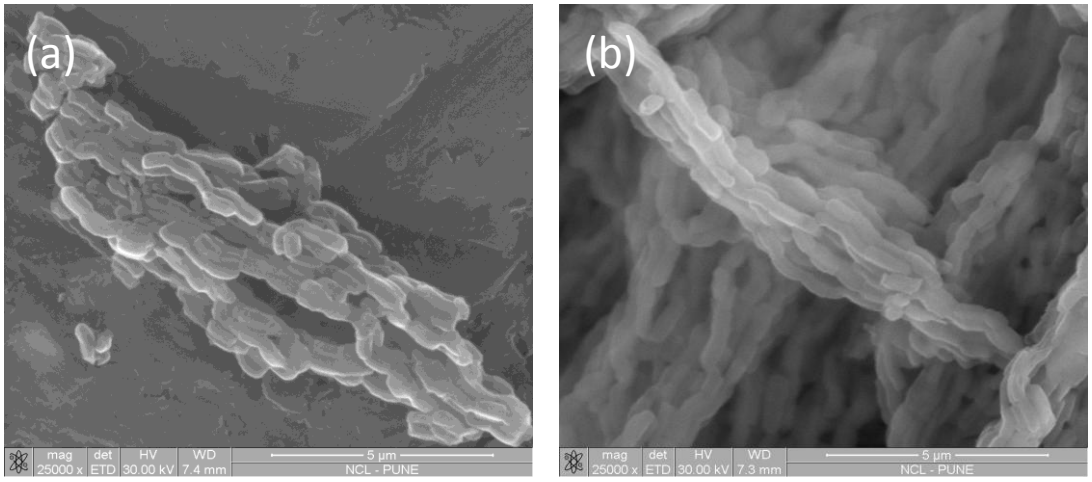


**Fig. 3.3.** SEM of (a) AlSBA-15 (Si/Al=10) and (b) AlSBA-15 (Si/Al=40)

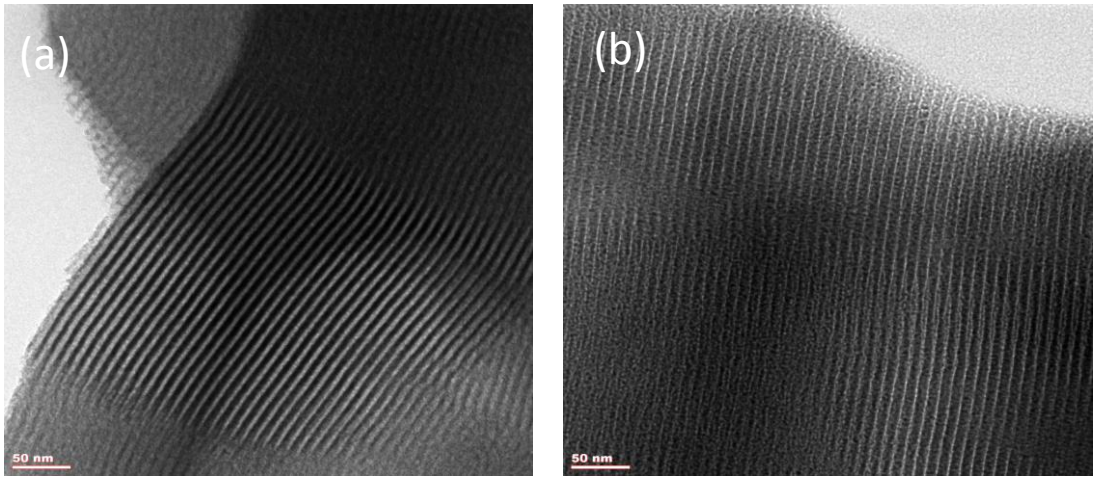


**Fig. 3.4.** TEM of (a) AlSBA-15 (Si/Al=10) and (b) AlSBA-15 (Si/Al=40).

### 3.3.2.1.4. TPD of $NH_3$

The acidity of the AlSBA-15 samples was determined by TPD of $NH_3$. The TPD profiles of the samples with different Si/Al ratios are given in Fig. 3.5. The total

acidity of materials is expressed in mmol.g$^{-1}$ of desorbed $NH_3$ under each temperature maximum and these values are listed in Table 1. All AlSBA-15 samples show two peaks, one pertaining to weak acidity (100-250 °C) and the other to moderately strong acidity (250-400 °C). With the decrease in the Si/Al ratio (or increasing aluminium content) from 40 to 10, the total acidity, in terms of ammonia desorbed, increased from 0.147 to 0.267 mmol.g$^{-1}$. This shows that the acidity increased with aluminium content. The parent mesoporous SBA-15 has very weak acidity due to the presence of surface silanol groups. However, this acidity is very low as compared to aluminium containing AlSBA-15 samples, suggesting the formation of acid sites on post modification with aluminium. Thus, the total acidity is dependent on the amount of aluminium present in the samples, but the acidity did not increase linearly with aluminum content, particularly in the higher aluminium containing samples.

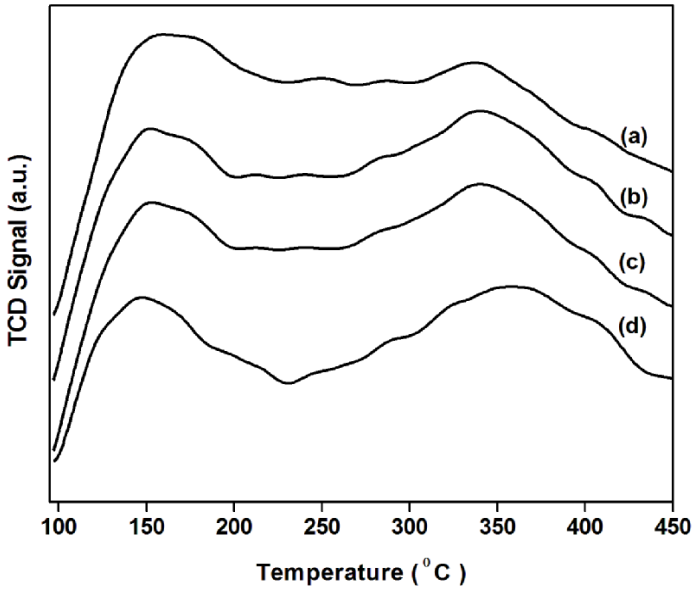


**Fig. 3.5.** TPD of (a) AlSBA-15 (Si/Al=10), (b) AlSBA-15 (Si/Al=20), (c) AlSBA-15 (Si/Al=30) and (d) AlSBA-15 (Si/Al=40).

### 3.3.2.1.5. $^{27}$Al Magic angle spinning nuclear magnetic resonance

Solid state $^{27}$Al MASNMR is an excellent technique to probe the local environment of aluminium. The spectra of the AlSBA-15 samples (Fig. 3.6) show two peaks; one peak at 53 ppm is indicative of aluminium in tetrahedral coordination, in which it is covalently bound to four Si atoms via oxygen bridges and the other peak at nearly 0 ppm is attributed to octahedrally coordinated aluminium species in extra framework positions [109]. With the decreasing Si/Al ratio (increasing Al content),

higher proportion of aluminium is substituted in the octahedral coordination, suggesting lower incorporation of Al into the tetrahedral framework and the presence of extra framework/non-framework species at higher Al loadings. It is expected that only tetrahedral Al generates Brönsted acid sites [110]. Hence, $^{27}$Al MASNMR results show that the acidity is not expected to increase linearly with Al content. The TPD of $NH_3$ results confirm this aspect.

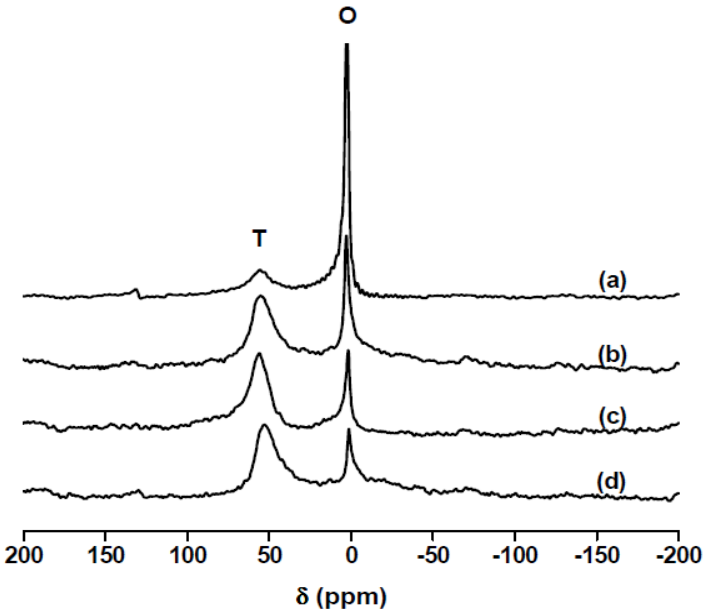


**Fig. 3.6.** $^{27}$Al MAS NMR spectra of (a) AlSBA-15 (Si/Al=10), (b) AlSBA-15 (Si/Al=20), (c) AlSBA-15 (Si/Al=30) and (d) AlSBA-15 (Si/Al=40).

### 3.3.2.1.6. FTIR of chemisorbed pyridine

Infrared spectroscopy of adsorbed pyridine is a well established tool for investigating the nature of acid sites of various solid acid catalysts. Apart from acid strength, it is important to investigate the nature of acid sites since these can alter the extent of polarization of a given bond in the reactant molecule and is a decisive factor for the type of reaction catalysed by the solid acids. The Brönsted and Lewis acidity of AlSBA-15 samples has been monitored by the bands in the range of 1350–1600 $cm^{-1}$ arising from its ring vibration modes of pyridine. The characteristic absorption band for Brönsted acidity(B) appeared at 1540 $cm^{-1}$, for Lewis acidity (L) appeared at 1450 $cm^{-1}$ and the band at 1490 $cm^{-1}$ is due to Brönsted and Lewis acidity (B+L) [111]. The spectra recorded after outgassing at 200 °C is shown in Fig. 3.7. All the samples exhibited the three characteristic adsorption bands. The intensities of the B and L peaks were taken into account for calculating the ratios. The B/B+L ratio is

found to be 0.459, 0.465, 0.526 and 0.545 for Si/Al ratio 10, 20, 30 and 40, respectively. This increase can be attributed to decreasing octahedral aluminium species from Si/Al ratio 10 to 40, as witnessed by $^{27}$Al MAS NMR studies.

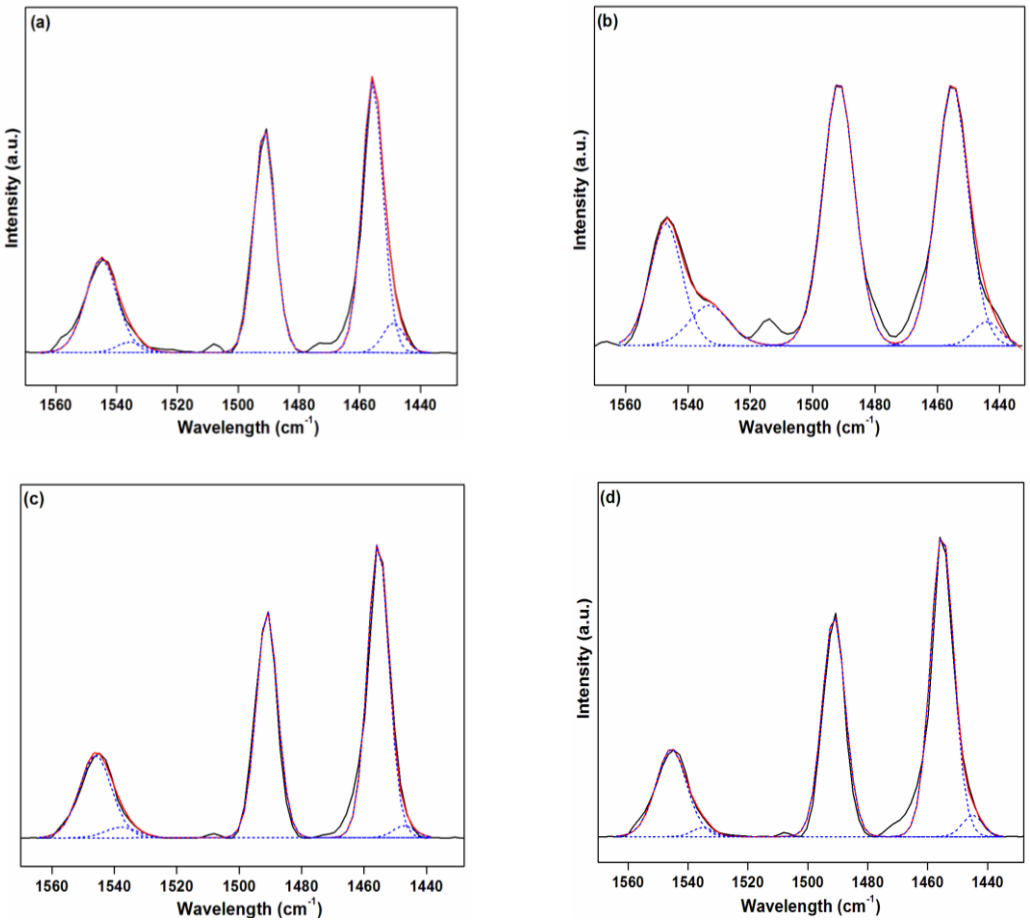


**Fig. 3.7.** FTIR pyridine adsorption of (a) AlSBA-15 (Si/Al=10), (b) AlSBA-15 (Si/Al=20), (c) AlSBA-15 (Si/Al=30) and (d) AlSBA-15 (Si/Al=40).

### 3.3.2.2. Catalytic activity in dehydration of fructose

The dehydration of fructose to HMF was used for testing the catalytic activity and selectivity of various catalysts. This reaction can yield numerous products (Scheme 3.1), but we had targeted for high HMF yield/selectivity. The results of the catalytic activity are given in Table 1. We have used three zeolites for this reaction, namely H-beta (Si/Al = 19), H-ZSM-5 (Si/Al = 23) and H-mordenite (Si/Al = 10), the later is reported to be selective for HMF in biphasic conditions [77]. Under the reaction conditions employed, the highly acidic zeolites demonstrated high fructose conversion (94, 79 and 70 mol% for beta, mordenite and ZSM-5, respectively) but gave lower selectivity for HMF (40–50%). The higher conversion on H-beta can be attributed to its stronger acidity and three dimensional pore structure. Mordenite has

two dimensional pore system with 12-membered ring large pores and 8-membered ring small pores, while H-beta has three dimensional pore system with all 12-membered ring large pores [112]. This along with smaller crystallite size of H-beta facilitates easier diffusion of reactants/products, leading to high conversion of fructose. Though ZSM-5 has three dimensional pore structure along with strong acidity, its medium size pores may be responsible for lower conversion. Moreover, selectivity and yields are affected because of strong acidity and confinement of reactants/products in the medium pores of the zeolite for longer duration. Even, increasing the stirring speed from 500 to 800 RPM had only a marginal effect with the conversion increasing from 70 to 73 mol%.

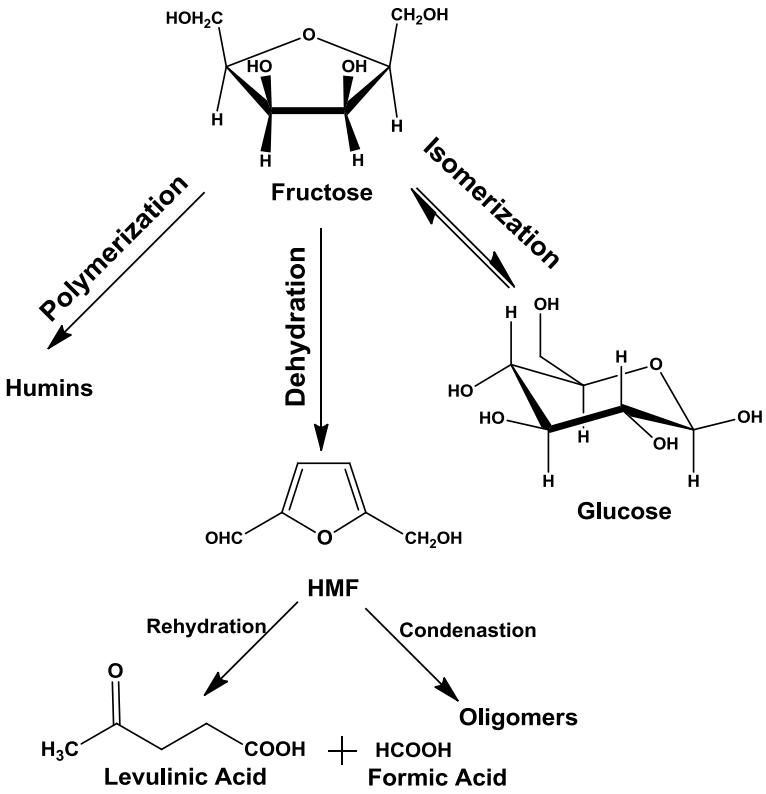


**Scheme 3.1.** Dehydration of C-6 sugars to HMF.

The results of the catalytic activity of zeolites are in good agreement with the earlier findings which shows that targeted furan compounds undergo humin formation in the intrazeolitic channels thus lowering its yield [113]. Hence, the poor efficiency of zeolites can be attributed to their strong acidity and local constraints within the pore system. In contrast, the mesoporous materials have weaker acidity than zeolites, but gave superior catalytic performance. In order to thoroughly investigate the

superiority in catalytic activity of mesoporous AlSBA-15, the activity of other catalysts was compared at similar conversion as that of AlSBA-15 (Si/Al = 40) and results are shown in Table 1. In case of zeolites, HMF yield was poor even at lower conversion levels compared to mesoporous catalysts. The inferior performance of zeolites is attributed to strong acidity as it has been observed that heterocyclic molecules specifically interact with Brönsted acid sites strongly and undergo oligomerization in the zeolitic channels [114]. Whereas, weaker acidity of AlSBA-15 prevents further reaction of the product furan, resulting in enhanced selectivities leading to higher HMF yields. On the other hand, when 15TZ750 (tungstated zirconia) is employed as catalyst, fructose conversion and HMF yield were 84 mol% and 24 mol% respectively, while HMF selectivity was only 28%. At lower conversion (62 mol%) the selectivity was almost the same. This shows that surface acidity has to be optimum for attaining good HMF yield/selectivity. The superiority of the AlSBA-15 catalysts with tunable acidity can be inferred from the results.

For the AlSBA-15 with varying Si/Al ratio, the conversion of fructose decreased from 68 to 59 mol% with increasing Si/Al ratio, but the HMF yield increased from 40 to 52 mol%. The decrease in conversion and increase in yields are a result of improved selectivity from 59% to 88%. The fall in conversion is a result of decrease in total acidity as a result of less Al content with increasing Si/Al ratio of the catalyst samples. The increase in HMF yield/selectivity is connected to the non-framework Al at higher Si/Al ratio (as evident from $^{27}$Al MAS NMR profile). It is known that non-framework aluminium cations in porous materials acts as Lewis acid centers [115-117], which accelerate the formation of humins from the carbohydrate and furan compounds [113], thereby reducing the HMF yield/selectivity. Yield of HMF was plotted against acidity for understanding the role of acidity on the reaction. Fig. 3.8 shows plot of total acidity against fructose conversion and HMF yield. The plot clearly shows that though the conversion increased with total acidity, yield of HMF follows exactly opposite trend. To understand the variation of HMF yield with weak and strong acidity, these were plotted against HMF yield as a ratio to total acidity, as given in Fig. 3.9. It is interesting to see that HMF yield increased against moderately strong acidity/total acidity ratio showing that moderately strong acidity contributes to higher formation of HMF (Fig. 3.9b). On the other hand, against weak acidity/total acidity ratio (Fig. 3.9a), it follows opposite trend. This clearly shows that high acidity and weaker acid sites do not aid HMF formation, though the higher

acidity leads to increased fructose conversion. For proper elucidation of nature of acid sites, HMF yield was also plotted against B/B+L ratio (Fig. 3.10). A good linear graph was obtained between the two parameters clearly showing that higher ratio of Brönsted sites favour HMF formation in biphasic medium. Among the samples investigated, AlSBA-15 (Si/Al = 40) showed maximum HMF yield/selectivity. Hence, it was used for further optimization of reaction conditions.

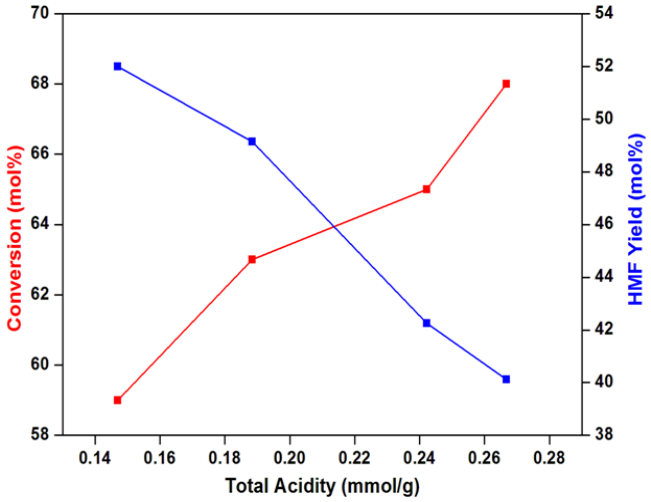


**Fig. 3.8.** Effect of total acidity on fructose conversion and HMF yield.

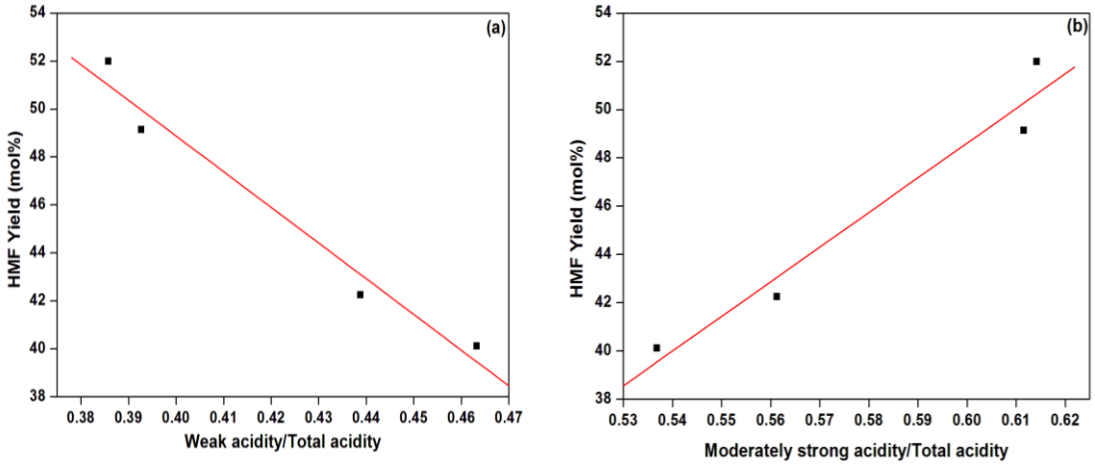


**Fig. 3.9.** HMF yield vs. (a) weak acidity/total acidity ratio , (b) moderately strong acidity/total acidity ratio.

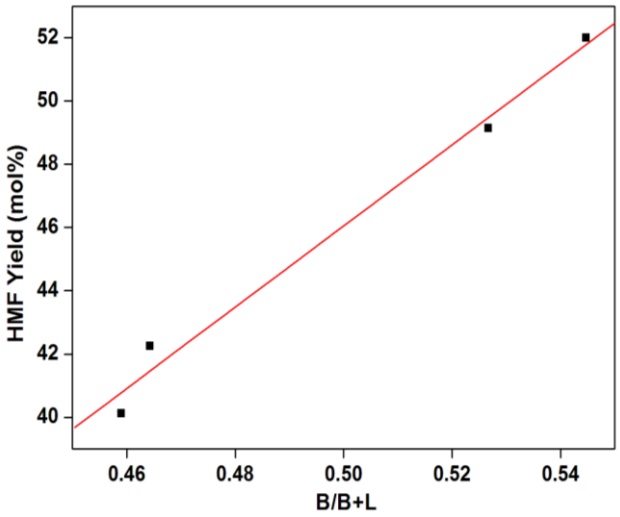


**Fig. 3.10.** HMF yield vs. B/B+L ratio.

### 3.3.2.2.1. Effect of temperature

The liquid phase dehydration of fructose with AlSBA-15 (Si/Al =40) was studied by varying the reaction temperatures in the 155-185 °C range; the results are shown in Fig. 3.11. Increasing temperature from 155 to 185 °C, leads to rise in fructose conversion from 59 to 91 mol%, respectively. However, the HMF yields increase from 20 to 52 mol% with the increase in temperature from 155 to 165 °C and remained constant thereafter. Therefore, 165 °C was considered as optimum temperature. Since there was an increase in fructose conversion but not the HMF yield, it is expected that the reactant undergoes unwanted side reactions at higher temperatures. For proper understanding of the effect of temperature on the complex reaction pathway, the product distribution was evaluated. The product distribution shows that at higher temperature, selectivity to HMF decreased from 88 to 54%, whereas selectivity to the formation of other compounds (mostly humins) has increased (Scheme 1). Additionally, very low levulinic acid (LA) selectivity was seen (< 5%); as MIBK suppresses the rehydration of HMF [118]. Furfural which can be obtained by decarboxylation of HMF [77] was almost insignificant. At higher reaction temperatures the colour of the reaction mixture darkened, which may be attributed to the presence of soluble oligomers. Thus it can be concluded that at higher reaction temperatures, in presence of MIBK, formation of humins and oligomerization (i.e. the condensation reaction) is dominant among the other side reactions.

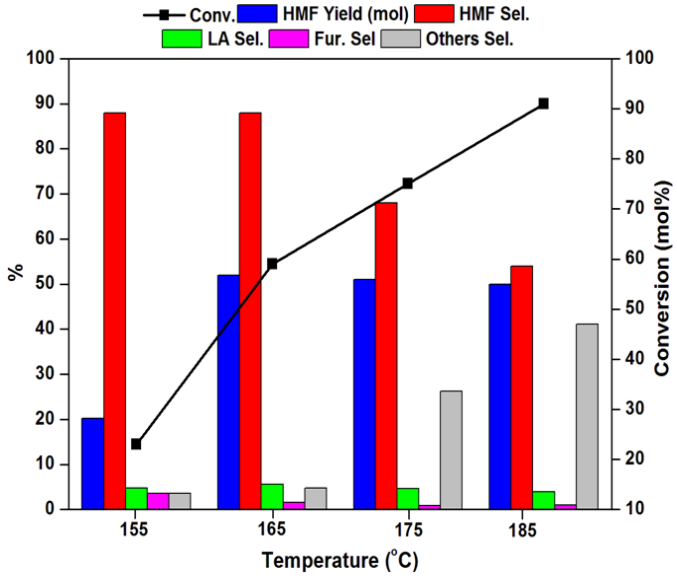


**Fig. 3.11.** Effect of temperature on dehydration of fructose.

Reaction conditions: Fructose = 1 g (in 10 mL water), catalyst = 0.15 g, water : MIBK = 1 : 5 (v/v), time = 1 h, RPM = 500.

### 3.3.2.2.2. Effect of catalyst content

The effect of catalyst content on fructose dehydration is shown in Fig. 3.12. It was observed that when the catalyst amount increased from 7.5 to 30 wt%, the fructose conversion increased from 33 to 77 mol%. Whereas, the HMF yield increased from 29 to 52 mol% with the increase in catalyst amount from 7.5 to 15 wt%, but remained constant on further increase in catalyst content. By observing the

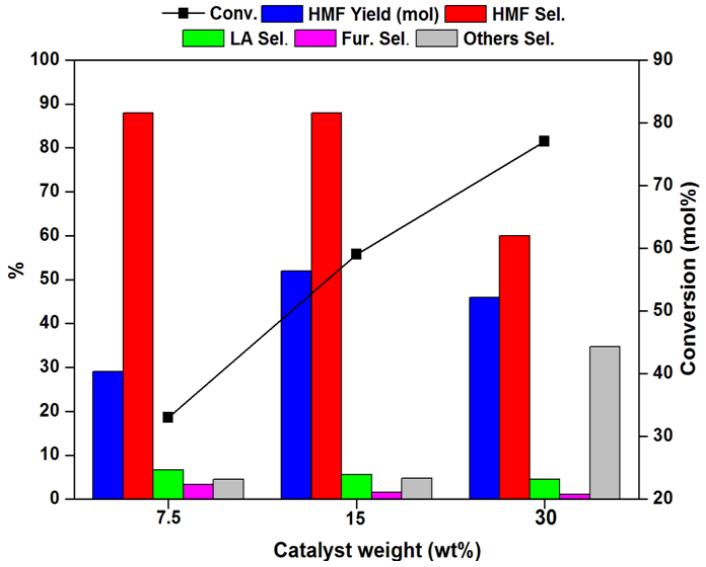


**Fig. 3.12.** Effect of catalyst content on dehydration of fructose.

Reaction conditions: Fructose = 1 g (in 10 mL water), temperature = 165 °C, water : MIBK= 1: 5 (v/v), time = 1 h, RPM = 500.

product distribution, it can be deduced that the HMF selectivity of 88% was constant up to a catalyst weight of 15 wt%, which then decreased with further increase in catalyst content. The increase in conversion is attributed to increase in the number of active sites; while the availability of more active sites drives the reaction towards more condensed products (due to enhanced selectivity of others). Furfural and LA are not formed in significant quantities clearly demonstrating that availability of more active sites favors the condensation reactions, decreasing the selectivity of HMF. From this study, 15 wt% of catalyst was found to be optimal for this reaction.

### 3.3.2.2.3. Effect of solvent

The effect of solvent on the reaction was investigated by using different polar and non-polar solvents. The results are shown in Fig. 3.13.

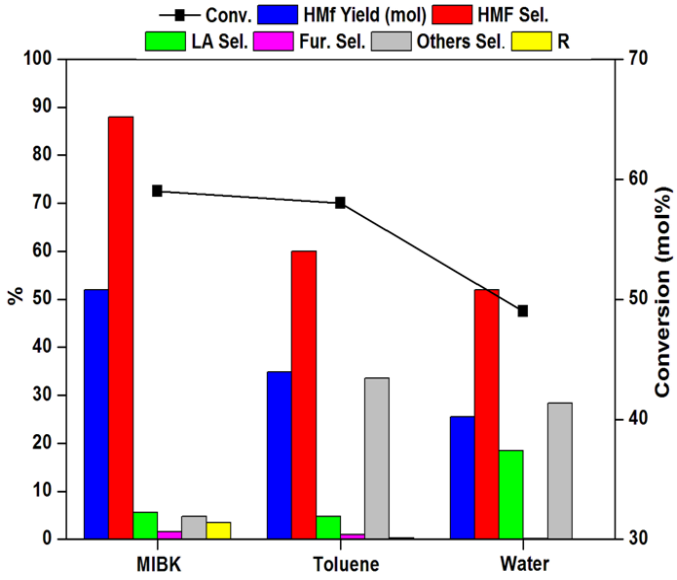


**Fig. 3.13.** Effect of solvent on dehydration of fructose.

Reaction conditions: Fructose = 1 g (in 10 mL water), temperature = 165 °C, catalyst = 0.15 g, water : organic solvent = 1: 5 (v/v), time = 1 h, RPM = 500.

The fructose conversion is almost same for MIBK and toluene (59 and 58 mol%, respectively), however in water the conversion of fructose was lower (49 mol%), as water is a polar solvent and a Lewis base, it has high affinity for the active acidic sites leading to blockage of acid sites thereby reducing conversion. Among the various solvents MIBK gave maximum HMF yield and selectivity (52 mol% and 88%) since its polar nature maximizes the dissolution of HMF. Lower yield of HMF was obtained in water (25 mol%) and toluene (35 mol%). Water being most polar

solvent offers less HMF selectivity (52%) and more LA (18.5%) demonstrating that rehydration of HMF to LA is dominant in water. With toluene, more of insoluble humins and soluble oligomers were obtained as the selectivity of others increased. The values of extraction coefficient R = $HMF_{org}/HMF_{aq}$ is 3.2, 0.236 and 0 for MIBK, toluene and water, respectively, revealing that MIBK is the most efficient extracting solvent as HMF is rapidly dissolved in it [119].

### 3.3.2.2.4. Effect of time

The effect of reaction time on fructose conversion and product yields was also investigated. The results are shown in Fig. 3.14. It may be seen that with the increasing time of reaction from 0.5 to 2 h, fructose conversion increased from 44 to 86 mol%, whereas the HMF yield increased from 38 to 52 mol% in the first hour of reaction, which has decreased marginally on further increasing the reaction time.

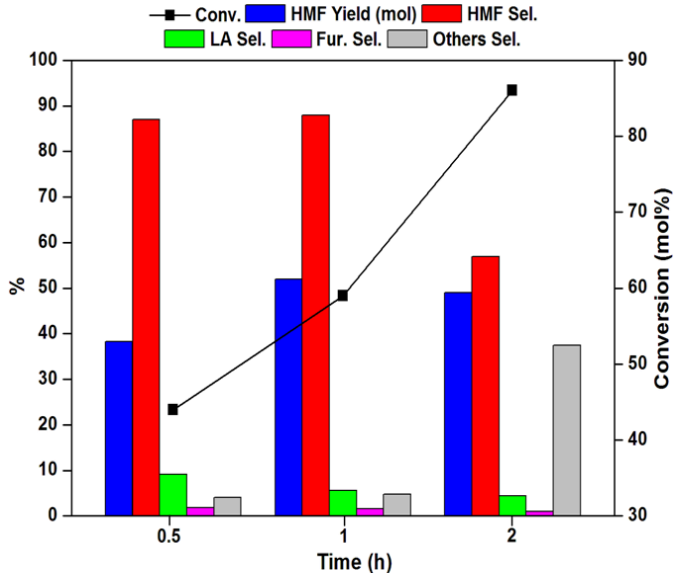


**Fig. 3.14.** Effect of time on dehydration of fructose.

Reaction conditions: Fructose = 1 g (in 10 mL water), temperature = 165 °C, catalyst = 0.15 g, water : MIBK = 1: 5 (v/v), RPM = 500.

Hence, 1 h of reaction time was considered as optimum. The product distribution shows that HMF selectivity decreased from 88 to 57% with the increasing time, while the selectivity to other byproducts increased (4.1 to 37.4 %). This shows that with increasing duration of the reaction, the HMF formed either degraded or undergoes further condensation reactions leading to a reduction in selectivity.

### 3.3.2.2.5. Effect of saccharides

In order to assess the effectiveness of the catalyst to convert other saccharides to HMF, various carbohydrates were used for dehydration reaction, the results are compared in Fig. 3.15. It was found that fructose gave maximum yield of HMF, i.e. 52 mol%, while sucrose; a disaccharide of fructose and glucose also gave moderate yield of 25 mol%. Glucose and maltose gave lower conversion and HMF yield (~7 mol%) since the isomerization of glucose to fructose is slow over acid catalysts, it reduces the overall rate of dehydration. Thus ketose sugars can be efficiently converted to HMF, while aldose sugars scarcely yielded the furan compound.

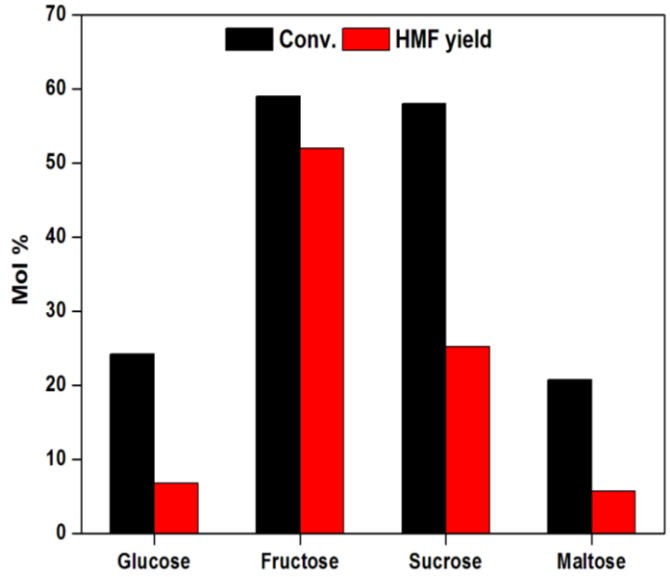


**Fig. 3.15.** Effect of saccharide on dehydration to HMF.

Reaction conditions: Sachharide = 1 g (in 10 mL water), temperature = 165 °C, catalyst= 0.15 g, $H_2O$ : MIBK= 1 : 5 (v/v), time = 1 h, RPM = 500.

### 3.3.2.2.6. Recyclability studies

To check the recyclability of the catalyst, used catalyst was calcined in air at 550 °C for 5 h in order to oxidize the carbonaceous species deposited on the catalyst (C = 13.2%, H = 1.5%, N = nil, estimated by micro analysis). The calcined (AlSBA-15, Si/Al=40) catalyst was used for the reaction that gave a fructose conversion of 51 mol% and HMF yield of 30 mol%. In order to investigate the reasons for this decrease in catalytic activity, the catalyst was subjected to $^{27}$Al MAS NMR and XRD studies, the results are shown in Fig. 3.16 and Fig. 3.17, respectively. From the NMR studies it can be seen that the peak around 0 ppm assigned to octahedral aluminium is absent,

showing the leaching of Al species. Due to leaching of tetrahedral and octahedral species, the overall catalytic activity decreased. The XRD patterns of fresh and used catalysts reveal that the peaks in the used catalyst shifted to higher 2θ values for all the three reflections indicating the structural deformation, as a result of hydrothermal treatment.

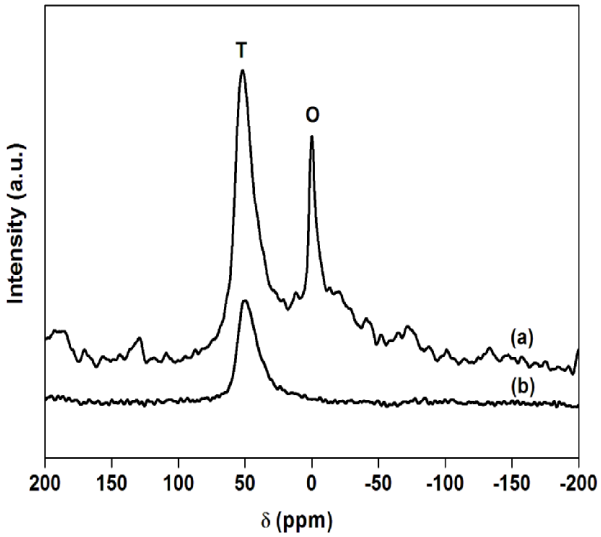


**Fig. 3.16.** $^{27}$Al MAS NMR of (a) fresh catalyst and (b) used catalyst.

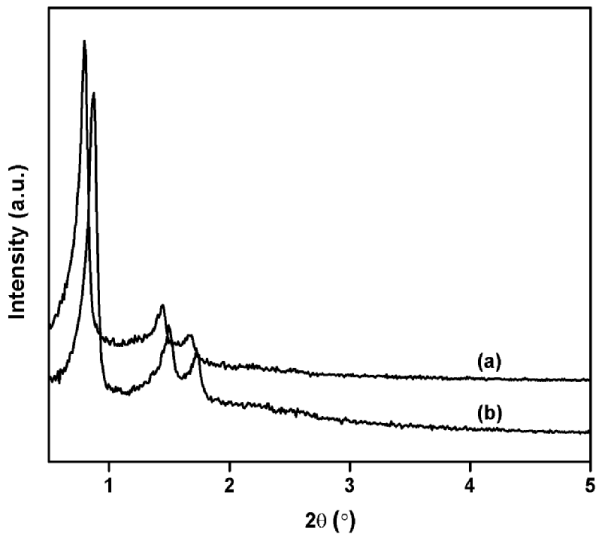


**Fig. 3.17.** XRD pattern of (a) fresh catalyst and (b) used catalyst.

When DMSO was used as solvent under these conditions, fructose conversion of 98 mol% and HMF selectivity of 76% was obtained. The used catalyst was washed with acetone, dried and used for next cycle. The results of recyclability of AlSBA-15 (Si/Al = 40) in DMSO are shown in Table 3.2. There was only a slight drop in fructose conversion; with only little change in HMF selectivity. Thus, the catalyst

could be recycled effectively up to 3 cycles without much loss in catalytic activity. These results show the usefulness of AlSBA-15 catalysts for dehydration of saccharides with DMSO as solvent. However, the recyclability of catalysts is not good when mixed solvents containing water are used.

**Table 3.2:** Recyclability studies of AlSBA-15(Si/Al =40) in DMSO

| S.N. | Recycle | Fructose conv.(mol%) | HMF Sel. (%) |
|---|---|---|---|
| 1. | - | 96 | 77 |
| 2. | 1st | 91 | 80 |
| 3. | 2nd | 80 | 75 |
| 4. | 3rd | 79 | 76 |

Reaction conditions: Fructose = 0.5 g, DMSO = 20 mL, temperature = 120 °C, catalyst weight = 0.075 g, time = 2 h, RPM = 500.

### 3.3.3. Conclusions

The selective formation of HMF, an important platform chemical has been achieved using aluminium incorporated SBA-15 catalysts. These catalysts were prepared by post synthesis method using $AlCl_3$. Pore confinement in zeolites of substrates and products formed adversely affects HMF yield/selectivity; while the mesoporosity of AlSBA-15 catalysts comes handy in overcoming these constraints resulting in enhanced yield of desired HMF. The effect of Si/Al ratio on the catalytic activity and yield was systematically investigated. A good linear correlation between the moderately strong acidity/total acidity ratio and B/B+L ratio against HMF yield was obtained. These findings demonstrate the presence of moderately strong acidity with higher Brönsted acidity in Al incorporated SBA-15 as crucial for HMF synthesis through dehydration of fructose. AlSBA-15 works truly as heterogeneous catalyst if milder reaction conditions and non aqueous solvent systems are employed.

## 3.4. Part 3B: Dehydration of fructose to HMF over clay catalysts

AlSBA-15 could effectively catalyze the dehydration of sugars to give furan compound but the challenge is to get a catalyst that is easy to prepare and also cost effective. Hence, we tried cheap and abundantly available acid treated clays for the dehydration reaction. In case of acid treated clays, the basal spacing between the octahedral aluminate and the tetrahedral silicate layers varies between 10 to 50 Å depending on the amount of occluded water in the interlamellar space. Bönsted acidity is generated by the presence of protons, terminal hydroxyl groups, bridging oxygen atoms in the layers and polarizing cations (e.g. $Al^{3+}$) present in the interlayer region. These properties make clay an efficient acid catalyst [120-122]. In addition, Al pillared clays consist of $Al_{13}$ poly-oxocations intercalated in the lamellar spaces leading to enhanced thermal stability, basal spacing, higher surface area and good acid strength. Hence, this study was aimed at employing different acid treated clays for the dehydration reaction and to investigate the synergistic effects of the acid sites and basal space of these materials for the formation of HMF.

### 3.4.1. Experimental

#### 3.4.1.1. Materials

Montmorillonite K10 was sourced from Sigma-Aldrich; while K20, K30 and Al pillared clay (ALPC) were procured from Fluka. Fructose, glucose, sucrose, maltose, MIBK, HCl and $HNO_3$ were procured from Loba Chemie Pvt. Ltd. India.

#### 3.4.1.2. Catalytic activity

The reaction method and analysis of the products is the same as described in Section 3.3.1.2.

### 3.4.2. Result and discussion

#### 3.4.2.1. Catalyst characterization

##### 3.4.2.1.1. X-ray diffraction

The structure of catalysts was investigated by powder X-ray diffraction and is shown in Fig. 3.18. The ordered lamellar structure of montmorillonites is marked by a strong reflection at $2\theta = 6.46°$, of basal d (001) [123]. This strong reflection of Al pillared clay show that this material is fairly well ordered. For the acid treated clays (K10, K20 and K30) the intensity of the reflection decreases indicating the destruction

of lamellar structure. The basal spacing of the acid treated clays is lower than that pillared clays because of the replacement of interlayer ions by protons which leads to lesser interlamellar water and decreased basal spacing. Interestingly, the basal spacing of all the acid treated clays is not altered significantly, probably due to the presence of similar interlayer ions [124]. In addition to this reflection the presence of higher order reflections at 2θ = 19.8°, 34.8° and 53.6° are also indicative of the reminiscent lamellar structure in acid activated clays. The peak at 2θ = 26.2° is attributed to α-quartz arising from the dealumination of clay on acid treatment [125,126].

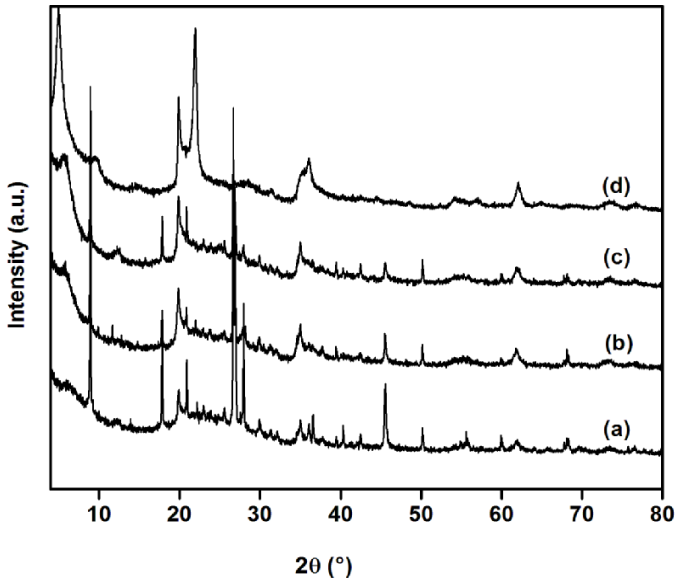


**Fig. 3.18.** XRD pattern of (a) K10, (b) K20, (c) K30 and (d) ALPC.

### 3.4.2.1.2. Chemical composition

The results of the chemical compositional analysis of various samples are given in Table 3.3. It was observed that depending on the severity of acid treatment (from K10 to K30) the amount of $Al_2O_3$ decreased from 14.4 to 11.8, while the amount of silica increased from 75.0 to 77.1 % . In case of Al pillared clays, the increase in the amount of $Al_2O_3$ is due to the presence of $Al_{13}$ polyoxo cations used as pillaring species as witnessed by $^{27}Al$ NMR studies.

**Table 3.3.** Chemical analysis of the clay samples.*

| Catalyst | Chemical Analysis (%) | | | | | | | |
|---|---|---|---|---|---|---|---|---|
| | $SiO_2$ | $Al_2O_3$ | CaO | $K_2O$ | MgO | $Na_2O$ | $Fe_2O_3$ | $H_2O^{\#}$ |
| K10 | 75.0 | 14.4 | 0.2 | 1.5 | 1.1 | 0.6 | 2.7 | 9.88 |
| K20 | 75.1 | 13.8 | 0.3 | 1.1 | 1.2 | 0.3 | 2.4 | 9.78 |
| K30 | 77.1 | 11.8 | 0.2 | 0.5 | 1.0 | 0.3 | 1.8 | 9.60 |
| ALPC | 72.4 | 20.1 | 0.2 | 0.9 | 2.5 | 0.2 | 1.8 | 12.17 |

* Determined by ICP-OES, #Determined by TGA

### 3.4.2.1.3. Surface area

The surface areas of the clay samples are shown in Table 3.4. The order of surface area was found to be K10 < K20 <K30 <ALPC. For the acid treated clays K10, K20, K30 there is an increase in surface area from 165 to 230 $m^2.g^{-1}$. The pore diameter also increased from 21.1 to 23.3 Å. This increase in surface area and pore diameter may be attributed to the generation of mesoporosity arising out of the leaching of the octahedral ions on acid activation [127]. The extent of leaching is proportional to the amount of acid [124] used, which explains the trend observed in surface area and pore diameter for acid activated clays. ALPC has a surface area of 235 $m^2.g^{-1}$ and pore diameter of 14.3 Å which is indicative of the formation of micropores after pillaring. This finding is consistent with the earlier studies that showed the formation of micropores during pillaring of montmorillonites [128].

**Table 3.4:** Physiochemical properties of clay catalysts.

| Catalyst | SA ($m^2g^{-1}$) | PD (Å) | B/B+L* | Acidity# (mmol/g) | Fruct. Conv. (mol %) | HMF Yield (mol %) | HMF Sel. (%) |
|---|---|---|---|---|---|---|---|
| K-10 | 165 | 21.1 | 0.82 | 0.20 | 80 | 61 | 76 |
| K-20 | 215 | 23.8 | 0.62 | 0.19 | 69 | 49 | 72 |
| K-30 | 230 | 25.3 | 0.57 | 0.18 | 49 | 38 | 77 |
| ALPC | 235 | 14.3 | 0.29 | - | 70 | 25 | 36 |

* determined by Pyridine IR, # Ref [129]
Reaction conditions: Fructose = 1g (in 10mL water), temperature = 165 °C, catalyst = 0.15 g, water : MIBK= 1: 5 (v/v), reaction time = 1 h, RPM = 500.

Legend: SA = surface area, PD = pore diameter, Fruct. conv. = fructose conversion, Sel. = selectivity, ALPC = Aluminium pillared clay.

### 3.4.2.1.4. $^{27}$Al MAS Nuclear magnetic resonance

The $^{27}$Al MASNMR spectra are shown in Fig. 3.19., all the clay samples show two resonances ~ 0 ppm and ~ 67 ppm accompanied by spinning side bands. The signal at ~ 0 ppm is attributed to Al ions in octahedral symmetry which is due to presence of Al in octahedral sheet of clay or alumina impurities. The signal at ~67 ppm is attributed to Al in tetrahedral symmetry. Usually the signal for tetrahedral Al is around ~54 ppm in zeolites, however the signal is slightly at lower field for acid treated montmorillonite [130]. Thus, for K10, K20, K30, the presence of Al in octahedral symmetry is the evidence of remaining 2:1 montmorillonite structure which corroborates with the XRD findings. The presence of Al in tetrahedral symmetry supports the dehydroxylation phenomena arising from the acid treatment [123]. For Al pillared clay also two peaks pertaining to tetrahedral and octahedral Al are observed, with the latter being most intensive. The presence of Al in both the coordination can be explained by the structure of $Al_{13}$ polyoxo cation as the pillaring species. Plee *et al* [131] have proved the structure of the cation to be a Keggin type tridecamer $[AlO_4Al_{12}(OH)_{24}(H_2O)_{12}]^{+7}$ using NMR techniques which shows the presence of Al in both coordination, supporting the observations of the present studies.

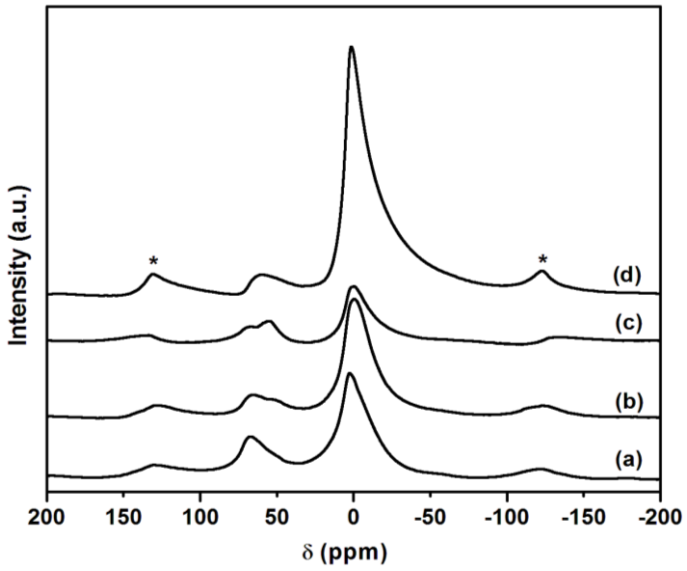


**Fig. 3.19.** $^{27}$Al MAS NMR of (a) K10, (b) K20, (c) K30 and (d) ALPC.

### 3.4.2.1.5. $^{29}$Si Nuclear magnetic resonance

$^{29}$Si MASNMR is an excellent tool for probing the structural changes as it is sensitive to environment of atoms even for short range ordering. The acid treatment at higher temperatures induces some surface modification in the clays which can be easily probed by this technique. The spectra (Fig. 3.20) of all the acid treated clays (K10, K20, K30) show three resonances around -110 ppm, -100 ppm and -94 ppm. The signal at ~94 ppm is associated with silicon atoms occupying the tetrahedral lattice layer and are coordinated *via* oxygen to three other silicon atoms in the same layer plus a fourth atom (usually aluminium, but also hydrogen, magnesium and iron) in the central, octahedral lattice layer, which is the characteristic peak of lamellar structure [123, 131]. The appearance of this band indicates the retention of layered structure as witnessed by XRD and $^{27}$Al MAS NMR studies. The appearance of high field signals at ~ 100 and ~110 ppm is associated with the crystalline siliceous impurities arising due to acid treatment [123] which are also evident in XRD. For Al pillared clay a broad resonance at ~94 ppm is associated with Si in the laminar montmorillonite lattice and the presence of the small high field resonance is due to siliceous impurities present in the basic montmorillonite structure [126].

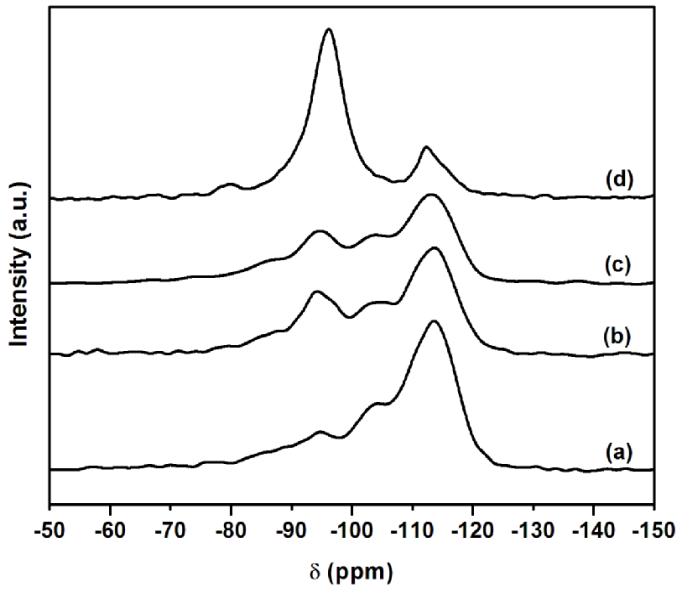


**Fig. 3.20.** $^{29}$Si NMR of (a) K10, (b) K20, (c) K30 and (d) ALPC.

### 3.4.2.1.6. FTIR of chemisorbed pyridine

The results of pyridine adsorbtion measurements of clay catalyst are depicted in Fig. 3.21. All samples exhibited three peaks at 1540 cm$^{-1}$, 1450 cm$^{-1}$ and 1490

$cm^{-1}$ pertaining to Brönsted acidity (B), Lewis acidity (L) and a combined band for Brönsted and Lewis acidity (B+L) respectively. The B/B+L ratios are listed in Table 3.3. The B/B+L ratio decreased in the order from K10, K20, K30 to ALPC clearly indicating that amongst all the clays K10 possesses maximum Brönsted acidity. The Brönsted acidity in acid treated clays is due to the presence of protons of terminal hydroxyl groups and bridging oxygen atoms present in the interlayer region. The Lewis acidity arises from the presence of metal centers. From K10 to K30 there is a decrease in Brönsted acidity since it is known that Brönsted acidity is higher for the samples prepared by mildest acid treatment and decreased as the octahedral layer became increasingly depleted [132]. For the pillared clay, the lower value of B/B+L (value) shows that Brönsted acidity is less in them, whereas they have high Lewis acidity associated with the pillars. The results are in agreement with the findings of Kloprogge *et al* who has shown that there is no reaction between the pillars and tetrahedral sheet in the montmorillonite which was the key requirement for generation of Brönsted acidity in the pillared clays [130].

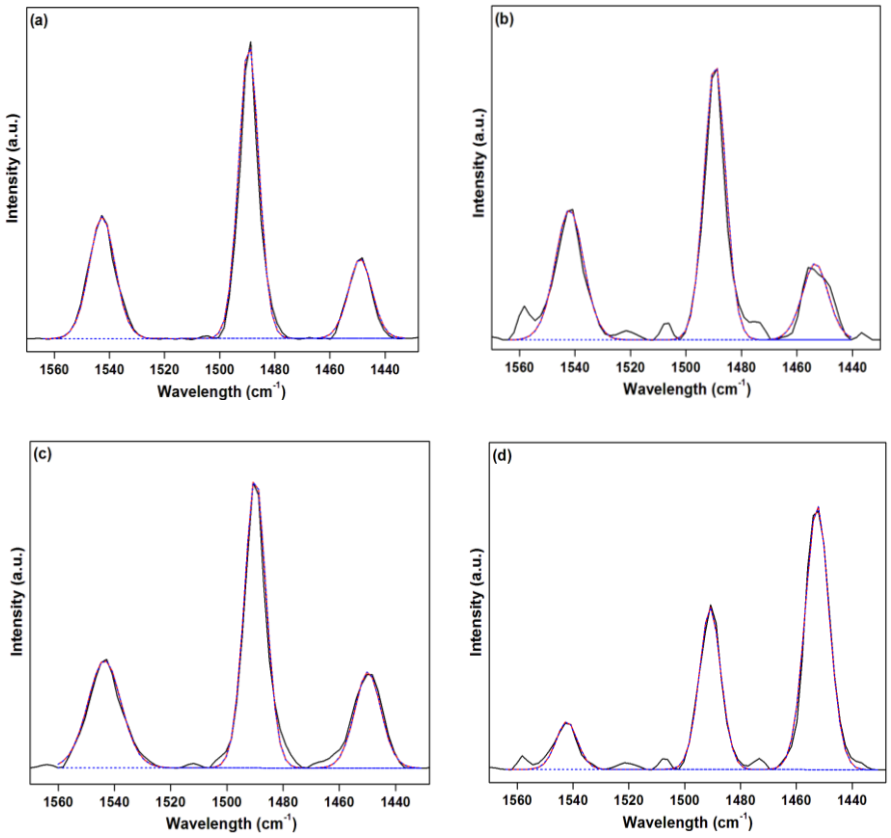


**Fig. 3.21.** FTIR of chemisorbed pyridine; (a) K10, (b) K20, (c) K30 and (d) ALPC.

### 3.4.2.2. Catalytic activity

The catalytic activity of the acid treated and pillared clay catalysts is shown in Table 3.3. From the results, it can be seen that the fructose conversion decreased with reduction in acidity. It was high for K10 at 80 mol%, which fell to 49 mol% for K30. This may be due to decrease in the total acidity. Whereas, pillared clay catalyst (ALPC) gave 70 mol% conversion of fructose, as the pillaring of aluminium species leads to enhanced acidity [131]. For K series catalysts, the selectivity's changed only marginally, though HMF yields differed. Based on the HMF yields, the clay catalysts may be ranked in the order K10> K20> K30> ALPC. To furnish insights into the type of acidity responsible for the formation of HMF, its yield was plotted against B/B+L ratio. A good linear correlation was seen between HMF yield and B/B+L ratio (Fig. 3.22.) suggesting that Brönsted acid sites are responsible for dehydration of fructose to HMF. K-10 gave maximum conversion and yield which may be attributed to its acid strength and higher Brönsted acidity. Hence, this catalyst was used for further optimization of reaction conditions.

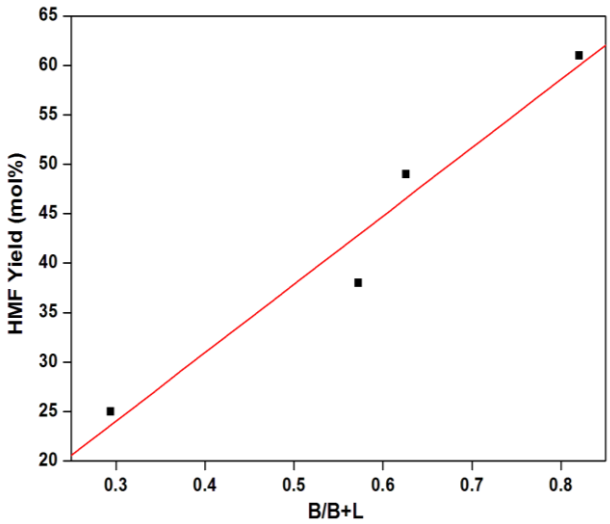


**Fig. 3.22.** HMF yield vs. B/B+L ratio.

#### 3.4.2.2.1. Effect of temperature

The effect of temperature on the reaction was investigated by varying the temperature in the 155-185 °C range; these results are shown in Fig. 3.23. Increase in temperature from 155 to 185 °C, led to increase in conversion from 66 to 98 mol %. The HMF yield increased from 51 to 61 mol% with the increase in temperature from 155 to 165 °C and decreased on further increasing the temperature. For understanding

the reason for this drop in HMF yields and to investigate the effect of temperature on various competitive reactions, the distribution of products was investigated. It was observed that HMF selectivity constantly decreased from 77 to 53% with the increase in temperature from 155 to 185 °C. Low selectivity's of side products like LA and furfural (< 5%) revealed that rehydration and decarboxylation are not dominant at higher temperatures. However, the enhanced selectivity of others (17 to 40%) clearly shows that even on clay catalysts increase in temperature promotes condensation and oligomerization. In addition, the dark colour of reaction mixture at high temperatures is indicative of the formation of condensation products. Since, maximum HMF yield was achieved at 165 °C it was considered as optimum temperature.

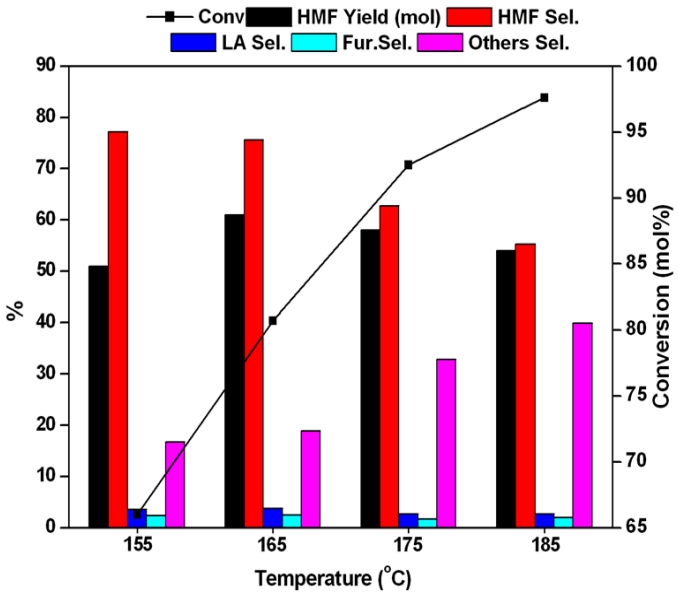


**Fig. 3.23.** Effect of temperature on fructose dehydration.

Reaction conditions: Fructose = 1 g (in 10 mL water), catalyst = 0.15 g, water : MIBK= 1 : 5 (v/v), time = 1 h, RPM = 500.

### 3.4.2.2.2. Effect of catalyst content

The effect of catalyst content on dehydration reaction is shown in Fig. 3.24. When the catalyst amount increased from 7.5 to 30 wt %, the conversion increased from 49 to 88 mol%. However, the HMF yield increased only upto 15 wt% catalyst content, by reaching 61 mol% and remained more or less flat on further increasing the catalyst content. By looking at the product distribution, it can be inferred that there was no appreciable change in selectivity with the increase in catalyst weight up to 15 wt%, but it decreased with further increase in the catalyst content. The increase in

conversion is attributed to increase in the number of active sites; while availability of more active sites drives the product selectivity towards the condensation products since LA and Furfural are not formed in significant amounts. Hence, 15 wt% of the catalyst (of substrate) was found to be optimum.

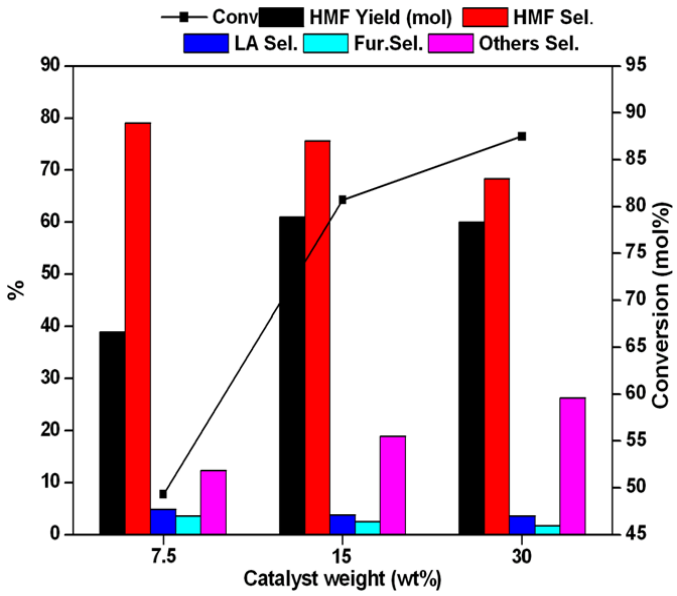


**Fig. 3.24.** Effect of catalyst content on fructose dehydration.

Reaction conditions: Fructose = 1 g (in 10 mL water), temperature = 165 °C, water : MIBK= 1: 5 (v/v), time = 1 h, RPM = 500.

### 3.4.2.2.3. Effect of solvent

The effect of solvent on the reaction has been studied by using different polar and non-polar solvents; these results are shown in Fig. 3.25. Fructose conversions of 80 and 73 mol% were obtained for MIBK and toluene as solvents. In water, the conversion of fructose was lower (53 mol %), due to high affinity of active acidic sites to water, as it acts as a Lewis base, thereby reducing the availability of catalytically active sites. The highest HMF yield of 61 mol% was achieved for MIBK followed by 38 mol% for toluene and only 28 mol% for water. To understand the effect of polarity on the reaction; the product distribution was analyzed. Among the polar solvents, water showed less (53%) selectivity to HMF and more to LA (25%) showing that rehydration of HMF to LA is predominant in water medium. MIBK gave maximum HMF selectivity (76%) due to its ability for dissolution of HMF [119]. With toluene as solvent, more insoluble humins and soluble oligomers were obtained.

The values of extraction coefficient R can be ranked as 6.03 for MIBK, 0.31 for toluene and 0 for water clearly show the superiority of MIBK over other solvents.

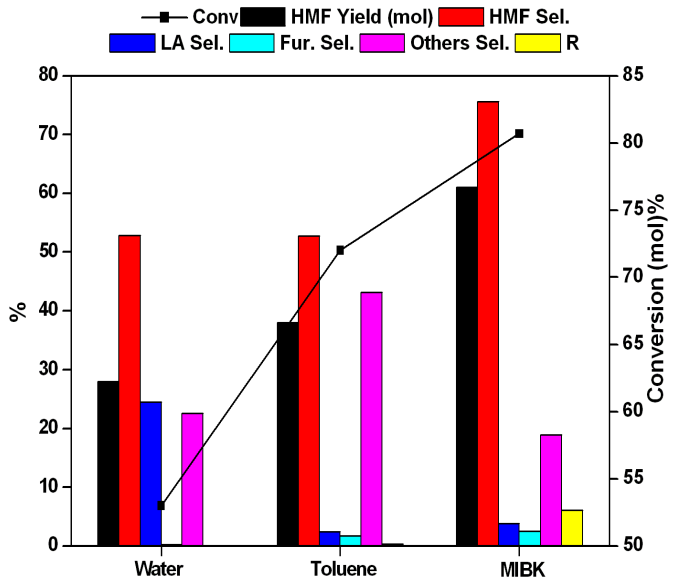


**Fig. 3.25.** Effect of solvent on fructose dehydration.

Reaction conditions: Fructose = 1 g (in 10 mL water), temperature = 165 °C, catalyst = 0.15 g, water : organic solvent = 1: 5 (v/v), time = 1 h, RPM = 500.

### 3.4.2.2.4. Effect of ratio of extracting solvent to water

The effect of ratio of extracting solvent to water was also studied and the results are given in Fig. 3.26. It was seen that the amount of extracting solvent has no appreciable effect on conversion of fructose. However HMF yields increased from 37 to 61 mol% on increasing the water: MIBK ratio from 1:2.5 to 1:5 and remained constant on further increasing the ratio (1:7.5). In order to investigate the role of water:MIBK ratio, the selectivity's of all the products formed were investigated. HMF selectivity increased from 47 to 76% on increasing the ratio from 1:2.5 to 1:5. With further increase in the ratio no profound effect on selectivity was observed. Exactly the opposite trend was observed for selectivity of others, revealing that less quantity of extracting solvent can extract only limited amount of HMF and the remaining HMF undergoes condensation and oligomerization. In this study, 1:5 was inferred to be the optimum water:MIBK ratio.

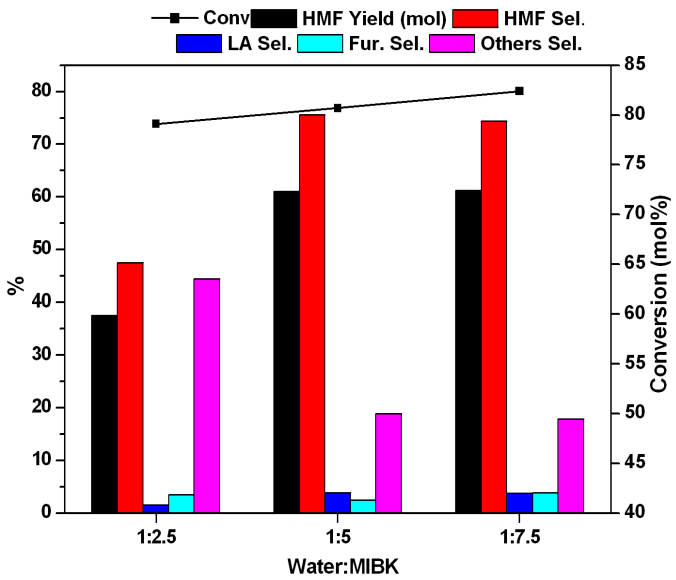


**Fig. 3.26.** Effect of ratio of extracting solvent on fructose dehydration.

Reaction conditions: Fructose = 1 g (in 10 mL water), temperature = 165 °C, catalyst = 0.15 g, time = 1 h, RPM = 500.

### 3.4.2.2.5. Effect of saccarides

In order to check the efficacy of the catalyst to transform other carbohydrates to HMF, different sugars were used as starting substrates for dehydration reaction. The reaction results are shown in Fig. 3.27. The HMF yields follow the order 61 mol% for fructose, 32 mol% for sucrose, 9 mol% for glucose and 6 mol% for maltose.

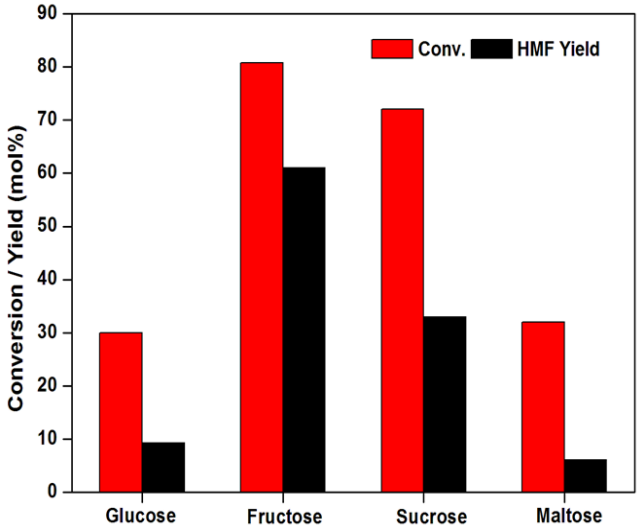


**Fig. 3.27.** Effect of saccharide on fructose dehydration.

Reaction conditions: Sachharide = 1 g (in 10 mL water), temperature = 165 °C, catalyst = 0.15 g, water : MIBK= 1 : 5 (v/v), time = 1 h, RPM = 500.

The above results can be explained on the basis of nature of sugars. The mono and disaccharides with keto groups gave higher HMF yields, whereas aldose sugars gave lesser yields. Since, in case of aldose sugars, the isomerization to ketose is slower over the acid catalyst, the overall dehydration to HMF deteriorates leading to poor yields of the furan compound.

**3.4.2.2.6. Recyclability study**

For recyclability study, the used catalyst was filtered, washed with water and acetone and was dried at 110 °C for 10 h, before it was used for next cycle. When used for next cycle it gave 64 mol% conversion of fructose and 27 mol% yield of HMF. To investigate the deterioration in catalytic activity further, the used catalyst was subjected to chemical analysis and X-ray diffraction (Fig. 3.28). XRD shows that the used catalyst retains the structure of parent K-10, however chemical analysis showed C = 6.48%, H = 1.02%, N= nil, which reveals the deposition of carbonaceous material on the catalyst. The presence of these species blocks the active sites of the catalyst leading to a decrease in the catalytic activity.

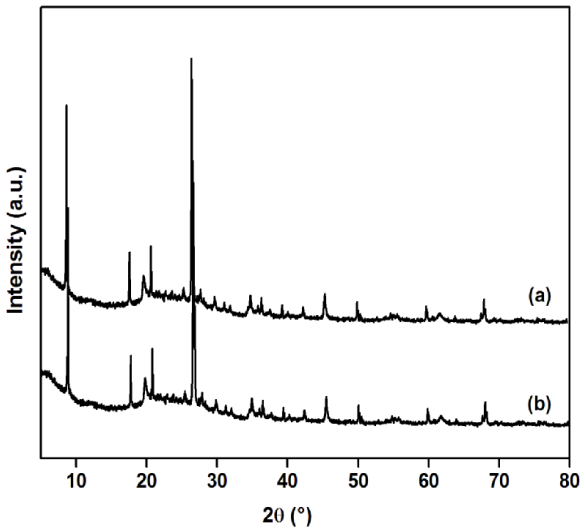


**Fig. 3.28.** XRD pattern of (a) Fresh catalyst and (b) Used catalyst.

### 3.4.3. Conclusions

Cheap and abundant clay catalysts were utilized for the synthesis of HMF from renewable carbohydrates in biphasic solvent system. The acid treated clays were subjected to various physico-chemical characterizations for proper understanding of structure activity relationships. Among the various treated clays the acid treated K10 clay showed the greatest catalytic activity. The present study envisages the nature of acidic sites responsible for higher yield/selectivity for furan compound. A linear correlation was obtained for B/B+L ratio and HMF yields displaying that the Brönsted sites are crucial for fructose dehydration to HMF. The findings accomplished through the present studies definitely furnish important insights into the acidic requirements of heterogeneous catalyst for such complex reactions.

### 3.5. References


1. P. Gallezot, Green Chem. 9 (2007) 295.
2. F.W. Lichtenthaler, S. Peters, C.R. Chim. 7 (2004) 65.
3. A. Corma, S. Iborra, A. Velty, Chem. Rev. 107 (2007) 2411.
4. A. Rosatella, S. Simeonov, R. Frade, C. Afonso, Green Chem. 13 (2011) 754.
5. S.E. Davis, L. Houk, E.C. Tamargo, A.K. Datye, R.J. Davis, Catal. Today 160 (2011) 55.
6. N.K. Gupta, S. Nishimura, A. Takagaki, K. Ebitani, Green Chem. 13 (2011) 824.
7. M.A. Lilga, R.T. Hallen, M. Gray, Top. Catal. 53 (2010) 1264.
8. O. Cassanove, S. Iborra, A. Corma, ChemSusChem. 2 (2009) 1138.
9. T. Thannatthanachon, T.B. Rauchfuss, Angew. Chem. Int. Ed. 49 (2010) 6616.
10. W. Yang, A. Sen, ChemSusChem. 3 (2010) 597.
11. Y.R. Leshkov, C.J. Barett, Z.Y. Liu, J.A. Dumesic, Nature Lett. 447 (2007) 982.
12. R. Leonard, Ind. Eng. Chem. 48 (1956) 1331.
13. V. Ghorpade, M. Hanna, US Patent 5859263 (1996).
14. A. Gandini, M.N. Belcacem, Prog. Polym. Sci. 22 (1997) 1203.
15. H. Koch, F. Krause, R. Steffan, H.U. Woelk, Starke. 35 (1983) 304.
16. W.N. Haworth, W.G.M. Jones, J. Chem. Soc. (1944) 667.
17. S. De, S. Dutta, B. Saha, Green Chem. 13 (2011) 2859.
18. K.B. Sidhpuria, A.L. Daniel-da-silva, T. Trindade, J.A.P. Coutinho, Green Chem. 13 (2011) 340.
19. A.S. Amarasekara, L.D. Williams, C.C. Ebede,Carbohydr. Res. 343 (2008) 3021.
20. K. Seri, Y. Inoue, H. Ishida, Chem. Lett. 29 (2000) 22.
21. F. Wang, A.W. Shi, X.X. Qin, C.L. Liu , W.S. Dong, Carbohydr. Res. 346 (2011) 982.
22. S. De, S. Dutta; B. Saha, Green Chem. 13 (2011) 2859.
23. Y. Nakamura, S. Morikawa, Bull. Chem. Soc. Jpn. 53 (1980) 3705.
24. G.A. Halliday, R.J. Young, V.V. Grushin, Org. Lett., 5 (2003)2003.
25. X. Tong, Y. Wang, G. Nie, Y. Yan, Environ. Prog. Sustain. (2014) DOI:10.1002/ep

26. Y. Wang, X. Tong, Y. Yan, S. Xue, Y. Zhang, Catal. Commun. 50 (2014) 38.
27. X. Qi, M. Watanabe, T.M. Aida, R.L. Smith, Catal. Commun. 10 (2009) 1771.
28. E. Ngee, Y. Gao, X. Chen, J.M. Lee, Z. Hu, D. Zhao, Ind. Eng. Chem. Res. dx.doi.org/10.1021/ie501980t|
29. Y. Lee,K.C.W. Wu., Phys. Chem. Chem. Phys. 14 (2012) 13914.
30. J. Wang, W. Xu, J. Ren, X. Liu, G. Lu, Y. Yang, Green Chem. 13 (2011) 2678.
31. J. Chen, K. Li, L. Chen, R. Liu, X. Huang, D. Ye, Green Chem. 16 (2014) 2490.
32. K.B. Sidhpuria, A.L. Daniel-da-silva, T. Trindade, J.A.P. Coutinho, Green Chem. 13 (2011) 340.
33. J. Lan, Z. Zhang, Ind. Eng. Chem. Res. (2014) DOI:10.10.16/j.jiec.2014.08.016
34. K. Shimizu, R. Uozumi, A. Satsuma, Catal. Commun. 10 (2009) 1849.
35. A. Tagaki, M. Ohara, S. Nishimura, K. Ebitani, Chem. Commun. (2009) 6276.
36. A.J. Sanborn, U.S. Patent 7317116 (2008).
37. X. Tong, M. Li, N. Yan, Y. Ma, P.J. Dyson , Y. Li, Catal. Today 175 (2011) 524.
38. X. Qi, M. Watanabe, T.M. Aida , R.L. Smith Jr., Ind. Eng. Chem. Res. 47 (2008) 9234.
39. J.B. Binder, R.T. Raines, J. Am. Chem. Soc. 131 (2009) 1979.
40. E. Nikolla, Y. Román-Leshkov, M. Moliner, M.E. Davis, ACS Catal. 1 (2011) 408.
41. K. Beckerle, J. Okuda, J. Mol. Catal A: Chem. 356 (2012) 158.
42. Y. Li, X. Lu, L. Yuan, X. Liu, Biomass Bioenergy 33 (2009) 1182.
43. Z. Zhang, Q. Wang, H. Xie, W. Liu, Z. Zhao, ChemSusChem. 4 (2011) 131.
44. Q. Ren, Y. Huang, H. Ma, F. Wang, J. Gao, J. Xu, Bioresources 8(2) (2013) 1563.
45. H. Yan, Y. Yang, D. Tong, X. Xiang, C. Hu, Catal. Commun. 10 (2009) 1558.
46. A. Osatiashtiani, A.F. Lee, D.R. Brown, J.A. Melero, G. Morales, K. Wilson, Catal. Sci. Technol. 4 (2014) 333.
47. R. Otomo, T. Yokoi, J.N. Kondo, J. Tatsumi, Appl. Catal. A. 470 (2014) 318.
48. J. Wang, J. Ren, X. Liu, J. Xi, Q. Xia, Y. Zu, G. Zu, Y. Wang, Green Chem. 14 (2012) 2506.
49. M. Ohara, A. Takagaki, K. Ebitani, Appl. Catal. A. 383 (2010) 149.

50. B.R. Caes, M.J. Palte, R.T. Raines, Chem. Sci., 4 (2013) 196.
51. M. Bicker, D. Kaiser, L. Ott, H. Vogel, J. Supercrit. Fluids 36 (2005)118.
52. L. Lai, Y. Zhang, ChemSusChem 4 (2011) 1745.
53. V.E. Tarabanko, M.A. Smirnova, M.Y. Chernyak, Chem. Sustain. Dev. 13 (2005) 551.
54. J. Liu, Y. Tang, K. Wu, C. Bi, Q. Cui, Carbohydr. Res. 350 (2012) 20.
55. H. Wang, T. Deng, Y. Wang, Y. Qi, X. Hou, Y. Zhu, Bioresour. Technol. 136 (2013) 394.
56. H. Li, Q. Zhang, S. Yang, Int. J. Chem. Eng. (2014) doi.org/10.1155/2014/481627.
57. J. Jeong, C. A. Antonyraj, S. Shin, S. Kim, B. Kim, K. Lee, J. K. Cho, J. Ind. Eng. Chem. 19 (2013) 1106.
58. (a) M.H. Tucker, R. Alamillo, A.J. Crisci, G. M. Gonzalez, S. L. Scott , J. A. Dumesic,ACS Sustain. Chem. Eng. 1 (2013) 554. (b) J.M.R. Gallo, D.M. Alonso, M.A. Mellmer, J.A. Dumesic, Green Chem. 15 (2013) 85.
59. M.L. Mednick, J. Org. Chem. 27 (1962) 398.
60. B.F.M. Kuster, H. S. van der Baan, Carbohydr. Res. 54 (1977)165.
61. F. H. Snyder, U.S. Patent 2851468 (1958).
62. Y. Li, X. Lu, L. Yuan, X. Liu, Biomass Bioenergy 33 (2009) 1182.
63. K. Nakajima, Y. Baba, R. Noma, M. Kitano, J. N. Kondo, S. Hayashi, M. Hara, J. Am. Chem. Soc. 133 (2011) 4224.
64. X. Qi, M. Watanabe, T.M. Aida, R.L. Smith Jr., Catal. Commun. 9 (2008) 2244.
65. F. Benvenuti, C. Carlini, P. Patrono, A.M. Raspolli Galletti, G. Sbrana, M.A. Massucci, P. Galli, Appl. Catal. A. 193 (2000) 147.
66. Y. Zang, J. Wang, J. Jiawen Ren, X. Liu, X. Li, Y. Xia, G. Lu, Y. Wang, Catal. Sci. Technol. 2 (2012) 2485.
67. F.S. Asghari, H. Yoshida, Carbohydr. Res. 341 (2006) 2379.
68. (a) A.H. Jadhav, H. Kim, I.T. Hwang, Bioresour. Technol. 132 (2013) 342 (b) Q. Wu, Y. Yan, Q. Zhang, J. Lu, Z. Yang, Y. Zhang , Y. Tang, ChemSusChem. 6 (2013) 820.
69. C.B. Rasrendra, I.G.B.N. Makertihartha, S. Adisasmito, H.J. Heeres, Top. Catal. 53 (2010) 1241.

70. A. Chareonlimkun, V. Champreda, A. Shotipruk, N. Laosiripojana, Fuel 89 (2010) 2873.
71. S. Zhao, M. Cheng, J. Li, J. Tian, X. Wang, Chem. Commun. 47 (2011) 2176.
72. Y. Román-Leshkov, J.N. Chheda, J.A. Dumesic, Science 312 (2006) 1933.
73. J.N. Chheda, Y. Román-Leshkov, J. A. Dumesic, Green Chem. 9 (2007) 342.
74. (a) Y. Román-Leshkov, J.A. Dumesic, Top. Catal. 52 (2009) 297 (b) J.N. Chheda, J.A. Dumesic, Catal. Today 123 (2007) 59 (c) A.J. Crisci, M.H. Tucker, J.A. Dumesic, S.L. Scott, Top. Catal. 53 (2010)1185.
75. Y. Roman-Leshkov, C.J. Barrett, Z.Y. Liu, J.A. Dumesic, Nature 447 (2007) 982.
76. (a) T. Thananatthanachon, T.B. Rauchfuss, Angew. Chem., Int. Ed. 49 (2010) 6616 (b) M. Kröger, U. Prüße, K.D. Vorlop, Top. Catal. 13 (2000) 237 (c) A. Takagaki, M. Takahashi, S. Nishimura, K. Ebitani, ACS Catal. 1 (2011) 1562.
77. C. Moreau, R. Durand, S. Razigade, J. Duhant, P.F. Augeras, P. Rivalier, P. Ros, G. Avignon, Appl. Catal. A. 145 (1996) 211.
78. (a) V.V. Ordomsky, J. vander Schaaf, J.C. Shouten, T.A. Nijhuis, J. Catal. 287 (2012) 68 (b) V.V. Ordomsky, J. vander Schaaf, J.C. Shouten, T.A. Nijhuis, ChemSusChem. 5 (2012) 1812.
79. Q. Zhao, L. Wang, S. Zhao, X. Wang, S. Wang, Fuels 90 (2011) 2289.
80. I. Morales, A. Teckehandani-oritiz, J. Santamaria, P. Maireless-Torres, A. Lopez, Appl. Catal. B. 144 (2014) 22.
81. F. Yang, Q. Lui, M. Yue, X. Bia, Y. Du, Chem. Commun. 47 (2011) 4469.
82. E. Nikolla, Y. Roman-Leshkov, M.E. Davis, ACS Catal. 1 (2011) 408.
83. C. Bispo, K. Vigier, M. Sardo, N. Bion, L. Mafia, P. Ferreria, F. Jerome, Catal. Sci. Technol. 4 (2014) 2235.
84. I. Morales, J. Santamaria, A. Lopez, P. Maireless-Torres, Fuel 118 (2014) 265.
85. C.V. McNeff, D.T. Nowlan, L.C. McNeff, B. Yan, R.L. Fedie, Appl. Catal. A. 384 (2010) 65.
86. C. Fan, H. Guan, H. Zhang, J. Wang, S. Wang, X. Wang, Biomass Bioenergy 35 (2011) 2659.
87. Y. Yang, C. Hu, M. Mahdi, A. Omar, Green Chem. 14 (2012) 509.
88. Y.J. Pagan-Torres, T. Wang, J.M. Gallo, B.H. Shanks, J.A. Dumesic, ACS Catal. 2 (2012) 930.

89. N. Shi, Q. Lui, Q. Zhang, T. Wang, L. Ma, Green Chem. 15 (2013) 1967.
90. T.S. Hansen, J. Mielby, A. Riisager, Green Chem. 13 (2011) 109.
91. (a) N. Jiang, R. Huang, W. Qi, R. Su, Z. He, Bioenergy Resources 5 (2012) 380 (b) H. Yousef, E.B. Hassan, Fuel 137 (2014) 115.
92. C. Fayet, J. Gelas, Carbohydr. Res. 122 (1983) 59.
93. C. Lansalot-Matras, C. Moreau, Catal. Commun. 4 (2003) 517.
94. C. Moreau, A. Finiels, L.J. Vanoye, J. Mol. Catal. A: Chem. 253 (2006) 165.
95. A. Stark, B. Ondruschka, Handbook of Green Chemistry Volume 6, Ionic Liquids, ed. P. Wasserscheid, A. Stark, Wiley-VCH Verlag GmbH & Co. KGaA, Weinheim, Germany, 2010.
96. F. Liu, J. Barrault, K. De Vigier, F. Jerome, ChemSusChem 5 (2012) 1223.
97. G. Tian, X. Tong, Y. Cheng, S. Xue, Carbohydr. Res. 370 (2013) 33.
98. S. Lima, P. Neves, M.M. Antunes, M. Pillinger, N. Ignatyev, A.A. Valente, Appl. Catal. A. 363 (2009) 93.
99. H. Zhao, J.E. Holladay, H. Brown , Z.C. Zhang, Science 316 (2007) 1597.
100. G. Yong, Y. Zhang , J.Y. Ying, Angew. Chem., Int. Ed. 47 (2008) 9345.
101. (a) F. Ilgen, D. Ott, D. Kralisch, C. Reil, A. Palmberger, B. König, Green Chem. 11 (2009) 1948 (b) M. Tan, L. Zhao, Y. Zhang, Biomass Bioenergy 35 (2011) 1367.
102. Y. Zhang, H. Du, X. Qian, E.Y.X. Chen, Energ. Fuels 24 (2010) 2410.
103. (a) H. Jadhav, E. Taarning, C.M. Pedersen, M. Bols, Tetrahedron Lett. 53 (2012) 983 (b) Y. Zhang, E.A. Pidko, E.J.M. Hensen, Chem. Eur. J. 17 (2011) 5281 (c) L. Hu, Y. Sun, L. Lin, Ind. Eng. Chem. Res. 51 (2012) 1099.
104. T. Stahlberg, W. Fu, J.M. Woody, A. Riisager, ChemSusChem. 4 (2011) 451.
105. S.P. Teong, G. Yi, Y. Zhang, Green Chem. 16 (2014) 2015.
106. O. Casanova, S. Iborra, A. Corma, J. Catal. 275 (2010) 236.
107. D. Zhao, J. Feng, Q. Huo, N. Melosh, G.H. Fedrickson, B.F. Chemlka, G.D. Stucky, Science 279 (1998) 548.
108. G.V. Shanbhag, T. Joseph, S.B. Halligudi, J. Catal. 250 (2007) 274.
109. H. Kosslick, G. Lischke, G. Walther, W. Storek, A. Martin, R. Fricke, Microporous Mater. 9 (1997) 13.
110. R.A. Beyerlein, C. Choi-Feng, J.B. Hall, B.J. Huggins, G.J. Ray, Top. Catal. 4 (1997) 27.

111. E.R. Parry, J. Catal. 2 (1963) 371.
112. W.M. Meier, D.H. Olson, Atlas of zeolite structure types, 3rd addition, published on behalf of structure commission of the international zeolites association, 1992.
113. R. Weingarten, J.A. Tomsett, W.C. Conner, G.W. Huber, J. Catal. 279 (2011) 174.
114. A. Chica, K.G. Strohmaier, E. Iglesia, Appl. Catal. B 60 (2005) 223.
115. G.H. Kuehl, H.K. Timken, Micropor. Mesopor. Mater. 35–36 (2000) 521.
116. A. Lucas, P. Canizares, A. Duran, A. Carrero, Appl. Catal. A. 154 (1997) 221.
117. N.E. Poh, H. Nur, M. Muhid, H. Hamdan, Catal. Today 114 (2006) 257.
118. T.S. Hansen, J. Meilby, A. Riisager, Green Chem. 13 (2011) 109.
119. A. Torres, P. Dautidis, M. Tsapatsis, Environ. Sci. 3 (2010) 1560.
120. K. Toshima, Y. Ushiki, G. Matsuo, S. Matsumara, Tet. Lett. 38 (1997) 7375.
121. T. Huang, R. Wang, L. Shi, X. Lu, Catal. Commun. 9 (2008)1143.
122. F. Bigi, S. Carloni, B. Frullanti, R. Maggi, G. Sartori, Tet. Lett. 40 (1999) 3465.
123. C.N. Rhodes, D.N. Brown, J. Chem. Soc. Faraday Tran. 88(15) (1992) 2269.
124. R. Mokaya, W. Jones, J. Catal. 153 (1995) 76.
125. M.A. Rodriguez, D.L. Gonzalez, M.A. Banaresmunoz Clay Miner. 29 (1994) 361.
126. C. Pesquera, F. Gonzalez, I. Benito, C. Blanco, S. Mendioroz, J. Pajares, J. Mater. Chem. 2 (9) (1992) 907.
127. M. Onal, Y. Sarikaya, T. Alemdaroglu, Turk. J. Chem. 26 (2002) 409.
128. J.T. Kloprogge, E. Booy, J.B.H. Jansen, J.W. Geus, Clay Miner. 29 (1994) 153.
129. V. Flessner, D.J. Jones, J. Roziere, J. Zajac, L. Storaro, M. Lenarda, M. Pavan, A. lopez, E.R. Castellon, M. Trombetta, G. Busca, J. Mol. Catal. A: Chem. 168 (2001) 247.
130. J.T. Kloprogge, J. Porous. Mater. 5 (1998) 5.
131. D. Plee, F. Borg, L. Gatineau, J.J. Fripiat, J. Am. Chem. Soc. 107 (1985) 2362.
132. C. Breen, F.D. Zahoor, J. Phys. Chem. B 101 (1997) 5324.

# *Chapter 4*

## Synthesis of biomass derived levulinic acid using beta zeolite catalyst

## 4.1. Introduction

Substituting fossil feedstocks with sustainable carbon sources for deriving transportation fuels, an energy and bulk chemical is not only a scientific challenge but also need of the hour [1]. An important option is the synthesis of platform chemicals like 5-Hydroxymethyl furfural (HMF) and bulk chemicals such as levulinic acid (LA) from biomass [2]. Levulinic acid, with two reactive groups is a versatile building block for the synthesis of bulk chemicals for numerous applications [3]. For instance, LA is a starting chemical for the preparation of polymers, pharmaceutically active compounds, organic chemicals, dyestuffs and flavour substances. LA is also an inhibitor of chlorophyll synthesis [4]. Levulinic esters possess attractive properties as fuel additives and are also useful as solvents and plasticizers [5,6]. δ-Aminolevulinate is a herbicide and its bisphenol derivative could be an interesting substitute for bisphenol A [7]. Additionally, LA can be an important constituent of hydraulic brake fluids, useful in the manufacture of nylon, rubber and glass like synthetic resins. Moreover, it has been proposed that its sodium salt can replace ethylene glycols as an antifreeze compound [4]. Visualizing the importance of LA, it was reported to be synthesized from various feedstocks using homogeneous as well as heterogeneous catalysts. The following sections discuss several important reports for the synthesis of LA from biomass to provide literature background.

## 4.2. Literature background for the synthesis of LA from biomass

The most prominent route for the production of LA is the dehydration of hexoses to HMF followed by its rehydration in acidic media [8]. Various other substrates can replace hexoses for making the process economically viable. Currently, significant attention is bestowed on utilization of various agricultural and biomass wastes as raw materials for LA production since it would render the process cheaper due to their low cost and copious availability. To get LA from this diversified feedstocks, a variety of acid catalysts were employed which are either homogeneous or heterogeneous in nature.

### 4.2.1. Preparation of LA using homogeneous catalysts

Various homogeneous acids (HCl, $H_2SO_4$, HBr, $H_3PO_4$) are highly effective as catalysts for LA production from hexoses, cellulose and other ligninocellulosic biomass. The use of inorganic acids for the production of LA from sugars dates back

to the early 19$^{th}$ century when Thomas *et al* dehydrated sucrose in the presence of HCl. They studied the effect of various reaction conditions like temperature, acid concentration and time to get high yield (42 mol%) of LA. With dextrose and starch as feedstocks ~37 mol% yield was achieved [9]. This was followed by Kuster *et al* who dehydrated fructose to HMF with its subsequent rehydration to LA. The effect of pH on the reaction path was investigated. At 175 °C, the HMF formation was feasible in the pH between 2.7 to 3.9, whereas LA formation was effective for lower pH (< 1) [10]. Followed by this, several researchers used HCl as catalyst for various biomass feedstocks that include sugars to lignocelluloses wastes. For example, Yoshida *et al* executed dehydration of fructose in subcritical water and could achieve LA yield as high as 64.5 mol% at 270 °C, 0.1 MPa, pH = 1.8 in 3.3 min [11]. They have also studied the effect of pH on the reaction pathway and deduced that lower pH favours LA formation and higher pH favours HMF, corroborating the earlier findings of Kuster. From their studies it was also revealed that this reaction is independent of pressure, while higher LA yields are associated with enhanced temperature and time. Wyman *et al* explored LA synthesis from cellulose and its kinetic studies. They achieved high LA yields (61 mol%) at 180 °C, with 99.6 mM cellulose concentration, 0.927 M HCl concentration, in 20 min [12]. Yan *et al* extended the scope of HCl as catalyst for LA production by using bagasse and paddy straw as feedstocks. They could attain 23.7 mol% yields of LA at 220 °C, 4.45 % HCl, in 45 min [13]. A study by Galletti *et al* [14] involved use of diverse lignocellulosic biomass like poplar sawdust, tobacco chops, wheat straw, olive tree pruning and waste (paper mill sludge) to produce LA with HCl as catalyst. Interestingly, the effect of microwave heating was also investigated. At 200 °C with 11.5 Meq HCl in 1 h 37, 55, 49.3 and 20.8 mol% LA yields (based on cellulose content) were obtained from, poplar sawdust, paper sludge, wheat straw and tobacco chips, respectively. When the reactions were performed under microwave heating, shorter duration (0.25 h) led to higher yields (45.8, 55.5 and 52.5 mol% for sawdust, sludge waste and tobacco chops, respectively), which clearly demonstrated the effectiveness of microwave heating over traditional thermal heating. The authors also compared the activity of HCl with $H_2SO_4$ and found that the former was more selective for LA production.

Though, HCl is reported to be an efficient and selective acid catalyst for LA synthesis, Girisuta *et al* focused on the use of $H_2SO_4$ as catalyst [15-17]. Initially they carried out the rehydration of HMF to LA using 0.1 M $H_2SO_4$ and achieved LA yield

of 94 mol% at 98 °C. Kinetic studies were performed to understand the formation of humins. The rate expressions were applied to furnish optimal reaction conditions [15]. Followed by this, they studied the conversion of glucose to get high LA yields (55 mol%) at 140 °C, using 0.1 M glucose and 1M $H_2SO_4$ in 2 h. The striking feature of the study was that higher LA yields were achieved at high acid concentration and with dilute glucose solution [16]. After hexoses, they focused on lignocellulosic biomass and synthesized LA from cellulose. They obtained high LA yields of 60 mol% at 150 °C with 1.7 wt% of cellulose concentration while acid concentration was unaltered (1 M). Kinetic studies were performed to understand the complex reaction network and optimize the reaction conditions [17]. All these important findings showed the potential of $H_2SO_4$ and paved the way for several other approaches employing diverse feedstocks. In the hunt for milder operating conditions for dextrose decomposition, Tarabanko *et al* [18] performed the dehydration reaction at 98 °C with high acid concentration (5.8 M of $H_2SO_4$) and achieved 38 mol% of LA in 12 h. With sucrose, 50 mol% of LA was accomplished. They also performed a comparative study of various acids in which selectivity's of HCl and $H_2SO_4$ were the same, while $H_3PO_4$ was too weak for this application as it rendered only 5 mol% of LA. Phosphoric acid was selective towards HMF formation due to high pH in accordance with the findings of Kuster. A similar comparative study was undertaken by Tanskanen *et al* in which they compared the activity of mineral acid ($H_2SO_4$) with organic acid (HCOOH) for glucose decomposition. They investigated the effect of concentration of protons at different temperatures and acid concentrations. The study revealed that the glucose decomposition is dependent on proton concentration at the reaction temperature and is independent of the source of the protons. This important finding furnished the apt parameters for activity comparison [19].

Later, targeting the economic viability of the process, various biomass resources were utilized for LA synthesis. Hanna *et al* used whole kernel sorghum grain and achieved 32.6 mol% of LA yield at 200 °C with 8 % $H_2SO_4$ and 10 % flour loading. The authors prepared a linear regression model capable of predicting LA yields with process conditions like reaction temperature, acid concentration and flour loading [20]. Corn starch was employed as the reactant for LA production by Cha *et al* in which blends of corn starch (70 %), water (25 %) and $H_2SO_4$ (5 %) were extruded at 180 °C. This was followed by heating at 200 °C for 1 h which yielded LA in significant amounts (47.5 %) [21]. Chang *et al* used wheat straw and attained 19.8

mol% of LA yield working with 3.5 % of $H_2SO_4$ concentration, 15.6 as liquid to solid ratio at 210 °C in 38 min [22]. Zhang *et al* exploited hybrid poplar wood chips and synthesized LA using a two stage process. In the first stage, pentoses were extracted in the liquid form leaving solid residue of hexoses (160 °C, 1 wt% $H_2SO_4$, and liquor to wood ratio of 6). The solid residue was then subjected to acid catalyzed dehydration to LA (second stage). Various process parameters were optimized and at 190 °C, 5 wt% $H_2SO_4$, at liquor to wood ratio of 10, LA yield of 60.3 % of theoretical value (17.3 wt% of original biomass content) was obtained in 50 min [23]. Similarly, Rivas *et al* used pine wood for the production of LA. The pine wood was treated in hot compressed water and the resultant liquor was mixed with $H_2SO_4$ and thermally heated. Different process parameters like acid concentration, temperature, time were studied. In the optimized conditions (135 °C, 10 % $H_2SO_4$, 10 h), 66 % LA yield of the stoichiometric value was achieved [24]. Researchers also focused on other interesting feedstocks like glucosamine (from chitosan) and red algae gracilaria verlucosa for LA synthesis. When glucosamine was used as starting material by Jeong [25] it gave 25.3 wt% LA yield at 188 °C, with 4 wt% $H_2SO_4$, 120 $gL^{-1}$ substrate concentration in 50 min. This study also showed that the reaction temperature, time and substrate concentration have pronounced effect on LA yields than catalyst concentration. However, by using red algae gracilaria verlucosa as substrate, only 18.64 wt% yield of LA was obtained with 2.85 % $H_2SO_4$ at 180 °C in 50 min. Another important feedstock to be used was wastewater slurry from starch industry containing $H_2SO_4$ which rendered excellent yields of LA (91.4 mol%) at 140 °C in 4 h [27]. Thus, a variety of biomass feedstocks for LA production using $H_2SO_4$ were reported.

Apart from employing diverse reactants, the current research is more focused towards finding appropriate process parameters for enhancing LA yield. In this context, biomass pretreatment has emerged as an attractive step. Retsina *et al* [28] treated the wood and agricultural residues with steam whereas Vries *et al* [29] pretreated the lignocellulosic biomass with acidic slurry. The outcome in both the cases was an increment in LA yields. Biomass pretreatment was coupled with continuous extraction of the reactive system by organic solvent by Fan *et al* to attain 30.6 mol% of LA from wheat straw [30]. Another impressive approach was adopted by Daniel [31] in which the carbohydrate feed was added in controlled manner to the reactor for acid catalyzed dehydration. 90 mol% of LA was obtained from fructose

(1.5 %) using 0.3 M $H_2SO_4$ (630 μL) at 180 °C in 20 min. However, when dextrose was used, $AlCl_3$ was added with the acid to give 74 mol% of LA. Similar approach was used by Mullen *et al* who altered the rate of addition of fructose feed and could achieve 92.8 mol% of LA with 1.05 mol $H_2SO_4$ at 200 °C [32]. In addition to this screening and modifications, researchers also opted for different informative studies. For example, kinetic modelling of switchgrass cellulose to LA was performed by Yan *et al* in which the release patterns of glucose, HMF and LA was studied [33]. Thermodynamic properties of LA were investigated [34] and computational studies were performed by Curtiss *et al* [35] in which they illustrated that glucose dehydration to HMF is endothermic but HMF rehydration is exothermic, so aqueous reaction environment and elevated temperature are predicted to make the dehydration step thermodynamically more favourable. Thus, it can be inferred that highly important synthesis of LA has been investigated on all fronts and the role of mineral acids for LA production is unrivalled.

Various other homogeneous catalysts and alternatives like microwave irradiation and use of ionic liquids as reaction medium have been deployed for LA production. Inorganic salts were used as catalysts. Glucose dehydration to LA was studied with Al, Cr and Zn salts by Rasrendra *et al* in which low yields of LA were obtained when glucose was used as stating material. However, from HMF 50 mol% of LA was obtained using $AlCl_3$ as catalyst (5 mM) at 180 °C in 1 h. For glucose, Zn salts were selective for HMF while Al salts were selective for lactic acid [36]. Shen *et al* carried dehydration of glucose and fructose with $InCl_3$ as catalyst and achieved 57 mol% of LA from glucose (2.5 mol% $InCl_3$, 180 °C, 1 h) and 45 mol% LA from fructose under similar reaction conditions. It was found that $InCl_3$ could effectively execute glucose to fructose isomerization. Reaction mechanism was also proposed [37,38]. Cellulose depolymerization and dehydration was accomplished with transition metal chlorides ($CrCl_3$, $FeCl_3$, $CrCl_2$) and $AlCl_3$ by Peng *et al* [39]. Amongst the catalysts studied, $CrCl_3$ excelled in catalytic performance and gave excellent yields of LA (67 mol%) with 0.2 M of salt, 5 wt% substrate concentration at 200 °C in 3 h. Following this, cellulose transformation to LA was studied by Khan *et al* with $AlCl_3$ and achieved 36.5 mol% of LA at 180 °C in 4 h [40]. In addition to salts, very interestingly glycine betadine hydrochloride was used to catalyze wheat straw dehydration to furfural and LA [41].

Recently, ionic liquids have emerged as excellent medium/catalysts for biomass valorization and dehydration of biomass to LA is no exception. Although, they have been mostly screened for HMF synthesis, there were reports about their utility for LA synthesis also. Ren *et al* conducted highly useful comparative study of sulphonic acid functionalized ionic liquids (SFIL). The catalytic activities of SFIL's depends on the anions and the performance can be ranked as $HSO_4^-$ > $CH_3SO_3^-$ > $H_2PO_4^-$. Under microwave irradiation, 55 mol% of LA was obtained from cellulose [42]. Heteropoly acid ionic liquids were deployed for cellulose dehydration to HMF by Sun *et al*, however, with water-MIBK biphasic systems 22.3 mol% LA yields were attained using 0.1 g cellulose, 0.5 mL water, 5 mL MIBK, 0.07 mol catalyst ([MIMPSH]$H_2PW$) at 140 °C in 7 h. On prolonging the duration of reaction to 12 h, LA yields drastically increased to 60 mol% [43]. Another acidic ionic liquid 1-(1-propylsulfonic)-3-methyl imidazolium chloride was used as catalyst in ethanol water system which rendered 23.7 mol% LA yields with 54 % water content in 48 h at 150 °C [44]. Ionic liquids were also exploited for other biomass feedstocks. Using [$C_4$mim]$H_2SO_4$ as catalyst, excellent LA yields (71 mol%) were achieved from bamboo shoot shell at 0.9 mol.$L^{-1}$ of catalyst in 105 min [45].

Apart from straight forward usage of homogeneous catalysts, other approaches have been adopted for effective LA production. Microwave heating appeared to be quite promising. Mika *et al* converted a range of biomass {glucosamine, low molecular weight (LMW)-chitosan and high molecular weight (HMW)-chitosan} to LA under microwave irradiation at 190 °C in 0.5 h with 2M $H_2SO_4$. With glucosamine and LMW-chitosan, LA yields between 20.6-32.7 mol % were obtained while HMW-chitosan gave 37.8 mol% yield [46]. Another, interesting approach was using $SO_2$ in hot water as catalyst for LA synthesis from cellulose. In this study it was found that $SO_2$ acts as a source of $H^+$ ions (as it forms $H_2SO_4$ in water) and lewis acid centers. 20 mol% of LA was achieved with 0.055gcm$^{-3}$ of $SO_2$ concentration, 0.5g cellulose at 210 °C in 0.5 h [47].

The homogeneous catalysts effectively catalyze the dehydration yielding the targeted compounds like LA, but the problems like handling issues, recyclability and environmental concerns associated with them are significant drawbacks hindering their application. As an alternative, heterogeneous acid catalysts were employed to overcome the problems associated with the homogeneous acids.

### 4.2.2. Levulinic acid production using heterogeneous catalysts

Several types of solid acids were used for LA synthesis, though the investigations were originated using acidic ion resins. Rase *et al* performed a comparative study of various acidic ion-exchange resins for the dehydration of sucrose to LA and inferred that selectivity of the acid was affected by the pore size of the resin. Among the resins studied, Dowex MSC-1H was found to be good and rendered 24 mol% yield of LA at 100 °C in 24 h. Lower yields were attributed to low reaction temperature as the resin is not stable at higher temperature [48]. Later, the discovery of hydrothermally more stable resins extended the use of resins for the targeted reaction. Amberlyst-70 was used as catalyst for two step transformation of cellulose to LA. In the first step non-catalytic hydrothermal decomposition of cellulose was carried at moderate temperature (190-270 °C) to produce water soluble compounds. The second step comprised of dehydration of water soluble compounds using Amberlyst-70. Under the optimized reaction conditions (160 °C, 8 h, 0.1 M total acid sites) moderate LA yields were obtained (21 % of theoretical value) [49]. This application extended the scope of resins for lignocellulosic biomass. Composite of silica and Nafion resin (Nafion SAC-13) was tested for transformation of cellulose to LA but only 11 % yield of glucose and LA were attained at 190 °C in 24 h [50]. The study was extended by using NaCl with the catalyst which resulted in tremendous enhancement of LA yield (from 14 to 72 %) at 200 °C in 120 h. The addition of the salt increased the ion concentration which leads to increased interaction with H-bonded network of cellulose structure facilitating the cellulose hydrolysis and improving the overall performance [51]. A similar approach was adopted by Yang *et al* [52] in which they used Fe modified Dowex-50 resin with 5 wt% NaCl for dehydration of cellulose to LA. Moderate yield of 33.3 % LA was achieved in 5 h at 200 °C. The authors claimed that Lewis acidity of Fe increases cellulose depolymerization in addition to the salt effect.

Considering the short comings of resins as catalysts, zeolites and pillared clays were preferred. LA was synthesized from glucose using MFI-type catalyst which gave 36 mol% LA yield at 180 °C in 8 h at a high catalyst loading (75 wt% of substrate). But, the recyclability studies were not undertaken [53]. Modification of the zeolite with $SO_4^{2-}/ZrO_2$ moieties could enhance the yields upto 55 %, however recyclability was a major issue due to leaching of the anchored acidic moieties. Kinetic studies of

glucose dehydration were performed by Rorrer *et al* [54] using H-Y zeolite. At 160 °C in 8 h low LA yield (~20 %) was obtained for 12 wt% of glucose solution using 50 wt % (w.r.t. substrate) catalyst. Jow *et al* dehydrated fructose with LZY zeolite and achieved 67 % of theoretical yield of LA at 140 °C in 15 h [55]. Pillared clays were also exploited for glucose dehydration where Fe pillared montmorillonite exhibited low yield of levulinic acid (<20 %) at 150 °C in 12 h. The activation energies were calculated and insights into the formation of humins (condensation products) were provided. Aluminium pillared clay was most susceptible to humin formation [56]. Mesoporous solid acids were also used for carbohydrate dehydration. In this context the accomplishments of Wang *et al* [57] are worth mentioning. The authors employed Al modified mesoporous niobium phosphate for the dehydration of cellulose and got 50 % yield at 180 °C in 24 h. However these studies did not include results of recyclability.

Apart from porous solids, numerous acid functionalized oxides, mixed oxides, carbon, polymers were screened for the reaction. Cellulose was dehydrated using sulphated titania ($SO_4^{2-}/TiO_2$) which gave 27.2 % of LA at 170 °C in 0.25 h [58]. Chen *et al* [59] used superacid ($S_2O_8^{2-}/ZrO_2–SiO_2–Sm_2O_3$) for producing LA from rice straw. The feedstock was pretreated with steam and then subjected to dehydration. Under the optimal conditions 70 % of theoretical yield of LA was obtained. However, the results were achieved for a high solid acid catalyst concentration (13.3 wt%), which corresponds to more than four times the cellulose weight content in the feedstock. Catalyst recycling was a major issue for former and leaching of sulphate species from the support is another drawback. Upare *et al* [60] showed successful transformation of glucose to LA with sulphonic acid functionalized graphene oxide as catalyst. Excellent yield of 78 mol% was achieved at the optimum reaction conditions (200 °C, 2 h, 30 g glucose in 200 ml water and 0.5 g catalyst). Interestingly, the catalyst exhibited good recyclability. Sulphonated hyperbranched poly(arylene oxindioles) was evaluated for cellulose dehydration, rendering 25 mol% of LA [61]. The catalyst system corresponds to a new class of water-soluble acid catalysts which can be separated by ultrafiltration after the reaction. In the context of facile separation, an attractive concept of magnetic catalyst was deployed by Lai *et al* [62] for cellulose dehydration. They used sulfonated mesoporous silica modified with magnetic iron oxide particles and attained 38 mol% of LA with 10 wt% cellulose

concentration after 12 h at 150 °C. Due to the magnetic properties, the catalyst was effortlessly separated post-reaction.

Ionic liquids with solid acid catalyst have exhibited promising results for LA synthesis. Jia *et al* studied cellobiose dehydration to acids in ionic liquids using polyoxometallate hybrid catalyst. Under optimal conditions LA yield of 46.3 % was achieved. A detailed mechanism of the organic transformation was also postulated [63]. Fe modified H-Y zeolite was used in BMIM[Br] ionic liquid for obtaining LA from oil palm fronds which resulted in 24.7 % LA at 153 °C, 1.1 g ionic liquid, 0.96 g catalyst in 6 h [64,65]. In conclusion, it can be deduced that production of LA is efficiently investigated by several acid catalysts and offers a green protocol of transforming renewable feedstocks to important platform chemicals.

### 4.3. Dehydration of carbohydrates to LA using beta zeolite catalysts

From the earlier reported studies it can be seen that various homogeneous and heterogeneous catalysts have been explored for LA synthesis from various feedstocks aiming at higher yields of the targeted compound. However, for such cascade reactions, proper insights into the nature of acidic sites and the interplay of these species for LA formation are lacking. Using solid acid catalysts which have several advantages over the homogeneous catalyst, the above mentioned findings are important to be noted. Because of non-uniformity of catalytic sites in solid acids, it is of prime importance to envisage the role of nature of acid sites responsible for LA formation as the type of acid sites can change the reaction pathway. In order to address this challenge, Beta zeolite with different $SiO_2/Al_2O_3$ ratios were used. The catalysts were subjected to detailed characterization for understanding of their catalytic activity. Importantly, the role of acidity and nature of acidic sites crucial for the reaction were investigated which will be highly useful in employing solid acid catalyst for such cascade reactions. Various process parameters were also optimized for the dehydration reaction with an aim to improve the LA yield. Attempts were made to correlate the acidity and particularly the type of acidity with LA yield.

### 4.3.1. Experimental procedures

#### 4.3.1.1. Materials

Fructose, glucose, sucrose, maltose, ethanol, 25% $NH_3$ solution and zirconium oxychloride ($ZrOCl_2.8H_2O$) were purchased from Loba Chemie Pvt. Ltd. 5-hydroxymethyl furfural, levulinic acid, lactic acid, furfural, acetic acid, ethyl levulinate, montmorillonite K-10 and ammonium metatungstate were procured from Sigma-Aldrich. Cellobiose and Inulin were purchased from Alfa Aesar. All the chemicals were of research grade and were used after drying following standard procedures. Zeolites $NH_4^+$-Y ($SiO_2/Al_2O_3$ = 30) and $NH_4^+$-Beta were ($SiO_2/Al_2O_3$ = 38, 75, 150) were obtained from Zeolyst International, USA. Zeolite $NH_4^+$-Beta ($SiO_2/Al_2O_3$ = 28) was prepared in our laboratory. These were calcined at 450 °C for 4 h in air before using them for the reaction.

#### 4.3.1.2. Catalytic activity

The dehydration reaction was carried out in 300 mL Parr (SS 316) autoclave that has a teflon liner. In a typical reaction, sugar was dissolved in Millipore water, to which freshly activated catalyst was added. The closed vessel was purged with nitrogen and the reaction was conducted at the desired temperature. At the end of reaction, the reaction mixture was filtered using nylon 0.22 μm filter and the filtrate was analyzed using HPLC, equipped with RI detector and Resex ROA Organic Acid $H^+$ column (300 mm × 7.8 mm) with 5 mM $H_2SO_4$ as the mobile phase at a flow rate of 0.6 $mL.min^{-1}$ at 60 °C.

### 4.3.2. Results and discussion

#### 4.3.2.1. Catalyst characterization

##### 4.3.2.1.1. X-ray diffraction (XRD)

The XRD powder patterns of the beta zeolite with $SiO_2/Al_2O_3$ = 28 (Beta-28), $SiO_2/Al_2O_3$ = 38 (Beta-38), $SiO_2/Al_2O_3$ = 75 (Beta-75) and $SiO_2/Al_2O_3$ = 150 (Beta-150) are shown in Fig. 4.1. The XRD pattern showed the characteristic reflection of BEA topology with intense diffraction peaks at 2θ =7.6 and 22.4° [66]. Though the position of the peaks was not affected significantly, a decrease in crystallinity was observed with increasing $SiO_2/Al_2O_3$ ratio, as a result of dealumination process used

for increasing the $SiO_2/Al_2O_3$ ratio [67]. No additional peaks pertaining to crystalline impurities or amorphous phases were observed in 2θ = 20-30°.

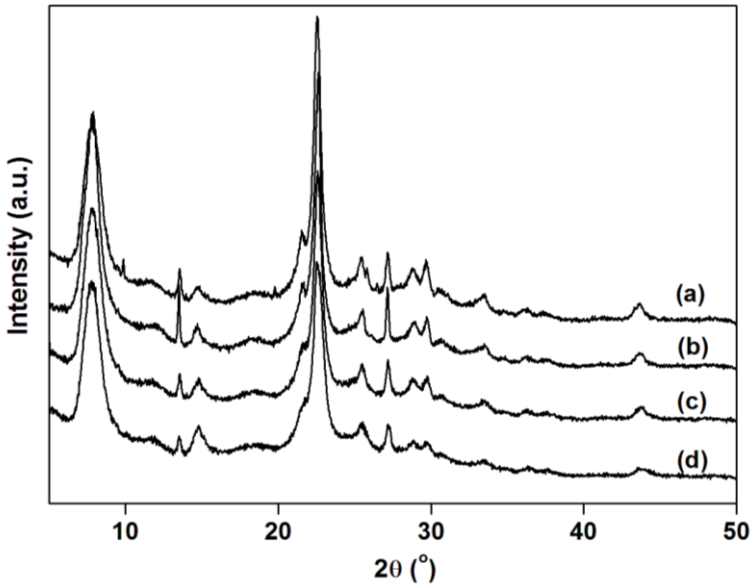


**Fig. 4.1.** XRD pattern of (a) Beta-28, (b) Beta-38, (c) Beta-75 and (d) Beta-150.

#### 4.3.2.1.2. Surface area

The textural properties of the catalyst are depicted in Table 4.1. The change in $SiO_2/Al_2O_3$ ratio has no significant effect on surface area but an increase in BJH pore volumes for the dealuminated samples (Beta-75,-150). This clearly shows that dealumination treatment induced significant structural changes in the zeolites leading to appearance of large pores. The results are consistent with earlier findings [68].

**Table 4.1:** Textural and physiochemical properties of catalyst used in dehydration.

| Catalyst | $SiO_2/Al_2O_3$ | S.A. ($m^2/g$) | P.D. (Å) | P.V. (cc/g) | Acidity (mmol/g) | B/B+L | $H_2O$ (%) |
|---|---|---|---|---|---|---|---|
| H-Beta-28 | 28 | 611 | 5.7x7.5 6.5x 5.6 | 0.64 | 0.96 | 0.55 | 15.05 |
| H-Beta-38 | 38 | 632 | 5.7x7.5 6.5x 5.6 | 0.78 | 0.87 | 0.63 | 14.87 |
| H-Beta-75 | 75 | 612 | 5.7x7.5 6.5x 5.6 | 0.89 | 0.50 | 0.58 | 6.47 |
| H-Beta-150 | 150 | 582 | 5.7x7.5 6.5x 5.6 | 0.84 | 0.19 | 0.42 | 3.45 |
| H-Y | 30 | - | 7.4 | - | | - | - |
| K-10 | - | 165 | 21.1 | - | 0.21 | - | 9.88 |
| 15WZ750 | - | 53 | - | - | 0.29 | - | - |

Legend: S.A. = surface area, P.D. = pore diameter, P.V. = pore volume

#### 4.3.2.1.3. Scanning electron miscroscopy (SEM)

The morphology of the samples was studied using SEM (Fig. 4.2). The presence of tiny spherical crystallites is evident from the micrographs of parent zeolites Beta-28 and Beta-38. The crystallite sizes are in 0.5-1.3 micron range. For the zeolite samples Beta-75 and Beta-150, the spherical morphology of the parent zeolite is completely absent. This clearly reveals that the dealumination process not only affects the crystallnity (as evident from XRD) but also the morphology of the zeolite.

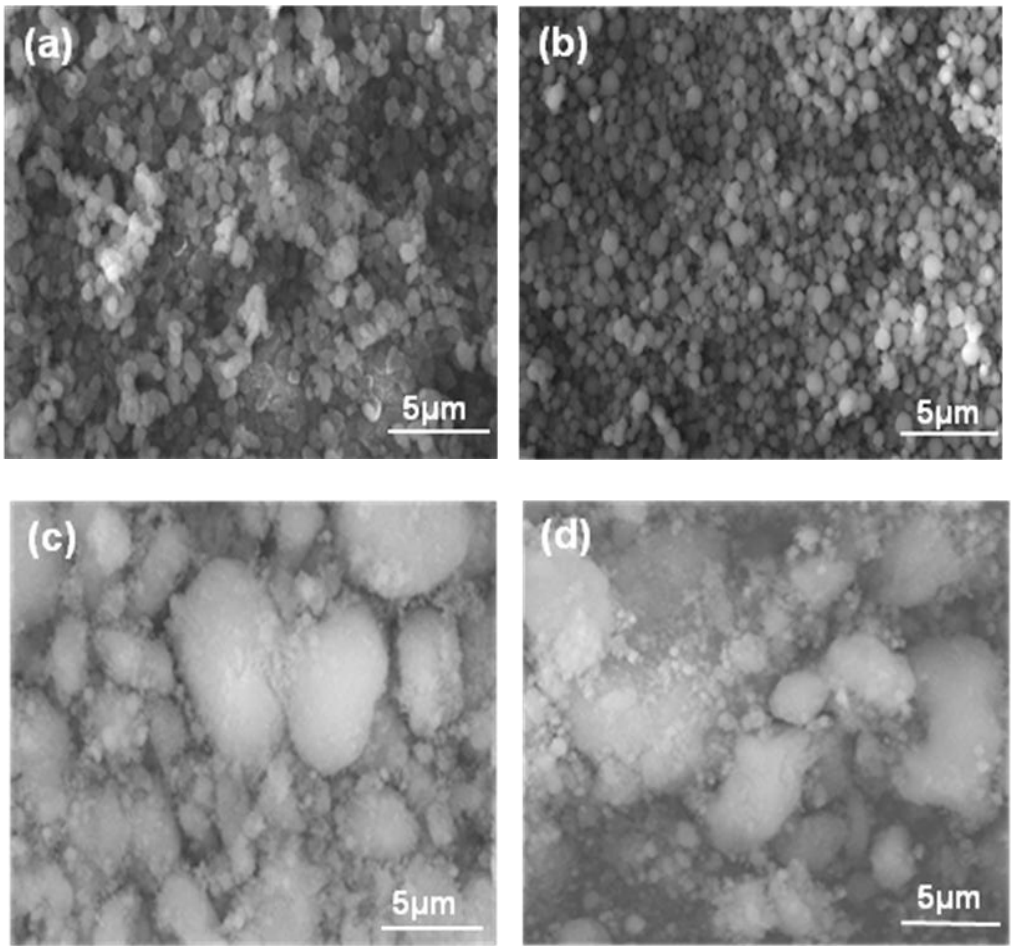


**Fig. 4.2.** SEM images of (a) Beta-28, (b) Beta-38, (c) Beta-75 and (d) Beta-150.

#### 4.3.2.1.4. $^{27}$Al MAS Nuclear magnetic resonance

Solid state $^{27}$Al MAS NMR is an excellent tool to probe the local environment of aluminium species. The spectra of the beta zeolite samples are shown in Fig. 4.3. The spectra are characterized by an intense and sharp peak at 53 ppm which is indicative of aluminium in tetrahedral coordination, which is covalently bounded to four Si atoms *via* oxygen bridges. Beta-28, -75,-150 exhibited another peak at nearly

0 ppm which is attributed to octahedrally coordinated aluminium species in extra framework positions [69]. The generation of octahedral aluminium species occurs during the dealumination process [70,71]. No signals around -30 ppm, due to pentacoordinated [72] or hexacoordinated extraframework [73,74] aluminium were observed. It is expected that only tetrahedral Al generates Brönsted acidity. Hence, $^{27}$Al MAS NMR results show that the acidity is not expected to increase linearly with Al content. The TPD of $NH_3$ results confirm this aspect.

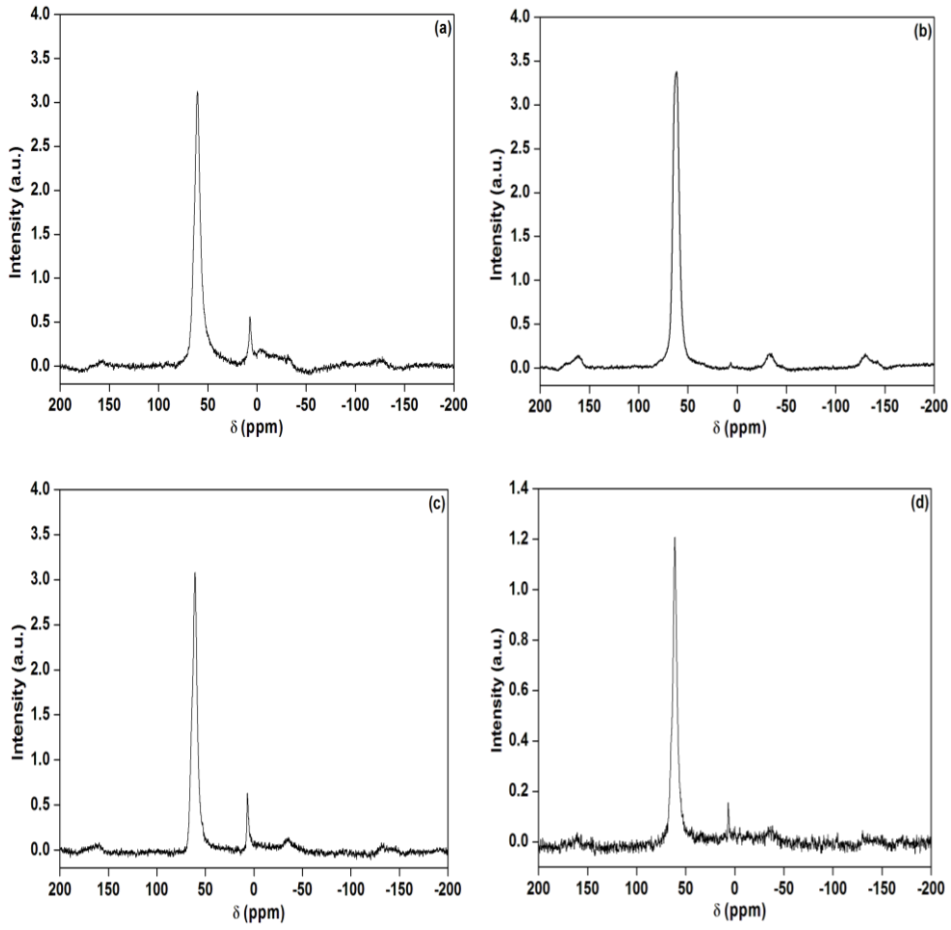


**Fig. 4.3.** $^{27}$Al MAS NMR of (a) Beta-28, (b) Beta-38, (c) Beta-75 and (d) Beta-150.

### 4.3.2.1.5. TPD of $NH_3$

The acidity of the beta samples was determined by TPD of $NH_3$. The TPD profiles of the samples with different $SiO_2/Al_2O_3$ ratios are given in Fig. 4.4. The total acidity of materials is expressed in mmol.g$^{-1}$ of $NH_3$ desorbed in the temperature range of 100-450 °C, and these values are listed in Table 4.1. All beta zeolite samples show two peaks, one pertaining to weak acidity (100-250 °C) and the other to moderately strong acidity (250-450 °C). Beta-28, -75 and -150 show an additional

peak at higher temperatures (500-700 °C), which is attributed to the desorption of $H_2O$ formed on condensation of silanol groups present in these samples. With the decrease in the $SiO_2/Al_2O_3$ ratio (or increasing aluminium content) from 150 to 28, the total acidity, in terms of ammonia desorbed, increased from 0.186 to 0.961 $mmol.g^{-1}$. This shows that the acidity increased with aluminium content. Thus, the total acidity is dependent on the amount of aluminium present in the samples, but the acidity did not increase linearly with aluminum content, particularly in the higher aluminium containing samples.

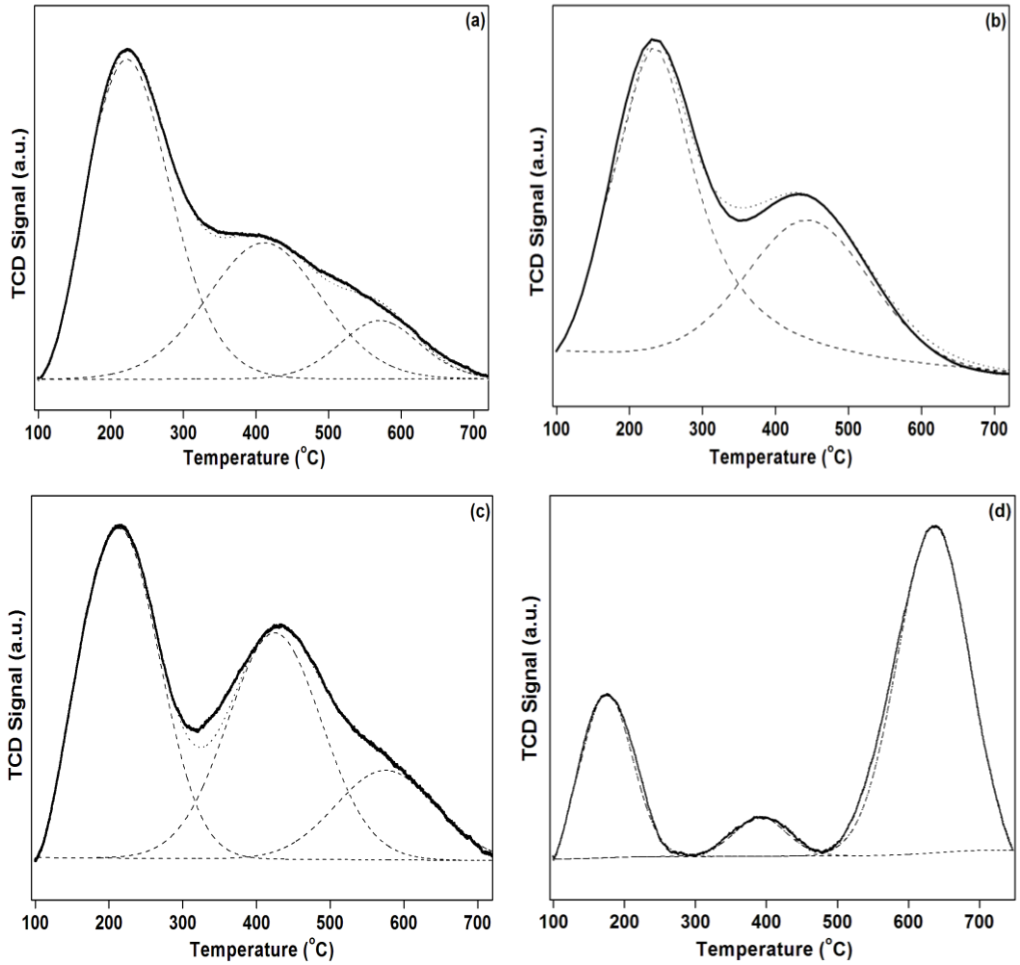


**Fig. 4.4.** $NH_3$-TPD profile of (a) Beta-28, (b) Beta-38, (c) Beta-75 and (d) Beta-150.

Brönsted acidity was investigated by TPD-MS using isopropyl amine as a probe. Isopropyl amine reacts with Brönsted acid sites leading to the formation of propylene and $NH_3$. Hence it is a good probe for the estimation of Brönsted acidity.

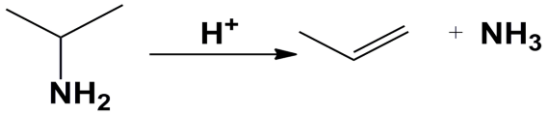

The results of TPD-MS of isopropyl amine are shown in Fig. 4.5. All samples exhibited two peaks, one at lower temperature (< 300 °C) and the other at higher temperature (> 300 °C). The peak at lower temperature is due to the desorption of isopropyl amine and water as evident from mass spectrum and the one at higher temperature is of propene and ammonia. The formation of propene clearly reveals the presence of Brönsted acid sites in zeolites. For Beta-150 an additional peak is witnessed at much higher temperature (> 500 °C), which is attributed to water formed due to condensation of silanol groups. Thus, the peak at higher temperature obtained in $NH_3$-TPD profile of Beta-150 is of water formed during condensation reaction and does not pertain to desorbed ammonia, which many reports assign to strong acidity. From propene concentration profile of all the zeolites, it is formed maximum on Beta-38 followed by -28, -75 and -150. The maximum propene concentration or Brönsted acidity in Beta-38 is due to the presence of all Al in tetrahedral coordination (as evident from $^{27}$Al MAS NMR) whereas propene formation is lower on others due to presence of octahedral Al species which is responsible for decreased Brönsted acidity.

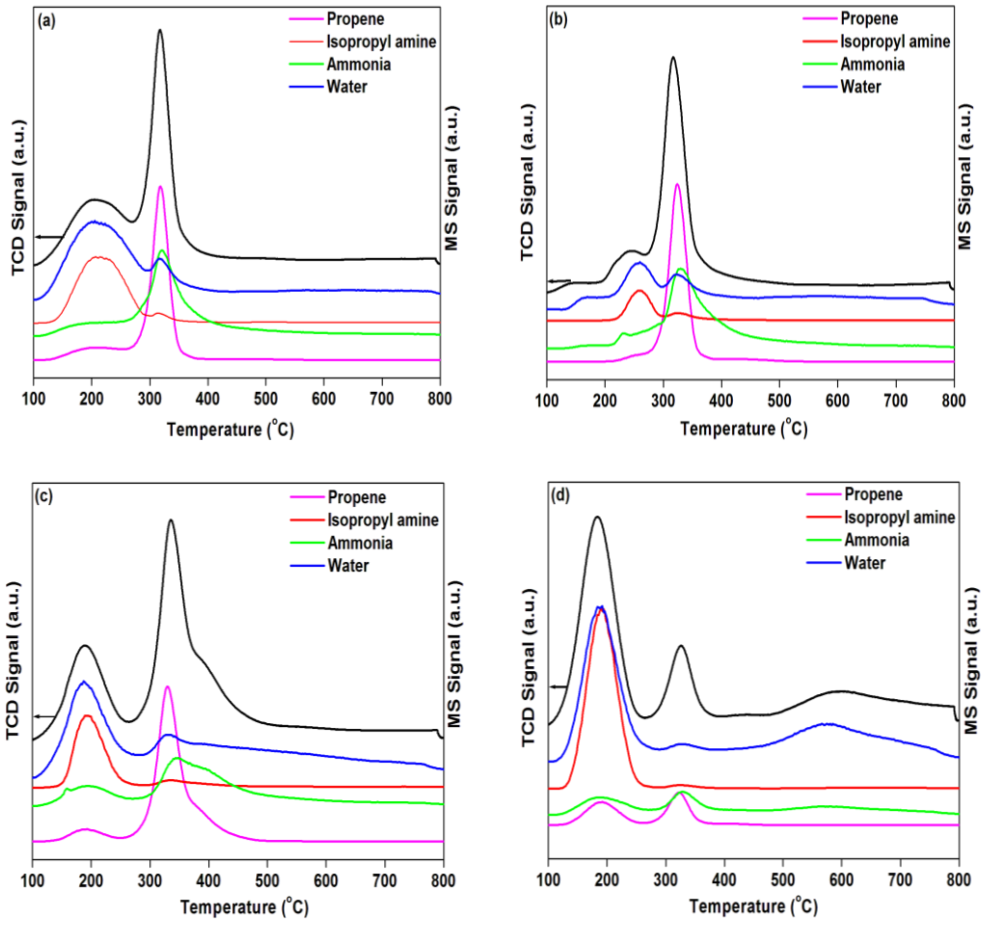


**Fig. 4.5.** TPD-MS profile of (a) Beta-28, (b) Beta-38, (c) Beta-75 and (d) Beta-150.

#### 4.3.2.1.6. FTIR of chemisorbed pyridine

The results of pyridine adsorbtion measurements of beta zeolite catalysts are shown in Fig. 4.6. All samples exhibited three peaks at 1540 $cm^{-1}$, 1450 $cm^{-1}$ and 1490 $cm^{-1}$ pertaining to Brönsted acidity (B), Lewis acidity (L) and combined peak for Brönsted and Lewis acidity (B+L), respectively. The value of B/B+L ratio is listed in Table 4.1. The Beta-38 has the greatest value of B/B+L ratio followed by -28, -75 and -150. This is in accordance with the findings of TPD-MS studies of isopropyl amine desorption, that shows Beta-38 possessing maximum Brönsted acidity. The diminishing value of B/B+L ratio can also be attributed to the enhanced Lewis acidity arising from non-framework aluminium shown by $^{27}$Al MAS NMR.

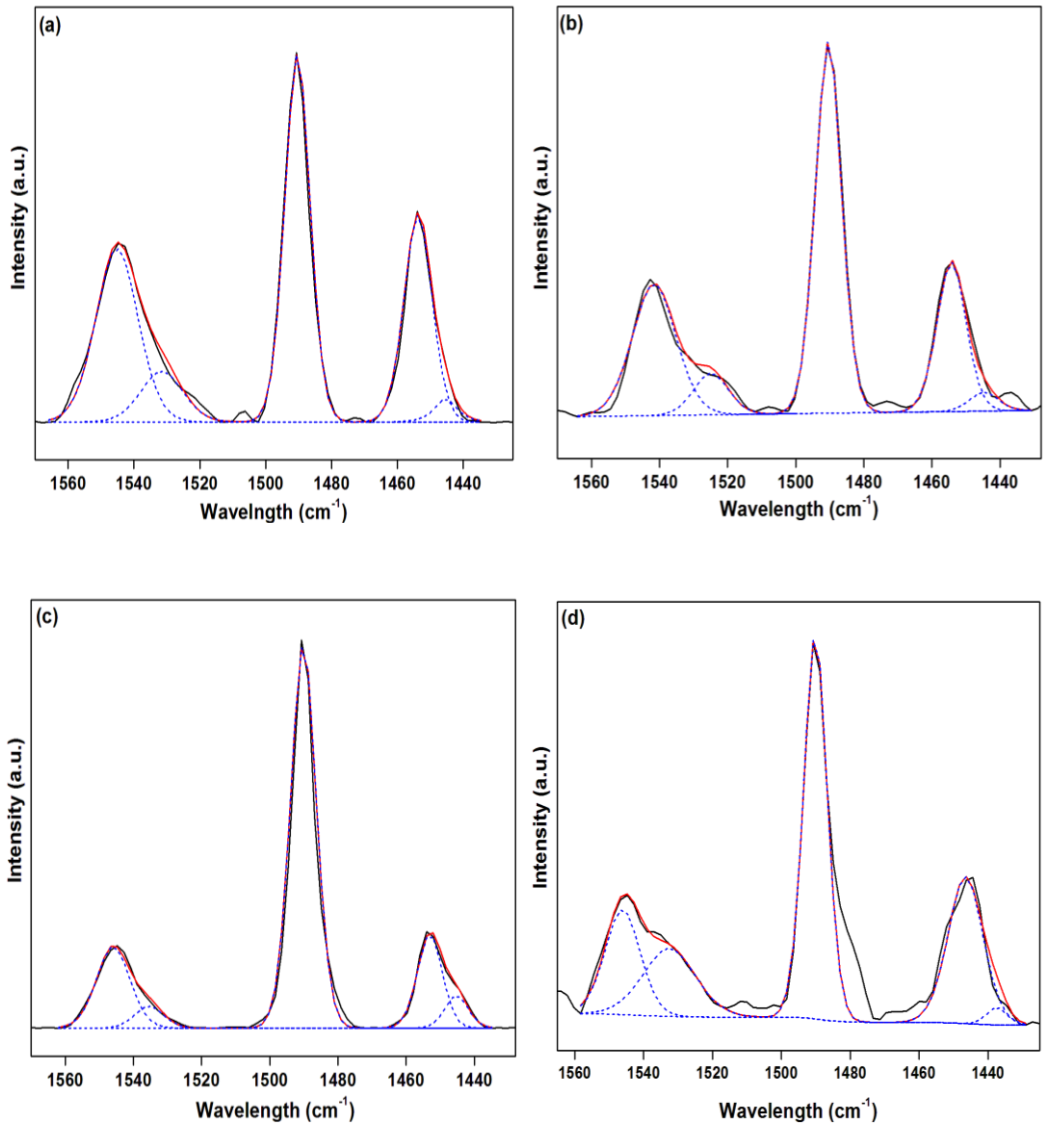


**Fig. 4.6.** FTIR of chemisorbed pyridine spectra; (a) Beta-28, (b) Beta-38, (c) Beta-75 and (d) Beta-150.

### 4.3.2.2. Catalytic activity in sucrose dehydration

The dehydration of sucrose to LA was used for testing the catalytic activity of various catalysts. This reaction can yield numerous products (Scheme 4.1), but we had targeted primarily LA yields. The results of the catalytic activity are given in Fig. 4.7. Initial screening was done using two zeolite structures and compared with other solid acids. Beta zeolite with various $SiO_2/Al_2O_3$ ratios (28, 38, 75 and 150), H-Y ($SiO_2/Al_2O_3 = 30$), acid treated montmorillonite K-10 and 15WZ-750 were compared.

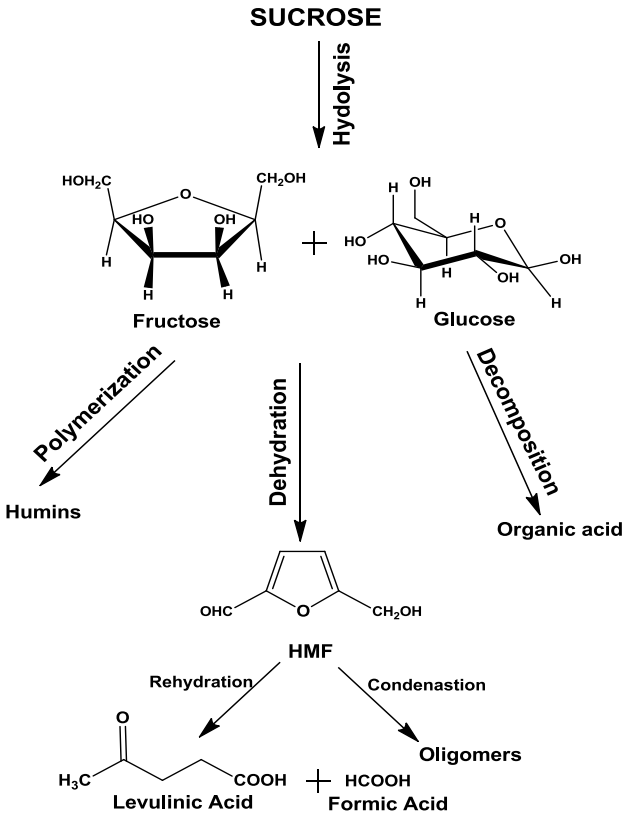


**Scheme 4.1.** Dehydration of sugars to LA.

Under the reaction conditions employed, the H-Y zeolite which is reported to be efficient solid acid catalyst for sugar dehydration to LA gave lower yields than beta zeolite. The superiority of the beta zeolite can be ascribed to its 3 dimensional free channels in contrast to cages of H-Y zeolite [66]. The channels of the beta zeolite facilitate the easy desorption of LA moieties without further degradation in contrast to their further reaction in the cages of Y zeolite. In addition, smaller crystallite size of H-beta also facilitates easier diffusion of reactants/products which results in higher yields of LA. It was seen that K-10, an acid treated clay, was also active for the

reaction and gave 66.7 mol% conversion and 16.56 mol% of LA yields. The inferior performance of K-10 was due to weaker acidity than zeolites [75]. On the other hand, when we have employed 15TZ750 (tungstated zirconia) as catalyst, which has no pore constraints, sucrose conversion was 93.3 mol% while LA yield was only 8.6 mol% because of competitive condensation reactions which are more feasible on the surface acidic sites of the catalyst. This shows that surface acidity has to be optimum for attaining good LA yields. The superiority of the beta zeolite can be inferred from these results.

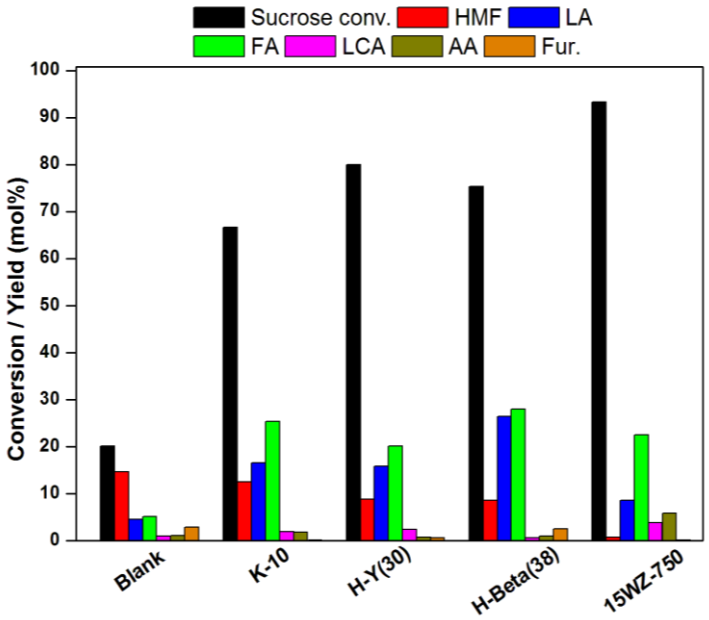


**Fig. 4.7.** Catalytic activity of various catalysts for dehydration of sucrose. Reaction conditions: Sucrose = 1 g in 60 mL water, temperature = 150 °C, catalyst = 50 wt% of sucrose, time = 24 h.

Among the H-Beta zeolites with varying $SiO_2/Al_2O_3$ ratios, the conversion of sucrose decreased from 81.7 to 62.4 mol% with increasing $SiO_2/Al_2O_3$ ratio (Fig. 4.8.), but the LA yields increased from 22.6 to 26.4 mol% with increasing $SiO_2/Al_2O_3$ ratio from 28 to 38 and decreased to 23.3 and 17.03 mol% for $SiO_2/Al_2O_3$ ratio 75 and 150, respectively. The reduction in conversion can be attributed to the decrease in total acidity as a result of lower aluminium content with increasing $SiO_2/Al_2O_3$ ratio of the catalyst. For a better understanding, the LA yield was plotted against total acidity for understanding the role of acidity on the reaction. Fig. 4.9. shows plot of total acidity against sucrose conversion and LA yields. The plot clearly shows that conversion increased linearly with total acidity; however LA yields exhibited some

deviation (since Beta-28 had more acidity as compared to Beta-38 but gave lesser yields of LA). For improved understanding, the effect of weak and strong acidity was studied, these were plotted against LA yields as a ratio to total acidity, as given in Fig. 4.10. It is interesting to note that LA yields increased against moderately strong acidity/total acidity ratio showing that moderately strong acidity contributes towards the formation of LA (Fig. 4.10b). On the other hand, against weak acidity/total acidity ratio (Fig.4.10a), it follows opposite trend.

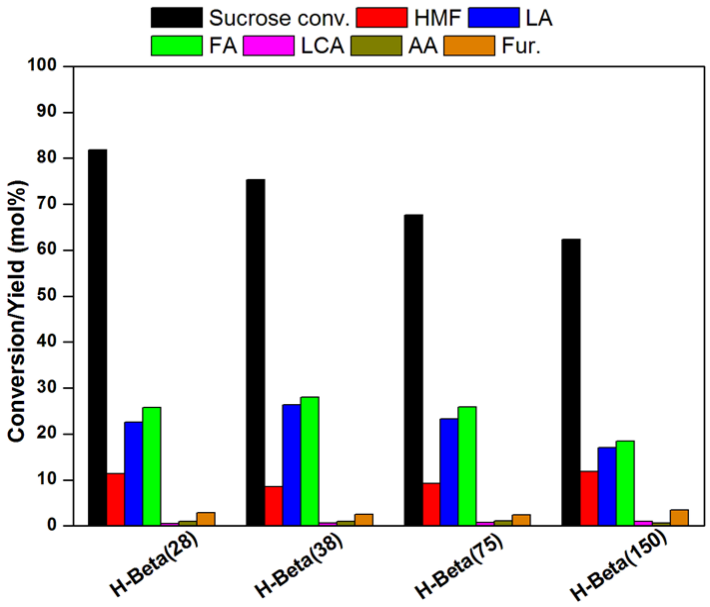


**Fig. 4.8.** Effect of H-Beta with varying $SiO_2/Al_2O_3$ on dehydration of sucrose.

Reaction conditions: Sucrose = 1 g in 60 mL water, temperature = 150 °C, catalyst = 50 wt% of sucrose, time = 24 h.

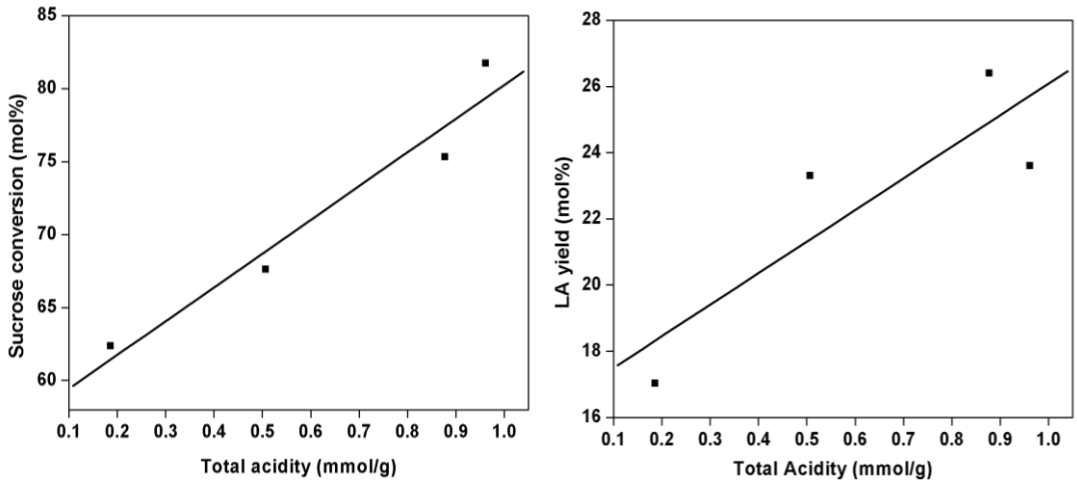


**Fig. 4.9.** Effect of total acidity on (a) sucrose conversion (b) LA yield.

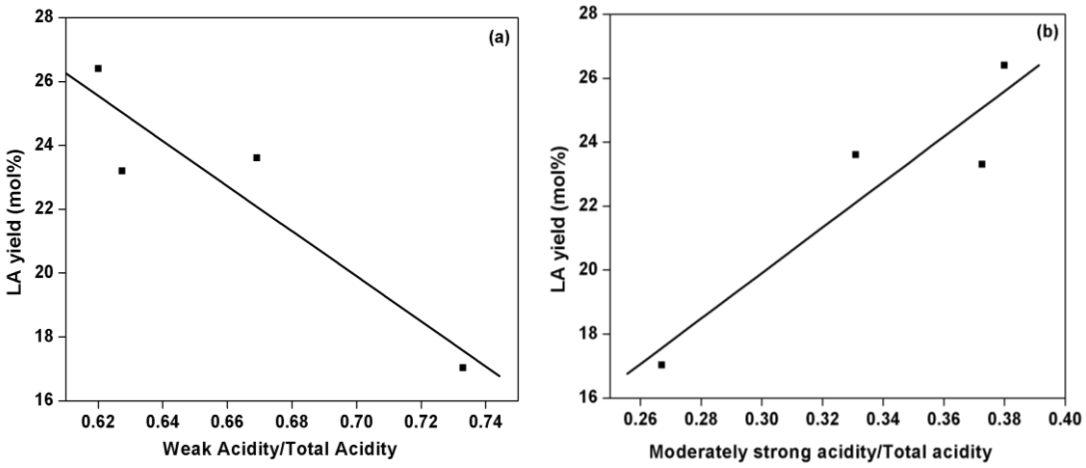


**Fig. 4.10.** Effect of (a) weak acidity/total acidity on LA yield (b) moderately strong acidity/total acidity on LA yield.

Since the LA synthesis is a typically Brönsted acid catalyzed reaction, it becomes important to investigate the effect of Brönsted acidity on LA yields. The propene traces/Brönsted acidity, obtained from TPD-MS, was plotted against LA yields (Fig. 4.11) and a good linear correlation was obtained. This observation is supported by a linear dependence obtained for B/B+L ratio and LA yields (Fig. 4.12) clearly elucidating that the presence of Brönsted acidity favours LA formation.

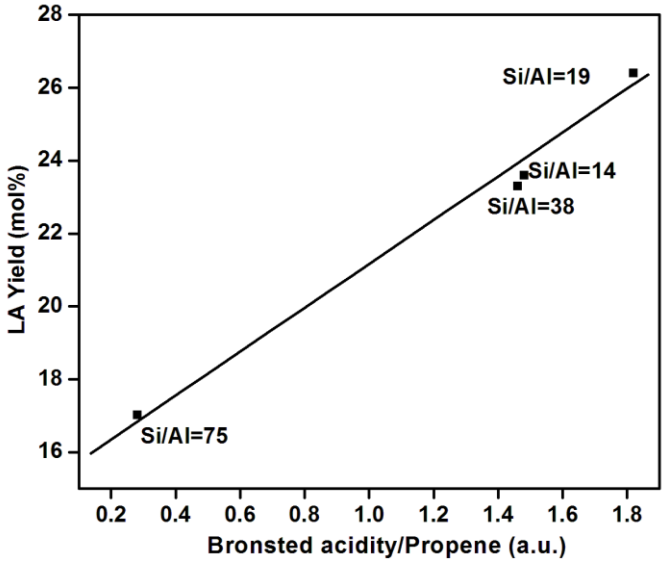


**Fig. 4.11.** Effect of Brönsted acidity on LA yields.

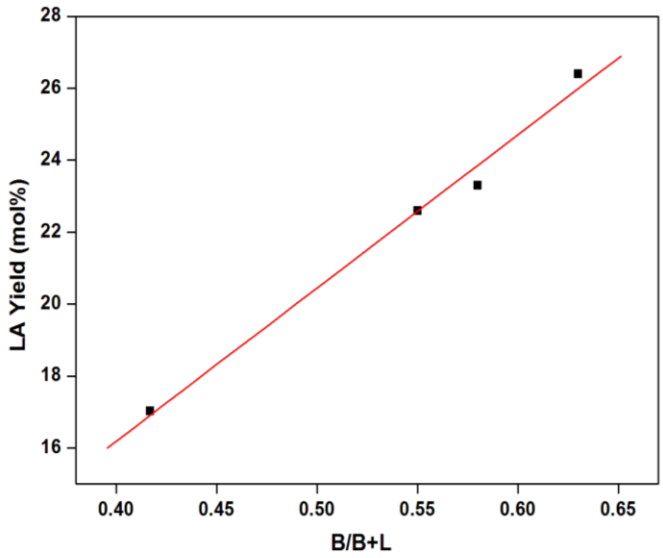


**Fig. 4.12.** B/B+L ratio vs. LA yields.

Thus, from the acidity studies it can be inferred that higher concentration of moderately strong acid sites, which are primarily Brönsted acid sites (as evident from TPD-MS) are crucial for LA formation. As a result, among the samples studied, Beta-38 gave maximum LA yield due to higher concentration of moderately strong Brönsted acidity which arises due to the presence of tetrahedral aluminium (as evident from $^{27}$Al MAS NMR) in contrast to other zeolites. Hence, it was used for further optimization of reaction conditions.

#### 4.3.2.2.1. Effect of temperature

The liquid phase dehydration of sucrose with Beta-38 was studied by varying the reaction temperature in the 130-190 °C range; these results are shown in Fig. 4.13. Conversion increased with temperature as well as with time of the reaction. After 24 h, the conversion increased from 29.2 to 99.8 mol% when temperature was increased from 130 to 190 °C. Time on stream study also reveals that higher conversions (>90 mol%) can be accomplished in less duration (~12 h) at higher temperatures. Evaluating the product distribution, it was found that higher temperatures upto 170 °C and longer duration (20 h) results in higher yields of LA (30.8 mol%) clearly demonstrating that such cascade reactions require high activation energy and time which corroborates with the earlier findings [48,76]. Other products like acetic acid (hereafter AA), lactic acid (hereafter LCA) and furfural were formed in minor concentrations (<3 mol%) suggesting that under the reaction conditions, the decomposition of sugars [77] and decarboxylation of HMF [78] are not dominant. It

was observed that formic acid (hereafter FA) yields were always greater than LA yields as some FA is formed on decomposition of sugars, though it is to a minor extent [79]. With increasing course of reaction the yields of the LA and furans decreased as they undergo side reactions and the yields of AA, LCA increased because of higher sugar decomposition [11, 77]. With further increase in temperature to 190 °C, LA yields decreased indicating side reactions of LA at higher temperature. Additionally, yields of LCA, AA and furfural also decreased and interestingly FA yields were less than LA yields indicating the decomposition of all the products towards coke [80]. At 170 °C, highest yield of LA was obtained, hence it was chosen for further study. The results are consistent with previous studies which show that around 170 °C is the optimal temperature for LA synthesis above which side reactions are dominant due to higher concentration of protonated pyranose form of sugars [46].

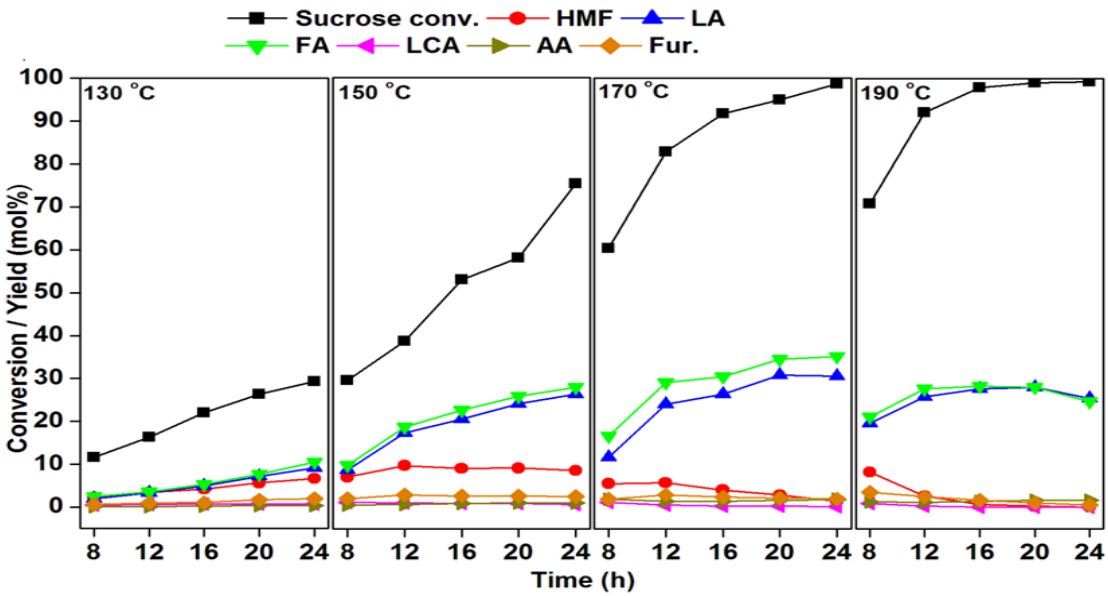


**Fig. 4.13.** Effect of temperature on dehydration of sucrose.

Reaction conditions: Sucrose = 1 g in 60 mL water, catalyst = 50 wt% of sucrose.

#### 4.3.2.2.2. Effect of substrate concentration

The effect of concentration of sucrose on the reaction was studied by varying the reactant concentration from 1.6 to 5 wt%, the results are shown in Fig. 4.14. The change in concentration has marginal effect on conversion with the course of the reaction. However, it has a profound effect on LA yields. On increasing the concentration from 1.6 to 5.0 wt%, LA yields increased from 34.5 to 41.1 mol% in 20

h. Time on stream study also reveals that LA yields increased with time i.e from 8 to 20 h, then decreased thereafter suggesting that LA undergoes further reactions. Yields of HMF and furfural also decrease with increasing time as they can undergo further acid catalyzed polymerization [11]. When substrate concentration is high, rate of the reaction increases leading to higher LA yields [81,82]. Additionally, the available acid sites are mostly occupied with the conversion of sucrose rather than participating in consecutive reactions that convert LA formed to byproducts. Hence, the increase in concentration of substrate has only marginal effect, while it helps to improve the LA yield.

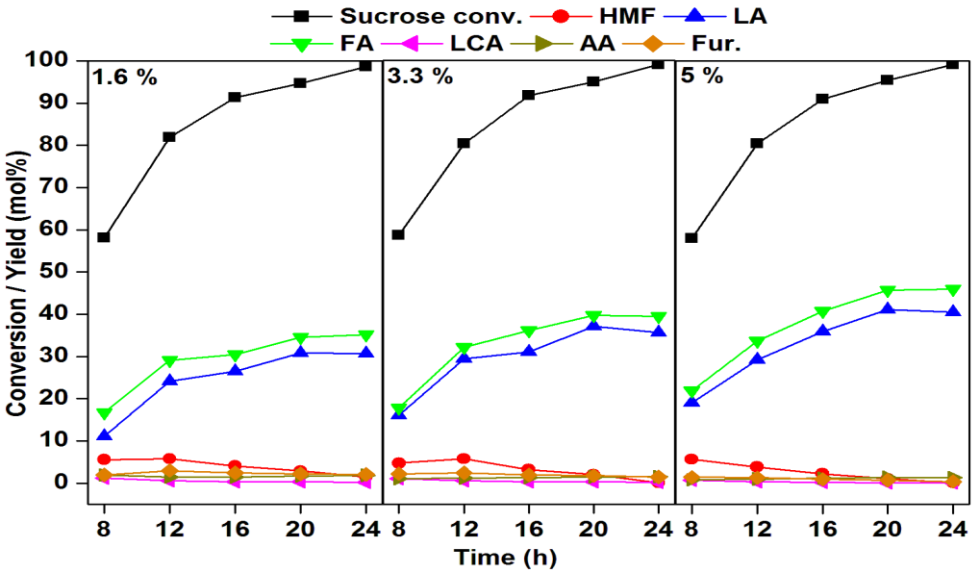


**Fig. 4.14.** Effect of reactant concentration on dehydration.

Reaction conditions: temperature = 170 °C, catalyst = 50 wt% of sucrose.

### 4.3.2.2.3. Effect of catalyst content

The effect of catalyst weight on the reaction has been studied by using different catalyst contents; results of these experiments are shown in Fig. 4.15. There is some increase in conversion with the catalyst content thus helping to reduce the time required for the reaction. After 8 h, conversion increased from 44.6 to 59.1 mol% when the catalyst amount is increased from 25 to 50 wt%. Additionally, LA yields also increased from 10.7 to 19.1 mol%. The enhancement in catalytic activity can be attributed to the presence of more active acidic sites. However, the effect on conversion with the increase in catalyst amount becomes marginal at longer reaction times, though its effect on LA yields remain significant, which clearly shows the necessity of optimum catalyst content to drive the reaction towards LA formation.

After 20 h on stream, with the increase in catalyst content from 25 to 37.5wt%, the conversion increased from 91.7 to 95.5 mol% and the LA yields increased from 32.3 to 40.4 mol%. Under the reaction conditions employed, since the other products are formed in minor concentrations (< 2 mol%) and only LA yields are increased it can be deduced that presence of moderately strong acidic sites which are primarily Brönsted in nature (as evident from TPD and TPD-MS) promotes rehydration of HMF leading to enhanced LA formation. Accordingly, previous reports states that LA is exclusively produced on Brönsted sites [83]. With further increase in catalyst amount to 50 wt% the conversion and yields were almost unaltered. Thus, 37.5 wt% was found to be the optimum catalyst content. These results are consistent with the earlier findings in which there was no appreciable change in catalytic activity beyond the optimum catalyst content [39, 22].

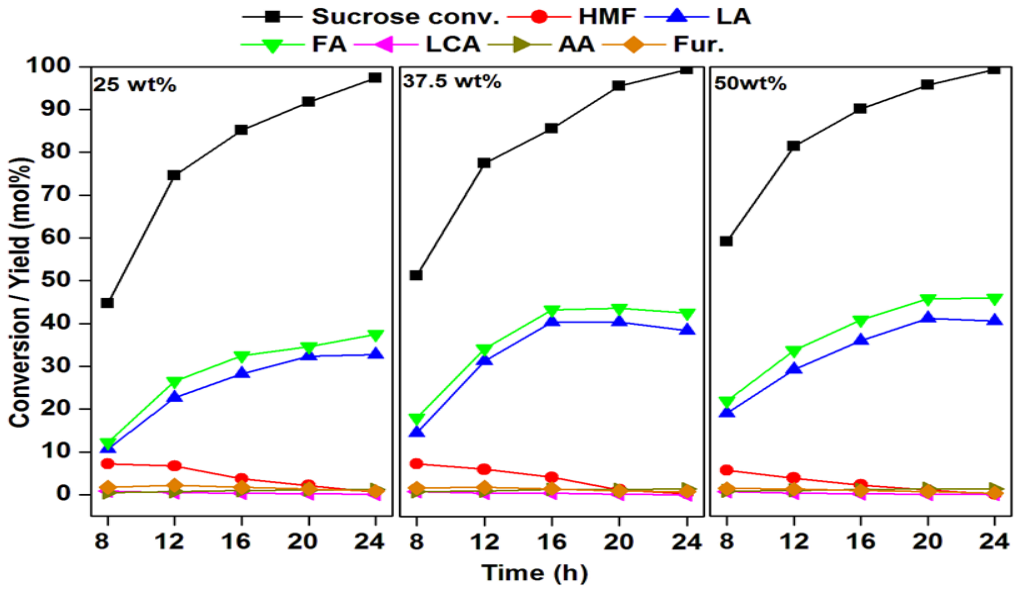


**Fig. 4.15.** Effect of catalyst content on dehydration on sucrose.

Reaction conditions: Sucrose = 3 g in 60 mL water, temperature = 170 °C.

#### 4.3.2.2.4. Kinetic studies

In order to find the activation energy of the reaction, rates of reaction at various temperatures (130-170 °C) were determined. Utilizing these rates, Arrhenius plot was obtained (Fig. 4.16). From the Arrhenius plot, the activation of sucrose to LA was calculated to be 20 kcal/mol which is comparable with the activation energy of other solid acid catalyst used for dehydration reaction [57,56].

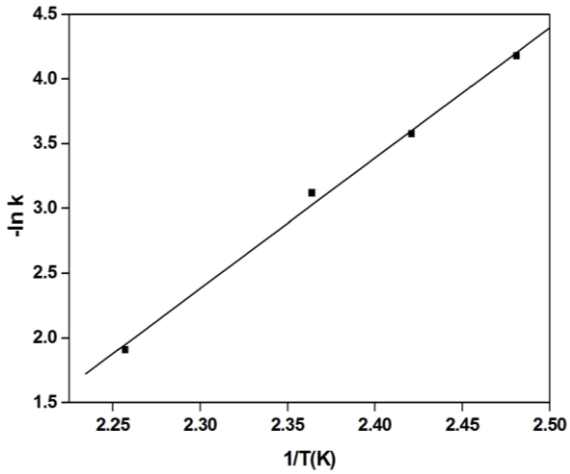


**Fig. 4.16.** Arrhenius plot for dehydration of sucrose to LA.

#### 4.3.2.2.5. Recyclability studies

To check the recyclability of the catalyst, used catalyst was calcined in air at 450 °C for 3 h to oxidize the carbonaceous deposits on the catalyst. The calcined (Beta-38) catalyst was used for the reaction. The results of recyclability are shown in Fig. 4.17. There was marginal effect on the sucrose conversion; however the LA yields detoriated from 41 to 25 mol% from 1$^{st}$ run to recycle 3 after which the yields of LA were stable.

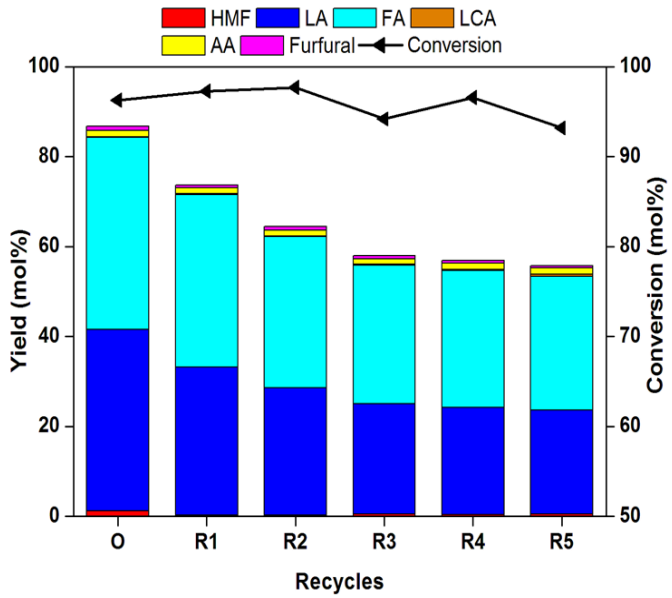


**Fig. 4.17.** Recyclability studies of sucrose dehydration to LA.

Reaction conditions: Sucrose = 3 g in 60 mL water, temperature = 170 °C, catalyst = 37.5 wt% of sucrose, time = 20 h.

In order to investigate the decrease in LA yields, the reaction mixture was analyzed by ICP-OES which showed the leaching of aluminium from zeolite lattice. In order to investigate structural changes, the catalyst was subjected to XRD and NMR studies, the results are shown in Fig. 4.18 and Fig. 4.19, respectively. From the XRD studies it can be seen that the BEA structure of the catalyst is retained, but there was decrease in peak intensity and absence of certain peaks clearly exhibits the decrease in crystallinity. The $^{27}$Al MAS NMR of the fresh catalyst shows only one peak at ~50 ppm pertaining to tetrahedral Al species, however reused catalyst shows an additional peak at ~0 ppm pertaining to octahedral Al species, which might have been due to dealumination in the harsh acidic reaction conditions (products FA as well as LA are acids). Due to dealumination, the overall acidity and particularly the Brönsted acidity decreases leading to inferior catalytic performance.

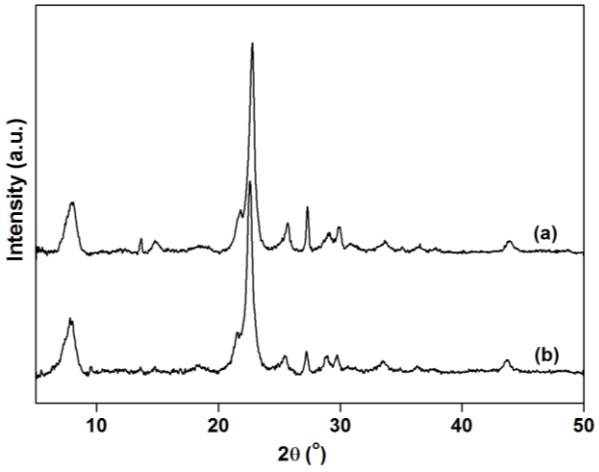


**Fig. 4.18.** XRD pattern of (a) fresh and (b) used catalyst.

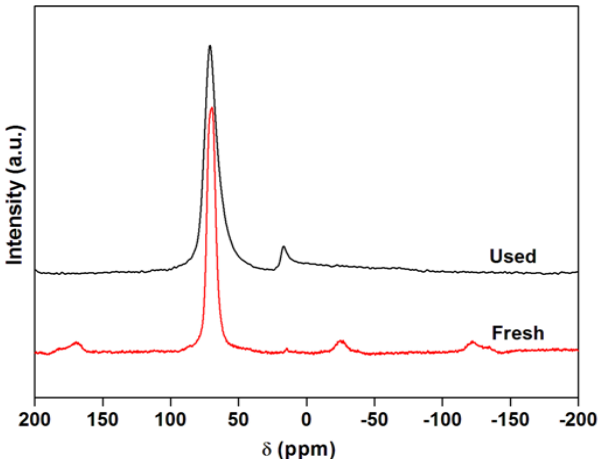


**Fig. 4.19.** $^{27}$Al MAS NMR of fresh and used catalyst.

### 4.3.2.3. Dehydration of glucose to LA

Since glucose is the most abundant and readily available sugar, it was used for dehydration reaction to get LA. The effect of temperature was studied in the temperature range of 130-190 °C; results are shown in Fig. 4.20. Glucose conversion increased with temperature as well as with increase time of the reaction. After 20 h on stream, the conversion increased from 11.3 to 97.1 mol% when temperature was increased from 130 to 190 °C. Similar to sucrose dehydration, good conversions (>90 mol%) were accomplished in less duration (~12 h) at higher temperatures. Evaluating the product distribution, it was found that the formation of products followed a similar pattern as that in sucrose dehydration giving higher yields of LA at higher temperatures (upto 170 °C) and on longer duration. At 20 h, the LA yields increased from 1.2 to 39.6 mol%, when temperature was raised from 130 to 170 °C. Other products like AA, LCA and furfural were formed in minor concentrations (<3 mol%). With further increase in temperature to 190 °C, LA yields decreased from 39.6 to 32.3 mol%, thus 170 °C was the optimum temperature which is in accordance with the previous study [46].

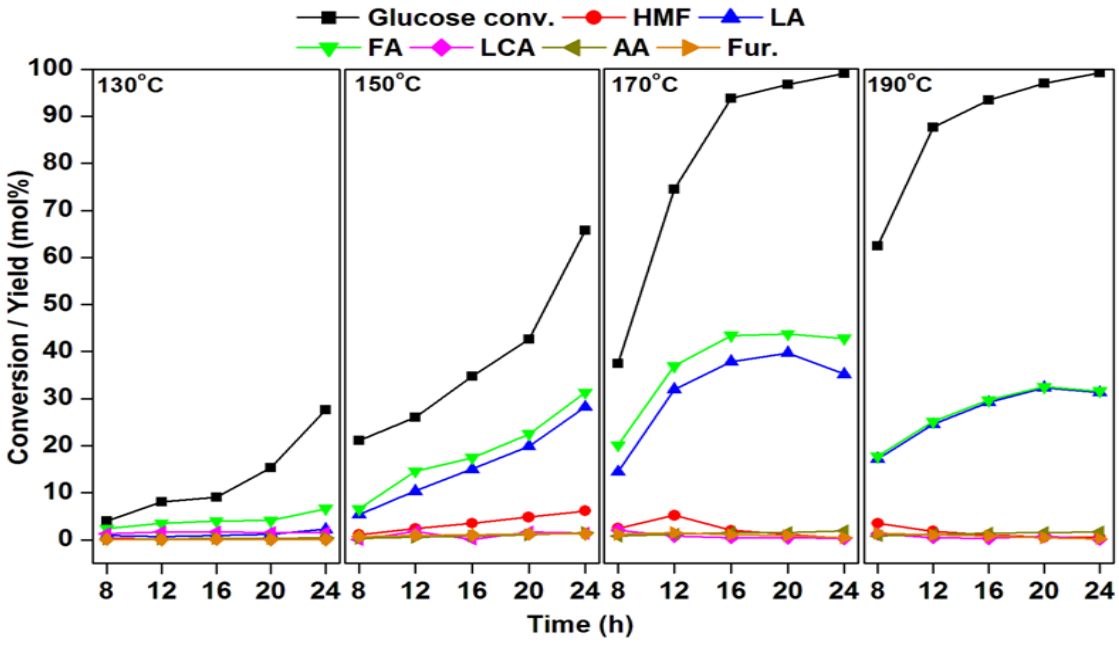


**Fig. 4.20.** Effect of temperature on dehydration of glucose.

Reaction conditions: Glucose = 3 g in 60 mL water, catalyst = 37.5 wt% of glucose.

In the case of glucose dehydration, the effect of catalyst weight was also studied and results are shown in Fig. 4.21. Increasing the catalyst amount from 25 to

50 wt% leads to enhanced conversion in less duration of the reaction. After 8 h the conversion increased from 21.9 to 37.4 mol% when catalyst amount was increased from 25 to 50 wt%. However, this increase in conversion becomes marginal with further course of the reaction. LA yields also increased with the catalyst content and reaction time. After 20 h, the LA yields increased from 30.9 mol% to 39.6 mol% when the catalyst content is increased from 25 to 37.5 wt% and remains same on further increasing the catalyst content i.e. 50 wt%. Hence, 37.5 wt% was found to be the optimum catalyst content. Similar observations were made by Peng *et al* [39] where optimum catalyst content was needed to achieve higher yields of LA, but beyond this optimum content there was no marked difference. The formation of other products is in accordance with sucrose dehydration clearly demonstrating that over the Brönsted sites of the catalyst LA formation is preferred over to other competitive side reactions [84].

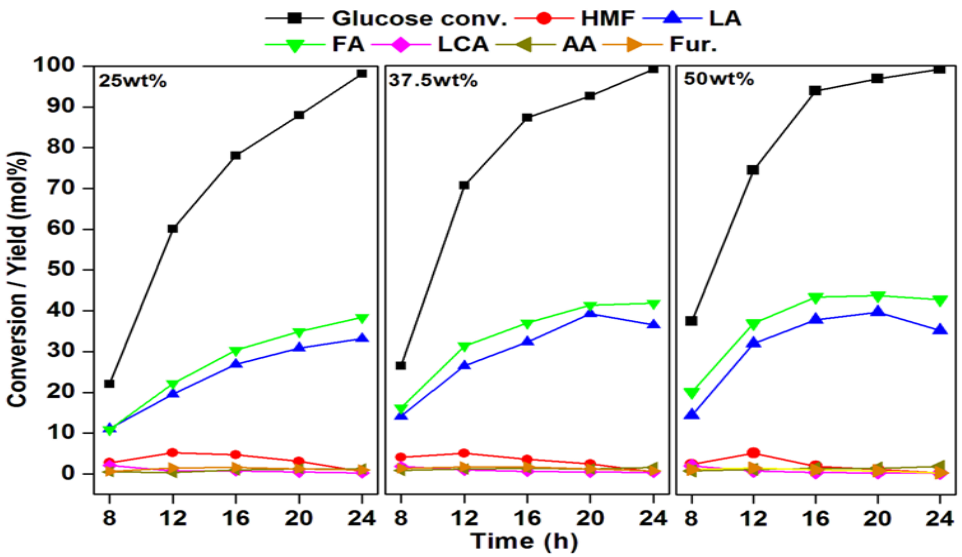


**Fig.4.21.** Effect of catalyst weight on dehydration of glucose.

Reaction conditions: Glucose = 3 g in 60 mL water, temperature = 170 °C.

### 4.3.2.4. Dehydration of other saccharides to LA

In order to evaluate the effectiveness of the catalyst to convert other saccharides to LA, various carbohydrates were used for dehydration reaction, the results are shown in Table 4.2. It was found that sucrose gave maximum yield of LA, i.e. 41 mol%. Since sucrose releases its monosaccharides slowly into the reaction solution [85], side (condensation) reactions are significantly suppressed. With

fructose, almost complete conversion (99 mol%) was observed with 31 mol% LA yield in 12 h. Fructose being a ketose sugar is more reactive leading to complete conversion in less reaction time which is in accordance with the study of Jow *et al* [55]. But the lower yield of LA suggests that acidity and small crystallite size of the catalyst promotes the condensation reactions when ketose sugar is employed for dehydration reaction. On the contrary, aldose sugar gave higher yields than ketose sugar exhibiting the efficiency of catalyst to promote isomerization of aldose to ketose followed by subsequent dehydration and rehydration. Similar observations were made by Riisager *et a*l where the zeolites were found to be efficient for aldose to ketose isomerization [86]. In addition to glucose, maltose and cellobiose; disaccharides of glucose also gave good LA yields (~37 mol% and ~35 mol% respectively). Inulin, a polysaccharide was also utilized for dehydration reaction and 37 mol% of LA was formed with the polysaccharide. Thus, the efficacy of the catalyst to convert various saccharides to LA can be clearly visualized.

**Table 4.2:** Dehydration of sugars to LA catalyzed by Beta-38.

| S.N | Substrate | Conv. | Yield (mol%) | | | | | |
|---|---|---|---|---|---|---|---|---|
| | | (mol%) | HMF | LA | FA | LCA | AA | Fur |
| 1. | Fructose[*] | 91.3 | 7.77 | 31.7 | 35.3 | 0.07 | 1.0 | 2.3 |
| 2. | Fructose[$] | 99.1 | 0.56 | 30.8 | 37.5 | 0.09 | 1.2 | 2.2 |
| 3. | Glucose | 92.5 | 2.37 | 39.2 | 41.3 | 0.41 | 1.5 | 1.1 |
| 4. | Maltose | 90.1 | 1.23 | 37.4 | 40.6 | 0.30 | 1.4 | 0.6 |
| 5. | Sucrose | 95.5 | 1.20 | 40.5 | 42.7 | 0.15 | 1.3 | 0.9 |
| 6. | Cellobiose | 91.9 | 2.29 | 34.8 | 36.2 | 0.41 | 0.9 | 1.1 |
| 7. | Inulin | 98.4 | 0.28 | 36.7 | 39.2 | 0.19 | 1.2 | 0.5 |

Reaction conditions: sugar = 3 g in 60 mL water, temperature = 170 °C, catalyst = 37.5 wt% of sugar, time = 20 h.

[*] temperature = 150 °C, [$] time = 12 h.
Legend: HMF = 5-Hydroxymethyl furfural, LA = Levulinic acid, FA = Formic acid, AA = Acetic acid, LCA = Lactic Acid, Fur = Furfural.

#### 4.3.2.5. Synthesis of ethyl levulinate

For evaluating the effectiveness of the catalyst in non-aqueous solvents synthesis of ethyl levulinate (EL) from glucose was carried out using Beta-38 under the optimized reaction conditions by replacing water with ethanol. Ethyl levulinate,

which is a bio-derived fuel additive, was obtained in good yields (39 mol%). The used catalyst was washed, dried and calcined in air at 450 °C for 4 h and used for further recyclability studies. The results of this study are shown in Table 4.3. It can be seen that the catalyst can be recycled upto three cycles with marginal decrease in ethyl levulinate yields. Thus, replacing the harsh, acidic hydrothermal reaction conditions with milder conditions by employing the non-aqueous solvents, the catalyst can retain its acidity and activity.

**Table 4.3:** Recyclability of Beta-38 for conversion of glucose to EL.

| S.N. | Recycles | Glucose conversion (mol%) | Ethyl Levulinate (mol%) |
|---|---|---|---|
| 1. | Fresh | 99 | 39 |
| 2. | 1st | 98 | 36 |
| 3. | 2nd | 98 | 35 |
| 4. | 3rd | 98 | 34 |

Reaction conditions: Glucose = 3 g in 60 mL EtOH, catalyst = 37.5 wt% of glucose, temperature = 170 ºC, time = 20 h.

### 4.3.3. Conclusions

Levulinic acid, a highly important bulk chemical, was effectively synthesized from various saccharides in good yields using beta zeolite catalyst. Insights into the requirement of acidic sites and their nature for such cascade reactions are also furnished. The effect of $SiO_2/Al_2O_3$ ratio on the catalytic activity and yield was systematically investigated. A good linear correlation between LA yield and moderately strong acidity/total acidity ratio, particularly the Brönsted acidity was obtained. These findings demonstrated that the presence of moderately strong acidity which is primarily Brönsted in nature is crucial for higher LA yields in such cascade reactions. These key findings pave the way for a rationale designing of a solid acid catalyst for LA from various saccharides. The acidic, harsh hydrothermal reaction conditions leads to detoriated catalytic performance which could be retained by employing non-aqueous systems. Thus, the important criteria of optimum/type of acidity and the recyclability issues have been efficaciously addressed in the present study.

## 4.4. References


1. C.H. Zhai, X. Xia, D.S. Tong, J. Beltramini, Chem. Soc. Rev. 40 (2011) 5588.
2. P. Gallezot, Chem. Soc. Rev. 41 (2012) 1538.
3. A. Corma, S. Iborra, A. Velty, Chem. Rev. 107 (2007) 2411.
4. V. Ghorpade, M. Hanna, US Patent 5859263 (1996).
5. G.W. Huber, S. Iborra, A. Corma, Chem. Rev. 106 (2006) 4044.
6. P.D. Bloom, US Patent 0216915 (2010).
7. J.J. Bozell, L. Moens, D.C. Elliott, Y. Wang, G.G. Neuenscwander, S.W. Fitzpatrick, R.J. Bilski, J.L. Jarnefeld, Resources Conser. Recycl. 28 (2000) 227.
8. J. Horvat, B. Klaic, B. Metelko, V. Sunjic, Tetrahedron Lett. 26 (1985) 2111.
9. R.W. Thomas, H.A. Schuette, J. Am. Chem. Soc. 58 (1931) 2324.
10. B.F. Kuster, H.M.G. Temmink, Carbohydr. Res. 54 (1977) 185.
11. F.S. Asghari, H. Yoshida, Ind. Eng. Chem. Res. 46 (2007) 7703.
12. J. Shen, C.E. Wyman, AIChE J. 58 (2012) 236.
13. L. Yan, N. Yang, H. Pang, B. Liao, Clean 36 (2008) 158.
14. A. Galletti, C. Antonetti, V.D. Luise, D. Licursi, N.N. Dinasso, Bioresources, 7 (2012) 1824.
15. B. Girisuta, L. Janssen, H.J. Heeres, Green Chem. 8 (2006) 701.
16. B. Girisuta, L. Janssen, H.J. Heeres, Che. Eng. Res. Des. 84(A5) (2006) 339.
17. B. Girisuta, L. Janssen, H.J. Heeres, Ind. Eng. Chem. Res. 46 (2007) 1696.
18. V.E. Tarabanko, M.Y. Chernyak, S.V. Aralova, B.N. Kuznetsov, Reac. Kinet. Catal. Lett. 75 (2002) 117.
19. L. Kupiainen, J. Ahola, J. Tanskanen, Ind. Eng. Chem. Res. 49 (2010) 8444.
20. Q. Fang, M.A. Hanna, Bioresour. Technol. 81 (2002) 187.
21. J.Y. Cha, M.A. Hanna, Ind. Crop Prod. 16 (2002) 109.
22. C. Chang, P. Cen, X. Ma, Bioresour. Technol. 98 (2007) 1448.
23. T. Runge, C, Zhang, Ind. Eng. Chem. Res. 51 (2012) 3265.
24. S. Rivas, M.J. Ganzales-Munoz, C. Vila, V. Santos, J.C. Parajo, Ind. Eng. Chem. Res. 52 (2013) 3951.
25. G.T. Jeong, Ind. Crop Prod. 62 (2014) 77.
26. G.T. Jeong, C.H. Ra, Y.K. Hong, J.K. Kim, I. Kong, S.K. Kim, D.H. Park Bioprocess Biosyst. Eng. DOI 10.1007/s00449-014-1259-5.

27. W. Kraithong, N. Viriya, N. Laosiripojana, Innov. Syst. Des. Eng. 5 (2014) 1.
28. T. Retsina, V. Pylkkanen, R. O'Connor, US0308720A1 (2014).
29. G.D. Vries, J.A. Kroon, J. Parton, P.L. Woestenborghs, A.De Rijke, US0018555A1 (2014)
30. M.H. Fan, L.F. Yan, Chin. J. Chem. Phys. 27 (2014) 92.
31. A. Daniel, US0316159A1 (2014).
32. B.D. Mullen, D.J. Yontz, C.M. Leibig, US012634A1 (2014).
33. L. Yan, A.A. Greenwood, A. Hossain, B. Yang, RSC Adv. 4 (2014) 23492.
34. H. Guerrero, C. Lafuente, F. Royo, L. Lomba, B. Giner, Energ. Fuel 25 (2011) 3009.
35. R.J. Assary, P.C. Redfern, J.R. Hammond, J. Greedy, L.A. Curtiss, J. Phys. Chem. B 114 (2010) 9002.
36. C.B. Rasrendra, I. Makertihartha, S. Adisasmita, H.J. Heeres, Top. Catal. 53 (2010) 1241.
37. Y. Shen, J. Sun, Y. Yi, B. Wang, F. Xu, R. Sun, J. Mol. Catal. A. 394 (2014) 114.
38. Y. Shen, Y. Xu, J. Sun, B. Wang, F. Xu, R. Sun, Catal. Commun. 50 (2014) 17.
39. L. Peng, L. Lin, J. Zhang, B. Zhang, Y. Gong, Molecules 15 (2010) 5258.
40. A.S. Khan, Z.B. Man, M.A. Bustan, C.F. Kait, A.S. Maulad, Appl. Mech. Mater. 625 (2014) 353.
41. B. Estrine, K.O. Vigier, F. Jerome, RSC Adv. 4 (2014) 28836.
42. H. Ren, Y. Zhou, L. Liu, Bioresour. Technol. 129 (2013) 616.
43. Z. Sun, M. Cheng, H. Li, T. Shi, M. Yuan, X. Wang, Z. Jiang, RSC Adv. 2 (2012) 9058.
44. A.S. Amarasekara, B. Wiredu, Bioenerg. Res. DOI 10.1007/s12155-014-9459-z.
45. C. Zhou, X. Yu, M.A. Haike, H.E. Ronghai, S. Vittayapadung, Chi. J. Chem. Eng. 21 (2013) 544.
46. A. Szabolcs, M. Molnar, G. Dibo, L.T. Mika, Green Chem. 15 (2013) 439.
47. L. Hu, G. Zhao, W. Hao, X. Tang, Y. Sun, L. Lin, S. Lin, RSC Adv. 2 (2012) 11184.
48. R.A. Schraufnagel, H.F. Rase, Ind. Eng. Chem. Prod. Res. Dev. 14 (1975) 40.

49. R. Weingarten, W.M. Conner, G.W. Huber, Energy Environ. Sci. 5 (2012) 7559.
50. J. Hegner, K.C. Pereira, B. DeBoef, B.L. Lucht Tetrahedron Lett. 51 (2010) 2356.
51. J. Potvin, E. Sorlien, J. Hegner, B. DeBoef, B.L. Lucht, Tetrahedron Lett. 52 (2011) 5891.
52. H. Yang, L. Wang, L. Jia, C. Qui, Q. Pang, X. Pan, Ind. Eng. Chem. Res. 53 (2014) 6562.
53. W. Zeng, D. Cheng, H. Zhang, F. Chen, X. Zhan, React. Kinet. Mech. Cat. 100 (2010) 377.
54. K. Lourvanij, G.L. Rorrer, Ind. Eng. Chem. Res. 32 (1993) 11.
55. J. Jow, G.L. Rorrer, M.C. Hawley, Biomass 14 (1987) 185.
56. K. Lourvanij, G.L. Rorrer, Appl. Catal. A Gen. 109 (1994) 147.
57. D. Ding, J. Wang, J. Xi, X. Liu, G. Lu, Y. Wang, Green Chem. 16 (2014) 3846.
58. P. Wang, S. Khan, H. Yu, Adv. Mater. Res. 96 (2010) 183.
59. H. Chen, B. Yu, S. Jin, Bioresour. Technol. 102 (2011) 3568.
60. P.P. Upare, J.W. Yoon, M.Y. Kim, M.Y. Kang, D.W. Hwang, Y.K. Hwang, H.H. Kung, J.S. Chang, Green Chem. 15 (2013) 2935.
61. S. Vyves, J. Thomas, J. Geboers, S. Keyzar, M. Smet, W. Dehaen, P.A. Jacobs, B.F. Sels, Energy Environ. Sci. 4 (2011) 3601.
62. D.M. Lai, L. Deng, Q.X. Guo , Y. Fu, Energy Environ. Sci. 4 (2011) 3552.
63. X. Jia, J. Lee, Y. Yang, ChemSusChem 7 (2014) 2670.
64. N.A.S. Ramli, N.A.S. Amin, Appl. Mech. Mater. 625 (2014) 361.
65. N.A.S. Ramli, N.A.S. Amin, Fuel Process Technol. 128 (2014) 490.
66. W.M. Meier, D.H. Olson, C.H. Barlocher, Atlas of Zeolite Structure Types, Elsevier, 1996.
67. D.M. Roberge, H. Hausmann, W.F. Holderich, Phys. Chem. Chem. Phys. 4 (2002) 3128.
68. A. Shrotri, A. Tanksale, J.N. Beltramini, H. Gurav, S.V. Chilukuri, Catal. Sci. Technol. 2 (2012) 1852.
69. H. Kosslick, G. Lischke, G. Walther, W. Storek, A. Martin, R. Fricke, Microporous Mater. 9 (1997) 13.

70. A. Omegna, M. Vasic, J.A. Bokhova, G. Pirngruber, R. Prins, Phys. Chem. Chem. Phys. 6 (2004) 447.
71. E.B. Lami, P. Massiani, F. Renzo, P. Espiau, F. Fagula, Appl. Catal. 72 (1991) 139.
72. J. Rocha, J. Klinowski, J. Chem. Soc., Chem. Commun. (1991)1121.
73. Q.L. Wang, G. Gianenetto, M. Guisnet, J. Catal. 130 (1991) 471.
74. G.J. Ray, B.L. Meyers, C.L. Marschall, Zeolites 7 (1987) 307.
75. U. Flessner, D.J. Jones, J. Rozière, J. Zajac, L. Storaro, M. Lenardac, M.Pavan, A. Jiménez-López, E. Rodrıguez-Castellón, M. Trombetta, G. Busca, J. Mol. Catal. A. Chem. 168 (2001) 247.
76. M. Kang, S.W. Kim, J.W. Kim, T.H. Kim, J.S. Kim, Renewable Energy 54 (2013) 54.
77. O. Novotny, K. Cejpek, J. Velisek, Czech J. Food. Sci. 26 (2008) 117.
78. C. Moreau, R. Durand, S. Razigade, J. Duhamet, P. Faugeras, P. Rivalier, P. Ros, G. Avignon, Appl. Catal. A Gen. 145 (1996) 211.
79. L. Deng, Y. Zhao, J. Li, Y. Fu, B. Liao, Q.X. Guo, ChemSusChem 3 (2010) 656.
80. N. Akiya, P.E. Savage, AIChE J. 44 (1998) 405.
81. S.S. Joshi, A.D. Zodge, K.V. Pandhare, B.D. Kulkarni, Ind. Eng. Chem. Res. 53 (2014) 18796.
82. J. Ahlkvist, Formic and levulinic acid from cellulose via heterogeneous catalyst
83. R. Weingarten, Y.T. Kim, G.A. Tompsett, A. Fernandez, K.S. Han, E.W. Hagaman, W.C. Conner, J.A. Dumesic, G.W. Huber, J. Catal. 304 (2013) 123.
84. V. Choudhry, S.H. Mushrif, C. Ho, A. Anderko, V. Nikolakis, N.S. Marinkovic, A.I. Frenkel, S.I. Sandler, D.G. Valchos, J. Am. Chem. Soc. 135 (2013) 3997.
85. M.S. Holm, S. Saravanamurugan, E. Taarning, Science 328 (2010) 602.
86. S. Saravanamurugan, M. Paniagua, J.A. Melero, A. Riisager, J. Am. Chem. Soc. 135 (2013) 5246.

# *Chapter 5*

Synthesis of 5-HMF and LA using nanocrystalline rare earth phosphates

## 5.1. Introduction

The plummeting reserves of fossil fuels, environmental concerns and energy crisis have driven the mankind to look for alternative and sustainable sources of energy, fuels and chemicals. Biomass, which has emerged as unrivalled renewable source of chemicals and fuels is indeed valorised by several interesting approaches [1]. As discussed earlier, synthesis of 5-Hydroxymethyl furfural (5-HMF) and levulinic acid (LA) from biomass derived carbohydrates is of paramount importance. These compounds have tremendous ability to render a wide array of highly important chemicals and fuels [2-4]. However, deriving these compounds is substantially difficult due to polyfunctionality of biomass feedstocks and instability of targeted molecules.

Levulinic acid forms through cascade reactions, whereas efficient production of HMF requires the minimization of unwanted side reactions originating from reactions between reactants, reaction intermediates and products. For HMF, the dehydration reaction is explored in various mediums like high boiling point aprotic solvent such as dimethylsulfoxide [5,6] and other organic solvents [7,8], ionic liquids [9,10] and biphasic systems [11,12] using various homogeneous and heterogeneous catalysts. Most of these processes are associated with disadvantages such as high energy inputs required for separation of products, environmental pollution, expensive solvents, mass transfer limitations and corrosion due to use of liquid acid catalysts. On the otherhand, water is a valuable solvent due to its easy availability, inexpensive, non-toxicity and ease of disposal in an environmentally benign manner. Therefore, research is now focussed on the partial or full substitution of organic solvents with water. Additionally, 5-HMF can be rehydrated to LA in water, furnishing another important bulk chemical. However, water being highly polar, maintaining the desirable activity and stability of the acid catalyst is a major challenge. The deactivation of the catalysts is caused due to their reaction with moieties that have an electron pair, leading to their strong adsorption. In order to overcome the aforementioned challenges it is necessary to use solid acid catalysts having unique stability and water tolerant acidic properties.

Rare earth orthophosphates ($LnPO_4$) possess numerous beneficial properties like low solubility in water [14], high refractive index, high thermal stability [13] and high concentration of lasing ions [15]. Due to these properties, they find wide range of

applications as luminescent materials, sensors, magnets and ceramics and as catalysts [16-20]. Additionally, they are highly stable in acidic and basic conditions [14]. Visualizing these properties, they were explored for the synthesis of 5-HMF and LA from carbohydrates in aqueous medium. As the effect of acidity and the nature of acid sites are crucial for targeted molecules, they are evaluated thoroughly and an attempt was made to correlate yields with acidity. In addition, various process conditions were optimized to get maximum yields of LA and 5-HMF.

## 5.2. Synthesis of 5-HMF and LA with lanthanide phosphates

### 5.2.1. Experimental procedures

#### 5.2.1.1. Materials

Fructose, glucose, sucrose and maltose were purchased from Loba Chemie Pvt. Ltd. 5-Hydroxymethyl furfural, levulinic acid, lactic acid, furfural, acetic acid were procured from Sigma Aldrich. Cellobiose and Inulin were purchased from Alfa Aesar. Rare earth (La, Ce, Nd, Sm) nitrates, gadolinium oxide, terbium chloride and dysprosium chloride were purchased from Indian Rare Earths Ltd, India. Ammonium dihydrogen phosphate was procured from Merck. All the chemicals were of research grade and were used without further purification. The catalysts were prepared by aqueous co-precipitation using lanthanide salts and ammonium dihydrogen phosphate. Section 2.2.3. describes the preparation of lanthanide phosphates in detail.

#### 5.2.1.2. Catalytic activity

The dehydration reaction was carried out in 300 mL Parr (SS 316) autoclave that has a teflon liner. In a typical reaction, sugar was dissolved in Millipore water, to which freshly activated catalyst was added. The closed vessel was purged with nitrogen and the reaction was conducted at the desired temperature. At the end of reaction, the reaction mixture was filtered using nylon 0.22 μm filter and the filtrate was analyzed using HPLC, equipped with RI detector and Resex ROA Organic Acid $H^+$ column (300 mm × 7.8 mm) with 5mM $H_2SO_4$ as the mobile phase at a flow rate of 0.6 $mL.min^{-1}$ at 60 °C.

### 5.2.2. Results and discussion

#### 5.2.2.1. Catalyst characterization

##### 5.2.2.1.1. X-ray diffraction (XRD)

The XRD powder patterns of the $LnPO_4$ (Ln = La-Dy) samples, are shown in Fig. 5.1. These patterns indicate that the samples are crystalline in nature. All lanthanide phosphate samples are isostructural as their reflections correspond to pure hexagonal phase of rhabdophane [21]. Moreover, the higher intensity of (200) plane indicates anisotropic growth along c-axis. The XRD analysis also shows a systematic shift in the position of diffraction peaks towards higher 2θ, reflecting the contraction of the ionic radii of the lanthanides. In order to investigate the lanthanide contraction, the unit cell dimensions were calculated from XRD data. The measured lattice parameters were plotted against the Shannon radii (Fig. 5.2a). The linear behavior of the graph clearly shows the effect of the lanthanide contraction. The XRD patterns also exhibit the increase in crystallinity from $LaPO_4$ to $DyPO_4$. To address this, the crystallite sizes were calculated from XRD patterns and plotted against the Shannon radii (Fig. 5.2b). The graph exhibits simosodal nature, showing that the crystallite sizes are nearly same for La to Sm phosphates, and increases steeply thereafter. This may be due to the morphological changes as seen in SEM studies. Additionally, absence of any peaks at low angles (11-12°) shows the absence of impurities, clearly showing the formation of pure hexagonal phase.

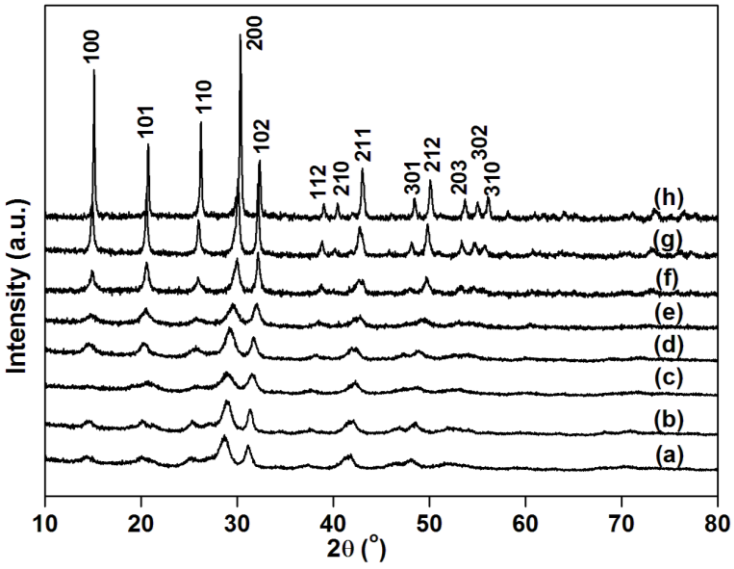


**Fig. 5.1.** XRD pattern of (a) $LaPO_4$, (b) $CePO_4$, (c) $PrPO_4$, (d) $NdPO_4$, (e) $SmPO_4$, (f) $GdPO_4$, (g) $TbPO_4$ and (h) $DyPO_4$

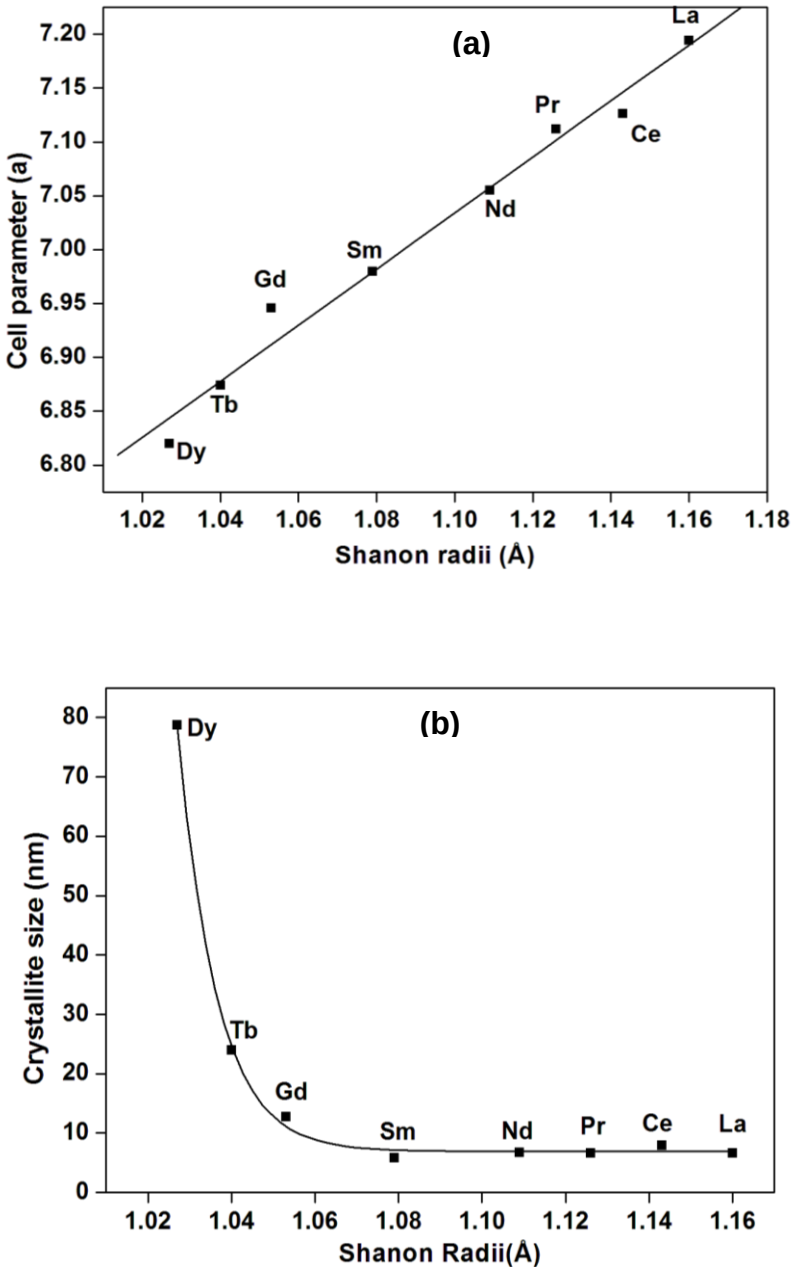


**Fig. 5.2. (**a) Plot of lattice prameter vs. lanthanide ionic radii
(b) Plot of crystallite size vs. lanthanide ionic radii.

### 5.2.2.1.2. Surface area

The textural properties of the catalyst materials are given in Table 5.1. The high surface areas of $LaPO_4$ to $SmPO_4$ samples are attributed to their nanocrystalline nature, while lower surface areas of $GdPO_4$ to $DyPO_4$ samples are due to their larger crystallite sizes. Thus, it can be inferred that a change in ionic radii of the lanthanide induces morphological changes in the structure which alters the crystallinity and textural properties of the material. The results are consistent with earlier findings [22].

**Table 5.1:** Textural and physiochemical properties of lanthanide phosphates.

| Catalyst | Ln:P* | S.A. ($m^2/g$) | Acidity (mmol/g) | | Weight Loss (%) | | B/B+L[#] |
|---|---|---|---|---|---|---|---|
| | | | Weak | Medium | 1st Peak | 2nd Peak | |
| $LaPO_4$ | 0.97 | 88 | 0.409 | 0.198 | 1.553 | 1.134 | 0.035 |
| $CePO_4$ | 0.99 | 72 | 0.403 | 0.102 | 1.198 | 1.168 | 0.032 |
| $PrPO_4$ | 0.99 | 102 | 0.418 | 0.184 | 1.765 | 1.139 | - |
| $NdPO_4$ | 0.82 | 87 | 0.391 | 0.199 | 1.831 | 1.812 | 0.025 |
| $SmPO_4$ | 1.00 | 108 | 0.413 | 0.208 | 1.546 | 1.822 | 0.040 |
| $GdPO_4$ | 0.97 | 61 | 0.301 | 0.174 | 1.285 | 2.581 | - |
| $TbPO_4$ | - | 11 | 0.192 | 0.138 | 0.991 | 3.28 | 0.002 |
| $DyPO_4$ | - | 9 | 0.067 | 0.068 | 0.77 | 3.29 | - |

*Determined by ICP-OES, [#]Determined by FTIR of chemisorbed pyridine

### 5.2.2.1.3. Scanning electron miscroscopy

Scanning electron microscopy (SEM) was used to examine the morphology of various lanthanide phosphate samples. These results are depicted in Fig.5.3. All the samples exhibit identical morphology of nanorod like structures. However, for $GdPO_4$, $TbPO_4$ and $DyPO_4$, the nanostructures become more pronounced, may be due to increase in crystallinity. This also leads to an increase in the length of nanorods from 100-200 nm to several μm. For lanthanide phosphates, researchers have demonstrated that the change in crystal structure induces changes in the morphology [23,21]. Thus, the identical morphology can be attributed to their similar hexagonal Rhabdophane crystal structure.

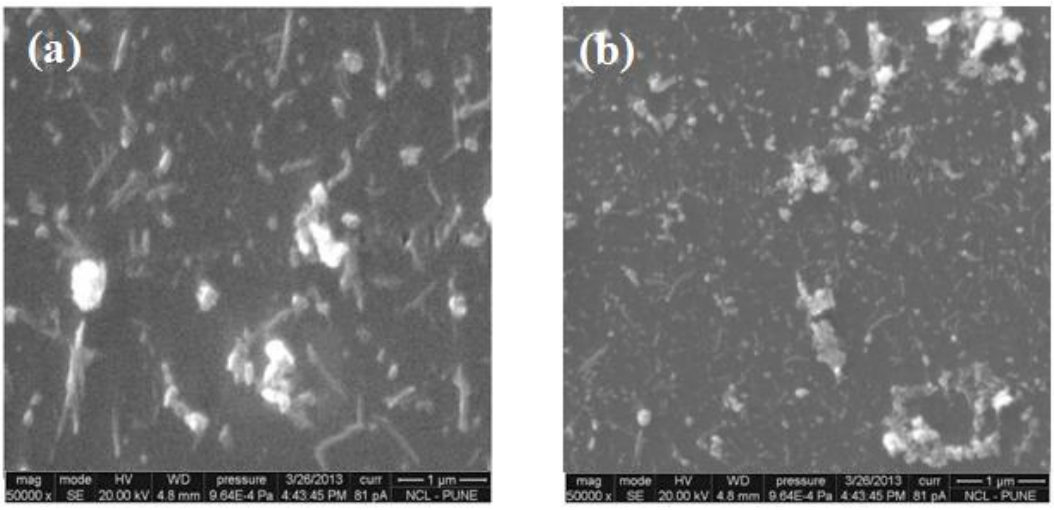

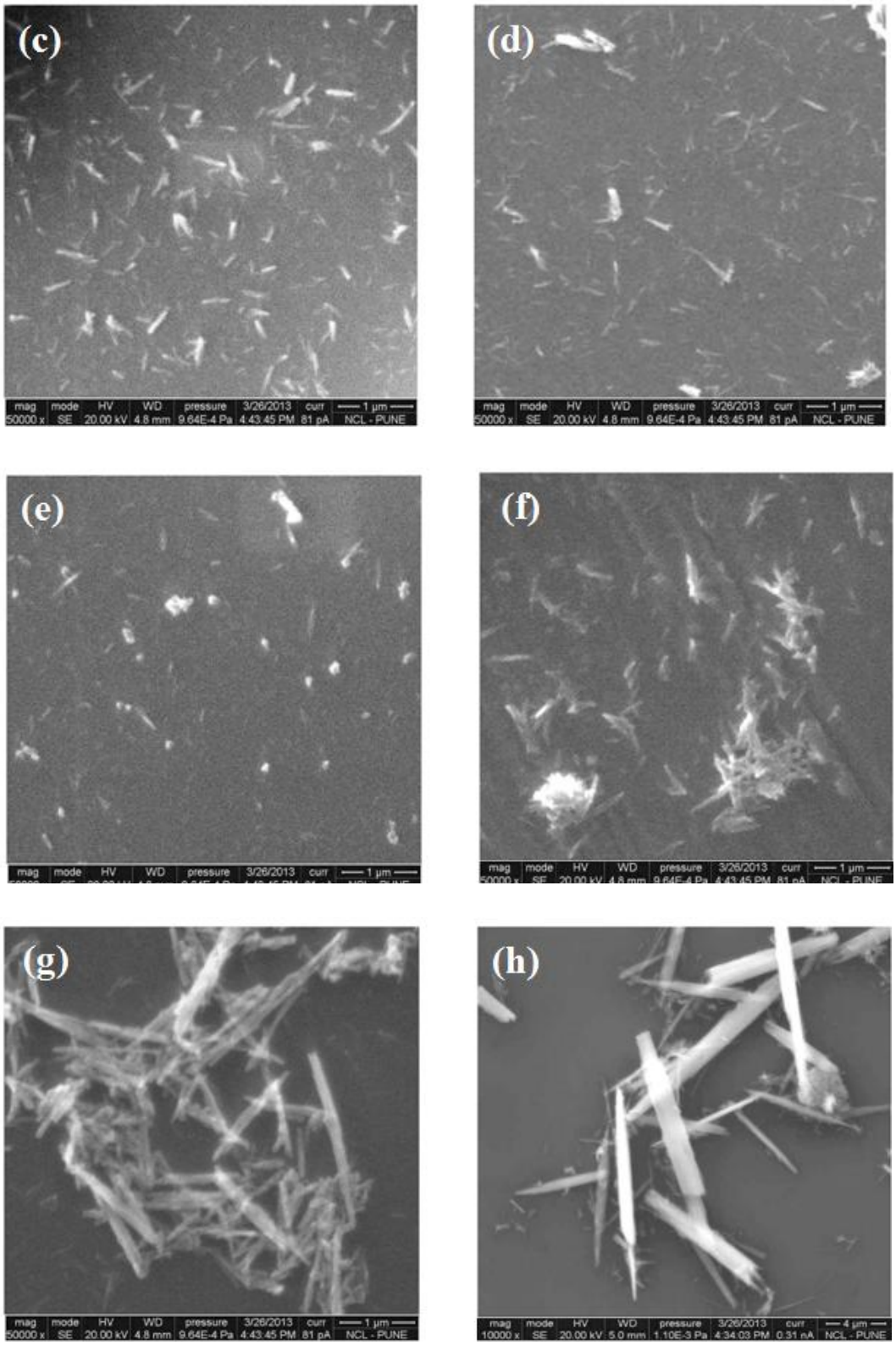


**Fig. 5.3.** SEM images of (a) $LaPO_4$, (b) $CePO_4$, (c) $PrPO_4$, (d) $NdPO_4$, (e) $SmPO_4$, (f) $GdPO_4$, (g) $TbPO_4$ and (h) $DyPO_4$.

### 5.2.2.1.4. Transmission electron microscopy

The structural aspect of the $LnPO_4$ samples was further investigated by TEM. The corresponding micrographs and selected area electron diffraction (SAED) patterns of lanthanide phosphates are presented in Fig. 5.4. TEM images further demonstrated that the obtained products have rod like morphology (Fig. 5.4 $a_1$-$g_1$). The clear lattice fringes in the TEM micrographs confirm the high crystallinity of the nanorods. The spacing between two adjacent planes were ~6.1 and 3.1 Å which are in agreement with the interplanar spacing of 6.12 and 3.072 Å corresponding to (100) and (200) crystal planes, respectively, and can be indexed to a pure hexagonal phase [21]. The SAED patterns of $LnPO_4$ are shown in Fig. 5.4 $a_2$-$g_2$. The continuous rings are obtained due to electron diffraction of a bunch of nanorods. The electron diffraction spots are calculated to have d spacing of 6.12, 4.46, 3.1, 2.86 and 2.16 Å, which corresponds to 100, 101, 200, 102, 003 crystal planes, respectively. All these planes are of pure hexagonal phase of Rhabdophane crystal structure which is in agreement with the XRD analysis.

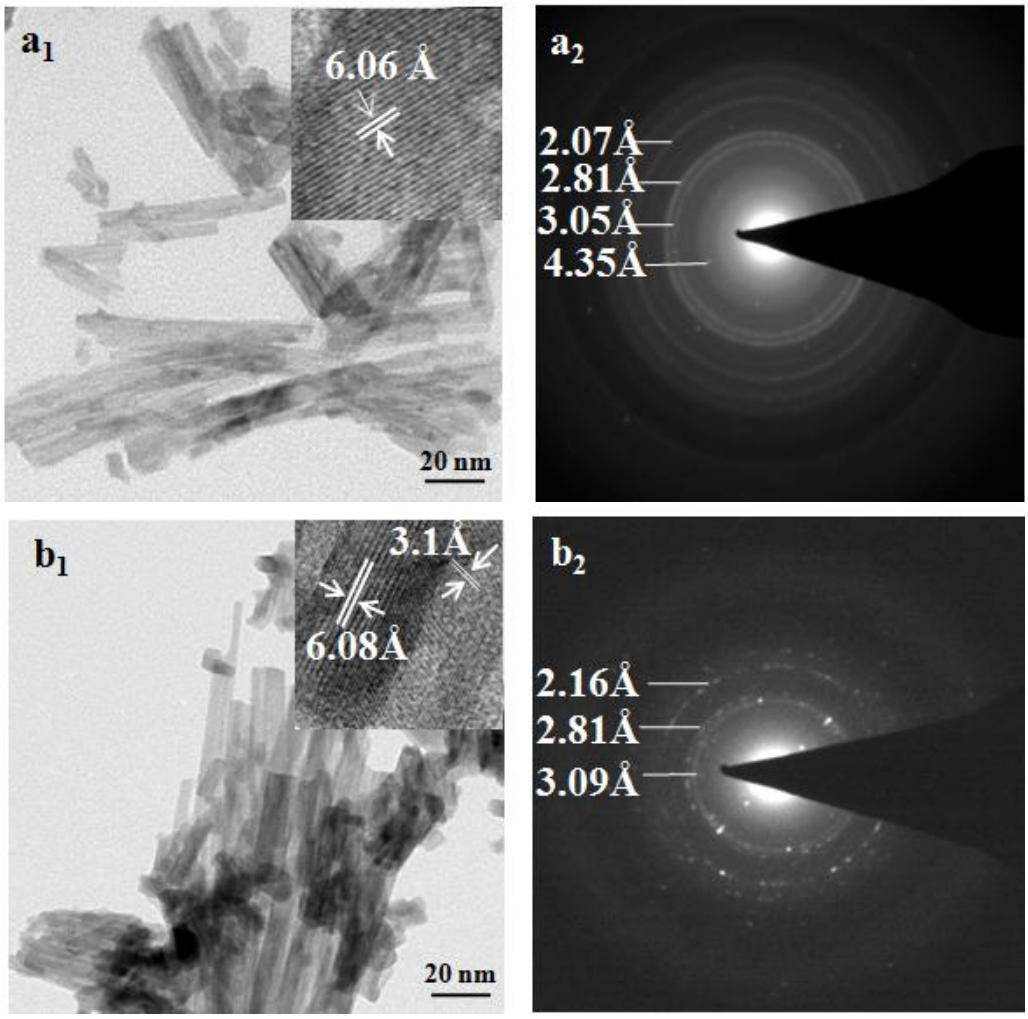

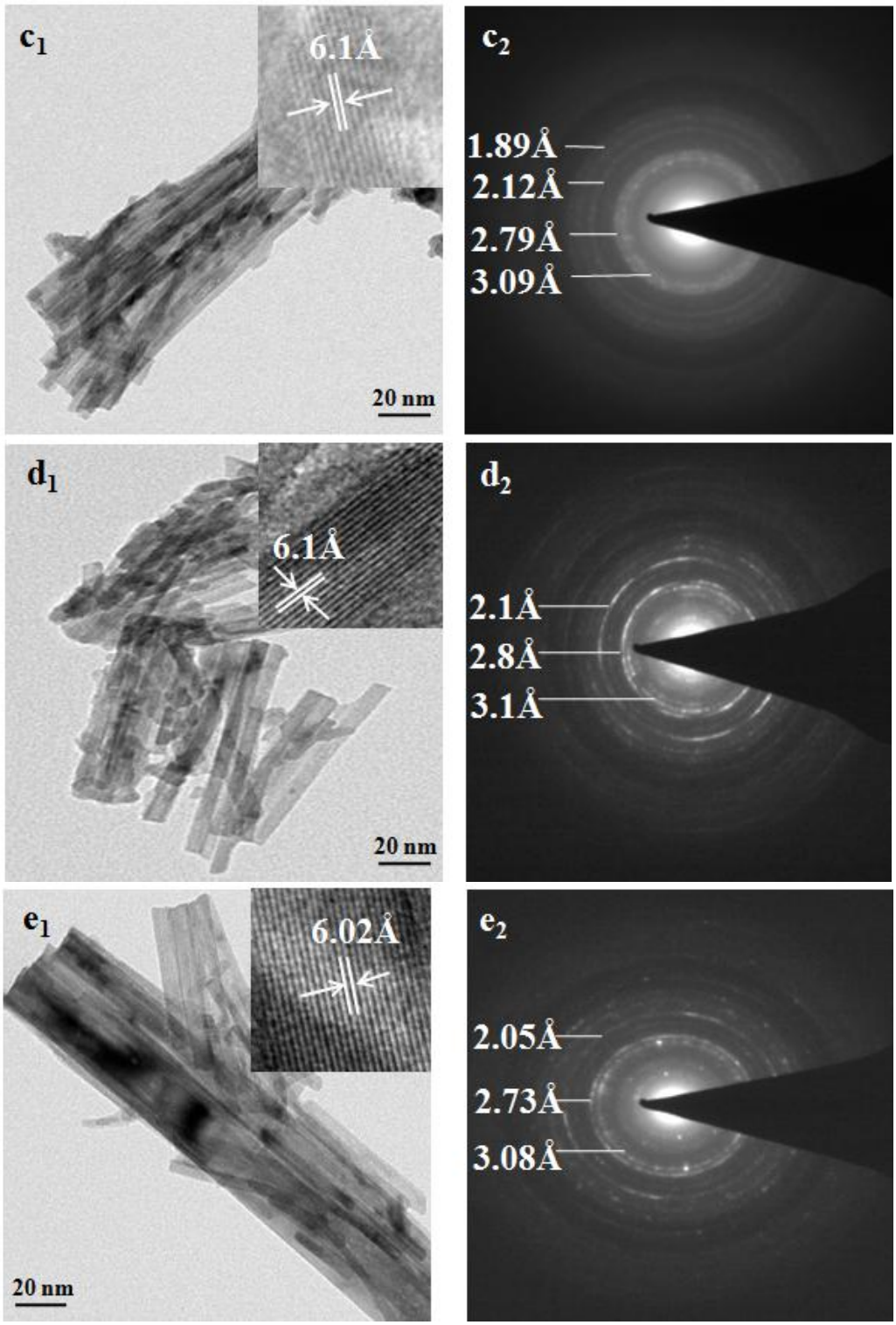
c1
6.1Å
20 nm
c2
1.89Å
2.12Å
2.79Å
3.09Å
d1
6.1Å
20 nm
d2
2.1Å
2.8Å
3.1Å
e1
6.02Å
20 nm
e2
2.05Å
2.73Å
3.08Å

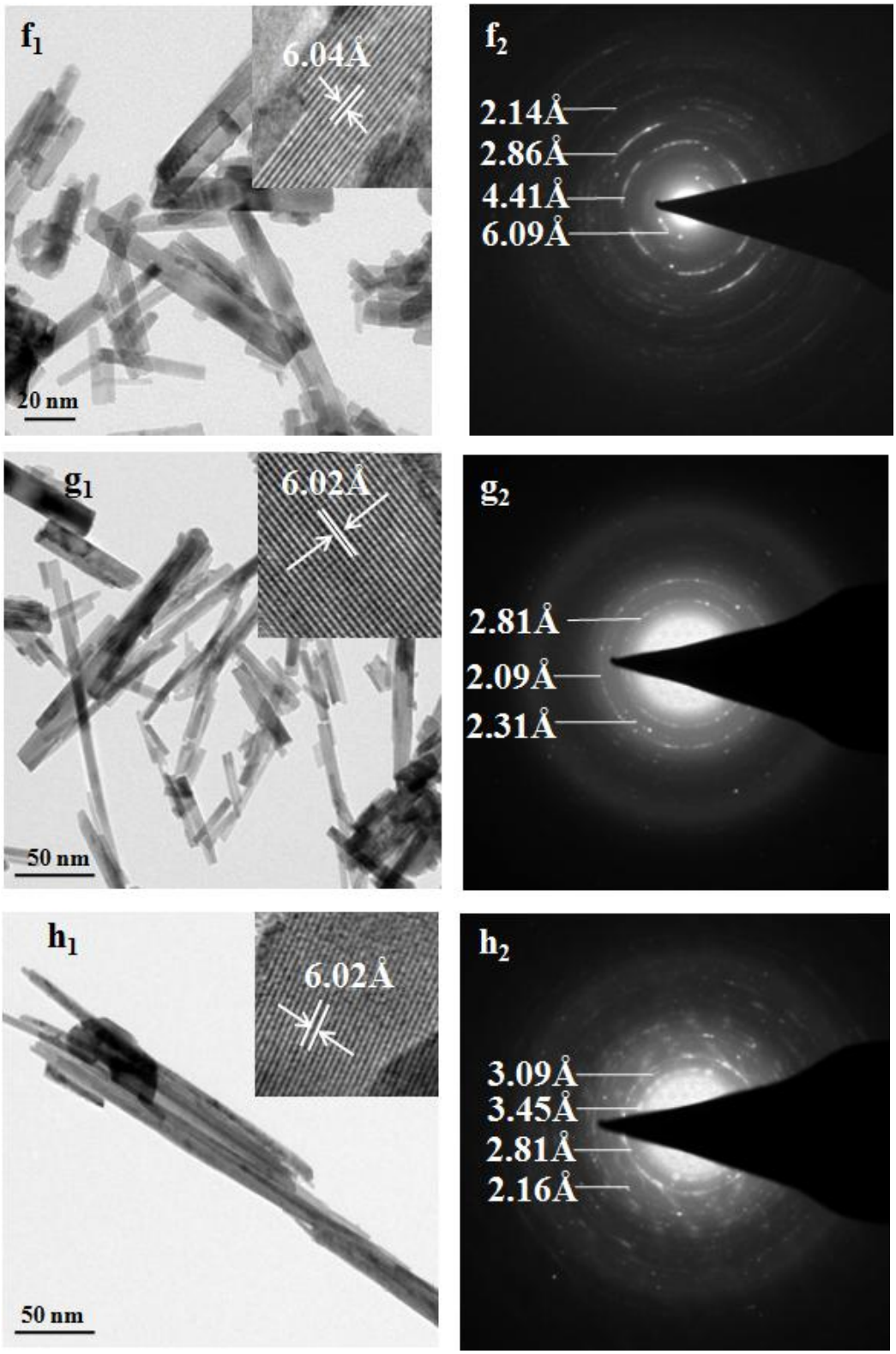


**Fig. 5.4.** TEM images of (a) $LaPO_4$, (b) $CePO_4$, (c) $PrPO_4$, (d) $NdPO_4$, (e) $SmPO_4$, (f) $GdPO_4$, (g) $TbPO_4$ and (h) $DyPO_4$ with lattice fringes as inset; along with SAED pattern of ($a_1$) $LaPO_4$, ($b_1$) $CePO_4$, ($c_1$) $PrPO_4$, ($d_1$) $NdPO_4$, ($e_1$) $SmPO_4$, ($f_1$) $GdPO_4$, ($g_1$) $TbPO_4$ and ($h_1$) $DyPO_4$

### 5.2.2.1.5. Thermogravimetric analysis

The TGA and DTG profiles of $LnPO_4$ samples are shown in Fig. 5.5. All $LnPO_4$ samples exhibited two types of weight losses, one upto temperature of 150 °C and the other in the temperature range of 150 to 250 °C. The values of weight losses are given in Table 5.1. The first weight loss is attributed to the release of the physically adsorbed water in the material. The second weight loss is due to the loss of water present in the channels. The results obtained are consistent with the earlier findings [21,24]. On evaluation it can be seen that the weight loss associated with physically adsorbed water decreases from $LaPO_4$ to $DyPO_4$ due to decrease in surface areas and the weight loss associated with water in the channels increases from $LaPO_4$ to $DyPO_4$ due to increase in the length of the rods. There are only marginal differences from $LaPO_4$ to $SmPO_4$ due to similar morphology (nanoparticles) and crystallite size.

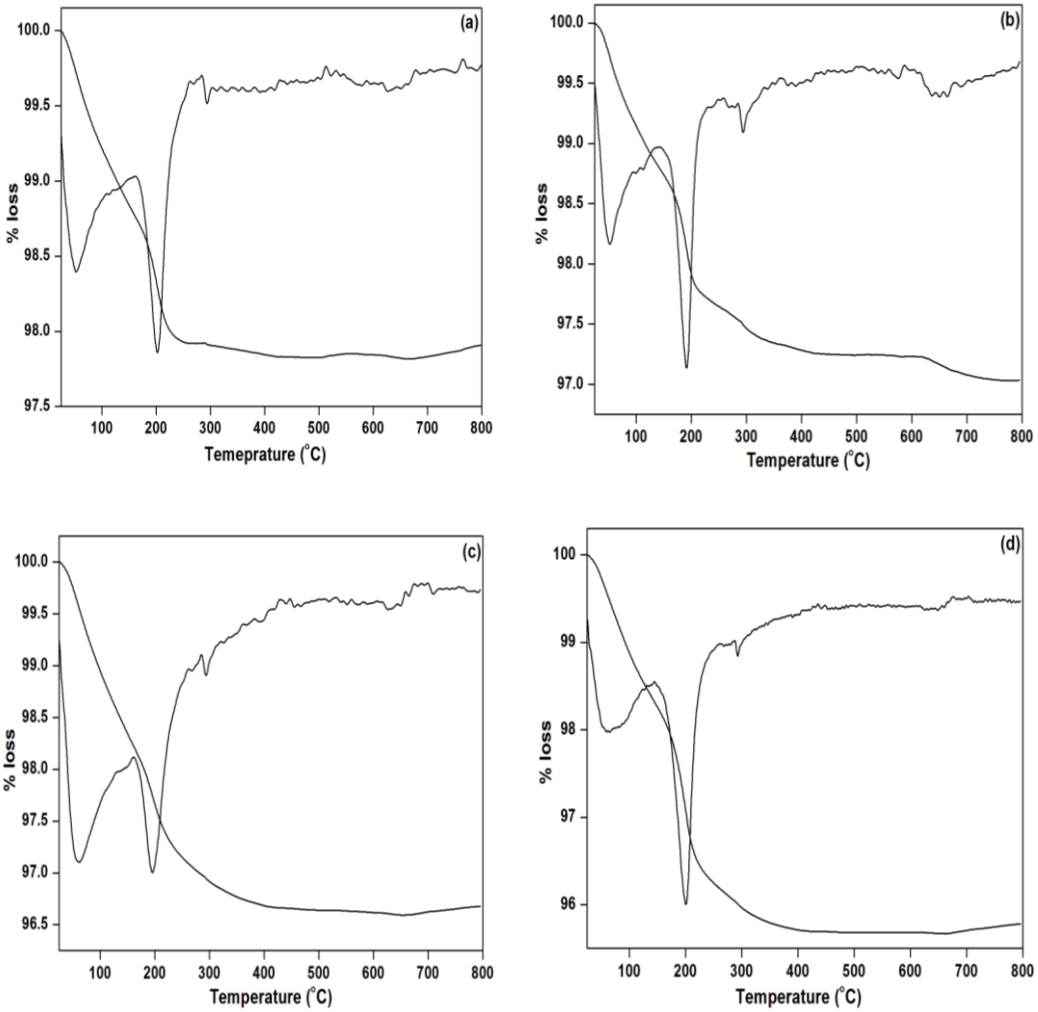

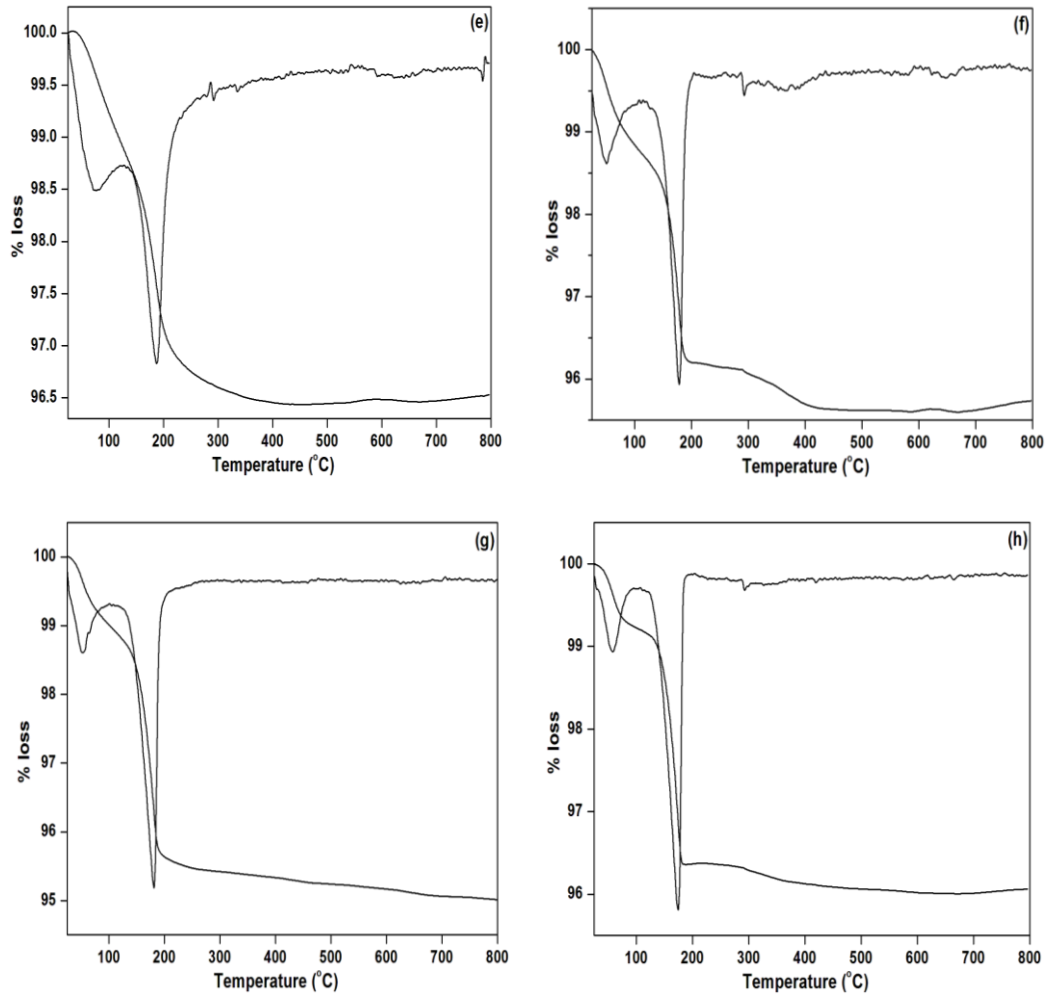


**Fig. 5.5.** TGA and DTG profile of (a) $LaPO_4$, (b) $CePO_4$, (c) $PrPO_4$, (d) $NdPO_4$, (e) $SmPO_4$, (f) $GdPO_4$, (g) $TbPO_4$ and (h) $DyPO_4$.

### 5.2.2.1.6. Fourier transform infrared spectroscopy

The IR bands of $LnPO_4$ samples show two groups of vibrations attributed to the characteristic vibrations of phosphate ($PO_4^{-3}$) group (Fig. 5.6) and bands at higher wave numbers in 3000-4000 $cm^{-1}$ range are assigned to coordinated water (Fig. 5.7). Three bands located at 542, 570 and 615 $cm^{-1}$ pertaining to $\nu_4$ O-P-O asymmetric bending vibrations of $PO_4^{-3}$ group [25] is clearly visible. For $\nu_3$ P-O asymmetric stretching vibration, two separate bands ~ 1015 and 1050 $cm^{-1}$ were observed. The shoulder peak at 960 $cm^{-1}$ is assigned for $\nu_1$ P-O symmetric stretching vibration of $PO_4^{-3}$ group. However, a significant shift in the absorption frequencies is observed depending on the lanthanide phosphate. The adsorption peaks at ~617 or 951 $cm^{-1}$ shift towards higher wavenumbers of 626 and 983 $cm^{-1}$ respectively for $LaPO_4$ and $DyPO_4$.The systematic frequency shifts can be associated with the effect of lanthanide

contraction as evident from XRD studies. The absence of bands at 1265 $cm^{-1}$shows the absence of pyrophosphate ($P_2O_7$) group [26]. Similarly, the absence of shoulder peak at 885 $cm^{-1}$, which is ascribed to the presence of $HPO_4^{-2}$, shows the decomposition of these species at higher temperatures [27]. The spectrum in high wavenumber region is shown in Fig. 5.7 as broad band ~ 3400 $cm^{-1}$. All samples displayed peaks from 3400 to 3800 $cm^{-1}$ in the O-H stretching region which can be ascribed to terminal P-OH groups [28-30], hydroxyl groups in defects [31] and coordinated water in the channels [32,33]. Broader peaks were observed for samples with higher surface area. With increase in surface area, intensity of hydroxyl groups increased, thereby increasing the interactions between adjacent hydroxyl species leading to broader peaks. The shift in the wavelength could possibly be due to decrease in M-O bonds from La to Dy. Thus, the FTIR data of lanthanide phosphates agree well with reported values showing the presence of discrete $PO_4$ groups, coordinated water and surface hydroxyl groups.

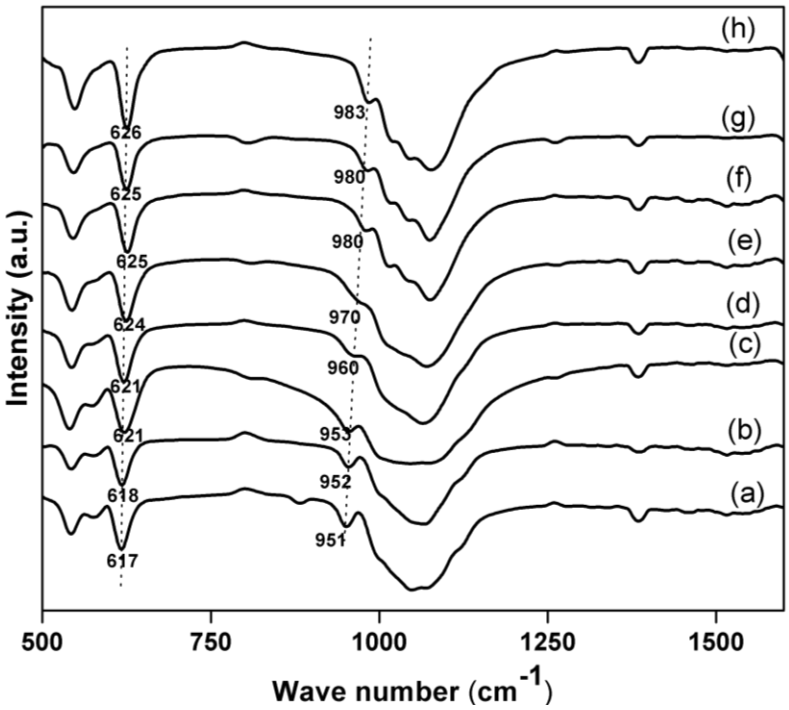


**Fig. 5.6.** FTIR spectrum of (a) $LaPO_4$, (b) $CePO_4$, (c) $PrPO_4$, (d) $NdPO_4$, (e) $SmPO_4$, (f) $GdPO_4$, (g) $TbPO_4$ and (h) $DyPO_4$.

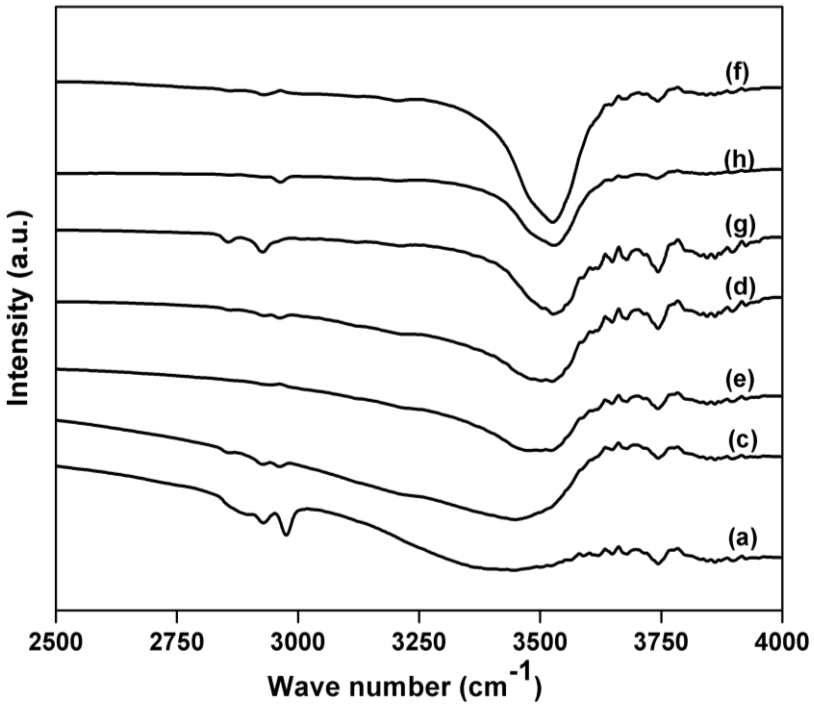


**Fig. 5.7.** Higher wavenumber FTIR spectrum of (a) $LaPO_4$, (c) $PrPO_4$, (d) $NdPO_4$, (e) $SmPO_4$, (f) $GdPO_4$, (g) $TbPO_4$ and (h) $DyPO_4$.

**5.2.2.1.7. Raman spectroscopy**

The Raman spectra of $LnPO_4$ samples are given in Fig. 5.8. A strong peak at 965 $cm^{-1}$ for $LaPO_4$ is assigned to the symmetric stretching mode ($\nu_1$) of the P-O bond in the $PO_4^{-3}$ group. The peak at 463 $cm^{-1}$ is assigned to the O-P-O bending modes [34]. These internal $PO_4^{-3}$ vibrations become irregular with the change in the ionic radii of the neighbouring atom [35]. Other researchers demonstrated that Raman spectra of $LnPO_4$ shows systematic peak shifts with decrease in ionic radius from $La^{+3}$ to $Dy^{+3}$ [21,36]. We have also observed a systematic trend in the behavior of internal $PO_4^{-3}$vibrations, as the peaks at 965 and 463 $cm^{-1}$ shifts to 998 and 472 $cm^{-1}$, respectively when we move from $LaPO_4$ to $DyPO_4$. Thus, the effect of lanthanide contraction witnessed by Raman spectroscopy corroborates the findings of XRD and FTIR spectroscopy.

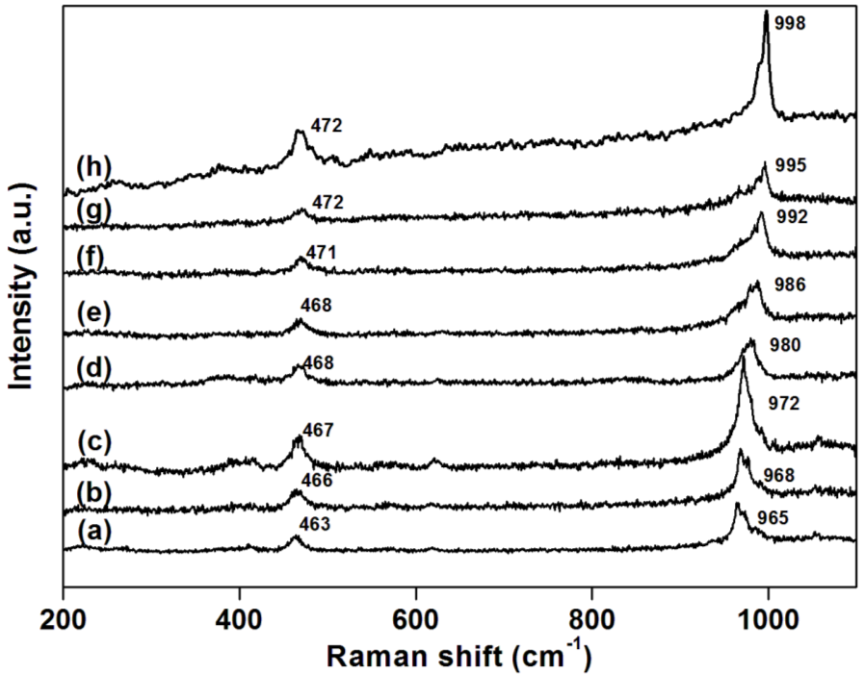


**Fig. 5.8.** Raman Spectra of (a) $LaPO_4$, (b) $CePO_4$, (c) $PrPO_4$, (d) $NdPO_4$, (e) $SmPO_4$, (f) $GdPO_4$, (g) $TbPO_4$ and (h) $DyPO_4$.

### 5.2.2.1.8. TPD of $NH_3$

The acidity of the $LnPO_4$ samples was determined by TPD of $NH_3$. The TPD profiles of the samples are shown in Fig. 5.9. The total acidity of the catalysts is expressed in mmol.$g^{-1}$ of desorbed $NH_3$ under each temperature maximum and these values are listed in Table 5.1. All lanthanide phosphate samples show two peaks, one pertaining to weak acidity (100-250 °C) and another assigned to moderately strong acidity (250-400 °C). With the decrease in the ionic radii from $LaPO_4$ to $DyPO_4$ the acidity of the samples gradually reduced. This decrease in acidity is attributed to decrease in P-OH groups, as a result of reduction in surface area which results from increase in crystallite size. A good linear correlation exists between the total acidity of the samples and the crystallite size (Fig. 5.10) clearly demonstrating that smaller crystallite size leads to the enhanced acidity in samples because the acid sites are generated at the lattice terminals of crystallites [22]. It was also observed that among the two types of acid sites, the surface area (crystallite size) has a profound effect on weak acidity. The smaller is the crystallite size (higher surface area), the higher is the weak acidity of the samples. However, the moderately strong acidity is found to be independent of the surface area and is almost same for all samples. Thus, the overall

decrease in acidity from $LaPO_4$ to $DyPO_4$ is due to decrease in weak acidity, which results from increase in the crystallite size of the samples [37].

The presence of Brönsted acidic sites on $LnPO_4$ was studied by TPD-MS using isopropyl amine as a probe molecule, the results are shown if Fig. 5.11. All samples exhibited three peaks, first in 100-200 °C region, the second in 200-300 °C region and the last in 300-450 °C temperature region. The peaks at lower temperatures (< 300 °C) are of desorbed isopropyl amine and water as evident from mass traces and the ones at higher temperatures are of propene and ammonia. The formation of propene clearly reveals the presence of Brönsted acid sites in lanthanide phosphates. It was observed that on $LaPO_4$ to $DyPO_4$ the intensity of first peak pertaining to water has decreased. This may be due to decrease in the surface area, which is responsible to decrease in P-OH groups, resulting in the low amount of physisorbed water on the surface. $DyPO_4$ exhibited an additional peak at higher temperature (> 500 °C) of water which may be emanating from condensation of P-OH groups.

The propene traces of the $LnPO_4$ are depicted in Fig. 5.12. The Brönsted acidity of lanthanide phosphates can be ranked as $SmPO_4$ > $LaPO_4$ > $CePO_4$ > GdPO4 > $PrPO_4$ > $NdPO_4$ > $TbPO_4$ > $DyPO_4$. Apart from the surface hydroxyl groups, researchers have demonstrated that the Brönsted acidity may arise from rare earth cations with incomplete coordination, the strength of which increases with the atomic number [38]. Another important parameter that contributes towards the Brönsted acidity of lanthanide phosphates is the Ln:P ratio [30]. Thus, the trend observed for the $LnPO_4$ is due to the combined effect of surface area, atomic number of lanthanides and Ln:P ratio.

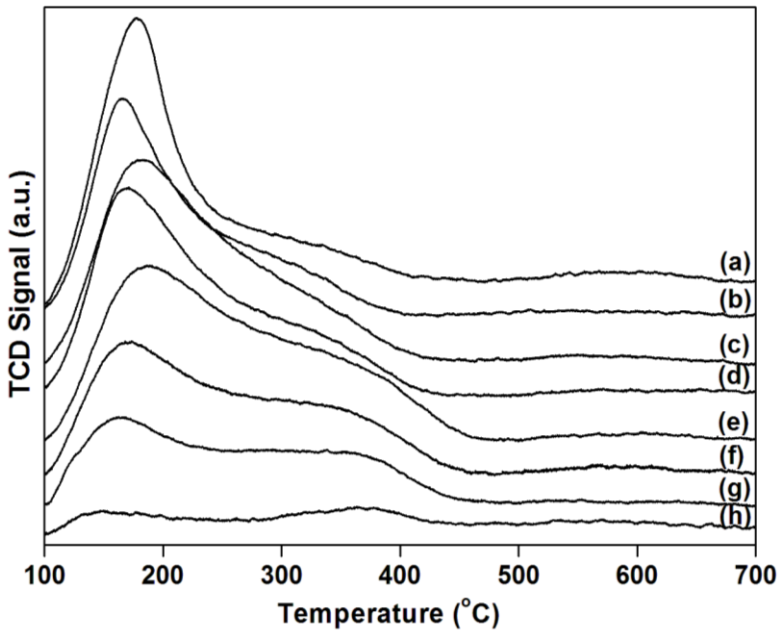


**Fig. 5.9.** $NH_3$-TPD profile of (a) $LaPO_4$, (b) $CePO_4$, (c) $PrPO_4$, (d) $NdPO_4$, (e) $SmPO_4$, (f) $GdPO_4$, (g) $TbPO_4$ and (h) $DyPO_4$.

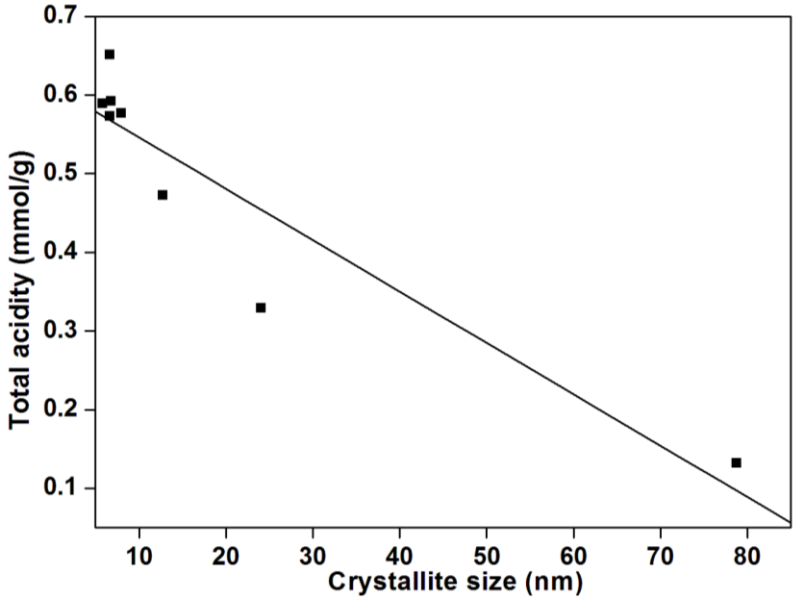


**Fig. 5.10.** Total acidity vs. crystallite size.

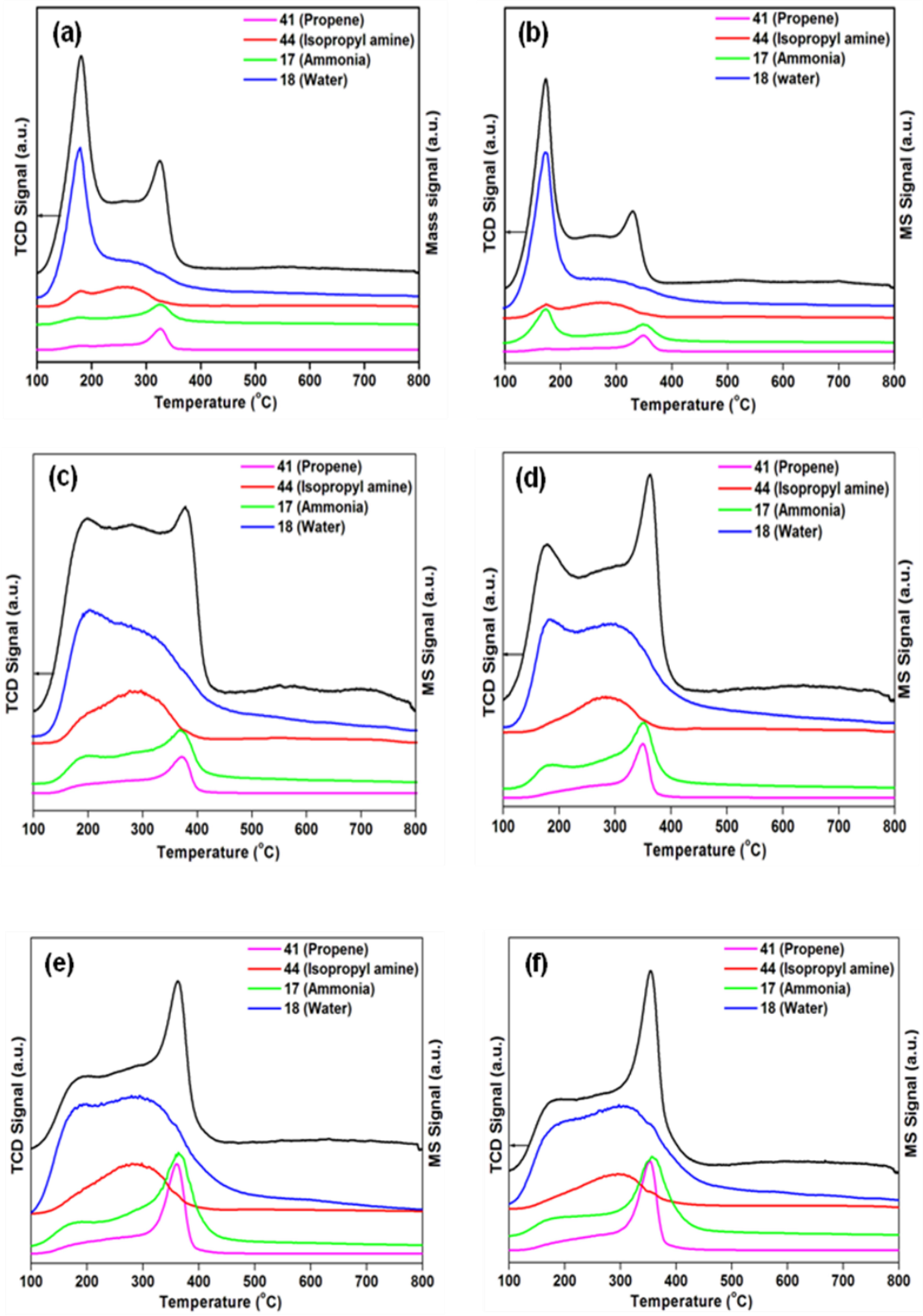
(a)
41 (Propene)
44 (Isopropyl amine)
17 (Ammonia)
18 (Water)
TCD Signal (a.u.)
Mass signal (a.u.)
Temperature (°C)
(b)
41 (Propene)
44 (Isopropyl amine)
17 (Ammonia)
18 (water)
TCD Signal (a.u.)
MS Signal (a.u.)
Temperature (°C)
(c)
41 (Propene)
44 (Isopropyl amine)
17 (Ammonia)
18 (Water)
TCD Signal (a.u.)
MS Signal (a.u.)
Temperature (°C)
(d)
41 (Propene)
44 (Isopropyl amine)
17 (Ammonia)
18 (Water)
TCD Signal (a.u.)
MS Signal (a.u.)
Temperature (°C)
(e)
41 (Propene)
44 (Isopropyl amine)
17 (Ammonia)
18 (Water)
TCD Signal (a.u.)
MS Signal (a.u.)
Temperature (°C)
(f)
41 (Propene)
44 (Isopropyl amine)
17 (Ammonia)
18 (Water)
TCD Signal (a.u.)
MS Signal (a.u.)
Temperature (°C)

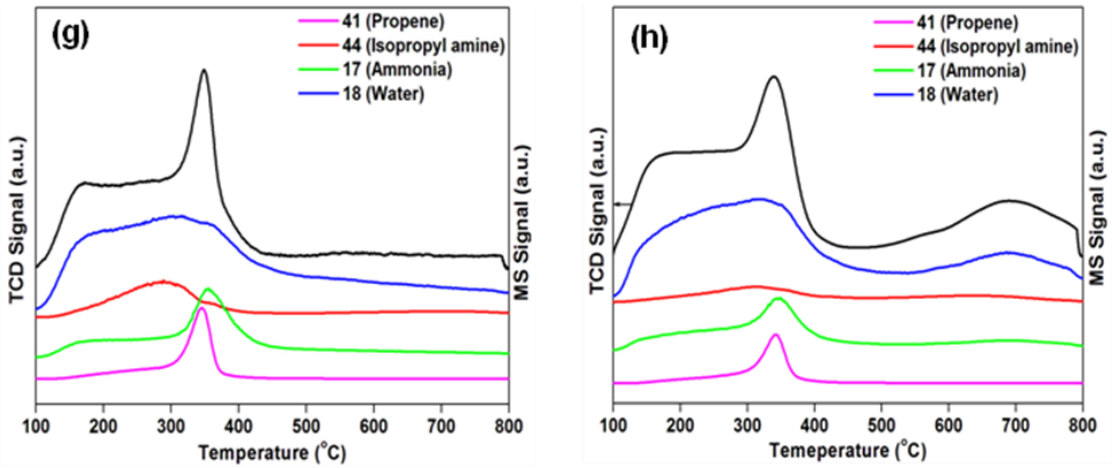


**Fig. 5.11.** TPD-MS profile of (a) $LaPO_4$, (b) $CePO_4$, (c) $PrPO_4$, (d) $NdPO_4$, (e) $SmPO_4$, (f) $GdPO_4$, (g) $TbPO_4$ and (h) $DyPO_4$.

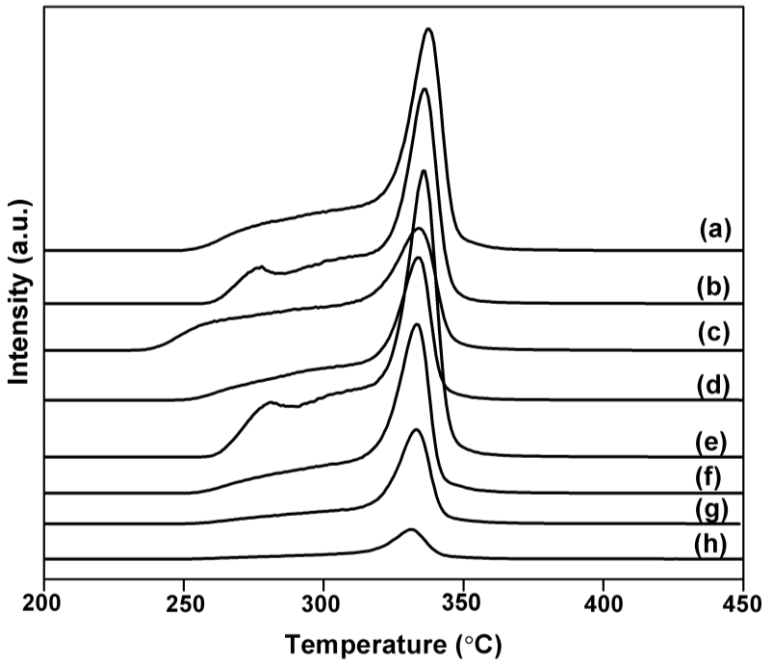


**Fig. 5.12.** Propene traces of (a) $LaPO_4$, (b) $CePO_4$, (c) $PrPO_4$, (d) $NdPO_4$, (e) $SmPO_4$, (f) $GdPO_4$, (g) $TbPO_4$ and (h) $DyPO_4$.

### 5.2.2.2. Catalytic activity for fructose dehydration to 5-HMF

#### 5.2.2.2.1. Effect of acidity

As inferred from the earlier studies, it is observed that change in ionic radii from La to Dy induces textural variations in $LnPO_4$ leading to changes in acidities. Therefore, to investigate the effect of acidity on fructose dehydration all the $LnPO_4$

catalysts were screened under similar conditions (Fructose = 4 g in 40 mL water, temperature = 150 °C, catalyst = 50 wt% of fructose, time = 2 h). The values of conversion (HMF yield) in mol% are 84.4 (42.1), 83.1 (39.1), 82.8 (41.5), 84.0 (40.8), 84.1 (42.5), 79.9 (40.9), 74.8 (39.3) and 72.1 (37.8) for $LaPO_4$, $CePO_4$, $NdPO_4$, $PrPO_4$, $SmPO_4$, $GdPO_4$, $TbPO_4$ and $DyPO_4$, respectively. The conversions decreased from 84.4 to 72.1 mol% from $LaPO_4$ to $DyPO_4$, which is attributed to decrease in total acidity. The decrease in total acidity results from decreasing surface area [37]. In order to confirm this aspect, surface areas were plotted against total acidity (Fig. 5.13) and a good liner correlation was obtained indicating that total acidity depends on smaller crystallite size (higher surface area). When conversion was plotted against total acidity, a linear behavior was observed (Fig. 5.14). But, the HMF yield was independent of the total acidity clearly indicating that total acidity does not contribute to higher yields of HMF. To investigate the acidity required for HMF formation, moderate strong acidity was plotted against HMF yield (Fig. 5.15), which shows a linear dependence of the two parameters. This drives us to conclude that moderately strong acidity converts fructose to HMF whereas weak sites are susceptible to side reactions.

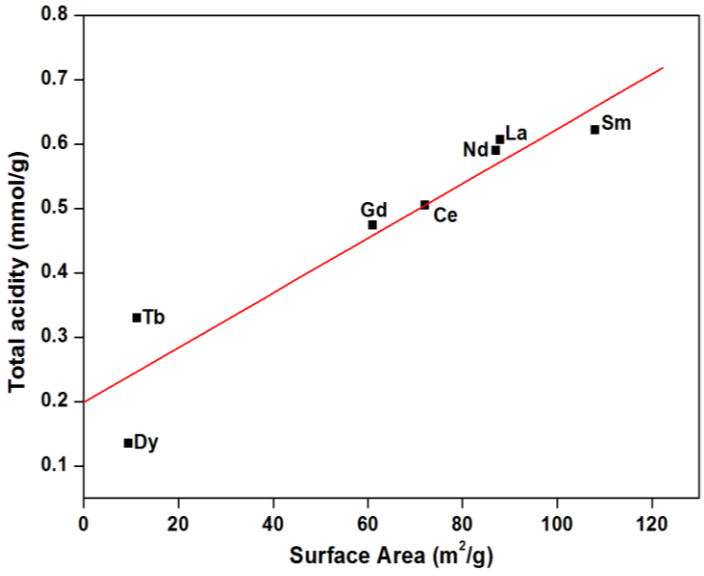


**Fig. 5.13.** Surface area vs. total acidity.

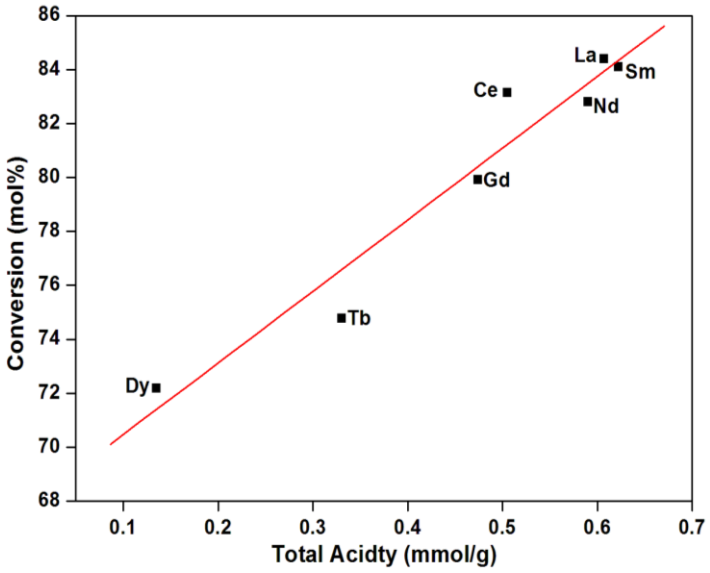


**Fig. 5.14.** Total acidity vs. fructose conversion.

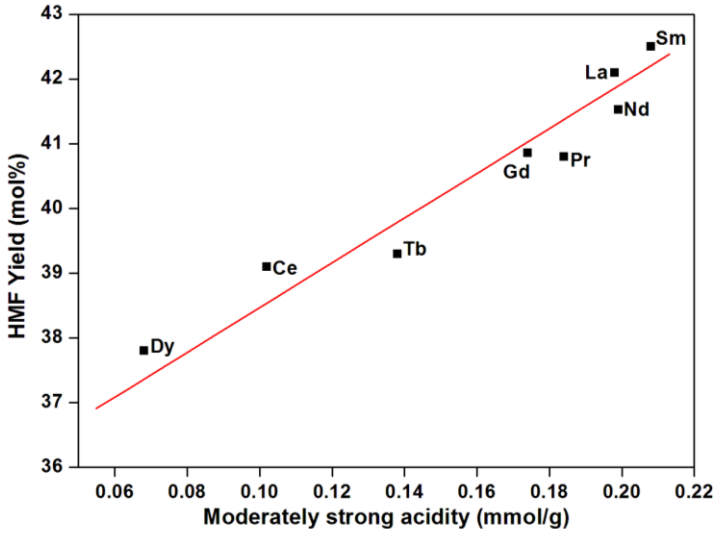


**Fig. 5.15.** Moderate strong acidity vs. HMF yield.

In order to investigate the nature of acidic sites responsible for HMF formation Brönsted acidity calculated from TPD-MS studies and B/B+L ratio calculated from Pyridine IR studies were plotted against HMF yield. Fig. 5.16 and Fig. 5.17 shows a good linear correlation between these parameters leading towards corroboration of our earlier findings that moderately strong Brönsted sites are the crucial ones for HMF formation from fructose. In terms of catalytic performance among different $LnPO_4$ catalysts, marginal differences were observed from $LaPO_4$ to $SmPO_4$ samples. Since, catalytic activity of $LaPO_4$ was slightly higher, it was chosen for further optimization of reaction conditions.

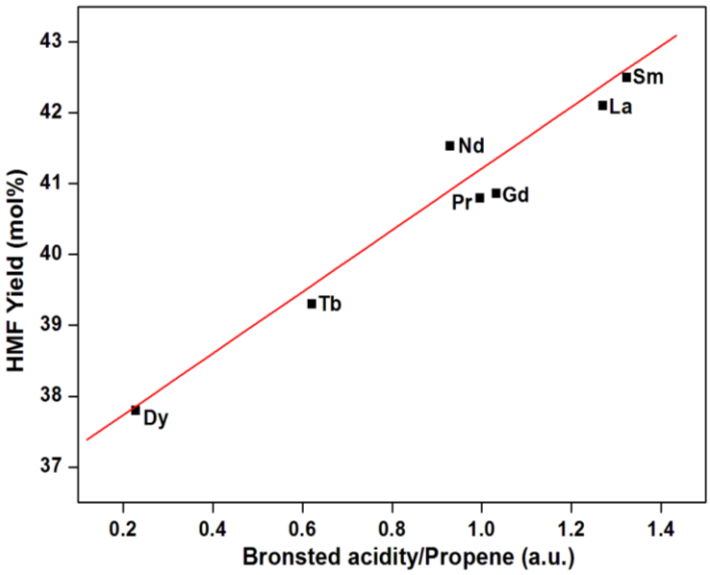


**Fig. 5.16.** Brönsted acidity in terms of propene formed vs. HMF yield.

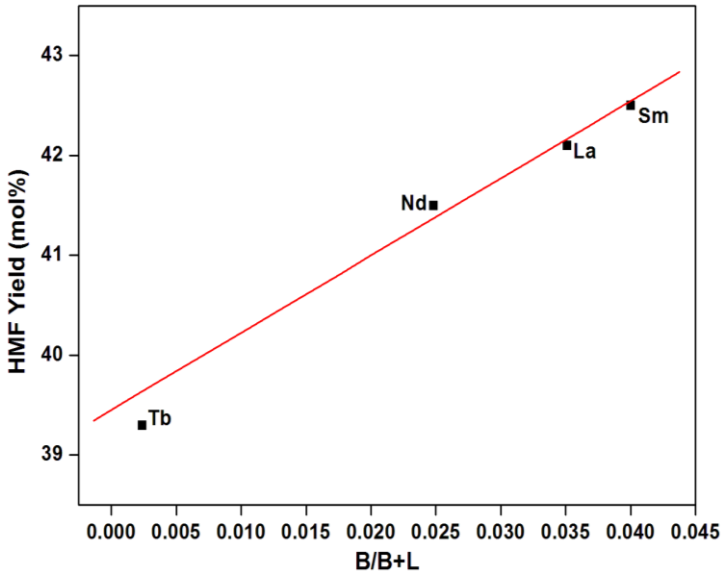


**Fig. 5.17.** B/B+L ratio vs. HMF yield.

### 5.2.2.2.2. Effect of temperature

The liquid phase dehydration of fructose with $LaPO_4$ was studied by varying the reaction temperature in the 130-160 °C range; the results are shown in Fig. 5.18 Increase in temperature from 130 to 160 $^{o}$C led to increase in conversion from 23.2 to 97.3 mol%. On evaluation of the product distribution, it was found that increase in temperature from 130 to 150 °C has enhanced the HMF yields from 7.9 to 40.24 mol%. With further increase in temperature to 160 °C the HMF yields fell to 31.6 mol%. At higher temperatures, the rehydration of HMF was dominant, hence higher

yields of Levulinic acid (LA) and Formic acid (FA) were obtained. Other products like acetic acid (AA) and furfural were formed in minor concentrations (< 3mol%) suggesting that under the reaction conditions studied, the decomposition of sugars [39] and decarboxylation of HMF [40] are not dominant. It was observed that FA yields were always greater than LA yields as some FA is formed due to decomposition of sugars, though to a minor extent [41]. Therefore, it can be clearly seen that higher temperature (>150 °C) promotes rehydration of HMF thereby lowering its yield, hence the optimum temperature was chosen as 150 °C for further study.

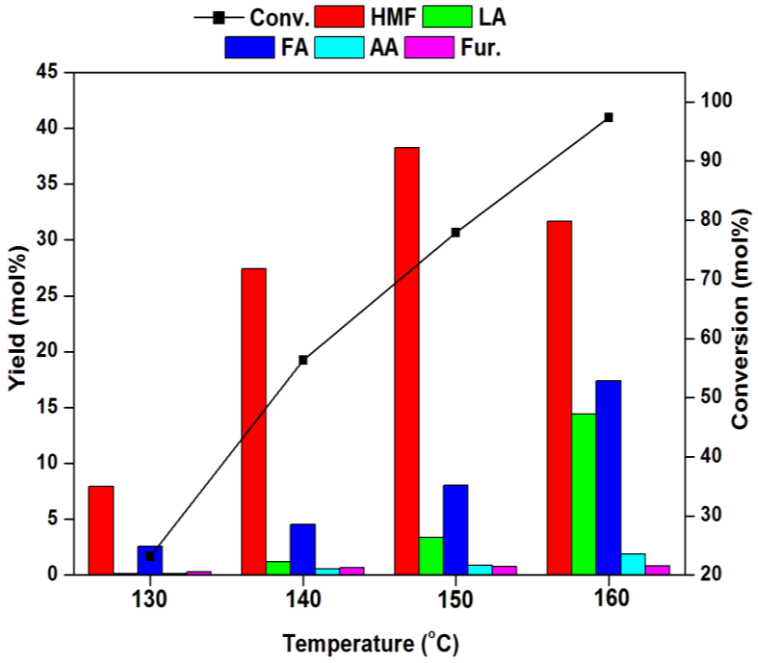


**Fig. 5.18.** Effect of temperature on fructose dehydration.

Reaction conditions: Fructose = 4 g in 40 mL water, catalyst = 50 wt% of fructose, time = 2 h.

### 5.2.2.2.3. Effect of catalyst content

The effect of catalyst content on the reaction was studied by using different catalyst amounts; results of which are shown in Fig. 5.19. There is substantial increase in conversion with the catalyst content. Conversion increased from 71.8 to 88.0 mol% when the catalyst content is increased from 25 to 62.5 wt% of substrate. The increase in conversion is due to availability of more active sites with increasing catalyst contents. HMF yields were found to increase from 38.2 to 42.1 mol% when the catalyst contents increased from 25 to 50 wt%, while it is reduced (35.4 mol%) on

further increasing the catalyst content. At very higher catalyst content (62.5wt%) neither the rehydration products nor the decomposition/decarboxylation products were formed in significant amounts clearly demonstrating that the condensation products (humins) are formed predominantly on increasing the available active sites. Based on this study, 50 wt% catalyst (of substrate) was found to be the optimum.

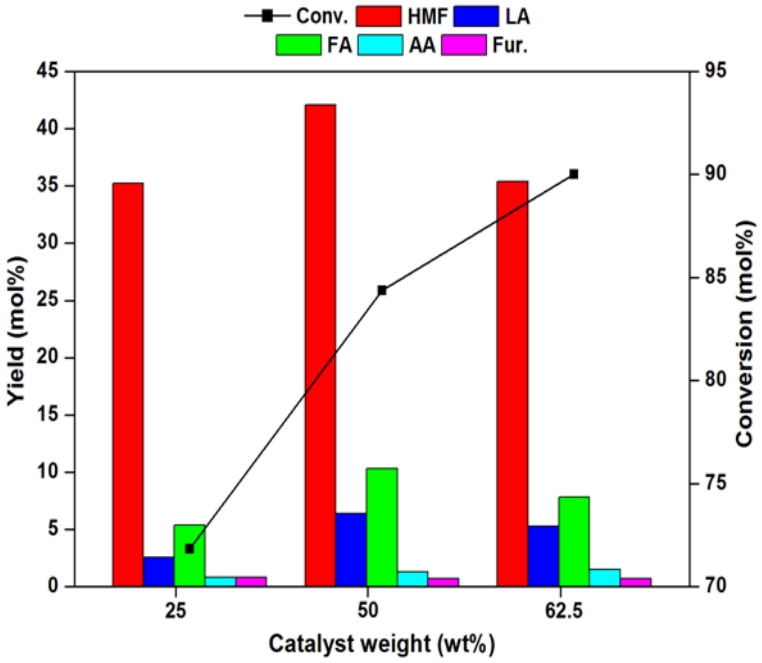


**Fig. 5.19.** Effect of catalyst content on fructose dehydration.

Reaction conditions: Fructose = 4 g in 40 mL water, temperature = 150 °C, time = 2 h

### 5.2.2.2.4. Effect of substrate concentration

The effect of fructose concentration on the reaction was studied by varying its concentration in water from 5 to 20 wt%. The change in concentration has profound effect on conversion and HMF yield (Fig. 5.20). The conversion increased from 70.7 to 90.5 mol% with the increasing concentration from 5 to 20 wt%, respectively. At higher concentrations of substrate, active sites are not occupied with water which is a strong Lewis base, leading to higher conversions. The HMF yield increased from 38.6 to 42.1 mol% with increase in concentration from 5 to 10 wt% respectively, which then reduces to 31.9 mol% on further increase in concentration to 20 wt%. The reduction in HMF yield on increasing the concentration is due to HMF undergoing condensation reactions. From the results it can be inferred that 10 wt% is the optimum concentration and the catalyst systems are efficacious to work in concentrated solutions.

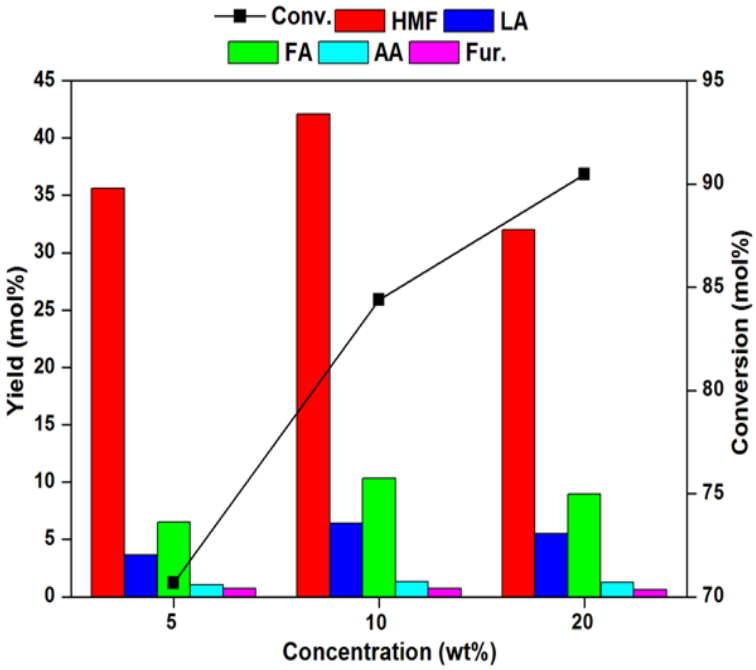


**Fig. 5.20.** Effect of substrate concentration.

Reaction conditions: temperature = 150 °C, catalyst = 50 wt% of fructose, time = 2h.

### 5.2.2.2.5. Effect of reaction time

The influence of reaction time on fructose dehydration was studied between 1 to 2.5 h, the results are depicted in Fig. 5.21.

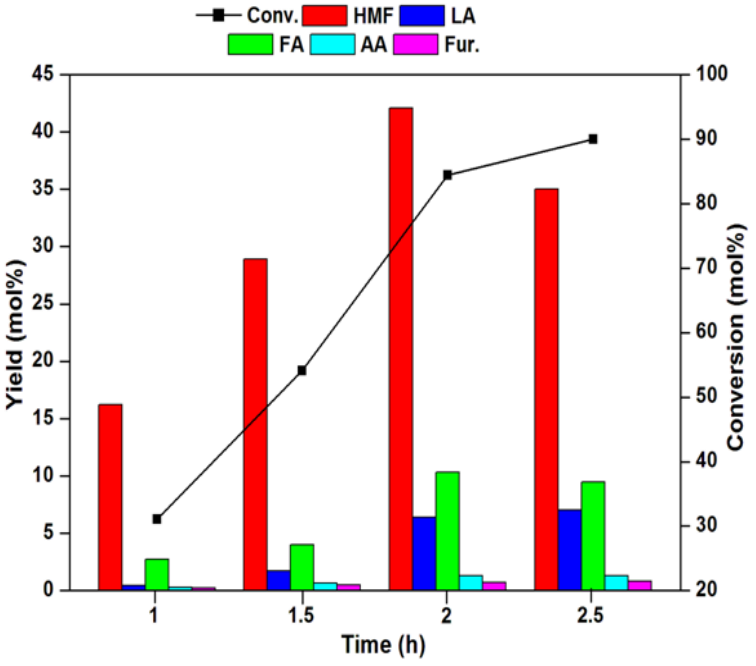


**Fig. 5.21.** Effect of time on fructose dehydration.

Reaction conditions: Fructose = 4 g in 40 mL, temperature = 150 °C
catalyst = 50wt% of fructose

With increase in reaction time, the conversion increased (31.1 to 90 mol%) whereas the HMF yield increased upto 2 h of reaction time (from 16.2 to 42.1 mol%) and detoriated with further increase in time. On evaluation of the product distribution, it can be deduced that the condensation reactions are dominant among other reactions as rehydration products (LA and FA), decomposition products (AA) and decarboxylation product (furfural) are not formed in substantial amount with increase in time. Thus, 2 h was found to be the optimum reaction time.

### 5.2.2.2.6. Effect of saccharide

In order to evaluate the effectiveness of the catalyst system to convert other saccharides to HMF, various carbohydrates were evaluated for dehydration reaction, the results are shown in Fig. 5.22.

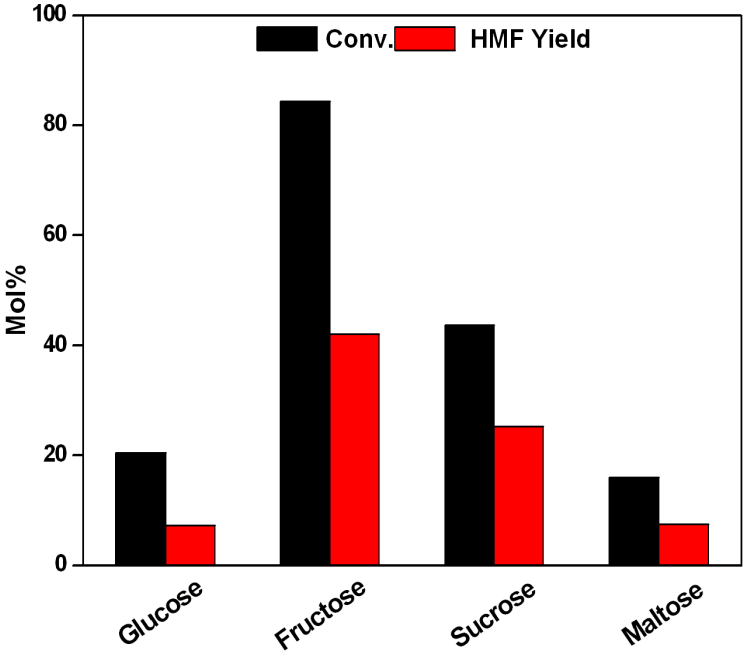


**Fig. 5.22.** Effect of saccharide on HMF yield.

Reaction conditions: sugar = 10 wt%, temperature = 150 °C, catalyst = 50wt% of sugar, time = 2 h.

It was found that fructose gave maximum yield of HMF, i.e. 42 mol% at 84.4 mol% conversion followed by sucrose (dissacharide of glucose and fructose) which gave moderate yield of HMF (25.3 mol%) at 43.7 mol% conversion. On the contrary, aldose sugars like glucose and maltose (dissacharide of glucose) gave lower yields of HMF (~ 7 mol%) at lower conversion, since the isomerization of glucose to fructose is slow over acid catalysts, it reduces the dehydration. Thus, ketose sugars can be

effectively converted to HMF whereas aldose sugars scarcely yielded the furan compound.

#### 5.2.2.2.7. Recyclability studies

To check the recyclability of the catalyst, the used catalyst was calcined in air at 500 °C for 3 h in order to oxidize the carbonaceous deposits on the catalyst and used for further reaction. The results are shown in Fig. 5.23. The catalyst was recycled for 3 times. It can be seen that the catalytic activity is regained after each use. There was marginal effect on conversion however, but the yields were unaltered. This shows the recyclability of the catalyst system and its effectiveness for use in aqueous conditions without any loss in catalytic activity.

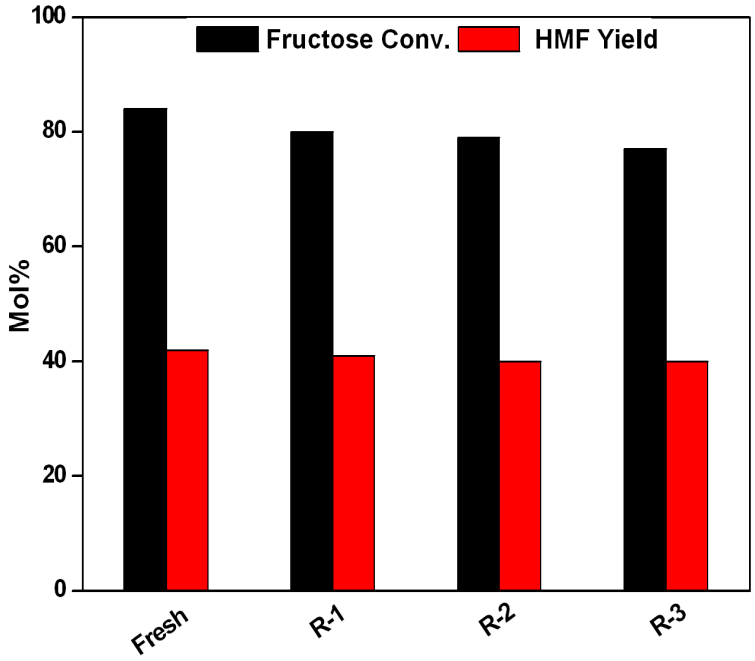


**Fig. 5.23.** Recyclability studies.

Reaction conditions: Fructose = 4 g in 40 mL water, temperature = 150 °C, catalyst = 50wt% of fructose, time = 2h.

### 5.2.2.3. Catalytic activity for glucose dehydration to LA

#### 5.2.2.3.1. Effect of acidity

The effect of acidity on glucose dehydration was investigated by deploying $LnPO_4$ catalysts in similar reaction conditions (glucose = 3g in 60 mL water, temperature = 170 °C, catalyst = 50 wt% of glucose, time = 20 h). The values of conversion (LA yield) in mol% are 90.5 (27.2), 90.0 (26.2), 91.8 (25.9), 91.6 (26.2),

92.2 (28.37), 85.4 (25.43), 82.0 (21.01) and 69 .0 (16.02) for $LaPO_4$, $CePO_4$, $PrPO_4$, $NdPO_4$, $SmPO_4$, $GdPO_4$, $TbPO_4$ and $DyPO_4$, respectively. The conversions decreased from 90.5 to 69 mol% from $LaPO_4$ to Dy $PO_4$ which is attributed to decrease in total acidity (Fig. 5.24). For LA also, the yields were found to be dependent on moderately strong acidity and not total acidity (Fig. 5.25) leading to a conclusion that moderate strong acidic sites are crucial and contributing to convert glucose to LA. Due to comparable catalytic activity from $LaPO_4$ to $SmPO_4$, $LaPO_4$ was used for further optimization of reaction conditions.

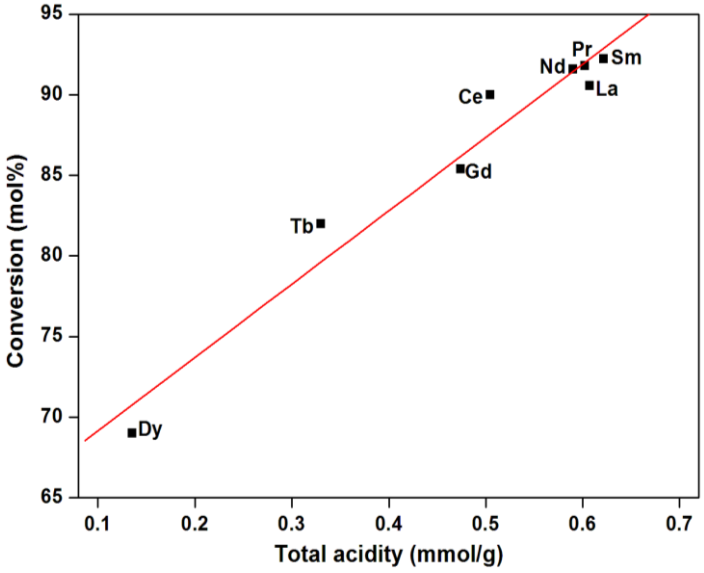


**Fig. 5.24.** Total acidity vs. glucose conversion.

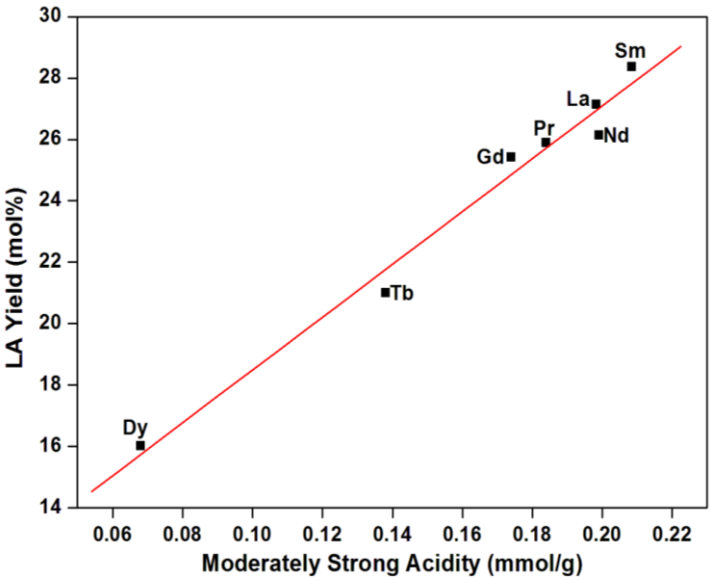


**Fig. 5.25.** Moderately strong acidity vs. LA yield.

In order to investigate the nature of acid sites responsible for LA formation, Brönsted acidity calculated from TPD-MS studies and B/B+L ratio calculated from Pyridine IR studies were plotted against LA yield (Fig. 5.26 and Fig. 5.27 respectively). Both the studies showed a linear graph demonstrating that Brönsted acid sites are required s for LA formation from glucose.

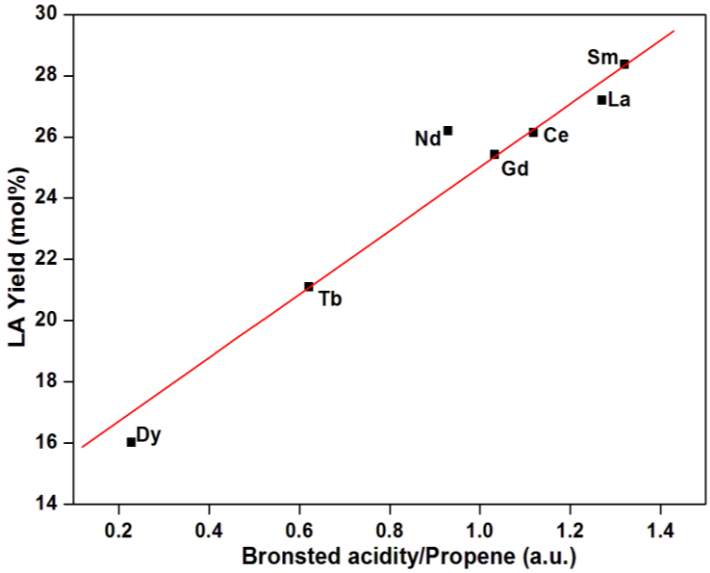


**Fig. 5.26.** Brönsted acidity in terms of propene formed vs. LA yield.

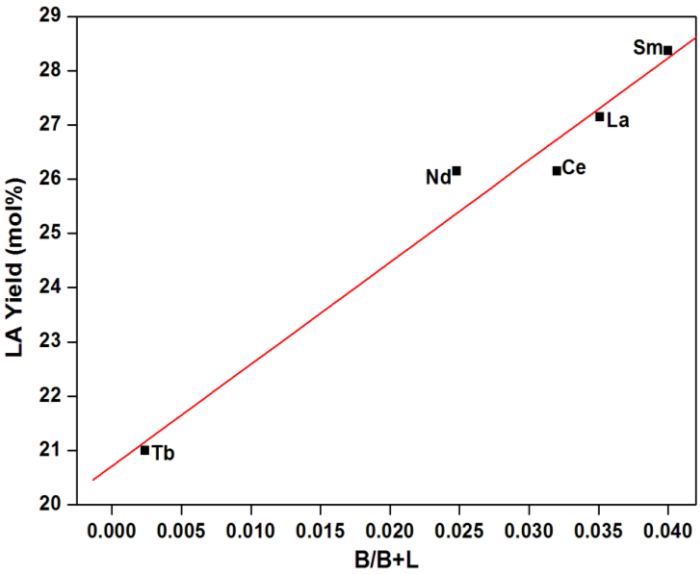


**Fig. 5.27.** B/B+L ratio vs. LA yield.

### 5.2.2.3.2. Effect of temperature and reaction time

The liquid phase dehydration of glucose with $LaPO_4$ was studied by varying the reaction temperatures in the 150-190 °C range with time on stream; the results are

shown in Fig. 5.28. Conversion increased with temperature and the course of the reaction. After 24 h, the conversion increased from 68.3 to 99.8 mol% for the increase in temperature from 150 to 190 °C. Time on stream study also reveals that higher conversions can be accomplished in less duration at higher temperatures. It was found that higher temperatures up to 170 °C and longer duration (up to 20 h) results in higher LA yields (27.5 mol%) clearly demonstrating that such cascade reactions require high activation energy and longer reaction time. Apart from LA, other products like acetic acid (hereafter AA), lactic acid (hereafter LCA) and furfural were formed in minor concentration (<3 mol%) suggesting that under the reaction conditions studied, the decomposition of sugars and decarboxylation of HMF are not dominant revealing that condensation is the dominant side reaction. As expected the yields of FA was more than LA. With further increase in temperature and time, LA yield decreased. Lesser yields of LA, LCA, AA, furfural and FA (than LA) indicate the decomposition of all the products towards coke. Thus, from these studies, 170 °C seems to be the optimum temperature.

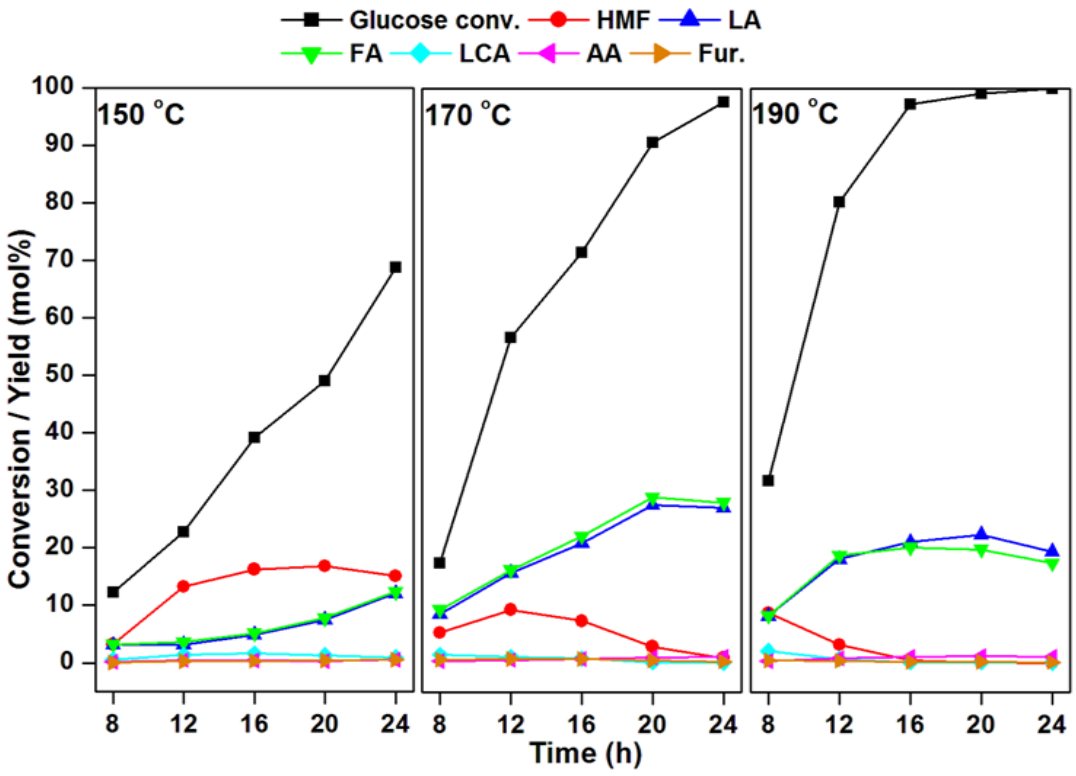


**Fig. 5.28.** Effect of temperature and reaction time on glucose dehydration.

Reaction conditions: Glucose = 3 g in 60 mL, catalyst = 50 wt% of glucose

### 5.2.2.3.3. Effect of catalyst content

The effect of catalyst content on the glucose to LA reaction was studied; results are shown in Fig. 5.29. With increase in the catalyst content from 25 to 50 wt%, glucose conversion and LA yields increased, showing that availability more active acidic sites promotes higher catalytic activity. Time on stream study depicts that highest LA yield (27.5 mol%) can be attained in 20 h with 50 wt% catalyst which remain almost unaltered with further increase in time. Increasing the catalyst weight to 65 wt% though increases the conversion slightly; the LA yields remained same indicating the possibility of side reactions with increasing catalyst content. Thus, 50 wt% can be inferred to be the optimum catalyst content.

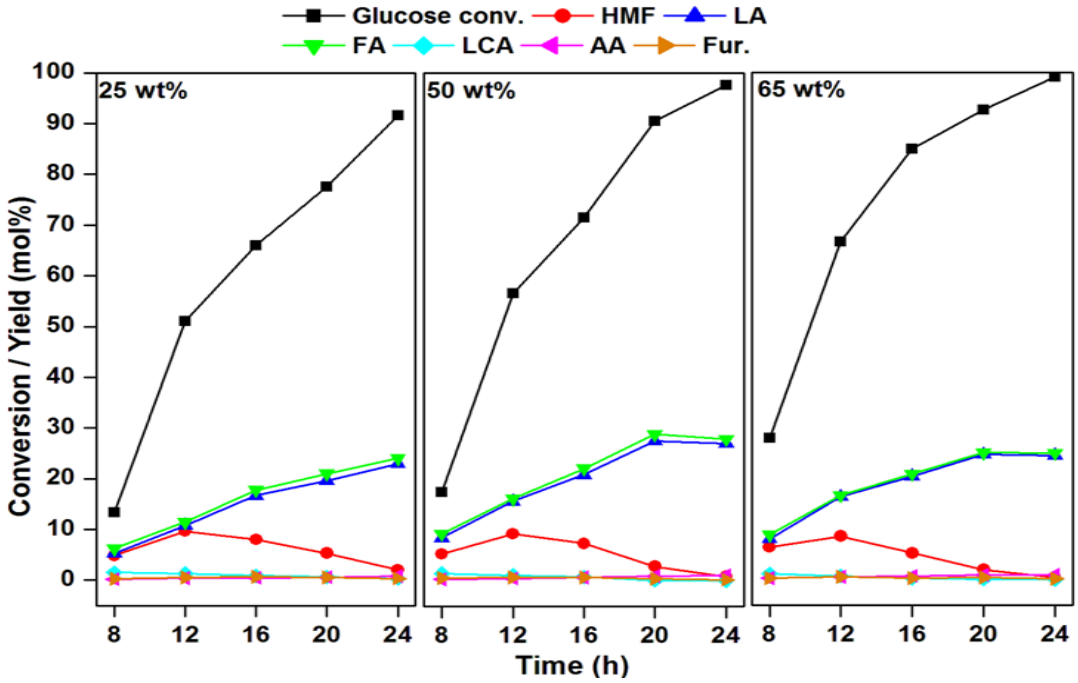


**Fig. 5.29.** Effect of catalyst content and reaction time on glucose dehydration.

Reaction conditions: Glucose = 3 g in 60 mL, temperature = 170 °C

### 5.2.2.3.4. Effect of sachharide

Several other sachharides were screened for the reaction to check the versatility of the catalyst. These results are shown in Table 5.2. It can be seen that saccharides with ketose sugar moieties in it gave higher yields of LA (33.1 and 31.3 mol% for fructose and sucrose, respectively) than the aldoses sugars. This can be attributed to the apt acidic sites on the catalyst which does not lead to further decomposition of ketose. Aldose sugars which require stronger sites rendered lower yields (~28 mol%)

**Table 5.2.** Dehydration of sugars to LA catalyzed by $LaPO_4$.

| S.N | Substrate | Conv. (mol%) | Yield (mol%) | | | | | |
|---|---|---|---|---|---|---|---|---|
| | | | HMF | LA | FA | LCA | AA | Fur |
| 1. | Fructose | 99.84 | 0.12 | 33.10 | 35.22 | 0.08 | 2.33 | 0.27 |
| 2. | Sucrose | 96.21 | 1.03 | 31.38 | 33.03 | 0.18 | 1.69 | 0.14 |
| 3. | Glucose | 90.56 | 2.91 | 27.55 | 28.90 | 0.18 | 0.99 | 0.49 |
| 4. | Maltose | 92.61 | 2.45 | 25.50 | 26.50 | 0.21 | 1.02 | 0.54 |
| 5. | Cellobiose | 90.08 | 2.56 | 27.18 | 29.14 | 0.43 | 0.85 | 0.57 |
| 6. | Inulin | 99.21 | 0.84 | 26.70 | 27.80 | 0.04 | 2.20 | 0.28 |

Reaction conditions: sugar = 3 g in 60 mL, temperature = 170 °C, catalyst = 50 wt% of sugar, time = 20 h.

Legend: HMF = 5-Hydroxymethyl furfural, LA = Levulinic acid, FA = Formic acid, AA = Acetic acid, LCA = Lactic Acid, Fur = Furfural.

### 5.2.2.3.5. Recyclability studies

To test the heterogeneity of the catalyst, the used catalyst was calcined in air at 500 °C for 3 h in order to oxidize the carbonaceous deposits on the surface and used for further reactions. The results are shown in Fig. 5.30. The catalyst was recycled for 3 times. There were only marginal decreases in conversion and yield displaying the effectiveness of the catalyst to work in aqueous acidic hydrothermal conditions.

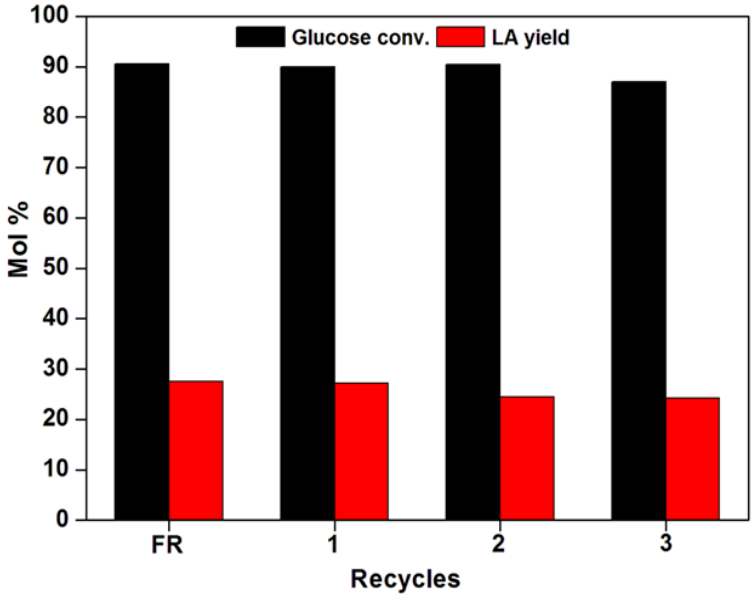


**Fig. 5.30.** Recyclability studies for glucose dehydration to LA.

Reaction conditions: Glucose = 3 g in 60 ml water, temperature = 170 °C, catalyst = 50 wt% of glucose, time = 20 h.

## 5.3. Conclusions

Synthesis of important platform and bulk chemicals like 5-HMF and LA from renewable sugars has been attempted with lanthanide phosphate in environmentally benign solvent (water). The $LnPO_4$ series of catalysts exhibited varied textural characteristics and its effect was studied on dehydration of sugars to 5-HMF and LA. Role of acidity was studied furnishing the type and nature of acidic sites required for the synthesis of furans and acids in water. Moderately strong Brönsted acid sites are crucial for higher yields of 5-HMF and LA in water as good linear correlation exists between the parameters. Various process parameters were optimized aiming for higher yields of targeted compounds. From the optimization studies it can be inferred that synthesis of 5-HMF requires lower temperature and time which may be attributed to its instability and reactivity. However, rehydration to LA requires higher temperature and longer time. Interestingly, the lanthanide phosphate catalysts exhibited good recyclability in the harsh hydrothermal reaction conditions exhibiting the true heterogeneous nature of the catalysts. Additionally, the catalyst system is found to be versatile to convert various other polysaccharides to targeted compounds. However, the catalyst being able to catalyze the dehydration reactions indicates the role of Lewis acidity in water, indicating to expand the scope of tailoring the Brönsted and Lewis sites for phosphate catalyst by improved synthesis approaches which could improve the yields of 5-HMF/LA retaining their heterogeneous nature.

## 5.4. References


1. J.B. Binder, R.T. Raines, J. Am. Chem. Soc. 131 (2009) 1979.
2. S.P. Teong, G.Yi, Y. Zhang, Green Chem. 16 (2014) 2015.
3. A.A. Rosatella, S.P. Simeonov, R.F.M. Frade, C.A.M. Afonso, Green Chem. 13 (2011) 754.
4. A. Corma, S. Ibbora, A. Velty, Chem. Rev. 107 (2007) 2411.
5. K. Shimizu, R. Uozumi, A. Satsuma, Catal. Commun. 10 (2009) 1849.
6. X. Qi, M. Watanabe,T.M. Aida, R.L. Smith, Catal. Commun. 10 (2009) 1771.
7. H. Zhu, Q. Cao, C. Li, X. Mu, Carbohydr. Res. 346 (2011) 2016.
8. J. Jeong, C.A. Antonyraj, S. Shin, S. Kim, B. Kim, K. Lee, J.K. Cho, J. Ind. Eng. Chem. 19 (2013) 1106.
9. H. Zhao, J.E. Holladay, H. Brown, Z.C. Zhang, Science 316 (2007) 1597.
10. T. Stalberg, M.G. Sorensen, A. Riisager, Green Chem. 12 (2010) 321.
11. Y. Román-Leshkov, J.N. Chheda, J.A. Dumesic, Science 312 (2006) 1933.
12. Y. Román-Leshkov, J.A. Dumesic, Top. Catal. 52 (2009) 297.
13. Y. Hikichi, T. Nomura, J. Am. Ceream. Soc. 70 (1987) C-252.
14. F.H. Firsching, S.N. Brune, J. Chem. Eng. Data 36 (1991) 93.
15. Y. Guo, P. Woznicki, A. Barkatt, E.E. Saad, I.G. Talmy, J. Mater. Res. 11 (1996) 639.
16. K. Riwotzki, H. Meyssamy, A. Komowski, M. Hasse, J. Phys. Chem. B 104 (2000) 2824.
17. H. Meyssamy, K. Riwotzki, Adv. Mater. 11 (1999) 840.
18. G. Carini, G.D. Angelo, G. Tripodo, A. Fontana, F. Rossi, G.A. Saunders, Europhys. Lett. 40 (1997) 435.
19. G. Sarala Devi, D. Giridhar, B.M. Reddy, J. Mol. Catal. A:Chem. 181 (2002) 173.
20. H. Onoda, H. Nariai, A. Moriwaki, H. Maki, I. Motooka, J. Mater. Chem. 12 (2002) 1754.
21. C.R. Patra, G. Alexander, S. Patra, D.S. Jacob, A. Gedanken, A. Landau, Y. Gofer, New J. Chem. 29 (2005) 733.
22. L. Ho, H. Nishiguchi, K. Nagaoka, Y. Takita, J. Porous. Mater. 13 (2006) 237.
23. Y. Fang, A. Xu, R.Q. Song, H. Zhang, L. You, J.C. Yu, H.Q. Liu, J. Am. Chem. Soc. 125 (2003) 16025.

24. B. Glorieux, M. Matecki, F. Fayon, J.P. Coutures, S. Palau, A. Douy, G. Peraudeau, J. Nucl. Mater. 326 (2004) 156.
25. P. Savchyn, I. Karbovnyk, V. Vistovs.kyy, V. Pankratov, M.C. Guidi, C. Mirri, O. Myahkota, A.Riabtseva, N. Mitina, A. Zaichenko, A.I. Popov, J. Appl. Phys. 112 (2012) 124309.
26. A. Hezel, S.D. Ross, Spectrochim. Acta. 22 (1966) 1949.
27. R. Kijkowska, E. Cholewka, B. Duszak, J. Mater. Science 38 (2003) 223 and W.W. Rudolph Dalton Trans. 39 (2010) 9642.
28. S.G. Hedge, P. Ratnaswamy, L.M. Kustov, V.B. Kazansky, Zeolites 8 (1988) 137.
29. J. Janchen, M.P.J. Peters, J. vanWolput, J.P. Wolthulzen, J.H.C. vanHoff, J. Chem. Soc. Faraday Trans. 90(7) (1994) 1033.
30. T.T. Nguyen, V. Ruaux, L. Massin, C. Lorentz, P. Afanasiev, V. Belliere-Baca, P. Rey, J.M. Millet, Appl. Catal. B Environ. 166-167 (2015) 432.
31. E. Astorino, J.B. Peri, R.J. Willey, G. Busca, J. Catal. 157 (1995) 482.
32. R.C.L. Mooney, Acta Crystallogr. 3 (1950) 337.
33. H. Assaaoudi, A. Ennaciri, A. Rulmont, Vib. Spectrosc. 25 (2001) 81.
34. K. Amezawa, H. Maekawa, Y. Tomii, N. Yamamoto, Solid State Ionics 145 (2001) 233.
35. A.M. Guillaume, R. Wirth, L. Nasdala, M. Gottschalk, J.M. Montel, W. Heinrich, Phys. Chem. Minerals 29 (2002) 240.
36. C.W.A. Paschoal, AP. Ayala, I. Guedes, C.K. Loong, L.A. Boatner, Proceedings of XV111th International Conference on Raman Spectroscopy 18 (2002) 577-578.
37. K. Rajesh, P. Shajesh, O. Seidel, P. Mukundan, K.G.K. Warrier, Adv.Funct. Mater. 17 (2007) 1682.
38. T.T.N. Nguyen, V. Ruaux, V. Belliece-Baca, P. Rey, J.M.M. Mullet, Appl. Catal. A. Gen. (2014) http://dx.doi.org/10.1016/j.apcata2014.12.026
39. O. Novotny, K. Cejpek, J. Velisek, Czech J. Food. Sci. 26 (2008) 117.
40. C. Moreau, R. Durand, S. Razigade, J. Duhamet, P. Faugeras, P. Rivalier, P. Ros, G. Avignon, Appl. Catal. A Gen. 145 (1996) 211.
41. L. Deng, Y. Zhao, J. Li, B. Liao, Q.X. Guo, ChemSusChem 3 (2010) 656.

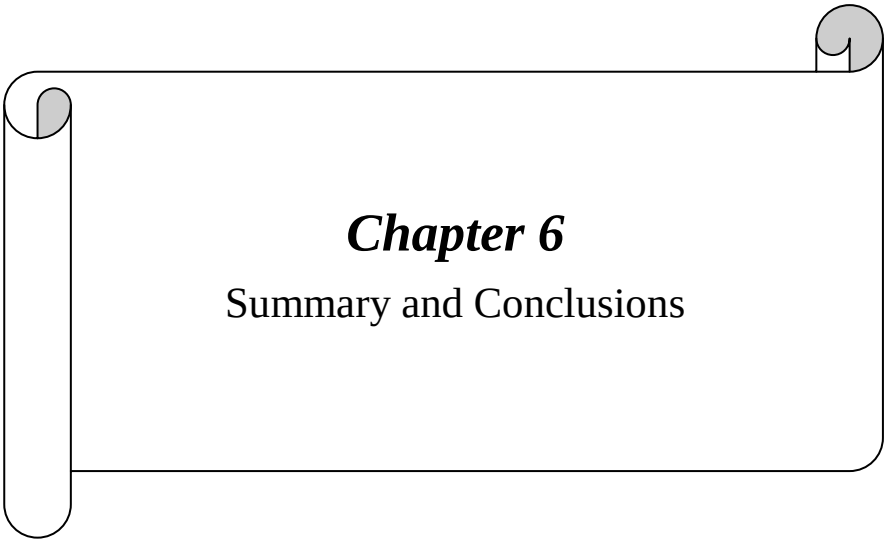

# *Chapter 6*

Summary and Conclusions

## 6.1 Summary and Conclusions

The present thesis has attempted to cover the efficacious conversion of renewable carbohydrate biomass to highly important platform chemicals 5-hydroxymethyl furfural (HMF) and levulinic acid (LA). Thus, the present study has high significance in the context of sustainability and green chemistry.

5-Hydroxymethyl furfural has been synthesized in various reaction mediums in order to evaluate the advantages and drawbacks of each system. Levulinic acid being a rehydration product of HMF is synthesized in environmentally benign solvent water. The important part of the study is to furnish insights into the role of acidity and investigate the type of acid sites responsible for the synthesis of HMF and LA. This is an important aspect to be investigated, if these catalysts have to be used as heterogeneous solid acid catalysts for these reactions. HMF is synthesized in biphasic medium from fructose using mesoporous Al incorporated SBA-15 and chemically treated clays. LA was synthesized from various saccharides with zeolite beta catalysts in aqueous medium. Lanthanide phosphates have been deployed for fructose dehydration to HMF and conversion of various sugars to LA. The characterization of the catalysts was carried out using X -ray diffraction (XRD), electron microscopy, Raman spectroscopy, chemical analysis, $^{27}Al$ and $^{29}Si$ nuclear magnetic resonance (NMR), thermo gravimetric analysis (TGA), infrared spectroscopy (IR) and $N_2$ sorption for BET surface area. The investigation of acidity was conducted using temperature programmed desorption of ammonia ($NH_3$-TPD), while the Brönsted acidity was monitored using temperature programmed desorption of isopropyl amine as a probe molecule using TPD instrument equipped with mass spectrometr (TPD-MS). Also, the nature of acid sites was evaluated using fourier transform infrared spectroscopy of pyridine (Pyridine–IR). Based on these investigations, the thesis is divided into 6 chapters which include a chapter for summarization of the work carried out for this dissertation.

**Chapter 1** gives a brief introduction to the heterogeneous catalysis. It provides an outlook of green chemistry and the potential of biomass derived carbohydrates for the production of chemicals. Prime importance is rendered to dehydration of sugars to 5-HMF; an important platform chemical and LA an important bulk chemical. It underlines the significance of these industrially important organic transformations. It also describes about the various catalysts used for this

work, like Al incorporated SBA-15, rare earth phosphates, zeolites and chemically treated clays. This chapter enumerates all the conclusions drawn upon the investigations conducted with regard to various catalysts in the conversion of carbohydrates to HMF and LA.

**Chapter 2** describes the methods of catalyst synthesis and important analytical techniques employed for their characterization. The catalysts synthesized were Al incorporated SBA-15, rare earth phosphates ($LaPO_4$ to Dy $PO_4$), whereas zeolite beta (with various $SiO_2/Al_2O_3$ ratios) and acid treated/pillared clays were commercially procured. This chapter also describes various experimental techniques deployed for their characterization. The characterization of these materials was carried out using powder X-ray diffraction (XRD), $N_2$ adsorption–desorption, scanning and transmission electron microscopy (SEM & TEM), $^{27}Al$ and $^{29}Si$ nuclear magnetic resonance (NMR), Fourier-transform infrared spectroscopy (FTIR), Raman spectroscopy, temperature programmed desorption of ammonia (TPD-$NH_3$), temperature programmed desorption coupled with mass spectrometry (TPD-MS) and pyridine IR. Detailed descriptions of these techniques, their theory and experimental procedures have been outlined in this chapter.

**Chapter 3** begins with an extensive introduction to the dehydration of sugars to HMF in various reaction mediums. It describes the results of investigations pertaining to the dehydration of fructose to HMF in biphasic conditions. This chapter is divided into two parts, 3A and 3B. Part 3A deals with the investigations relating to Al incorporated SBA-15 as catalysts for dehydration of fructose to HMF in biphasic medium. It presents the detailed textural characterization to study the change in structure, morphology and acidity before and after Al incorporation. The XRD pattern of Al containing samples show similar peaks that of parent SBA-15 clearly showing that on post synthesis modification (alumination), hexagonal mesoporous structure is retained. The retention in morpholology can also be clearly seen by SEM and TEM. Alumination leads to the formation of acidic sites and the total acidity depends on the amount of aluminium present in the samples. The increase in the aluminium content leads to increase in extraframework species as displayed by $^{27}Al$ MAS NMR thus altering the nature of acid sites which is studied by pyridine IR. In addition, the results of $N_2$ sorption etc were also discussed in detail.

The AlSBA-15 catalysts were evaluated for the dehydration of fructose to HMF. The effect of Si/Al ratio on the catalytic activity and yield were systematically investigated. A good linear correlation between the moderately strong acidity/total acidity ratio and B/B+L ratio against HMF yield was obtained. These findings demonstrated that the presence of moderately strong acidity particularly the Brönsted acid sites are crucial for HMF formation from dehydration of fructose in biphasic medium. Reaction temperature, catalyst amount and time have marked effect on catalytic activity. AlSBA-15 works truly as heterogeneous catalyst if milder reaction conditions and non aqueous solvent systems are employed. Conclusions drawn from the catalytic fructose dehydration reaction studies and their correlation with the characterization results are also discussed in this section.

Part-3B deals with the HMF synthesis from fructose in biphasic medium using acid treated and pillared clays. This part discusses the characterization and catalytic activity results of clay catalyst. The change in structure after the chemical treatment has been investigated by XRD and NMR studies. The studies show slight reminiscence of lamellar structure of the parent clay after acid treatment. However, pillaring imparts higher preservance and stability to the layered structure. The textural properties of the clays were studied by $N_2$ sorption which shows the formation of mesopores after acid treatment. The effect on acidity and nature of acidic sites after different chemical treatments was also investigated. The present study envisages the nature of acidic sites responsible for higher yield/selectivity for the furan compound. A linear correlation was obtained for B/B+L ratio and HMF yields demonstrating that the Brönsted acid sites are crucial for fructose dehydration to HMF. Among the various treated clays, the acid treated clay K10 demonstrated the greatest catalytic activity giving 61 mol% of HMF from fructose. The catalytic activity was correlated with various physiochemical properties of the catalyst.

**Chapter 4** commences with broad literature background of LA synthesis from various biomass feedstocks along with the significance and rationale of the compound. This is followed by results of dehydration of sugars to LA with zeolite beta in aqueous medium. This chapter is divided in to two parts. Part-4A provides the detailed studies of characterization of beta zeolite with different $SiO_2/Al_2O_3$ ratios. XRD shows the retention of BEA topology though some decrease in crystallinity was witnessed in dealuminated samples. The dealumination process also mars the

spherical morphology of the samples and induces textural changes which are addressed with SEM and $N_2$ sorption studies, respectively. The dealuminated samples have octahedral Al, in addition to tetrahedral Al, as part of the dislodged Al from the lattice is occluded in the zeolite pores. This is clearly demonstrated by $^{27}$Al MAS NMR. This change in aluminium coordination has a profound effect on acidity especially Brönsted acidity. TPD-MS studies were used for estimating the Brönsted acidity in the zeolite which was well corroborated with Pyridine IR investigations.

Part-4B presents the catalytic activity of beta zeolite catalysts in the dehydration of sucrose/glucose to LA. The role of acidity on the reaction was explored revealing that moderately strong acidity with more Brönsted acid sites is responsible for the formation of keto acid. The parameters like reaction temperature, catalyst content and substrate concentration plays an important role in sucrose/glucose dehydration and LA yields. Dehydration of other polysachharides was also studied. Recyclability studies show a decrease in catalytic activity due to acidic hydrothermal reaction conditions. The catalyst retains its activity when ethanol is used as reaction medium as ethyl levulinate is formed. The later is a good fuel additive. At the end of the chapter, conclusions were drawn and catalytic activity was correlated with characterization results.

**Chapter 5** focusses on the synthesis of HMF in green solvent water and discusses the pros and cons of the system. Synthesis of HMF and rehydration of HMF to LA were studied using lanthanide phosphate catalysts and reported in this chapter. This chapter is also divided into two parts. Part-5A describes the detailed results of characterization of lanthanide phosphates. XRD of the catalysts show that all lanthanide phosphates are nanocrystalline and isostructural with hexagonal structure of rhabdophane mineral. The crystallinity and cell parameters are affected by the ionic radii indicating the effect of lanthanide contraction which is in agreement with IR and Raman spectroscopy studies. This effect also alters the textural properties of the catalysts which in turn affects the acidity of the materials. Total acidity was found to be linearly dependent on the surface area. Scanning and transmission electron microscopic analysis suggest rod like morphology and also d-spacing of the material, respectively. Thermal stability of the material was studied by TGA analysis.

Part-5B describes the catalytic activity of lanthanide phosphates in fructose dehydration to HMF and glucose dehydration to LA. However, various other sugars

are also screened for both the transformations. Role of acidity was studied furnishing the type/nature of acidic sites required for the synthesis of furans and acids in water. Various process parameters were optimized aiming for higher yields of targeted compounds. From the optimization studies it can be inferred that synthesis of 5-HMF requires lower temperature and less reaction time, as otherwise the 5-HMF formed is converted to unwanted by-products, as a result of its instability. However, rehydration to LA requires higher temperature and time. Moderately strong Brönsted acid sites are crucial for higher yields of 5-HMF and LA in water as good linear correlation existed between the parameters. Interstingly, the lanthanide phosphate catalysts exhibited good recyclability in the harsh hydrothermal conditions exhibiting the true heterogeneous nature.

From the above studies, it can be concluded that HMF and LA were synthesized from renewable sugars. From the acidity studies, it can be inferred that both the compounds need moderately strong acid sites for their formation as linearity is observed between the two parameters. Comparing the catalytic performance of AlSBA-15 and K10 in biphasic medium it can be inferred that K10 rendered higher yields of HMF (61 mol%) than AlSBA-15 (52 mol%) which is due to higher value of B/B+L ratio (0.8 for K10 and 0.5 for AlSBA-15). Similarly, for LA synthesis from glucose, beta zeolite gave higher yield of LA (39 mol%) as compared to lanthanum phosphate (27 mol%) which is due to higher B/B+L ratio and Brönsted acidity. Thus, it can be seen that type/nature of acidic sites required for both compounds is same. However, higher total acidity and moderate acidity seems to be favorable for LA. Additionally, reaction conditions for HMF and LA vary. The temperature for both the transformations was nearly same but, HMF synthesis requires less duration, whereas LA needs higher reaction time. These findings are beneficial for developing efficient solid acid catalysts and apt process conditions for such cascade reactions.

It is mandatory at the end of all chapters in a dissertation to summarize the research work undertaken for the advantage of the reader. Hence, this chapter summarizes the conclusions reached based on the experimental results during these investigations. Initially it describes the content of each chapter in detail with glimpses of results at the end. This section also offers suggestions for further research work in given areas and scope of their applications.

## 6.2. Suggestions for future research

The aim of the present investigations is to utilize renewable carbohydrate biomass for the production of important platform and bulk chemicals, which in turn can lead to contributions towards the sustainable production of chemicals. Hence, the thesis dealt with the preparation and characterization of solid acid catalysts for dehydration of carbohydrates to HMF and LA. Since the reactant and the products are highly reactive due to their polyfunctionality, the acidity has to be fine tuned to minimize unwanted side reactions which will lead to higher yields of the targeted compounds. Towards this purpose, role of acidity is studied furnishing insights into the crucial acidic sites responsible for HMF and LA formation. Mesoporous aluminium incorporated SBA-15 and chemically treated clays were employed for fructose dehydration in biphasic reaction medium that gave good HMF yields. These catalysts also have potential to catalyze other reactions such as synthesis of other important chemicals like lactic acid or alkyl lactates, HMF ethers, alkyl levulinates from carbohydrates. The role of acidity for above mentioned reactions can also be studied. For understanding the interaction of complex reactants and improvisation of catalysts, DFT studies can also be undertaken which will lead to the tuning of catalyst and the reaction conditions. Currently there is no commercial production of HMF as higher yields of HMF can be obtained only in DMSO, this makes the product separation highly energy intensive. Therefore, study of process conditions that lead to economically viable solvent is important. This optimization can help to maximize HMF yield. This can be extended to studies pertaining to continuous production of HMF. In order to make the process more cost effective, lignocellulosic biomass can be used for the production of HMF.

Commercial production of LA uses homogeneous acids as catalyst, leading to handling issues and environmental degradation. Hence, to make the process greener and to reduce the environmental hazards, homogeneous acids must be replaced by heterogeneous catalysts. In the present study, beta zeolite has been screened for LA production from various polysaccharides, however, leaching of framework aluminium was observed in the acidic hydrothermal conditions. Switching from batch mode to continuous mode may overcome the leaching problem due to separation of acidic products thereby improving the performance. Additionally, the process conditions can be tackled leading to less coke formation. The provision of insitu carbon removal adds

to the benefits of continuous process. Moreover, the possibility of designing novel hierarchal zeolites expands the scope of zeotype materials for LA production. Thus, in future new hierarchal zeolites can be tested for dehydration reactions for HMF and LA in a fixed bed reactor.

Since, water is a valuable solvent due to its easy availability, non-toxicity and environmental friendliness, the present study focussed on using it partially or fully to substitute organic solvents for the green synthesis of HMF. However, water being highly polar, maintaining the desirable yield of HMF and stability of the catalyst are major challenges. Hence, rare earth phosphates were used as catalysts since they are highly stable in acid and basic solution. Good yields of HMF were obtained with $LaPO_4$ which could also work for further rehydration of HMF to LA. Since, rare earth phosphates have excellent hydrothermal stability, they can be exploited for cellulose transformation to HMF and LA. Other acid catalyzed reactions like esterification, etherification and dehydration of sugars can be tested with them. Additionally, tuning of acidity and enhancement of Brönsted sites can be achieved by addition of dopant. In future, they can be definitely exploited for HMF and LA synthesis from carbohydrates in continuous mode.

By and large, this study advances the knowledge on the conversion of carbohydrate biomass to value added chemicals. It describes the dehydration of carbohydrates to HMF and LA. Role of acidity is explored that will help to understand cascade reactions. Carrying out the reaction with right acidity and quenching the reaction at right duration of the reaction are important for the formation of furans and acids. Though good yields of targeted compounds could be achieved, there is still scope to improve and optimize the results. This needs more research to be carried out in these areas. The present investigations pertaining to acidity characterization should also pave the way for efficient design of solid acid catalyst in the very foreseeable future.

## List of Publications

1. Dehydration of fructose to 5-hydroxymethyl furfural over ordered AlSBA-15 catalyst.
   **Nishita Lucas**, Ganesh Kokate, Atul S. Nagpure and Satyanarayana Chilukuri Microporous and Mesoporous Materials 181 (2013) 38-46.
2. Novel catalysts for valorization of biomass to value added chemicals and fuels.
   **Nishita Lucas**, Narasimharao Kanna, Atul S. Nagpure, Ganesh Kokate and Satyanarayana Chilukuri, Journal of Chemical Sciences 126 (2014) 403-413.
3. Renewable fuels from biomass derived compounds: Ru containing hydrotalcites as catalysts for conversion of HMF to 2,5-dimethylfuran.
   Atul S. Nagpure, A.K. Venugopal, **Nishita Lucas**, M. Manikandan, Raja T., Satayanarayana Chilukuri, Catalysis Science and Technology, DOI:10.1039/c4cy01376.
4. Exploring the role of acidity for the synthesis of biomass derived levulinic acid with zeotype catalyst.
   **Nishita Lucas**, Atul S. Nagpure and Satyanarayana Chilukuri (communicated)
5. Green synthesis of 5-hydroxymethyl furfural from fructose over nanocrystalline rare earth phosphates.
   **Nishita Lucas**, Atul S. Nagpure and Satyanarayana Chilukuri (communicated)
6. Efficacy of clay catalyst for platform chemicals from renewable carbohydrates.
   **Nishita Lucas**, Atul S. Nagpure and Satyanarayana Chilukuri
   (Manuscript under Preparation).

## List of Patents

1. Efficient production of renewable liquid fuels and chemicals from biomass over Ruthenium supported catalyst.
   Satyanarayana V.V. Chilukuri, Atul Sopan Nagpure, **Nishita Satyendra Lucas**
   Patent application No. 0183DEL2014